Metaeffector regulation of *Legionella pneumophila* translation inhibiting effectors

by

Ashley Marie Joseph

B.S., California State University, Monterey Bay, 2014

AN ABSTRACT OF A DISSERTATION

submitted in partial fulfillment of the requirements for the degree

DOCTOR OF PHILOSOPHY

Division of Biology
College of Arts and Sciences

KANSAS STATE UNIVERSITY
Manhattan, Kansas

2022

Abstract

Legionella pneumophila is a facultative, intracellular bacteria that naturally infects free living amoeba and is an accidental human pathogen. *L. pneumophila* possesses a Dot/Icm type IV secretion system that transfers over 330 effector proteins directly into its host cell. This large arsenal of effectors contributes to the ability of *L. pneumophila* to establish infection in both environmental and immune phagocytes. Effectors modulate host cell processes to acquire nutrients and generate a camouflaged replication compartment called the *Legionella* containing vacuole (LCV) which mimics the appearance of rough endoplasmic reticulum. Survival within the host cell relies on proper coordination and regulation of effector activity throughout the infection process. *L. pneumophila* encodes a subset of effector proteins, called metaeffectors, that regulate the activity of another effector or family of effectors.

The metaeffector, MesI, is required for *L. pneumophila* intracellular replication in *Acanthamoeba castellanii* and bone marrow-derived macrophages in the context of its target effector, SidI. SidI is one of seven effectors known to inhibit host mRNA translation. We found that MesI suppresses both SidI translation inhibition and novel mannosyl hydrolase activity. It was additionally discovered that MesI binds SidI at two, non-overlapping regions on the N-and C- terminus and does not interfere with SidI binding to the eukaryotic elongation factor, eEF1A. Further investigation revealed that the deleterious phenotype associated with loss of *mesI* is due to SidI intrabacterial toxicity that can be replicated *in vitro* with overexpression of *sidI* uncoupled from *mesI.*

Given the importance of MesI regulation of SidI to *L. pneumophila* survival, we investigated another toxic translation inhibiting effector, SidL, that interacts with a putative metaeffector, LegA11. In addition to translation inhibition, SidL binds to filamentous actin and

inhibits actin polymerization *in vitro,* but the effects of LegA11 on these activities are unknown. We uncovered that LegA11 regulates both SidL translation inhibition and inhibition of actin polymerization, despite promoting binding to actin. Interestingly, we discovered that loss of *legA11* provided a replication advantage during intracellular replication in murine *Nlrc4*-deficient macrophages, but not in *Acanthamoeba castellanii*, THP-1 cells or the mouse lung. This advantage was not attributed to improved establishment of the LCV or an increase in bacterial growth rate and the cause of the replication advantage is unknown.

Here we highlight commonalities in metaeffector regulation of translation inhibiting effectors, while demonstrating the differential contributions of metaeffectors to *L. pneumophila* intracellular replication. This work provides valuable insight into the dynamic and intricate regulation of *L. pneumophila* effectors and contributes to the broader understanding of complex host-pathogen interactions exerted by intracellular pathogens.

Metaeffector regulation of *Legionella pneumophila* translation inhibiting effectors

by

Ashley Marie Joseph

B.S., California State University, Monterey Bay, 2014

A DISSERTATION

submitted in partial fulfillment of the requirements for the degree

DOCTOR OF PHILOSOPHY

Division of Biology
College of Arts and Sciences

KANSAS STATE UNIVERSITY
Manhattan, Kansas

2022

Approved by:
Co-major Professor
Dr. Stephanie Shames

Approved by:
Co-Major Professor
Dr. Sherry Fleming

Copyright

Abstract

Legionella pneumophila is a facultative, intracellular bacteria that naturally infects free living amoeba and is an accidental human pathogen. *L. pneumophila* possesses a Dot/Icm type IV secretion system that transfers over 330 effector proteins directly into its host cell. This large arsenal of effectors contributes to the ability of *L. pneumophila* to establish infection in both environmental and immune phagocytes. Effectors modulate host cell processes to acquire nutrients and generate a camouflaged replication compartment called the *Legionella* containing vacuole (LCV) which mimics the appearance of rough endoplasmic reticulum. Survival within the host cell relies on proper coordination and regulation of effector activity throughout the infection process. *L. pneumophila* encodes a subset of effector proteins, called metaeffectors, that regulate the activity of another effector or family of effectors.

The metaeffector, MesI, is required for *L. pneumophila* intracellular replication in *Acanthamoeba castellanii* and bone marrow-derived macrophages in the context of its target effector, SidI. SidI is one of seven effectors known to inhibit host mRNA translation. We found that MesI suppresses both SidI translation inhibition and novel mannosyl hydrolase activity. It was additionally discovered that MesI binds SidI at two, non-overlapping regions on the N-and C- terminus and does not interfere with SidI binding to the eukaryotic elongation factor, eEF1A. Further investigation revealed that the deleterious phenotype associated with loss of *mesI* is due to SidI intrabacterial toxicity that can be replicated *in vitro* with overexpression of *sidI* uncoupled from *mesI.*

Given the importance of MesI regulation of SidI to *L. pneumophila* survival, we investigated another toxic translation inhibiting effector, SidL, that interacts with a putative metaeffector, LegA11. In addition to translation inhibition, SidL binds to filamentous actin and

inhibits actin polymerization *in vitro,* but the effects of LegA11 on these activities are unknown. We uncovered that LegA11 regulates both SidL translation inhibition and inhibition of actin polymerization, despite promoting binding to actin. Interestingly, we discovered that loss of *legA11* provided a replication advantage during intracellular replication in murine *Nlrc4*-deficient macrophages, but not in *Acanthamoeba castellanii*, THP-1 cells or the mouse lung. This advantage was not attributed to improved establishment of the LCV or an increase in bacterial growth rate and the cause of the replication advantage is unknown.

Here we highlight commonalities in metaeffector regulation of translation inhibiting effectors, while demonstrating the differential contributions of metaeffectors to *L. pneumophila* intracellular replication. This work provides valuable insight into the dynamic and intricate regulation of *L. pneumophila* effectors and contributes to the broader understanding of complex host-pathogen interactions exerted by intracellular pathogens.

Table of Contents

List of Figures

List of Tables

Acknowledgements

The first person I would like to thank is my advisor, Dr. Stephanie Shames. Thank you for your support and guidance throughout my time at Kansas State University. You gave me the opportunity to learn, grow, fail, and succeed in your lab and taught me that it's ok to say "I don't know"- although I hope I didn't say it too much! I would also like to thank my co-mentor, Dr. Sherry Fleming. Your feedback may be tough, but its fair, and I am a better scientist because of it. Next, I would like to thank my committee members, Dr. Brian Geisbrecht, Dr. Jeroen Roelofs, Dr. Phil Hardwidge, and Dr. Revathi Govind for your feedback, support, and collaboration throughout my Ph.D. I would also like to thank my friend, colleague and mentor, Dr. Annette Angus for always taking the time to talk and remind me that I am a rockstar. I of course have to thank my fellow Shames Lab members, Dr. Deepika Chauhan and Tshegofatso Ngwaga. The friendship that we've built over the years got me through some of the toughest times of graduate school and I will forever cherish getting the chance to know you. I would also like to thank all the amazing undergraduate researchers I had the opportunity to work with in the lab, Adrienne Pohl, TJ ball, Will Sydzyik,and Sabrina Veith. Thank you for all your hard work and contributions to this research.

I owe a huge thank you to my family. Thank you to my parents, who have always supported me mentally, emotionally, and financially. I appreciate your patience and for always pretending to be interested when I talk about my research for hours on end. To my brother, Sean. Thank you for letting me think that I could beat you up when we were little, even though I have a Ph.D. in microbiology, and you have a black belt in jiu jitsu. I am more confident and stronger for that. It's nice of you to let Kevin win as well. To my sister-in-law, and cousins- thank you for all the light night calls, trips across the country, and laughs that kept me grounded. To my Friday

Night Happy Hour Crew- Cheers to surviving a global pandemic, Ph.D., and several Manhattans together! To my nieces and nephew, never let anyone tell you what you can or cannot do. You create your own journey. To all my friends, thank you for the laughs, smiles, hugs, and wine. I am truly blessed to have you in my life. ♦

Finally, I need to thank my amazing husband, Jesse. You are my partner and my rock. Even when I doubted myself and wanted to quit, you stood by my side and reminded me that we can accomplish anything together. We survived four and a half years, two Ph.D.s and 1,500 miles. I can't wait to see what the future has in store.

Dedication

I dedicate this work to my cousin Jacque. When told of her strength through unimaginable challenges she replied, “What other choice do I have?”, which became my motto throughout graduate school.

Chapter 1 - Introduction

I. *Legionella*

Bacteria of the genus *Legionella* are Gram-negative bacilli, abundantly found in fresh water and soil environments (1, 2). The *Legionella* genus encompasses 65 known species, covering 80 strains (3, 4). Approximately 20 of these species have been shown to cause disease in humans, although *Legionella pneumophila* accounts for >90% of infections in the United States (4, 5). Most species feature a single, monopolar flagellum, although some exist as non-flagellated cells (5, 6). In aquatic systems, *Legionella* can appear as either planktonic cells or more commonly, as part of diverse biofilms. *Legionella* replicate poorly within biofilms, mainly due to their inability to synthesize most amino acids (7, 8). They can persist in biofilms by capturing nutrients from dead microbial cell debris, but this is not sufficient to support substantial replication (9). However, persistence in biofilms permits predation by free-living amoeba such as *Acanthamoeba castellanii* and *Hartmannella vermiformis*, that naturally phagocytose and degrade bacteria as a food source (8, 10). Millions of years of co-evolution with protozoa have enabled *Legionella* to exploit vesicle trafficking and nutrient metabolism to successfully replicate within the eukaryotic cell (11, 12).

II. Establishment of Infection

Phagocytosis. The bacterial outer membrane protein, LaiA, collagen-like protein, Lcl, and lipopolysaccharides (LPS) on the bacterial cell surface are involved in host cell adherence (13–16). Uptake of *L. pneumophila* occurs through coiling phagocytosis in which a unilateral pseudopod engulfs the bacterium (17, 18). The significance of this noncanonical phagocytosis is unknown and is independent of bacterial virulence, as heat-killed *L. pneumophila* are also

internalized this way (17). Another intracellular pathogen, *Borrelia burgodorferi*, is engulfed by macrophages using coiling phagocytosis which requires regulation of the actin binding formins, FMNL1, mDial1, and Daam1 by Arp2/3 (19–21). During *L. pneumophila* infection, actin polymerization is induced at the site of bacterial entry and the bacteria are internalized into a membrane derived phagosome (22).

Intracellular Life Cycle. Critical for pathogenicity is the establishment of the *Legionella* containing vacuole (LCV). Biogenesis of the LCV begins when translocated virulence proteins called effectors recruit host organelle-derived vesicles to the surface of the phagosome (22–26). The membrane of the phagosome becomes studded with ribosomes, mimicking the appearance of the endoplasmic reticulum and successfully concealing the compartment from lysosomal fusion (4, 22). Bacteria contained in the LCV enter the replicative phase of their life cycle following signaling by the amino acid sensing phagosomal transporter (Pht) protein family (27).The proteome of replicative bacteria is enriched with DNA polymerases (DnaA), ribosomal subunits, aminoacyl-tRNA synthetases and other enzymes necessary for cellular division (28). The bacteria display decreased virulence and cease expression of the flagellin gene, which aids in the subversion of host cell detection (29). During intracellular growth, *L. pneumophila* relies on their host cell for nutrients such as amino acids. *L. pneumophila* detects depletion of host cell amino acid through the *Legionella* quorum sensing (Lqs) system and the protein LqsR regulates the transition into the transmissive phase (30–34). The bacterial protein, RelA, involved in guanosine pentaphosphate (ppGpp) metabolism accumulates and indicates a response to amino acid starvation and marks entrance into the transmissive phase (35, 36). Transmissive bacteria, also known as persisters, are non-growing but metabolically active. The membranes of persistent *Legionella* comprise higher levels of branch chained fatty acids (BCFA) and short chain fatty

acids characteristic of bacteria exposed to environmental stress (37). The change in fatty acid composition of the cell membrane in conjunction with activity of drug efflux pumps such as TolC, give transmissive *Legionella* a higher tolerance to antimicrobials (37–41). Additionally, expression of flagellin resumes, and expression of effectors are upregulated, causing the bacteria to be more infectious (28, 29).

Effectors. *Legionella* encodes a Dot/Icm T4SS that is required for creation of the LCV (11, 42). The T4SS localizes to the poles of intracellular bacteria and tethers it to the phagosome, traversing both bacterial and eukaryotic membranes and allowing for the translocation of effectors directly into the host cell (43–45). Effectors target host cell components and assist in subversion of the host defenses. Over 18,000 unique effectors have been identified in the *Legionella* genus, with hundreds featuring eukaryotic-like domains, suggesting evolutionary cross over events with protist host cell (3, 42). The number of effector proteins present in the *Legionella* genome varies by species, but *L. pneumophila* contains one of the largest collections with over 330 identified effectors (3, 42, 46). This large arsenal of effectors is a consequence of *L. pneumophila* interactions with various phagocytic protozoa and led to its emergence as an accidental human pathogen (46–50). The broad protozoan host tropism also explains the presence of effector redundancy within the *Legionella* genome (51). While many effectors appear functionally redundant, effector requirements vary by host cell, with only 7 effectors being universally required (50).

Biogenesis of the LCV. Bacteria are phagocytosed into a membrane-bound phagosome that is transported along microtubules to the perinuclear region where lysosomes are congregated (52, 53). This process can be impeded by the transient accumulation of actin filaments around immature phagosomes or supported by actin nucleation around docking sites (54, 55). The

vacuolar ATPase (V-ATPase) ATP6V0D2 interacts with the SNARE proteins to facilitate lysosomal fusion and the phagolysosome undergoes rapid acidification through V-ATPase activation and ROS production by NADPH oxidase (56–60). In protozoan and immunocompromised hosts, *L. pneumophila* can subverts normal vesicle trafficking and establish the LCV through the activity of effector proteins (61).

The effectors SidK and WipB prevent acidification of the vacuole by impairing V-ATPase function (62, 63). Members of the vacuole protein sorting inhibitor protein family (Vip), LegC3 and LegC7/YlfA interact with the host protein, VAMP4 (64, 65). VAMP4 regulates Golgi-to-late endosome trafficking through formation of a trans-SNARE complex (66). LegC3 and LegC7/ YlfA inhibit VAMP4 formation of the trans-SNARE complex and consequently modify normal vesicle trafficking (65, 67, 68). VipA, acts as an actin nucleator, enhancing polymerization of actin microfilaments around early endosomes that alters trafficking (69). In contrast, the effector kinase, LegK2, inhibits nucleation of branched actin filaments by phosphorylating the ARP2/3 complex on phagosomes to evade the late endocytic pathway (70). The effector WipA dephosphorylates multiple proteins involved in actin polymerization including ARP2/3, and a double mutant lacking *wipA* and *legK2,* displays impaired replication at late stages of infection (71). VipD prevents fusion of phagosomes with endosomes by altering endosome protein and lipid composition through interactions with Rab5 (72). The effector LidA localizes to the cytoplasmic surface of the phagosome where it works synergistically with SidM/DrrA to recruit the host small GTPase, Rab1 (73). Rab1 regulates ER-to-Golgi trafficking and binding to SidM/DrrA-LidA interferes with the host secretory pathway (73). Later, the effector, SidD, antagonizes the activity of SidM/DrrA by deAMPylating Rab1, allowing for its

release from the LCV membrane (74). The GTPase-activating (GAP) effector LepB then associates with GTP-bound Rab1 promoting its deactivation (75, 76).

During early LCV formation, mitochondria associate with the LCV in a T4SS-independent manner (77). The *L. pneumophila* chaperone, HtpB, located on the bacterial cell surface alters actin microfilament organization during ectopic expression and infection. It has also been implicated in the association of mitochondria with the LCV, however this has only been demonstrated with recombinant, purified protein (78). Upon association with the LCV, mitochondria fragmentation occurs in a T4SS-dependent manner. The effector MitF/ LegG1 regulates actin cytoskeleton dynamics and mitochondria fragmentation through the host Ran GTPase and phosphorylation of the large GTPase, DNM1L respectively. (23). Fragmentation by MitF/ LegG1 does not release death signals such as cytochrome C, but instead halts mitochondrial respiration and leads to Warburg-like metabolism within the cell that favors bacterial replication (23).

Actin Dynamics. Actin is present in eukaryotic cells as either monomeric (G) actin or as filaments (F), consisting of linked G-actin monomers. Efficient polymerization of G-actin into F-actin is facilitated by the protein, profilin (79). Profilin binds to ADP-actin monomers and catalyzes the exchange of ADP to ATP. The profilin-ATP-actin complex is recruited to the barbed end of unbranched actin filaments by formins or the ARP2/3 complex of branched filament networks (79, 80). Profilin releases the ATP-actin monomer to be added to the growing filament (81). In addition to proteins involved in polymerization of actin, proteins that contribute to mRNA translation assemble on actin filaments (82–85). Disruption of the actin cytoskeleton affects initiation of protein synthesis and decreases translational fidelity in yeast and activates MAP kinase and NF-κB signaling pathways in immune cells (82, 86, 87). Chemical inhibition of

actin polymerization decreases *L. pneumophila* uptake and intracellular growth, highlighting the importance of actin dynamics in pathogen survival (88, 89). The *L. pneumophila* effector, SidL binds to actin and has been shown to inhibit polymerization through unknown mechanisms (90). The activity and regulation of SidL is further examined in this dissertation (Chapter 4).

Acquisition of Nutrients. *L. pneumophila* is auxotrophic for the amino acids valine, isoleucine, leucine, proline, phenylalanine, methionine, arginine, and tyrosine with a partial requirement for cystine (7, 91). The bacterium must therefore acquire these amino acids from their environment (7). In addition to the use of amino acids in protein synthesis, *L. pneumophila* metabolizes serine, and to a lesser degree, threonine, as their main source of carbon during the replicative phase of growth (7, 92, 93). Release of amino acids from nearby bacteria can support *L. pneumophila* metabolism, however this process is inefficient, requiring 100 dead cells per one *Legionella* (9). Therefore, effective replication naturally occurs intracellularly where *L. pneumophila* can acquire amino acids from its host. *L. pneumophila* utilizes host proteasomal degradation to access amino acids by linking polyubiquitinated proteins to the LCV via the effector, AnkB (94). Substrates of the *L. pneumophila* type II secretion system, LapA and LapB are aminopeptidases that remove N-terminal amino acids from peptides (95–98). The *L. pneumophila* threonine phagosomal transporter A (PhtA) and the host neutral amino acid transporter, SLC1A5, are required for bacterial nutrient acquisition and transition from the transmissive to replicative phase of growth (27, 99). *L. pneumophila* also encodes at least seven effectors that inhibit host mRNA translation that generate a large pool of free amino acids and peptides (100–104).

Translation Inhibition. The effector family, Lgt, comprises 3 glucosyltransferases (Lgt1, Lgt2, and Lgt3) that modify serine-53 of the host elongation factor, eEF1A, leading to its inactivation and inhibition of mRNA translation (102, 105). This process is enhanced in the presence of

aminoacyl-tRNAs and GTP (106). The Lgts are >80% similar and are enzymatically comparable, yet they differ in their temporal activity. Lgt1 and 2 are robustly expressed during late stages of *L. pneumophila* infection and stationary phase of *in vitro* growth, while Lgt3 expression peaks during lag phase and early *L. pneumophila* infection (102). Translation inhibition increases cytosolic amino acid levels that trigger the host master growth regulator, mTORC1 (mechanistic target of rapamycin complex 1) protein kinase (107). When amino acid levels are high, V-ATPases relay an activating signal to Rag GTPases on the lysosomal surface. A trimeric Ragulator complex anchors the Rag GTPases to the lysosome and the subsequent heterodimer forms a docking site for mTORC1 (108, 109). mTORC1 is recruited to the surface of lysosomes by Rag GTPases where it becomes activated and upregulates translation by phosphorylating translation initiation factor 4E (eIF4E) binding proteins thus promoting the release of EIF4E from the 5'-cap of mRNAs (108, 110–112). Activation of mTORC1 by the Lgt effector family is countered by the SidE family of effectors through ubiquitylation of the Rag GTPases (107). When mTORC1 is inactivated, the AMP-activated protein kinase (AMPK) is phosphorylated, leading to an upregulation of autophagy (113–116). Autophagy is restrictive to *L. pneumophila* intracellular replication; however, effector regulation of autophagy can promote pathogen survival (117–120).

The effector LegK4 is a kinase that phosphorylates threonine-495 within the substrate binding domain of heat shock protein 70 (Hsp70) (104). Heat shock proteins (Hsp) are ATPases important for proper folding of nascent polypeptides and maintaining homeostasis during stress (121). Hsp70 forms a complex with the heat shock chaperone 70 (Hsc70) and associates with the exit tunnel of the ribosome during protein synthesis (122). Phosphorylation by LegK4 decreases the ATPase activity of Hsp70 yet encourages its association with the ribosome. While the root of

the prolonged interaction following LegK4 phosphorylation is unknown, it is hypothesized that the inability to correctly fold nascent polypeptides leads to extended interactions between Hsp70 and the ribosome (104).

The effector, SidI, was identified in a yeast lethality screen as a cytotoxic effector. SidI toxicity can be attenuated by an arginine to proline substitution at amino acid 453 (R453P) or a glutamine to lysine substitution at amino acid 482 (E482K). SidI inhibits mRNA translation *in vitro* and interacts with host Valyl-tRNA synthetase, eEF1A and eEF1Bγ translational components (101). SidI activity additionally induces interactions between eEF1A and heat shock factor 1 (HSF1) which indicates activation of the heat shock response in *L. pneumophila*-infected cells and during transfection (101, 123). *hsp70* transcription is upregulated in *sidI*-transfected cells, but this does not lead to an increase in Hsp70 protein levels, possibly due to suppression of translation by SidI (101). The mechanism behind SidI activity is unknown and further investigated in this dissertation (Chapters 2). Additionally, SidI toxicity is alleviated in the presence of another *L. pneumophila* effector, Lpg2505, and this relationship is also explored (Chapters 2 and 3).

Similar to SidI, the effector SidL was found to be toxic when expressed in yeast (90). SidL enhances inhibition of eukaryotic protein synthesis by four other translation inhibiting effectors (Lgt 1, 2 ,3 and SidI) and additionally inhibits actin polymerization *in vitro* (90, 100). Aberrant organization of the actin cytoskeleton attenuates mRNA translation (86), but whether SidL-mediated translation inhibition is a consequence of impaired actin polymerization is unknown (90, 124). SidL yeast toxicity can be suppressed by overexpression of the eukaryotic F-actin polymerization factor, profilin. SidL does not disrupt profilin binding to actin or affect profilin-mediated inhibition of actin polymerization (90). Profilin is connected to multiple

processes in the cell that could suppress SidL toxicity other than actin polymerization, including regulation of translation initiation and cell cycle progression (125). SidL toxicity can additionally be suppressed by interactions with another *L. pneumophila* effector, LegA11 (126). LegA11 is a predicted metaeffector and is further investigated in this dissertation (126)(Chapter 4).

The effector RavX (Lpg1489) has been shown to inhibit host mRNA translation (103), although the exact mechanism behind its activity has not been studied. It is possible that there are undiscovered effectors that target protein synthesis in the *L. pneumophila* genome, as a mutant lacking all seven known translation inhibiting effectors still inhibits host translation (103). Ribosome profiling of *L. pneumophila* infected cells provides evidence to support the presence of additional effectors targeting translation initiation (127). It is also possible that the host cell regulates translation initiation through the mTOR pathway in response to bacterial infection (100, 103, 107, 127, 128). Further investigation of *L. pneumophila* host-pathogen interactions will undoubtedly reveal additional mechanisms modulating host protein synthesis during bacterial invasion.

Host Cell Responses to Translation Inhibition. *L. pneumophila* effector-mediated translation inhibition triggers MAPK signaling in macrophages (129, 130). This response occurs through p38 and SAPK/JNK MAPK signaling and can lead to the production of proinflammatory cytokines as well as cell cycle arrest in G1 phase (130–132). Bacterial replication is favored during mitosis (M phase), or within Gap 1 or 2 (G phases) whereas replication is restricted during DNA synthesis (S phase)(124, 133). Chemical inhibition of p38 or SAPK/JNK significantly reduces *L. pneumophila* intracellular replication, demonstrating the necessity of these pathways in pathogen survival (134). Macrophages overcome translation inhibition and mount an immune response by superinducing proinflammatory cytokine transcripts and

selectively translating them in a MyD88-dependent manner (127, 130, 132). *L. pneumophila* can attenuate MAPK responses in macrophages by removing activating phosphates from p38 via the phosphotyrosine phosphatase effector, Ceg4 (135). Amoebae such as *Dictyostelium discoideum,* lack p38 MAP kinases, but instead contain two ERK MAP kinases that play a role in their developmental life cycle (136, 137). It is therefore unlikely that *L. pneumophila* evolved activity against p38, and is potentially the result of similarities between protozoan and mammalian host targets.

III. Metaeffectors *[This section and its contents are published. See reference* (138)*]*

The status quo pertaining to bacterial effectors is that they specifically target host proteins and pathways. However, *L. pneumophila* encodes a family of effectors, termed metaeffectors, which function as "effectors of effectors" through targeting and regulating the function of other effectors (126, 138). Metaeffectors contribute *to L. pneumophila* virulence and provide an additional mechanism by which bacteria regulate effector functions within host cells.

The term "metaeffector" was coined a decade ago when Kubori and colleagues discovered that the effector LubX spatiotemporally regulates the effector SidH within *L. pneumophila*-infected host cells (139, 140). LubX contains two regions with similarity to eukaryotic U-box domains, and functions as E3 ubiquitin ligase within eukaryotic cells (140). In conjunction with UbcH5a or UbcH5c E2 enzymes, LubX polyubiquitinates the host kinase, Clk1 (139, 141). LubX additionally co-opts E2 enzymes to ubiquitinylate its cognate effector, SidH, leading to its proteasomal degradation (Figure 1) (139). Like the majority of *L. pneumophila* effectors, genetic deletion of *sidH* has no discernable effect on intracellular replication within macrophages, and the function of SidH within host cells has yet to be elucidated (139, 141).

SidH is a paralog of the *L. pneumophila* effector SdhA, which promotes *L. pneumophila* intracellular replication through maintenance of LCV integrity (139, 142, 143). Thus, SidH may contribute to maintaining the integrity of the LCV during early infection. In a Drosophila melanogaster infection model, *L. pneumophila* Δ*lubX* mutants are hyper-lethal. However, loss of *lubX* results in decreased bacterial burden in flies compared to wildtype, Δ*sidH* and Δ*sidH*Δ*lubX* *L. pneumophila* strains (139). Loss of *lubX* has no discernable effect on *L. pneumophila* replication within mouse bone marrow-derived macrophages, suggesting that SidH may be detrimental in the absence of LubX specifically in vivo. It would be valuable to reveal whether loss of LubX-mediated regulation of SidH is also deleterious to *L. pneumophila* replication in a mouse model of Legionnaires' Disease. Interestingly, LubX expression peaks when the cells are nearing the stationary phase; much later than the critical window for SidH degradation, suggesting that mediation of SidH toxicity may not be the apogee of LubX activity (139).

Timing. Temporal regulation of effector translocation is likely important for other effector–metaeffector pairs. The metaeffector SidJ regulates the SidE family of effectors (SidE/SdeABC) to facilitate biogenesis of the LCV (Figure 1) (144, 145). SidJ is one of very few effectors individually important for *L. pneumophila* intracellular replication (146). While expression and translocation of the SidE effectors peaks during early infection, SidJ translocation increases gradually over the course of infection (145, 146). The SidE effectors are mono-ADP-ribosyltransferases that ligate ubiquitin to Rab GTPases independently of E1 and E2 enzymes (147–149). SidJ is a calmodulin-dependent glutamylase that spatiotemporally regulates the SidE effectors by breaking phosphodiester bonds between ubiquitin- and SidE-modified substrates (149). SidJ is a calmodulin-dependent glutamylase that temporally regulates the function of the SidE effectors (149–152). SidJ polyglutamylates Glu860 of the SidE family effector SdeA,

leading to its inactivation. In the absence of SidJ, SdeA fails to depart from the LCV surface, but robustly ubiquitinates several Rab and Rag GTPases (Figure 1) (145, 149). While SidE effectors are important at early stages of infection, their prolonged activity is deleterious to *L. pneumophila*. Delayed translocation of SidJ relative to the SidE family enables precise temporal regulation of SidE effector function (145). The timing of SidJ translocation is facilitated by an in-ternal secretion signal, present in addition to its canonical C-terminal secretion signal. Deletion of SidJ's internal secretion signal impairs *L. pneumophila* intracellular replication to the same extent as a loss-of-function mutation in sidJ (145). The importance of temporal regulation of the SidE family of effectors by SidJ within host cells demonstrates the critical role of metaeffectors in the establishment of *L. pneumophila's* intracellular replicative niche.

Identification. Urbanus and colleagues recently executed the most comprehensive effector toxicity suppression screen to date, resulting in the discovery of 17 effector-suppression pairs, including nine putative metaeffectors (126). The researchers used a high-throughput yeast toxicity assay to screen over 108,000 pairwise effector-effector genetic interactions. This study revealed the plasticity of metaeffector activity. In some cases, metaeffectors directly inactivate their cognate effector. For example, LegL1 deactivates its cognate effector through steric hindrance of its active site. Other metaeffectors, such as LupA and LubX, enzymatically modify their cognate effectors LegC3 and SidH (see above), respectively (Figure 1). LupA is a eukaryotic-like ubiquitin protease that catalyzes removal ubiquitin from LegC3 (126). LegC3 is one of three *L. pneumophila* effectors that mimic eukaryotic Q-SNAREs to recruit vesicles coated with VAMP4 to the LCV (67, 68). How ubiquitiniylation influences LegC3 activity and the contribution of its regulation by its metaeffector LupA are both unknown.

This screen not only identified novel metaeffector pairs, but also unveiled diversity in effector function and regulation. SidP is a phosphatidylinositol-3-phosphate (PI3P) phosphatase (153). SidP's PI3P phosphatase activity is dispensable for binding and suppressing the toxicity of its cognate effector MavQ. The phosphatase activity of SidP resides within its N-terminal domain, and the C-terminal domain alone is sufficient for binding and regulation of MavQ. MavQ is a predicted phosphoinositide (PI) kinase, and together with SidP, likely regulates PI metabolism within host cells. Interestingly, SidP is toxic to yeast when expressed together with the effector Lem14; however, the role of Lem14 in SidP metaeffector activity and PIP metabolism has not been fully elucidated (126). The putative role of MavQ as a PIP kinase, and the synergistic effects of SidP and Lem14 reveal a complex picture of effector regulation of host PIPs (Figure 1).

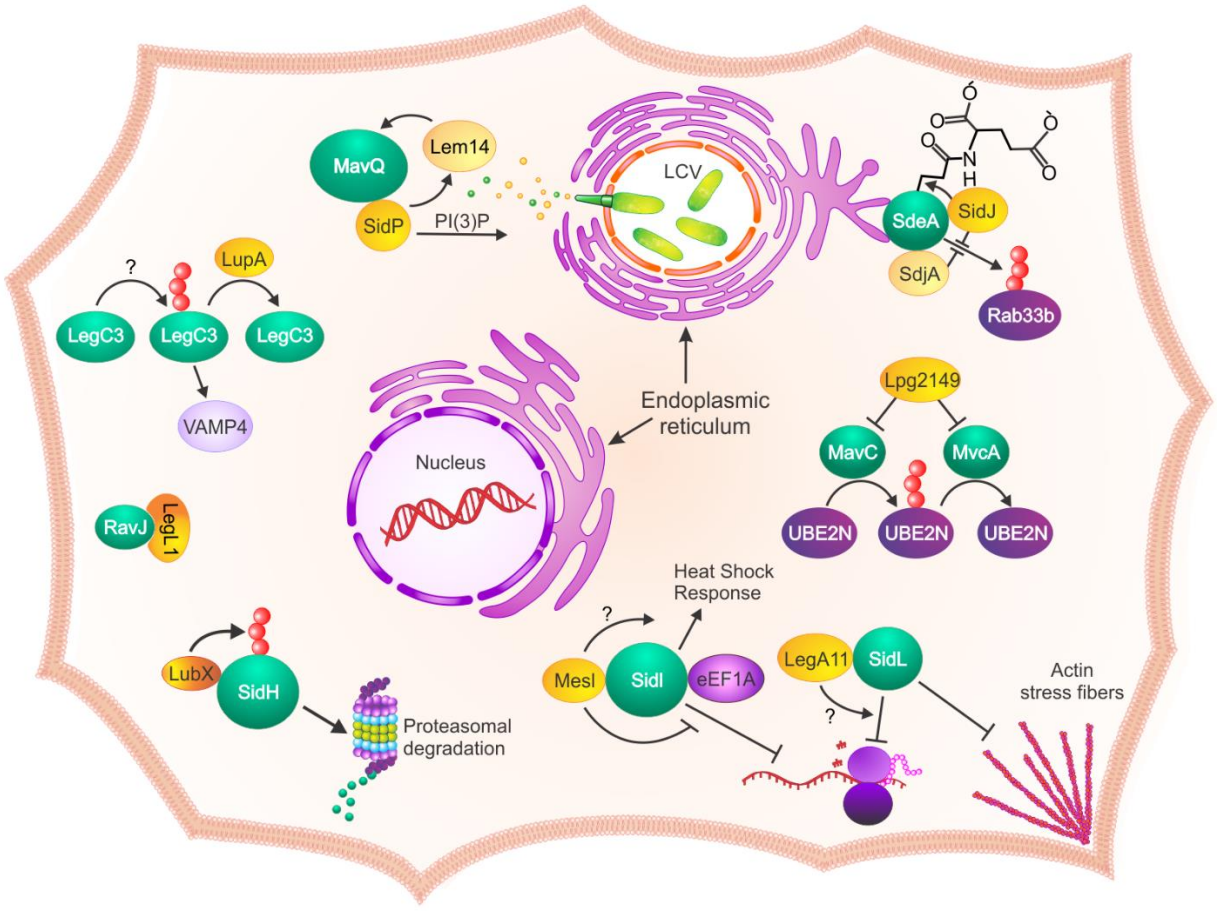

Figure 1.1. Known Activities of *L. pneumophila* metaeffectors

L. pneumophila metaeffectors exploit various modes of action against other effectors, many leading to the deactivation or degradation of their target. *L. pneumophila* which relies on complex regulation of effector synthesis and translocation to orchestrate successful host cell invasion, and it can be speculated that this intricacy applies to metaeffector regulation as well. Metaeffectors likely prevent overactivity of their target effectors, which can be detrimental to the *L. pneumophila* intracellular life cycle. While the activity of some effectors, such as the transglutamylation of SdeA by SidJ or interactions of SidI with MesI prevent toxicity attributed to their target, others like SidP and Lem14 with MavQ have a more complicated relationship with their target effector that has yet to be uncovered. Yellow, metaeffectors; Teal, effectors; Purple, host proteins and structures; Red, ubiquitin; Green-yellow, *L. pneumophila*. Figure from (138)

The effector deamidases MavC and MvcA are both regulated by a single metaeffector, Lpg2149 (Figure 1). MavC and MvcA are functional antagonists that temporally regulate the activity of the host E2 enzyme, Ube2N. MavC catalyzes E1-independent monoubiquitination and

inhibition of Ube2N (154). Prolonged inhibition of Ube2N is detrimental to *L. pneumophila* and is reversed through MvcA deubiquitination (Figure 1) (155). Lpg2149 binds and inhibits the deamidase activity of both MavC and MvcA; however, the biological significance of this inhibition and influence on temporal regulation of Ube2N ubiquitination are unknown. Further investigation is required to uncover the role of Lpg2149 in *L. pneumophila* virulence. Collectively, these studies underlie the importance of metaeffectors in spatiotemporal regulation of *L. pneumophila* effector function.

Characteristics. Classification of an effector as a metaeffector is based on two criteria, (1) binding; and (2) regulation of a cognate effector(s). Several metaeffectors, including LubX and SidJ, co-opt host proteins to regulate their cognate effectors (139, 150–152, 156). Moreover, LubX does not exclusively catalyze ubiquitination of SidH (see above), demonstrating the functional versatility of metaeffectors. Other metaeffectors, such as MesI, are able to regulate their cognate effectors in the absence of host components, but this does not preclude the involvement of host factors (157). A defining feature of metaeffectors is direct interaction with cognate effector proteins. However, other characteristics are shared amongst effector–metaeffector pairs.

In general, metaeffectors are smaller than their cognate effectors. This is a trend and not a rule, as several metaeffectors such as LegL1, LupA, and SidP are comparable in size to their targets (Table 1). It is also not uncommon for metaeffectors to contain interaction domains, such as the tetratricopeptide repeats (TPR) of MesI, ankyrin repeats of LegA11, or the leucine-rich repeats (LRR) of LegL1(158, 159). These interaction domains are likely important for the interaction of effectors with their cognate effector. For example, the LRR of LegL1 forms a canonical horseshoe shape over RavJ's active site, causing steric hindrance (126). The ankyrin

repeats in LegA11 likely facilitates protein–protein interactions (see above) (159, 160). Thus, several metaeffectors possess canonical protein–protein interaction motifs that are likely used to bind their cognate effector(s).

Metaeffectors are typically encoded in close proximity to their cognate effector within the genome (126). Some exceptions to this exist, as *mavQ* is not encoded in the vicinity of either *sidP* or *lem14* (126). Genomic analysis of 38 *Legionella* species revealed 143 effector pairs encoded in close proximity in at least two *Legionella* genomes. Nineteen of these effector pairs—including SidL-LegA11 and SidI-MesI—appear to have co-evolved; however, this number may be higher, as it only captures pairs found in multiple species and does not consider those unique to a single species (161). Some effector pairs, such as SidL and LegA11, are always found in conjunction, while others, such as SidI and MesI, occasionally occur in solidarity. *sidL* and *legA11* represent the most highly co-evolved effector pair in the *Legionella* genus (161). Relatively little is known about transcriptional regulation of effector–metaeffector gene expression. Interestingly, *legA11* and *sidL* are encoded adjacent to each other, but on different strands of the chromosome and initiate in opposite directions. Elucidating the timing and quantity of effector and metaeffector gene expression can provide additional spatiotemporal insights into mechanisms of metaeffector-mediated regulation of effectors. While effector pairs are present across the *Legionella* genus, only *L. pneumophila* metaeffectors have been studied to date (48). Although all Legionella species studied to date replicate within an endoplasmic reticulum-derived LCV, whether species-specific differences affect metaeffector-effector regulation and function exist has yet to be elucidated.

Although effectors are critical virulence factors for many Gram-negative bacterial pathogens, mechanisms by which effectors are regulated within host cells are poorly understood.

Metaeffectors provide an additional layer of regulation and spatiotemporal fine-tuning of effector function. Although metaeffectors are currently unique to the *Legionella* genus, it is tempting to speculate that other pathogen virulence strategies involve metaeffectors. Identification of metaeffectors is challenging and relies on robust phenotypes resulting from effector dysregulation. Urbanus and colleagues conducted the most extensive effector-pair screen to date using a yeast expression model. However, other metaeffector–effector pairs may be incognito within this unnatural expression in the absence of a toxic effector phenotype (126). Extreme functional redundancy within *L. pneumophila*'s effector repertoire creates challenges, as deletion of a single effector rarely leads to a discernable phenotype (141, 151). MesI and SidJ are two of less than a dozen effectors that are individually important for *L. pneumophila* intracellular replication (144, 146, 162). Thus, metaeffectors play a major role in the virulence strategy of *L. pneumophila*, which emphasizes the importance of both effector interplay and functional regulation.

Table 1.1. Known *L. pneumophila* effector-metaeffector pairs and their activities.*

Metaeffector	Gene ID	Activity	Size[a]	Effector	Gene ID	Activity[b]	Size[a]	Refs.
LegA11/ AnkJ	Lpg0436	Unknown	269	SidL/ Ceg14	Lpg0437	Translation inhibitor	666	(126)
LegL1	Lpg0945	Competitive inhibition	296	RavJ	Lpg0944	Putative transglutaminase	391	(126)
Lem14	Lpg1851	Synergistic with SidP	220	MavQ	Lpg2975	Putative kinase	871	(126)
Lpg2149	Lpg2149	Unknown	119	MavC	Lpg2147	Ubiquitinase	482	(155)
				MvcA	Lpg2148	Deubiquitinase	426	
LubX	Lpg2830	E3 Ubiquitin Ligase	246	SidH	Lpg2829	SdhA homolog	2225	(139)
LupA	Lpg1148	Deubiquitinase	503	LegC3	Lpg1701	Glutamine (Q)-SNARE-like protein	506	(67, 153)
MavE	Lpg2344	Unknown	208	YlfA/ LegC7	Lpg2298	SNARE-like Protein	425	(126)
MesI	Lpg2505	Unknown	295	SidI/ Ceg32	Lpg2504	Putative mannosyltransferase	942	(101, 157, 162)
SdbC	Lpg2391	Putative Lipase	434	SdbB	Lpg2482	Putative Lipase	448	(126)
SidJ	Lpg2155	Calmodulin-dependent transglutamylase	873	SidE	Lpg0234	Ubiquitin Ligases	1575	(144–146, 148–152)
				SdeA	Lpg2157		1506	
				SdeB	Lpg2156		1926	
				SdeC	Lpg2153		1533	
SidP	Lpg0130	PI3P Phosphatase	822	MavQ	Lpg2975	Putative PIP Kinase	871	(126)

*Table from (138)

IV. Legionnaires' Disease

Emergence as an Accidental Human Pathogen. The first reported outbreak of *L. pneumophila* in humans was in July of 1976 at the American Legion Conference being held at a hotel in Philadelphia, Pennsylvania. One hundred and eighty-two individuals associated with the hotel during this time developed similar symptoms and within 2 weeks, 29 individuals died from the illness. Patients experienced general discomfort (muscle aches, headache, and lethargy) that quickly escalated to chills and fever between 38.9–40.6 °C (102-105°F) (163). A non-productive cough and chest pains associated with inflammation of the pleura developed in roughly 30% of the cases. The idiopathic illness was dubbed Legionnaires' Disease in relation to the 72 American Legion Conference attendees who experienced it (163, 164).

The route of transmission was hypothesized to be airborne, given the symptoms associated with the illness and lack of evidence to support other modes. Silver staining of diseased alveoli revealed the presence of a large number of bacilli within macrophages (163). These bacilli were further implicated as the etiological agent of Legionnaires' Disease when guinea pigs infected with tissue suspensions from disease patients became ill and Gram-negative bacillary bacteria were recovered (165).

The outbreak of Legionnaires' Disease in 1976 was comparable to two other outbreaks in the 1960s. The District of Columbia outbreak in July 1965 was clinically similar to Legionnaires' Disease with 81 cases and 12 deaths. The Pontiac, Michigan outbreak in July 1968 consisted of 144 cases with no deaths and mild respiratory symptoms. Serological antigen evaluation of patients from all 3 outbreaks displayed commonalities and the diseases were henceforth referred to as Legionnaires' Disease and Pontiac Fever, collectively known as legionellosis (164, 165).

Immune Cell Response. During *L. pneumophila* infection of immunocompetent hosts, the nucleotide binding and leucine rich repeat (NLR) NLRC4 sensor protein detects bacterial flagellin and forms an inflammasome complex with the neuronal apoptosis inhibitory protein 5 (Naip5) adaptor protein (166–170). The NLRC4/Naip5 inflammasome binds and activates caspase-1 (CASP1) which in turn cleaves pro-interleukin-18 (IL-18) and pro-IL-1β into activated IL-18 and IL-1β (171). Gasdermin D (GSDMD) is additionally cleaved, and the N-terminal proteolytic fragment forms a pore in the cell membrane, inducing pyroptosis and restricting disease progression (172, 173).

Tumor Necrosis Factor (TNF) can also stimulate pyroptosis by activating caspase-8 through the kinase receptor-interacting protein 1 (RIP1) and the Fas-associated death domain protein (FADD) (174). Caspase-8 and caspase-3 cleave GSDMD and the tumor suppressor gene, gasdermin E (GSDME) respectively (174–177). The gasdermin proteins induce pyroptosis and form a pore in the mitochondrial membrane that release the death proteins cytochrome C and HtrA2/Omi protease, along with mROS (177). Pyroptosis releases intracellular bacteria and cytokines that recruit neutrophils to the site of infection (56, 103, 171, 178). Neutrophils take up extracellular bacteria and generate antimicrobial ROS and TNF. TNF further enhances macrophage killing of *L. pneumophila* by inducing fusion of the phagosome with lysosomal compartments (56).

L. pneumophila can subvert detection and modulate vesicle trafficking of immunosuppressed hosts, using strategies evolved in the natural protozoan host (50). In immunocompromised hosts, stimulation of the innate immune system by *L. pnuemophila* produces decreased secretion of cytokines including TNF-α and interferon gamma (IFN-γ)(179, 180). Production of IFN-γ by natural killer (NK) cells is essential for the clearance of *L.*

pneumophila infection and TNF signaling induces pyroptosis (181–183). Consequently, bacterial burden is increased in the lung resulting in Legionnaires' Disease (22, 163, 165, 184).

VIII. Model Systems for Studying *Legionella*

Infection. Mice are a commonly used model system for the study of pathogenic microorganisms. The ability of *L. pneumophila* to replicate within murine derived systems depends on the mouse strain (185). Inbred A/J mice lack the *lgn1* gene locus that encodes various *naip* proteins important for assembly of the NLRC4/NAIP5 inflammasome (185, 186). Intratracheal inoculation of A/J mice with 10^6 colony forming units (CFU) of *L. pneumophila* produces symptoms similar to Legionnaires' disease (187). A/J mice will succumb to infection doses greater than 10^8 CFU (187–189). Other inbred mouse stains such as C57BL/6 and BALB/c contain the *lgn1* locus and are therefore restrictive to *L. pneumophila* (190). However, these strains can be used pending genetic modification of either the mouse or *L. pneumophila*. Deletion of the flagellin gene, *flaA*, from *L. pneumophila* prevents activation of the NLRC4/Naip5 inflammasome and evasion of canonical pyroptosis (191). Alternatively, genetic knockout of the *Nlrc4* gene in C57BL/6 mice can be used to prevent canonical pyroptosis and promote a permissive host (169). *L. pneumophila* replicates within alveolar macrophages and bone marrow-derived macrophages (BMDM) are commonly used to study *L. pneumophila* infection (186, 192–194).

A human leukemic monocyte cell line, THP-1, can be used to evaluate *L. pneumophila* intracellular survival. Stimulation with phorbol 12-myristate 13-acetate (PMA) differentiates THP-1 cell into a macrophage-like adherent cell (195). While THP-1 cells are phagocytic and produce lysozymes characteristic of monocytes, they have reduced levels of the full length Naip

adaptor protein and have decreased sensitivity to intracellular bacterial flagellin. This renders them permissive to *L. pneumophila* intracellular replication (196). Intracellular replication in THP-1 cells peaks around 48-hours and *L. pneumophila* enter death phase by 72-hours, compared to replication in BMDMs where stationary phase occurs around 72-hours (195, 197).

Non-phagocytes such as human embryonic kidney cells (HEK293) and Chinese hamster ovary (CHO) cells can be engineered to express the opsonic FcγRII receptor (157, 198, 199). Fcγ receptors (FcγR) are transmembrane receptors that bind the carboxy terminal Fc region of immunoglobulins (IgG) following interactions with a target ligand. Upon ligand recognition, the inner membrane ITAM region of the receptor is phosphorylated, setting off a signaling cascade that generates phosphatidylinositol-3,4,5-triphosphate (PIP3). Generation of PIP3 regulates the activation of the GTPase Rac important for actin remodeling (200, 201). Opsonization of *L. pneumophila* with α-*Legionella* antibodies enables Fc-mediated uptake of bacteria (202, 203). HEK293 and CHO cell lines are easily cultured for up to 30 passages, making them a valuable resource in the lab. However, they are highly susceptible to *L. pneumophila* infection and are better suited for infection models less than 8-hours (204–206).

A secretion system deficient mutant is typically included during *L. pneumophila* infection models as a negative control. The *L. pneumophila dotA* gene encodes a component of the T4SS that is important for early phagosome trafficking (207, 208). Deletion (Δ*dotA)* or loss of function mutation (*dotA*::Tn) of *dotA* results in increased lysosomal fusion and subsequently decreased bacterial intracellular survival (207–209). Although the exact mechanism is unknown, *dotA* deficient bacteria are unable to translocate effectors into the host cell, making them susceptible to host defenses (210).

Recombinant and Ectopic Expression. Recombinant expression and purification of effectors from *Escherichia coli* enables efficient evaluation of individual protein function *in vitro* (211). Protein production is carried out in the BL21(DE3) *E. coli* strain which lacks the *ompT* gene that encodes the outer membrane protease, OmpT (212). Due to the overwhelming number and redundancy of *L. pneumophila* effectors, ectopic expression can be used to evaluate isolated function of effectors in eukaryotic cells such as HEK293T and African green monkey fibroblasts (COS7) (206, 213). COS7 cells also exhibit a low profile, making them an ideal cell for immunofluorescent and confocal microscopy (214).

IX. Overview of Dissertation

Here I examine metaeffector regulation of two translation inhibiting effectors, SidI and SidL, in the *L. pneumophila* Philadelphia-1 (SRS43) strain. The metaeffector, Lpg2505 (MesI), was originally identified using a high-throughput forward genetic screen for effector virulence phenotypes using transposon insertion sequencing (INSeq)(162). *L. pneumophila* lacking a functional *mesI* have a severe intracellular growth defect in both amoeba and macrophage hosts and are outcompeted in a mouse model of infection. However, the virulence phenotype associated with loss of *mesI* is solely due to the activity of its cognate effector, SidI, since a loss-of-function mutation in *sidI* rescues the growth defect (162). The putative metaeffector, LegA11, can suppress SidL-mediated yeast toxicity and the two proteins interact during ectopic expression in mammalian cells (159, 160). Deletion of *legA11,* causes a growth defect in some, but not all, species of amoeba as well as human monocyte-derived macrophages, but it is unknown if this is related to the activity of SidL (215).

Our lab sought to investigate these gaps in knowledge and expand our understanding of how metaeffector regulation of effectors contributes to *L. pneumophila* survival. We found that SidI possess mannosyl hydrolase activity and likely functions as a mannoysltransferase during infection. MesI was found to rescue SidI-mediated translation inhibition *in vitro*, possibly due to suppression of mannosyl hydrolase activity which was also observed (Chapter 2). Unexpectedly, MesI displayed chaperone-like activity by regulating SidI translocation into the host cell during late stages of infection (Chapter 3).

Most strikingly, it was discovered that *sidI* expression is toxic to *L. pneumophila* intracellular replication in the absence of *mesI* and this could be mimicked during *in vitro* growth by overexpression of *sidI* uncoupled from *mesI*. Visualization of infected macrophages revealed a high number of degraded Δ*mesI* bacteria, despite having poor localization with the lysosomal-associated membrane protein, LAMP1. Finally, a non-translocated MesI mutant was sufficient to rescue intracellular growth, further supporting that MesI metaeffector activity is critical intrabacterially (Chapter 3). From here the possibility of targeting MesI for the development of novel therapeutics was explored. In collaboration with the High-Throughput Screening Laboratory at the University of Kansas, a compound was identified that successfully attenuated *L. pneumophila* growth *in vitro* and during intracellular growth in *A. castellanii*. The inhibition was specific to the presence of *sidI* and *mesI,* although no disruption of binding or translation inhibition was observed (Chapter 3).

Finally, we investigated if SidL and LegA11 share a similar relationship to SidI and MesI. We found that LegA11 suppressed both SidL translation and actin polymerization inhibitory activities *in vitro.* This suppression was not the result of competitive inhibition as LegA11 did not disrupt SidL binding to actin and unexpectedly restored actin binding to an

inactive SidL mutant. In contrast to previous reports, we found that loss of *legA11* produced a replication advantage in murine *Nlrc4*-deficient BMDMs, but not in THP-1 cells or *A. castellanii*. This phenotype did not translate to a competitive advantage over wild type *L. pneumophila* during replication in the mouse lung (Chapter 4).

Metaeffectors represent a noncanonical effector regulatory system that is likely not unique to *L. pneumophila*. There is increasing evidence suggesting the presence of metaeffector-like interactions in other pathogens (216–218). Identification of metaeffector and metaeffector-like functions has been contingent on observable phenotypes, such as toxicity or intracellular replication; however, scrutiny of genomic organization of effector genes may lead to identification of additional metaeffectors encoded by other *Legionella* species and other bacterial pathogens. These findings demonstrate the importance of metaeffectors in *L. pnuemophila* virulence and survival. Further investigation will undoubtedly reveal additional mechanisms of metaeffector regulation of effectors arising from host-pathogen co-evolution.

Chapter 2 - The *Legionella pneumophila* Metaeffector Lpg2505 (MesI) Regulates SidI-Mediated Translation Inhibition and Novel Glycosyl Hydrolase Activity

Ashley M. Joseph[1], Adrienne E. Pohl[1], Theodore J. Ball[1], Troy G. Abram[2], David K. Johnson[3], Brian V. Geisbrecht[2], Stephanie R. Shames[1,4]

[1] Division of Biology, Kansas State University, Manhattan, Kansas, USA
[2] Department of Biochemistry and Molecular Biophysics, Kansas State University, Manhattan, KS, USA
[3] Molecular Graphics and Modeling Laboratory, Computational Chemical Biology Core, University of Kansas, Lawrence, Kansas, USA
[4] Microbiology and Molecular Genetics, Michigan State University, East Lansing, MI, USA

Author Contributions

Ashley M. Joseph
All experiments except what is indicated below
Writing (Manuscript Draft)

Adrienne E. Pohl
SidI truncation binding (Figure 4 B)

Theodore J. Ball
SidI-MesI binding (Figure 1 A + B)

Brian V. Geisbrecht and Troy G. Abram
SidI-MesI binding kinetics (Figure 1 C + D, Supplemental Figures 1 + 2)
BV- Writing (SPR) and editing

David K. Johnson
SidI molecular modeling (Supplemental Figure 6 + 8, Supplemental Table 1)
Writing (molecular modeling) and editing

Stephanie R. Shames
Conceptualization, editing, figure formatting and funding

ABSTRACT

Legionella pneumophila, the etiological agent of Legionnaires' disease, employs an arsenal of hundreds of Dot/Icm-translocated effector proteins to facilitate replication within eukaryotic phagocytes. Several effectors, called metaeffectors, function to regulate the activity of other Dot/Icm-translocated effectors during infection. The metaeffector Lpg2505 is essential for *L. pneumophila* intracellular replication only when its cognate effector, SidI, is present. SidI is a cytotoxic effector that interacts with the host translation factor eEF1A and potently inhibits eukaryotic protein translation by an unknown mechanism. Here, we evaluated the impact of Lpg2505 on SidI-mediated phenotypes and investigated the mechanism of SidI function. We determined that Lpg2505 binds with nanomolar affinity to SidI and sup-presses SidI-mediated inhibition of protein translation. SidI binding to eEF1A andLpg2505 is not mutually exclusive, and the proteins bind distinct regions of SidI. We also discovered that SidI possesses GDP-dependent glycosyl hydrolase activity, and that this activity is regulated by Lpg2505. We have therefore renamed Lpg2505 MesI (metaeffector of SidI). This work reveals novel enzymatic activity for SidI and provides insight into how intracellular replication of *L. pneumophila* is regulated by a metaeffector.

INTRODUCTION

Legionella pneumophila is the etiological agent of Legionnaires' disease, a severe inflammatory pneumonia that results from uncontrolled bacterial replication within alveolar macrophages. Upon phagocytosis, *L. pneumophila* avoids lysosomal degradation through establishment of an endoplasmic reticulum-derived compartment called the Legionella-containing vacuole (LCV) (17). For biogenesis of the LCV and acquisition of nutrients from the host cell, *L. pneumophila* is dependent on a massive arsenal of over 300 individual effector proteins that are translocated directly into the host cell through a Dot/Icm type IVB secretion system (T4BSS) (219). The cellular functions of the majority of effectors have yet to be elucidated, due in part to their functional redundancy within macrophages (reviewed in reference (141)). Metaeffectors, used by *L. pneumophila* to regulate effector function, have emerged as a common theme in *L. pneumophila* pathogenesis (126). Metaeffectors are defined as effectors that target and regulate the functions of other effector proteins within host cells (139). The first metaeffector described was LubX, which temporally regulates the function of its cognate effector, SidH, by hijacking host ubiquitination machinery to facilitate proteasomal degradation of SidH (139). At least 20 of the over 300 identified *L. pneumophila* effectors are capable of regulating the functions of other effectors (126). Two of them—SidJ and Lpg2505—are metaeffectors that are members of a small group of effectors that are individually important for *L. pneumophila* intracellular replication within macrophages (145, 146, 162). SidJ is a glutamylase that covalently modifies and abrogates the functions of the SidE family of effector ubiquitin ligases (149–151). Lpg2505 is an effector of unknown function that suppresses the toxicity of the effector SidI (Lpg2504) and is important for intracellular replication in macrophages only when wild-type *sidI* is expressed (162). We previously discovered that a loss-of-function mutation in lpg2505 attenuated *L.*

pneumophila replication within bone marrow-derived macrophages (BMDMs); the natural host, *Acanthamoeba castellanii*; and a mouse model of Legionnaires' disease (162). Restoration of *L. pneumophila* Δ*lpg2505* intracellular replication within BMDMs was observed upon either deletion of sidI or replacement of the wild-type sidI allele with a nontoxic sidI allele ($sidI_{R453P}$), suggesting that wild-type sidI was deleterious to *L. pneumophila* in the absence of Lpg2505 (162). Concomitantly, Lpg2505 was sufficient to suppress SidI-mediated toxicity toward the yeast *Saccharomyces cerevisiae* (162). Thus, SidI activity negatively impacts *L. pneumophila* in the absence of Lpg2505, a unique phenotype for a translocated effector.

SidI is one of seven cytotoxic *L. pneumophila* effector proteins that inhibit host cell protein translation (101). Like the majority of *L. pneumophila* effectors, *sidI* alone is dispensable for intracellular replication within macrophages (101), likely due to functional redundancy with other effectors. Other translation-inhibiting effectors include Lgt1 to -3, SidL, LegK4, and Lpg1489 (90, 100, 101, 103, 104). Lgt1 to -3 are glycosyltransferases that inhibit translation by glucosylating eukaryotic elongation factor 1A (eEF1A) at Ser-53 (102, 105, 106). LegK4 is an effector kinase that phosphorylates heat shock protein 70 (Hsp70), thereby reducing its ATPase activity and protein-refolding activities (104). SidL and Lpg1489 have been experimentally demonstrated to inhibit host protein synthesis (90, 103), but their modes of action are unknown. Like Lgt1 to -3, SidI also interacts with eEF1A; however, this interaction is insufficient for translation inhibition (101). SidI also interacts with eEF1Bγ and induces the host heat shock response (101). To date, the mechanism(s) by which SidI functions within the host cell to inhibit host protein synthesis have not been elucidated. In this study, we aimed to discern how Lpg2505 regulates SidI and to gain insight into the molecular mechanism of SidI function. We discovered that Lpg2505 and SidI bind with nanomolar affinity and that Lpg2505 suppresses SidI-mediated

translation inhibition in vitro. Furthermore, SidI interaction with Lpg2505 and eEF1A are not mutually exclusive, and the two proteins bind with distinct regions of SidI. Finally, we discovered novel GDP-mannose glycosyl hydrolase activity for SidI, which is regulated by Lpg2505. We have therefore named Lpg2505 metaeffector of SidI (MesI).

RESULTS

MesI and SidI bind with nanomolar affinity. Lpg2505 (MesI) is sufficient to suppress SidI-mediated cytotoxicity in yeast and to promote *L. pneumophila* intracellular replication within mouse models of infection and *A. castellanii* (162). To reveal a potential mechanism for MesI-mediated regulation of SidI, we first evaluated whether MesI interacts with SidI. Since effectors function within host cells, we investigated whether SidI and MesI interact in the presence of host cell lysates. HEK293 cells stably producing 3xFLAG-epitope tagged MesI were generated, and we initially attempted to ectopically express green fluorescent protein (GFP)-tagged sidI within these cells for coimmunoprecipitation. However, wild-type SidI could not be detected, likely due to potent translation inhibition. Since a glutathione S-transferase (GST)-tagged SidI fusion protein (GST-SidI) was used to initially identify eEF1A as a binding partner (101), we generated recombinant GST-SidI and evaluated its ability to interact with 3xFLAG-MesI within HEK 293 lysates (see Materials and Methods). We found that glutathione beads coated with recombinant GST-SidI, but not GST alone, retained 3xFLAG-MesI (Fig. 2.1A) (see Materials and Methods). Furthermore, using lysates from *Escherichia coli*, we found that GST-SidI, but not GST alone, was retained on Ni-nitrilotriacetic acid (NTA) beads. that had been coated with His6 -MesI (Fig. 2.1B). Thus, MesI interacts with SidI in the presence or absence of mammalian cell lysates.

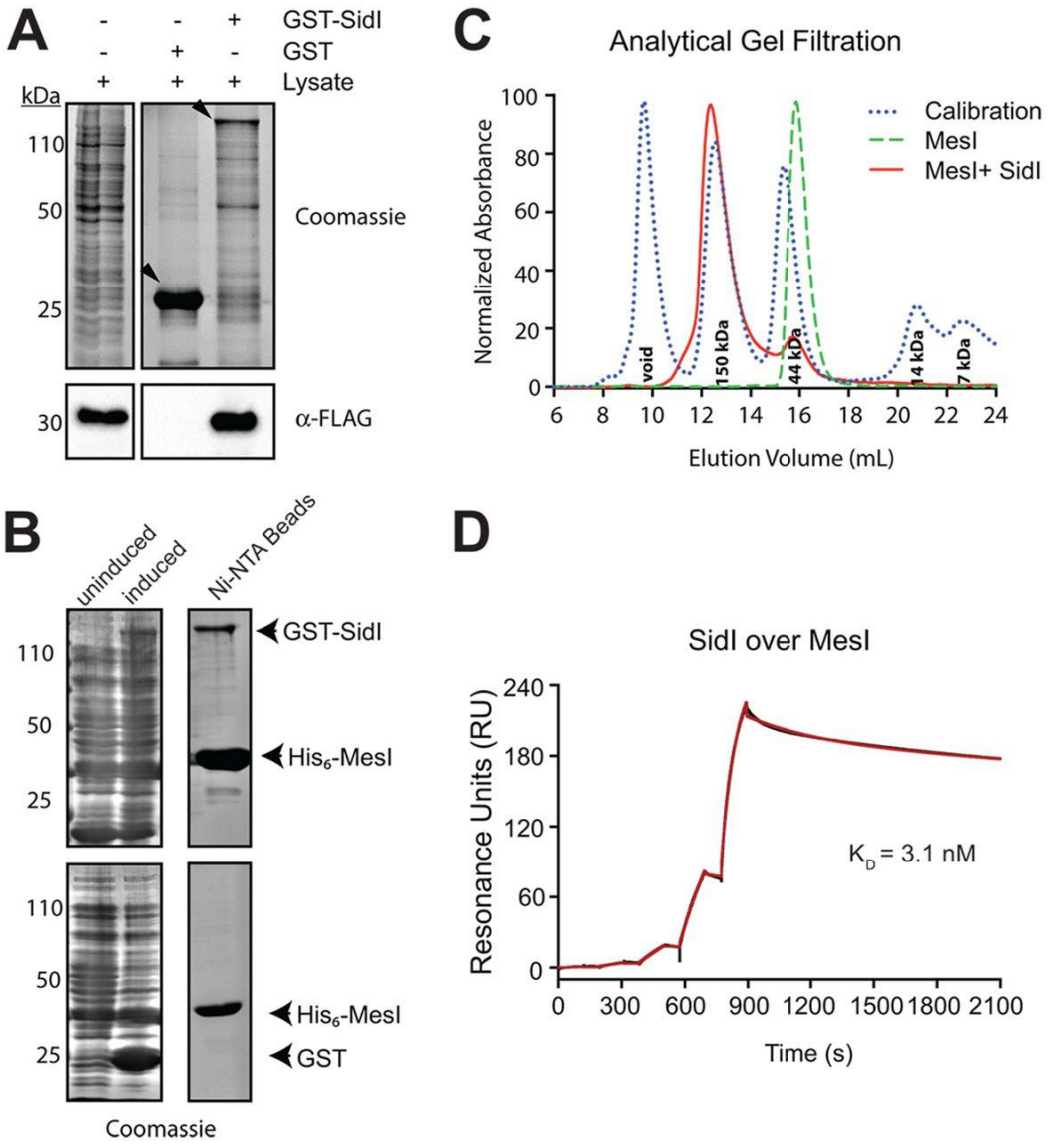

Figure 2.1 MesI and SidI interact directly with nanomolar affinity.

(A) Lysates from HEK293 FcγRII cells stably expressing 3xFLAG-MesI were incubated with glutathione beads coated with either GST or GST-SidI, followed by Coomassie staining for total protein and Western blotting for MesI (α-FLAG). The arrowheads indicate GST and GST-SidI proteins. (B) Lysates from *E. coli* overexpressing either GST or GST-SidI were incubated with Ni-NTA beads coated with His_6-MesI, followed by SDS-PAGE and Coomassie staining for proteins retained on the beads. (Left) Whole-cell lysates from uninduced and induced cultures of *E. coli* expressing GST and GST-SidI proteins. (Right) Proteins retained on Ni-NTA beads (see Materials and Methods). (C) Chromatograms resulting from analytical-scale gel filtration separation of either MesI alone (green trace) or MesI bound to SidI (red trace). A chromatogram of known size standards is provided for reference (blue trace). (D) Binding of His_6-SidI to immobilized MesI was assessed by SPR. The reference- corrected sensorgram from a single-cycle experiment is shown in black, while the outcome of fitting to a two-state binding model is shown in red. The interaction is described by an apparent KD of 3.1 nM, consisting of two

individual steps (association rate 1 [$k_{on,1}$] = 2.7 x 10^4 M^{-1} s^{-1}, dissociation rate 1 [$k_{off,1}$] = 5.1 x 10^{-4} s^{-1}, $k_{on,2}$ = 2.3 x 10^{-3} s^{-1}, and $k_{off,2}$ = 4.5 x 10^{-4} s^{-1}).

To determine if SidI and MesI bind directly, we examined the abilities of these proteins to associate with one another throughout the course of sequential column chromatography procedures. SidI and MesI were coexpressed in *E. coli* and purified by Ni-NTA affinity chromatography (see Materials and Methods), and the eluted proteins were separated by analytical-format size exclusion chromatography. We found that SidI (~110 kDa) and MesI (~35 kDa) coeluted from the column as a species corresponding to a molecular weight of ~145 kDa, as judged by comparison to a panel of known protein standards (Fig. 2.1C). As 145 kDa is the expected size of one molecule each of SidI and MesI, it is likely that SidI and MesI bind in a 1:1 stoichiometry. Bands corresponding to both proteins were detected in samples of column fractions that had been separated by SDS-PAGE and analyzed by Coomassie staining (see Fig. S1 in the supplemental material). Thus, SidI and MesI interact directly and appear to form a stable complex.

We subsequently used surface plasmon resonance (SPR) to investigate the affinity and kinetics of the MesI-SidI interaction. We immobilized MesI on an SPR surface using random amine chemistry and injected recombinant purified SidI at increasing concen- trations. We employed a single-cycle approach due to difficulty with regenerating the MesI surface following exposure to SidI. We found that the reference-corrected sen- sorgram could be described fairly well by a Langmuir binding model (KD [equilibrium dissociation constant] =0.89 nM and x^2 =3.26) (see Fig. S2 in the supplemental material) but was better fitted to a two-state reaction model (K_D=3.1 nM and x^2= 0.79) (Fig. 2.1D). A particularly noteworthy feature of the MesI-SidI interaction is its long half-life, with an estimated dissociation rate constant between 2x10^4 s^{-1} and 5x10^4 s^{-1} . This observation explains, at least in part, the abilities of MesI and SidI to remain associated with

one another throughout the copurification procedures described above. Taken together, these data indicate that MesI binds directly to SidI and forms a high-affinity complex with a K_D of ~3 nM.

MesI suppresses SidI-mediated translation inhibition. Based on the high-affinity interaction between SidI and MesI, we hypothesized that MesI represses SidI-mediated translation inhibition. To test this hypothesis, we quantified translation of firefly luciferase (Luc) mRNA in vitro (see Materials and Methods). The assay was used previously to demonstrate that ≥5 ng of recombinant SidI was sufficient to completely abolish translation (101). We confirmed that purified His_6-SidI significantly attenuates protein translation and additionally revealed that purified MesI alone has no impact on translation (Fig. 2.2A). We further determined that MesI significantly rescues translation in the presence of SidI ($P < 0.01$) (Fig. 2.2B). Rescue of protein translation by MesI was specific to SidI, since MesI had no impact on translation inhibition by Lgt1, a characterized *L. pneumophila* effector translation inhibitor (105, 220) (Fig. 2.2C). Furthermore, we confirmed previous reports that the $SidI_{R453P}$ mutant protein does not impair in vitro protein translation (101) and found that MesI has no impact on this phenotype (Fig. 2.2D). We further revealed that a nonspecific protein (GST) was unable to suppress SidI-mediated translation inhibition (see Fig. S3 in the supplemental material). Thus, MesI is sufficient to suppress SidI-mediated translation inhibition in vitro.

Our SPR data demonstrate that the SidI-MesI interaction occurs rapidly. We therefore hypothesized that preformation of the SidI-MesI complex would not result in further attenuation of SidI-mediated translation inhibition. To determine whether preformation of the SidI-MesI complex would enhance MesI-mediated suppression of translation inhibition, we incubated SidI with MesI for 30 min prior to addition to the in vitro translation reaction mixture and compared

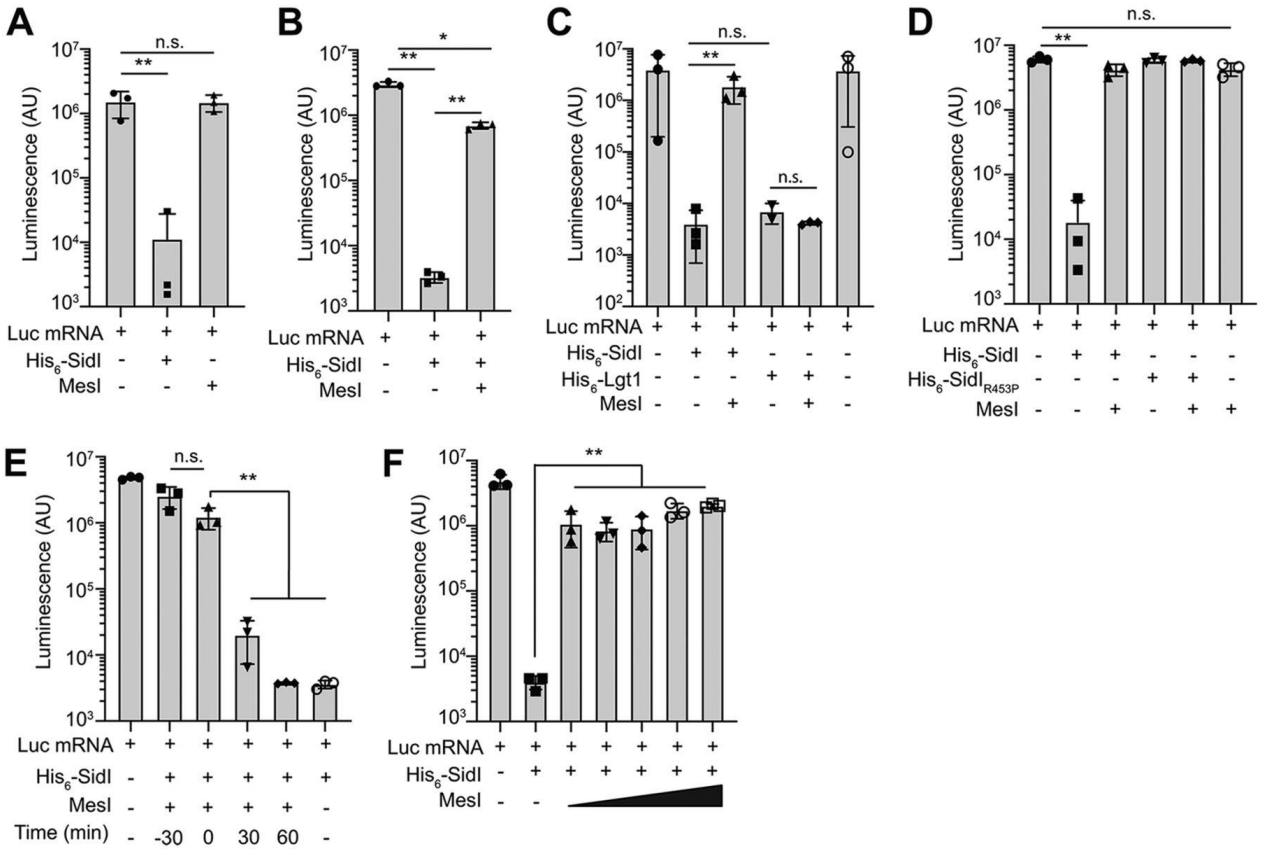

Figure 2.2 MesI modulates SidI-mediated translation inhibition in vitro

Translation of luciferase (Luc) mRNA was quantified using a rabbit reticulocyte lysate kit. (A to D) Translation of luciferase in the presence of 4 ng (37 fmol) His_6-SidI or 20 ng MesI (A), 4 ng (37 fmol) of His_6-SidI alone or with an equimolar amount of MesI (B), 37 fmol His_6-SidI or His_6-Lgt1 alone or with an equimolar amount of MesI (C), or 37 fmol His_6-SidI or His_6-$SidI_{R453P}$ alone or with an equimolar amount of MesI (D). (E) His_6-SidI alone or His_6-SidI and MesI were added to *in vitro* translation reaction mixtures at the indicated times (-30 indicates preincubation of His_6-SidI and MesI for 30 min prior to the translation reaction). (F) Quantification of *in vitro* translation of Luc mRNA in the presence of His_6-SidI alone or MesI and His_6-SidI at increasing molar ratios (1:1, 2:1, 3:1, 6:1, and 15:1 MesI/His_6-SidI molar ratios). AU, arbitrary units. The data are representative of the results of at least two independent experiments. The data are expressed as means ± standard deviations (SD) of samples in triplicate. The asterisks denote statistical significance by t test (*, $P < 0.05$; **, $P < 0.01$; n.s., not significant).

---

this to reactions where SidI and MesI were added simultaneously (time zero). Preformation of the SidI-MesI complex did not further attenuate SidI-mediated translation inhibition (Fig. 2.2E) (see Materials and Methods). Furthermore, MesI was insufficient to reverse SidI-mediated translation inhibition, since addition of MesI to the reaction mixture after either 30 min or 60 min

did not restore translation (Fig. 2.2E). Finally, we evaluated whether suppression of SidI-mediated translation inhibition by MesI was dose dependent. MesI was added in concentrations ranging from equimolar up to a 15-fold molar excess relative to SidI. An equimolar amount of MesI was sufficient to suppress SidI-mediated translation inhibition, and translation was not further enhanced by addition of up to a 15-fold molar excess of MesI (Fig. 2.2F). Thus, equimolar amounts of MesI are sufficient to suppresses SidI- mediated translation inhibition.

MesI does not affect the interaction between SidI and eEF1A. A previous report demonstrated that SidI interacts directly with the transcription factor eEF1A (101). We therefore investigated whether the interactions between SidI and eEF1A or MesI are mutually exclusive. GST-MesI or GST alone was immobilized on glutathione beads and incubated with His_6 -SidI that was preincubated with HEK 293T lysates. We found that eEF1A from HEK 293T lysates was retained on GST-MesI-coated beads only in the presence of SidI and that eEF1A did not impair interaction between MesI and SidI (Fig. 2.3A). We confirmed previous work demonstrating interaction between $SidI_{R453P}$ and eEF1A (101) and further revealed that $SidI_{R453P}$ also interacts with MesI (see Fig. S4 and S7A in the supplemental material) (101). These data demonstrate that MesI interacts specifically with SidI and confirm that SidI binding to eEF1A is insufficient for translation inhibition (101). Subsequently, we asked whether increasing the concentration of MesI would influence the SidI-eEF1A interaction. We incubated GST-SidI with eEF1A (from HEK 293T lysates) (see Materials and Methods) followed by increasing concentrations of purified recombinant MesI. Despite the MesI concentration increasing 100-fold, GST-SidI still retained eEF1A on the beads (Fig. 2.3B), suggesting that SidI interacts with MesI and eEF1A simultaneously. The same result was observed when MesI was incubated with GST-SidI prior to HEK 293T lysates (see Fig. S5A in the supplemental material). Thus, SidI

binding to eEF1A and MesI is not mutually exclusive.

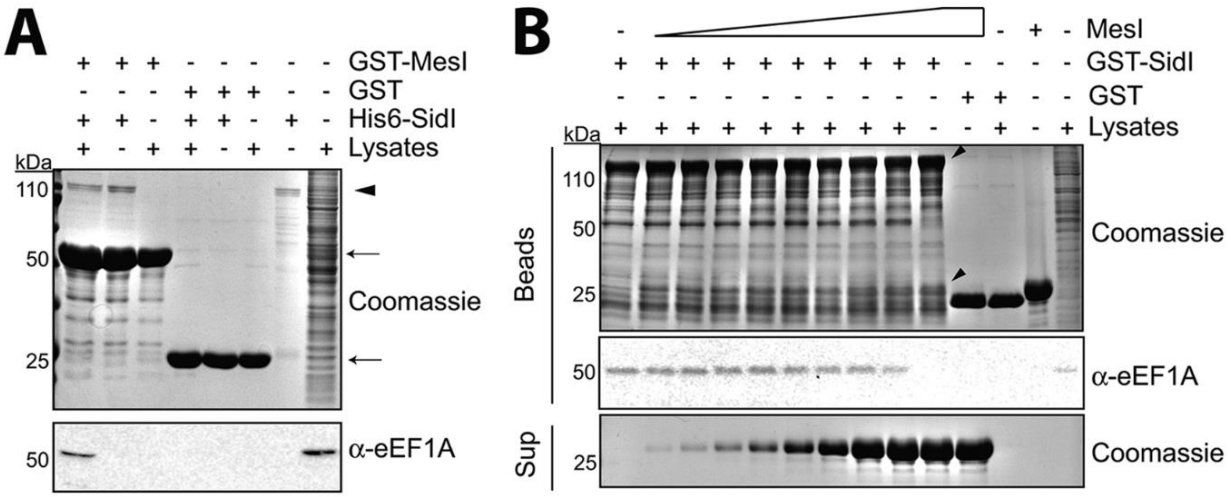

Figure 2.3 MesI does not impair interaction between SidI and eEF1A.

(A) GST-MesI or GST alone was immobilized on magnetic glutathione agarose beads, followed by incubation with 100 μg purified His_6-SidI alone or His_6-SidI that had been preincubated with lysates from HEK293T cells (Lysates), as indicated. Proteins were separated by SDS-PAGE and visualized by Coomassie staining or Western blotting for eEF1A, as indicated. The arrowhead indicates His_6-SidI, and the arrows indicate GST-MesI (lanes 1 to 3 from left) or GST (lanes 4 to 6). (B) Lysates from *E. coli* expressing GST-SidI or GST alone were incubated with magnetic glutathione agarose beads and lysates from HEK293T cells, followed by 10 to 1,000 μg of purified recombinant MesI (shown as increasing amounts in supernatants [Sup] from beads [an uncropped image is shown in Fig. S5B]). Proteins remaining on the beads were separated by SDS-PAGE and visualized by Coomassie staining or Western blotting for eEF1A, as indicated. GST-SidI (~130 kDa) and MesI (~27 kDa) are indicated with arrowheads. The data are representative of the results of at least two independent experiments.

MesI and eEF1A interact with distinct regions of SidI. Since MesI and eEF1A are capable of binding SidI simultaneously, we hypothesized that the proteins interact with SidI at distinct sites. SidI has a molecular weight of ~110 kDa and consists of 942 amino acids. Since the structure of SidI has not been solved, we used the RaptorX Web server (221) to predict the domain structure of SidI. Based on the predicted domains (see Fig. S6 in the supplemental material), we generated SidI truncations consisting of amino acid residues 1 to 268 ($SidI_N$), 269 to 942 ($SidI_C$), and 269 to 874 ($SidI_{C\Delta 68}$) (Fig. 2.4A). To determine which of these putative SidI

domains is involved in interaction with MesI and eEF1A, we immobilized GST-tagged full-length SidI, $SidI_N$, $SidI_C$, or $SidI_{C\Delta 68}$ or GST alone on glutathione beads, followed by incubation with lysates from HEK 293 cells stably producing 3xFLAG-MesI. Western blot analysis was used to detect 3xFLAG-MesI and eEF1A bound to SidI truncation proteins (see Materials and Methods). We confirmed that GST-SidI, but not GST alone, was capable of retaining both MesI and eEF1A on the beads. 3xFLAG-MesI was further retained on beads coated with GST-$SidI_N$ and GST- $SidI_C$, but not GST-$SidI_{C\Delta 68}$, whereas eEF1A was retained by GST-$SidI_C$ and GST-$SidI_{C\Delta 68}$ (Fig. 2.4B). As a negative control, we found that GST-Lgt1 retained neither eEF1A nor 3xFLAG-MesI with the same efficiency as GST-SidI and GST-$SidI_{R453P}$ (see Fig. S7A). To control for the potential influence of 3xFLAG-MesI on eEF1A binding to SidI fragments, we repeated the experiment using HEK 293 cells that did not produce 3xFLAG-MesI. We observed the same pattern of interactions between eEF1A and the C-terminal region of SidI in the absence of 3xFLAG-MesI (see Fig. S7B). Based on these data, we conclude that MesI interacts with SidI at regions within amino acid residues 1 to 268 and 874 to 942, with apparently higher affinity to the latter, whereas eEF1A interaction with SidI is dependent on amino acid residues 269 to 874. Together, these data suggest MesI interacts with two nonoverlapping regions of SidI that are distinct from the site of SidI interaction with eEF1A.

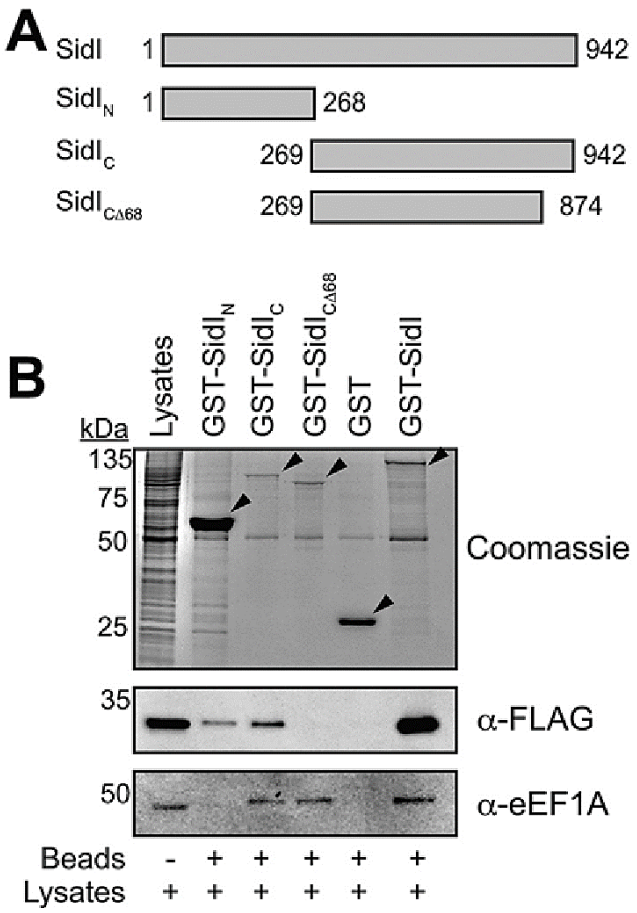

Figure 2.4. MesI and eEF1A interact with distinct regions of SidI.

(A) Schematic representation of SidI truncation proteins. (B) Lysates from *E. coli* expressing GST-SidI constructs were incubated with gluta- thione agarose beads, followed by washing and incubation with lysates from HEK293 FcγRII cells stably expressing 3xFLAG-MesI. Proteins were separated by SDS-PAGE and visualized by Coomassie staining (GST-SidI) or Western blotting. The arrowheads indicate GST fusion proteins. The data are representative of the results of three independent experiments.

Loss of MesI does not impact SidI translocation into host cells. The majority of *L. pneumophila* effector proteins rely on a C-terminal translocation signal for Dot/Icm-mediated translocation into host cells (222, 223). Based on the observed interaction between MesI and the C-terminal 68 amino acid residues of SidI, we evaluated whether Dot/Icm-mediated translocation of SidI requires MesI. Dot/Icm-dependent export of SidI fused to *Bordetella pertussis* adenylate cyclase (CyaA) was quantified (223). When CyaA fusion proteins reach the cytosol of eukaryotic

cells, they catalyze formation of cAMP, which can be quantified using a cAMP-specific enzyme-linked immunosorbent assay (ELISA). Based on potent toxicity associated with wild-type SidI, a nontoxic *sidI* allele (R453P; $SidI_{RP}$) was used for these experiments (101, 162). Expression of CyaA-$SidI_{R453P}$ was confirmed using Western blot analysis (Fig. 2.5A). Subsequently, we found that cAMP production within host cells was significantly increased following infection with wildtype and Δ*mesI* strains, but not the Dot/Icm-deficient Δ*dotA* strains, of *L. pneumophila* producing CyaA-$SidI_{R453P}$ (Fig. 2.5B). Translocation of CyaA-RalF was used as a positive control for Dot/Icm-dependent translocation and similarly confirmed by Western blot analysis (223) (Fig. 2.5A and B). Together, these data demonstrate that SidI translocation into host cells is not impacted by loss of MesI.

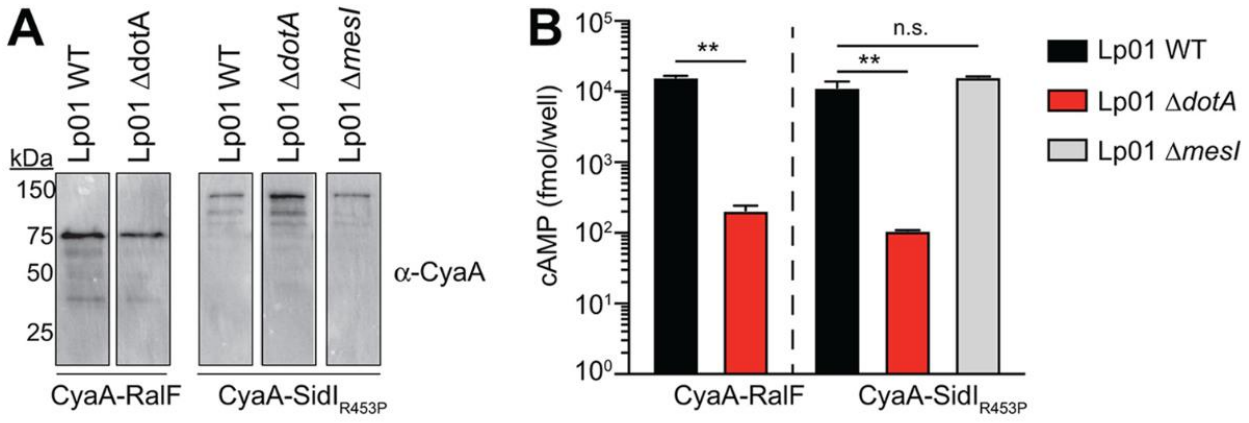

Figure 2.5. MesI is not required for Dot/Icm translocation of SidI into host cells.

(A) Western blot showing production of CyaA-RalF (~76 kDa) and CyaA-$SidI_{R453P}$ (~150 kDa) by the indicated *L. pneumophila* strains. WT, wild type. (B) Quantification of cAMP extracted from CHO FcγRII cells infected with the indicated *L. pneumophila* strains. The asterisks denote statistical significance by t test (**, $P < 0.01$; n.s., not significant). The data are representative of the results of two independent experiments. The data are expressed as means and SD of samples in triplicate.

Binding to eEF1A is insufficient for SidI-mediated translation inhibition.

Subsequently, we investigated the ability of truncated SidI proteins to influence protein

translation. At concentrations equivalent to that of SidI, neither $SidI_N$, $SidI_C$, nor $SidI_{C\Delta68}$ was sufficient to inhibit protein translation *in vitro* (Fig. 2.6A). Based on the interaction between $SidI_{C\Delta68}$ and eEF1A, we also quantified translation in the presence of increasing concentrations of His_6 -$SidI_{C\Delta68}$. We found that His_6-$SidI_{C\Delta68}$ significantly decreased translation at concentrations up to 25-fold greater than that of SidI (Fig. 2.6B), suggesting that the truncation retains some activity; however, $SidI_{C\Delta68}$ -mediated translation inhibition is modest in comparison to that with an equal amount of SidI despite the ability to interact with eEF1A (Fig. 2.4B; see Fig. S7B). These data further confirm that interaction with eEF1A is insufficient for SidI-mediated translation inhibition (101).

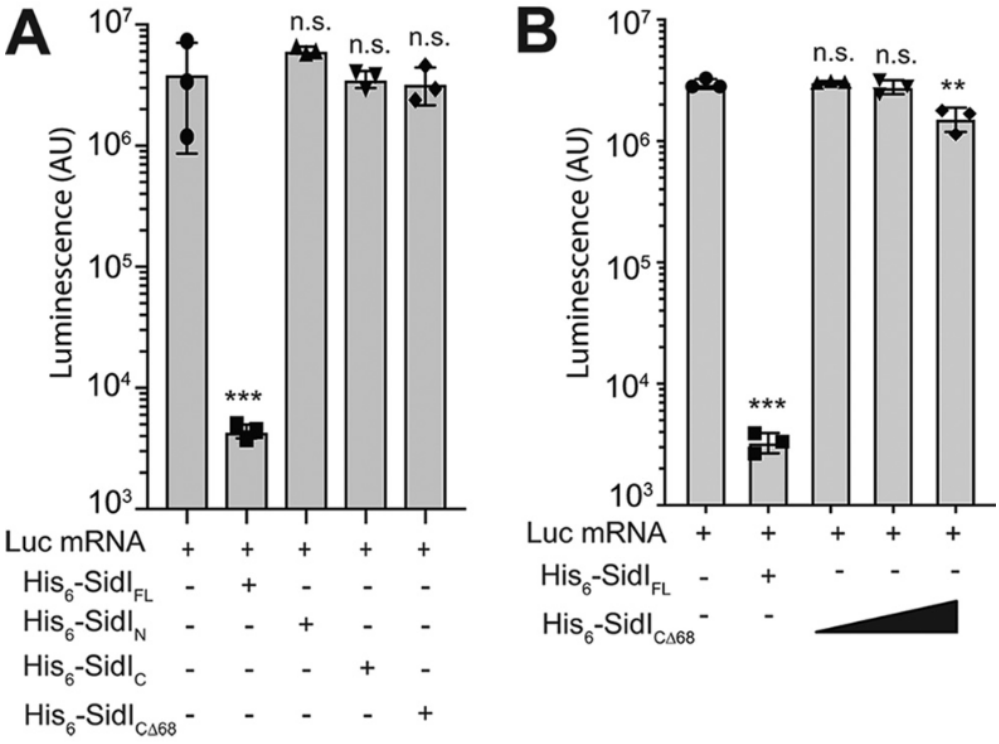

Figure 2.6. Full-length SidI is required for translation inhibition.

Translation of luciferase mRNA was quantified using a rabbit reticulocyte lysate kit. Shown is translation of luciferase mRNA in the presence of 4 ng His_6-SidI, His_6-$SidI_N$, His_6-$SidI_C$, or His_6-$SidI_{C\Delta68}$ (A) or 4 ng of His_6-SidI alone or increasing amounts of His_6-$SidI_{C\Delta68}$ (4 ng, 50 ng, or 100 ng) (B). The asterisks denote statistical significance by t test (***, $P < 0.001$; **, $P < 0.01$; n.s., not significant). The data are representative of the results of at least two independent experiments. The data are expressed as means ± SD of samples in triplicate.

SidI is a GDP-dependent glycosyl hydrolase. Like many other bacterial effectors, the primary amino acid sequence of SidI does not have obviously conserved motifs. Therefore, to gain insight into the putative function of SidI, we used a variety of computational methods to predict the structure and function of SidI. Though very low primary sequence identity was present in the templates used, the HHPred Web server (224), the Phyre2 Web server (225), the Raptor-X Web server (221), and the I-TASSER Web server (226–228) all produced models of various lengths but with the same fold for overlapping regions. A DALI search (229) for structural homologs against each of these models revealed that amino acid residues 368 to 868 of SidI have predicted structural homology to multiple bacterial and eukaryotic glycosyltransferases with GT-B folds, including PimB, a GDP-mannose-dependent mannosyltransferase (see Table S1 and Fig. S8 in the supplemental material). Orthogonally, the Ginzu domain parser on the Robetta server also predicted the presence of a glycosyltransferase domain (230). Based on the consensus between the orthogonal computational approaches, we hypothesized that SidI possesses GDP-dependent glycosyltransferase activity and that GDP-mannose could be a substrate. To test this hypothesis, we utilized a functional luminescence-based assay to quantify the cleavage of several nucleotide-sugars including GDP-mannose, GDP-fucose, UDP-glucose, and UDP-GlcNac (see Materials and Methods). As a positive control for nucleotide-sugar cleavage, we included the glucosyltransferase Lgt1, which cleaves UDP-glucose (231). MesI was included as a control, since it does not have predicted enzymatic activity (see Materials and Methods). We found a highly significant increase in liberation of GDP from GDP-mannose in the presence of purified recombinant His_6-SidI (Fig. 2.7A). We did not observe similar levels of nucleotide liberation catalyzed by SidI for GDP-fucose, UDP-glucose, or UDP-GlcNAc (Fig. 2.7A to D), suggesting that GDP-mannose is the preferred substrate for SidI. Interestingly, MesI

displayed mild activity against GDP-fucose but no activity against any other nucleotidesugars tested (Fig. 2.7A to D). As predicted, Lgt1 cleaved UDP-glucose, but no other nucleotide sugars were cleaved to a similar extent by either SidI or MesI (Fig. 2.7A to D). We further revealed that $SidI_{R453P}$ was unable to cleave GDP-mannose to the level of wild-type SidI (Fig. 2.7E), suggesting that the ability to cleave GDP-mannose is connected to inhibition of protein translation and toxicity phenotypes observed for SidI (101, 162).

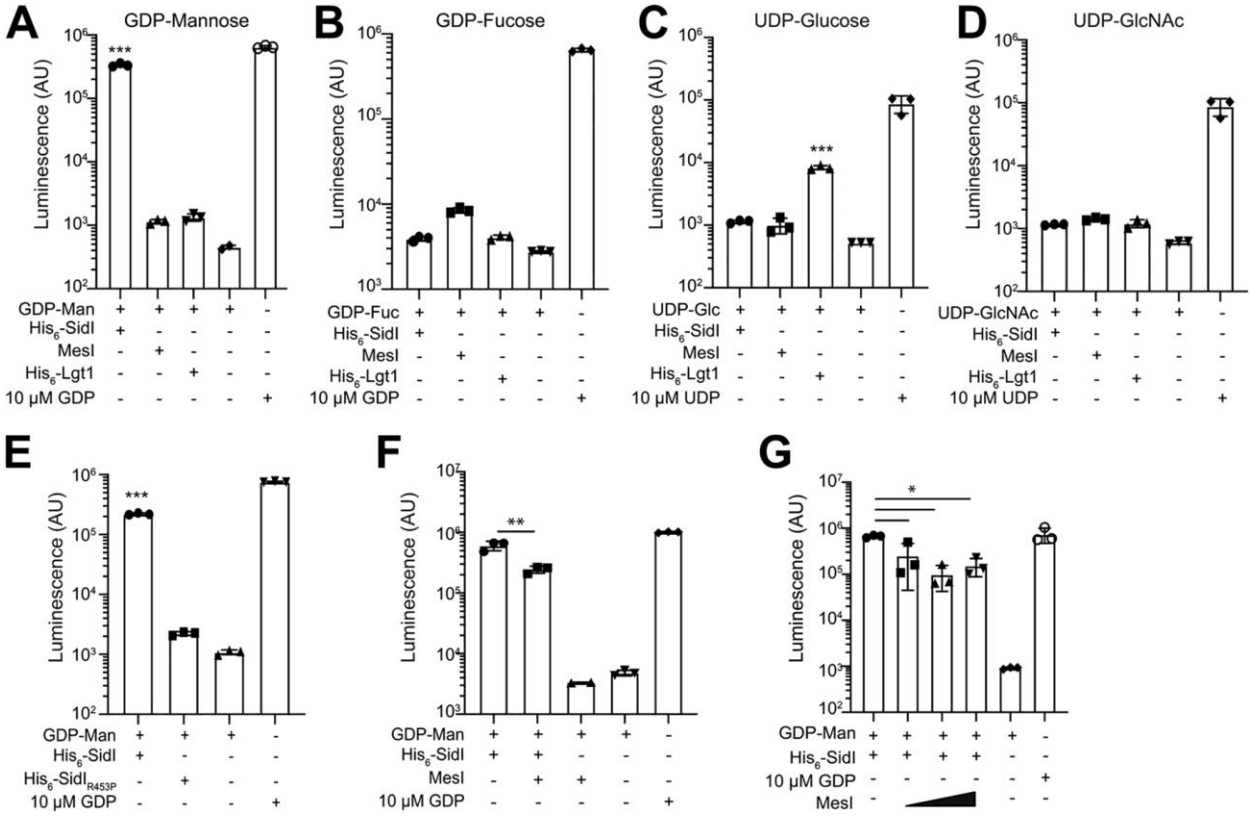

Figure 2.7. SidI possesses glycosyl hydrolase activity.

(A to D) Quantification of GDP or UDP liberated from GDP-mannose (A), GDP-fucose (B), UDP-glucose (C), or UDP-GlcNAc (D) in the presence or absence of 5 μg purified His6-SidI, His_6-Lgt1, or MesI, as indicated. (E) Five micrograms of His_6-SidI or His_6-$SidI_{R453P}$ was incubated with GDP-mannose. (F and G) Five micrograms of His_6-SidI and/or the molar equivalent of MesI incubated with GDP-mannose (F) or increasing molar amounts of MesI (1:1, 2:1, or 5:1 molar ratio of MesI to His_6-SidI) (G). The asterisks denote statistical significance by t test (***, $P < 0.001$; **, $P < 0.01$; *, $P < 0.05$). The data are representative of the results of at least two independent experiments. The data are expressed as means ± SD of samples in triplicate.

Together, these data demonstrate that SidI possesses glycosyl hydrolase activity and that GDP-mannose is the preferred substrate. The entire predicted GDP-dependent glycosyltransferase domain of SidI is encoded in amino acids 368 to 868, which are encompassed within the $SidI_{C\Delta 68}$ truncation (Fig. 2.4A; see Fig. S8). To determine whether $SidI_{C\Delta 68}$ alone is sufficient to cleave GDP- mannose, we incubated His_6 -$SidI_{C\Delta 68}$ with GDP-mannose and quantified the generation of free GDP. Full-length SidI and $SidI_N$, which is not predicted to possess glycosyl hydrolase activity, were included as controls. We also included His_6 -$SidI_C$, which includes the predicted enzymatic domain. Thus, we evaluated the abilities of $SidI_N$, $SidI_C$, and $SidI_{C\Delta 68}$ to cleave GDP-mannose compared to that of wild-type SidI. All the SidI proteins examined generated a luminescence signal upon incubation with GDP-mannose; however, the luminescence signals obtained by incubation of $SidI_N$, $SidI_C$, and $SidI_{C\Delta 68}$ in the absence of GDP-mannose did not differ significantly from when they were incubated with GDP-mannose (see Fig. S9 in the supplemental material). However, a very significant increase in luminescence was observed when full-length SidI was incubated with GDP-mannose compared to SidI alone (see Fig. S9). These data demonstrate that full-length SidI is required for glycosyl hydrolase activity.

SidI enzymatic activity is dampened by MesI. Based on the ability of MesI to suppress SidI-mediated translation inhibition, we hypothesized that MesI could regulate SidI-mediated GDP-dependent glycosyl hydrolase activity. Thus, SidI-mediated GDP-mannose cleavage in the presence of equimolar amounts of MesI was quantified as described above. We found that MesI was sufficient to significantly decrease— but not inhibit—SidI GDP-dependent glycosyl hydrolase activity ($P < 0.01$) (Fig. 2.7F). We further evaluated whether addition of a molar excess of MesI would further decrease SidI glycosyl hydrolase activity; however, addition of up to a 5-fold molar excess of MesI to SidI was not sufficient to significantly inhibit SidI activity

compared to equimolar quantities (Fig. 2.7G). Furthermore, attenuation of SidI enzymatic activity is specific, since addition of equal quantities of an unrelated protein (GST) was unable to attenuate GDP-mannose cleavage by SidI (see Fig. S10 in the supplemental material). Thus, MesI dampens SidI glycosyl hydrolase activity *in vitro.*

DISCUSSION

Legionella pneumophila is an opportunistic, intracellular pathogen that exploits host cell machinery to promote intracellular replication through the translocation of effector proteins. SidI is one of seven cytotoxic effectors that inhibit eukaryotic protein translation (SidI, SidL, Lgt1 to -3, LegK4, and Lpg1489) (90, 101–103). Within this family of effectors, SidI is distinct, as its regulation by the metaeffector Lpg2505 (MesI) is essential for intracellular replication (162). Our study aimed to explore the role of MesI in the regulation of SidI function and elucidate potential mechanisms behind SidI-mediated toxicity. Here, we demonstrate that MesI binds directly to SidI with high affinity and modulates both SidI-mediated translation inhibition and novel GDP-dependent glycosyl hydrolase activity, which has not been previously observed for a bacterial effector. We further demonstrate that SidI is able to simultaneously bind MesI and eEF1A, which interact with distinct regions of SidI. This work is the first to define the enzymatic activity of SidI and the contribution of MesI to SidI-mediated phenotypes. *L. pneumophila* is reliant on host cell-derived amino acids for intracellular replication (94). It can therefore be speculated that *L. pneumophila* utilizes multiple effector proteins to halt host protein synthesis at the elongation step in order to facilitate proteasomal degradation of partially folded polypeptides. The translation-inhibiting effectors characterized to date have diverse functions. The effector Lgt1 was found to target the host elongation factor eEF1A, and homology searches led to the

discovery of the orthologous effectors Lgt2 and -3 (106). The Lgt effectors function by glycosylation of eEF1A at Ser-53, which results in blockade of host protein synthesis (232). The Lgts also glycosylate a eukaryotic release factor-related protein (eRF3) and Hsp70 subfamily B suppressor 1 (Hbs1) (233, 234). Based on the function of Lgt1 to -3, attempts were made to identify SidI-mediated posttranslational modification of eEF1A; however, no modifications were discovered (101). Although SidI was previously assumed to lack glycosyltransferase activity (101, 235), we discovered that SidI is indeed able to cleave GDP-mannose, suggesting that SidI is a likely a mannosyltransferase. SidI also had low levels of activity against three other activated sugars; however, this is likely a consequence of relaxed sugar specificity by glycosyltransferases in vitro (236). Further investigation is required to reveal the target of SidI's glycosyltransferase activity in vivo and the molecular mechanism by which SidI inhibits translation.

SidI induces the host stress response through formation of a complex between heat shock factor 1 (HSF1) and eEF1A (101). The formation of this complex in conjunction with a noncoding RNA promotes the binding of HSF1 to the heat shock element (HSE), inducing host cell Hsp70 expression (101, 123). Notably, despite the upregulation of transcription, Hsp70 protein levels did not differ between infected and uninfected cells (101), likely due to robust translation inhibition by *L. pneumophila* effectors. A more recent study revealed that the eEF1A1 isoform facilitates expression of heat shock genes independently of its role in protein translation (237). Since SidI, but not Lgt1, induced expression of Hsp70 in addition to eEF1A-mediated activation of the HSF1 transcription factor, it could be hypothesized that SidI modulates eEF1A to specifically amplify heat shock genes, which could enhance the survival of *L. pneumophila*-infected cells. Moreover, the effector LegK4 phosphorylates Hsp70, which results in loss of protein translation. It is tempting to envision a scenario whereby SidI and LegK4 function in

concert to modulate host Hsp70 activity. The importance for modulation of heat shock proteins has also been demonstrated by previous observations that Hsp90 is essential for *L. pneumophila* replication in *A. castellanii* (238). Further investigation is required to define the influence of MesI on SidI-mediated modulation of the heat shock response.

Regulation of effector function by metaeffectors is an essential component of the *L. pneumophila* virulence strategy. The first identified *L. pneumophila* metaeffector, LubX, functions as an E3 ubiquitin ligase that is translocated into the host cytosol at late stages of infection and catalyzes ubiquitination of the effector protein SidH, targeting it for proteasomal degradation (139). *L. pneumophila* Δ*lubX* mutants replicate similarly to wild-type bacteria, suggesting that LubX is not individually required for intracellular replication in the host cells examined (139). Like MesI, the metaeffector SidJ directly contributes to intracellular replication by suppressing the toxicity of the SidE family of effectors (SdeA, SidE, SdeB, and SdeC) (144, 145). However, unlike MesI, overexpression of SidJ is toxic to eukaryotic cells (26, 144). The SidE family effectors also contribute directly to intracellular replication through a novel mechanism of phosphoribosyl-ubiquitin conjugation to host substrates (239–241). Unlike the SidE effectors, loss of *sidI* or the *sidI-mesI* operon has no effect on *L. pneumophila* intracellular growth (162), suggesting that SidI functions redundantly within macrophages. However, in the absence of MesI, SidI is deleterious to *L. pneumophila* intracellular replication (162), a phenotype not observed for any other effector.

Several modes of metaeffector function have been described. A large-scale screen by Urbanus and colleagues led to the discovery of 17 putative *L. pneumophila* metaeffectors that function to suppress the toxicity of other effectors (126). They uncovered several mechanisms by which metaeffectors regulate their cognate effectors through direct targeting and abrogation of

effector enzymatic activity in vitro (LegL1, SidP, and LupA). Similarly, we found that MesI dampens SidI activity in vitro; however, residual SidI activity is retained, suggesting that MesI functions to fine-tune or direct SidI activity. Interestingly, we did not observe substantial interaction between Lgt1 and eEF1A despite evidence that the Lgt1 enzyme is active (see Fig. S7A, S2C, and S7C), which is likely due to release of eEF1A following its glucosylation. Although we have not identified the bona fide substrate of SidI, our observation that SidI interacts with both MesI and eEF1A stably and simultaneously in distinct regions suggests that SidI may not target eEF1A but instead use interaction with eEF1A to gain access to a different host substrate. Moreover, the almost complete restoration of translation by MesI in the presence of SidI compared to the relatively modest decrease in SidI-mediated glycosyl hydrolase caused by MesI suggests that MesI does not function to suppress SidI enzymatic activity. Future investigation will reveal the target of SidI activity, the role of MesI in SidI function, and how these phenotypes contribute to *L. pneumophila* intracellular replication.

We discovered that MesI interacts with SidI in two nonoverlapping N- and C-terminal regions. This observation is unique, since no previously characterized metaeffectors and very few protein-protein interactions are facilitated through multiple nonoverlapping regions. For example, the metaeffector SidJ binds and polyglutamylates single sites on SdeA, SdeB, SdeC, and SidE (151), and the metaeffector LubX binds SidH through its U box 2 domain only (139). However, interaction of a protein with more than one nonoverlapping region of a binding partner is not unprecedented. Using affinity chromatography, Liang and Hai demonstrated that human activating transcription factor 4 (hATF4) interacts with four nonoverlapping domains within CREB (cAMP response element-binding protein)-binding protein (CBP). Moreover, hATF4 interacted with individual CBP domains with differing affinities (242). Similarly, MesI

interacted with the N- and C-terminal regions of SidI with lower efficiency than the full-length SidI protein (Fig. 2.4B). Based on our evidence that the SidI-MesI interaction has a 1:1 stoichiometry (Fig. 2.1C), it can be speculated that both the N- and C-terminal regions of SidI contribute to MesI binding. Nevertheless, since our SPR data were better described by a two-state model as opposed to a simple Langmuir model, we suspect that MesI binding to SidI may somehow alter the conformation of SidI. We are currently conducting further studies to help define these structural changes and are additionally optimistic that our efforts to solve the structure of the MesI-SidI complex will shed light on the molecular basis for this unique interaction. Interestingly, one of MesI's binding sites on SidI falls at the extreme carboxy terminus of SidI. The majority of Dot/Icm-translocated effectors are dependent on a C-terminal translocation signal for secretion into host cells (222). We revealed that loss of mesI did not impact SidI translocation into host cells (Fig. 2.5). However, that does not preclude the possibility of MesI interfering with SidI translocation, since *sidI*, but not *mesI*, was overexpressed. Further evaluation at more physiologically relevant expression levels is required to determine if MesI impairs Dot/Icm-dependent translocation of SidI into host cells. Through structural-homology prediction and biochemical analysis, we revealed that SidI likely possesses GDP-dependent glycosyltransferase activity. Although we have not directly demonstrated the transfer of mannose to a substrate protein, it is unlikely that SidI functions only as a nucleotide-sugar hydrolase in the context of infection. Moreover, free-nucleotide liberation from activated sugar donors is a prerequisite for transfer of glycans to substrate molecules and is an established method to identify glycosyltransferase activity without knowing the acceptor substrate (243). Several *L. pneumophila* effectors function as glycosyltransferases, including the translation inhibitors Lgt1 to -3; however, none have been shown to utilize GDP- conjugated sugars. In fact,

bacterial GDP-dependent glycosyltransferases seem to be involved primarily in biogenesis of cell surface structures (244–246). SidI has predicted structural homology to mycobacterial phosphatidylinositol mannosides (PIMs), which are GT-B glycosyltransferases (245, 247). To our knowledge, no other translocated bacterial effector has been demonstrated to have GDP-dependent glycosyltransferase activity. The primary site of protein glycosylation in eukaryotic cells is the Golgi apparatus; however, nucleotide sugars, including GDP-mannose, are synthesized in the cytoplasm of eukaryotic cells prior to transport into the Golgi apparatus (248, 249). Thus, SidI likely hijacks cytoplasmic GDP-mannose prior to its translocation into the Golgi apparatus. Based on the relatively low abundance of individual effectors in L. pneumophila-infected cells, it is unlikely that SidI function influences glycoprotein production by host cells. Thus, we predict SidI is a GDP-dependent glycosyltransferase, and this activity is likely critical for SidI-mediated translation inhibition and cytotoxicity. Further biochemical and structure-function analysis will reveal the detailed molecular mechanism by which SidI functions, its bona fide substrate in host cells, and how MesI regulates its activity to promote *L. pneumophila* intracellular replication. In this study, we have revealed a direct high-affinity interaction between SidI and its metaeffector, MesI; defined a novel enzymatic activity for SidI; and uncovered the fact that MesI can modulate SidI function in vitro. Our work has provided a foundation for future biochemical and cell biological studies to reveal how SidI functions to modulate host cell processes. The severe virulence defect resulting from expression of *sidI* in the absence of *mesI* underlines the importance of defining the molecular mechanism of SidI-MesI function. Moreover, the lack of precedent for a bacterial GDP-dependent glycosyltransferase effector protein suggests that SidI possesses novel enzymatic activity, which must be regulated by MesI to promote *L. pneumophila* intracellular replication. Our future work will focus on uncovering

this mechanism in order to gain critical insight into translation inhibition and metaeffector function.

MATERIALS AND METHODS

Bacterial strains, cell culture, growth conditions, and reagents. *E. coli* strains used for cloning (Top10; Invitrogen) and protein expression [BL21(DE3); a gift from Craig Roy, Yale University] were maintained in Luria-Bertani (LB) medium supplemented with antibiotics as appropriate for plasmid selection (50 μg ml^{-1} kanamycin [GoldBio], 100 μg ml^{-1} ampicillin [GoldBio], and 25 μg ml^{-1} chloramphenicol [GoldBio]). *L. pneumophila* Philadelphia-1 Lp01 (250) and Δ*dotA* (208) strains were cultured on supplemented charcoal–N-(2-acetamido)-2-aminoethanesulfonic acid (ACES)-buffered yeast extract (CYE) and grown at 37°C, as described previously (251, 252). CYE was supplemented with 10 μg ml^{-1} chloramphenicol for plasmid maintenance as required. Protein expression in *E. coli* and *L. pneumophila* was induced with 1 mM isopropyl- β-D-1-thiogalactopyranoside (IPTG) (GoldBio).

Table 2.1. Oligonucleotide primers used in this study

Name	Sequence (5′→3′)[a]
MesISalI-F	ATT**GTCGACA**ATGATAAAAGGAAAACTTATGCCC
MesIBglII-F	TGG**AGATCT**ATGATAAAAGGAAAACTTATGC
MesIPstI-R	GG**CTGCAG**TTATAAAATAATTGGTCGAG
SidIBamHI-F2	ATT**GGATCC**TTATGACTAAAATATACTTATTAACTGC
SidIBamHI-F	ATT**GGATCC**ATGACTAAAATATACTTATTAACTGC
SidINotI-R	ATT**GCGGCCGC**TCAAAATACCAGTATCGATTCTTTAAG
SidICBamHI-F	ATT**GGATCC**ATGAATTTTTATGATTTTGATGG
SidICΔ68NotI-R	ATT**GCGGCCGC**TCATATATTCTCTAATAAATGATC
SidINNotI-R	ATT**GCGGCCGC**TCATCTGAAACTTTTATCGTGCTC
SidIPstI-R	ATT**CTGCAG**TCAAAATACCAGTATCGATTC
Lgt1Sal1-F	ATT**GTCGACA**ATGAAAGCAAGAAGGGATCAAC
Lgt1_6p1Sal1-F	ATT**GTCGACTCA**TGAAAGCAAGAAGGGATCAAC
Lgt1Not1-R	ATT**GCGGCCGC**CTACCCTACTGAAGGCAACCAAC

[a]Restriction endonuclease cleavage sites are shown in boldface.

All mammalian cells were grown at 37°C-5% CO 2 for up to 30 passages. HEK 293 FcγRII (a gift from Craig Roy, Yale University (253)) and HEK 293T (ATCC) cells were cultured in Dulbecco's modified Eagle medium (DMEM) (Gibco) supplemented with 10% heat-inactivated fetal bovine serum (HIFBS) (U.S. origin; Gibco). CHO FcγRII cells (254) (a gift from Craig Roy) were cultured in MEMα (Gibco) supplemented with 10% HIFBS. Unless otherwise specified, all chemicals were obtained from Millipore Sigma (St. Louis, MO). The oligonucleotide primers used in this study are listed in Table 1.

Molecular cloning, plasmid construction, and generation of Legionella strains. *L. pneumophila* Lp01 genomic DNA (gDNA) was isolated using the Illustra genomicPREP DNA isolation spin kit (GE Healthcare) and used as a template for cloning *sidI* and *mesI* into the indicated plasmid vectors. For recombinant-protein production, *sidI* was amplified using the primer pair SidIBamHI-F/SidINotI-F and cloned as a BamHI/NotI fragment into pGEX-6P-1 (GE Healthcare) and pT7HMT (211). *mesI* was amplified using primer pairs MesIBglII-F/MesINotI-R and cloned as a BglII/NotI fragment into BamHI/NotI-digested pGEX-6P-1 and pcDNA4T/O-3xFLAG (251). For cloning into pT7HMT, *mesI* was amplified using the MesISalI-F/MesINotI-R primer pair and cloned as a SalI/NotI fragment. For generation of SidI truncations, the regions of interest were amplified with primer pairs SidIBamHI-F/SidINNotI-R ($SidI_N$), SidICBamHI-F/ SidINotI-R ($SidI_C$), and SidICBamHI-F/SidICΔ68NotI-R ($SidI_{C\Delta68}$) and cloned as BamHI/NotI fragments into pT7HMT or pGEX-6P-1. For generation of pcyaA::$sidI_{R435P}$, $sidI_{R453P}$ was amplified from pSR47S::$sidI_{R453P}$ (162) with SidIBamHI-F2/SidIPstI-R and cloned as a BamHI/PstI fragment into pcyaA (221). *sidI*$_{R453P}$ was cloned into pT7HMT or pGEX-6P-1 by amplification from pSR47S::$sidI_{R453P}$ (162) with primer pair SidIBamHI-F/ SidINotI-R and cloning as a BamHI/NotI fragment. *lgt1* was cloned into

pT7HMT or pGEX-6p-1 following amplification from Lp01 gDNA using primer pair Lgt1Sal1-F/Lgt1Not1-R or Lgt1_6p1Sal1-F/Lgt1Not1-R and cloning as a SalI/NotI fragment. DNA sequences were confirmed by Sanger sequencing (Genewiz, South Plainfield, NJ). *L. pneumophila* Lp01 wild type and Δ*dotA* producing CyaA-SidI constructs were generated by electroporation of pcyaA::sidI$_{R453P}$ into competent strains using a Bio-Rad gene pulser at 2.4 kV, 200 Ω, and 0.25 μF and plated on CYE supplemented with 10 μg ml^{-1} chloramphenicol. CyaA-SidI production was confirmed by Western blotting as described below. *L. pneumophila* strains harboring pcyaA::ralF (221) were a gift from Craig Roy (Yale University). Transfection and selection of stable tissue culture cells. HEK 293 FcγRII cells were transfected with pcDNA4T/O-3xFLAG::mesI using FuGENE HD (Roche) transfection reagent according to the manufacturer's instructions. At 48 h post-transfection, 500 μg ml^{-1} zeocin (Invitrogen) was added to the culture medium, and the selection was maintained for 10 days. Subsequently, the cells were maintained in 200 μg ml^{-1} zeocin, and production of 3xFLAG-MesI was confirmed by Western blotting as described above.

Recombinant-protein expression and purification. Overnight E. coli BL21(DE3) cultures were subcultured at 1:100 for 3 h in LB medium supplemented with the appropriate antibiotics, followed by induction of protein expression with 1 mM IPTG, and induced at 16°C overnight. Bacterial cultures were centrifuged at 4,200 relative centrifugal force (rcf) for 5 min at 4°C and washed with ice-cold phosphate- buffered saline (PBS), followed by incubation in bacterial lysis buffer (50 mM Tris, pH 8, 100 mM NaCl, 1 mM EDTA, 200 g ml1 lysozyme, 2 mM dithiothreitol [DTT], 10 μg ml^{-1} DNase, and complete protease inhibitor) for 30 min on ice. The bacteria were sonicated on ice, followed by centrifugation at 17,000 rcf for 30 min at 4°C. The clarified bacterial lysates were incubated with either Ni-NTA beads plus 5 mM imidazole (His

tag) or glutathione agarose beads (GST tag) for 1 to 2 h at 4°C with rotation. For His-tagged proteins, Ni-NTA agarose beads were transferred to 10-ml Poly-Prep chromatography columns (Bio-Rad) and washed with 20 ml of ice-cold wash buffer (50 mM Tris, pH 8, 100 mM NaCl, 1 mM EDTA, 40 mM imidazole), followed by elution in 7 ml of elution buffer (50 mM Tris, pH 8, 100 mM NaCl, 1 mM EDTA, 200 mM imidazole). For GST-tagged proteins, glutathione agarose beads were transferred to a 10-ml Poly-Prep chromatography column and washed with 20 ml wash buffer I (PBS, 0.05% Triton X-100), followed by wash buffer II (PBS, 0.05% Triton X-100, 0.5 M NaCl), and eluted in GST elution buffer (50 mM Tris, pH 9.5, 10 mM glutathione). The protein eluates were visualized by SDS-PAGE and Coomassie. brilliant blue staining. Elution fractions containing protein were combined, dialyzed into PBS, and quantified by Bradford assay (Thermo Scientific). In some cases, the polyhistidine tag was removed from recombinant proteins by site-specific proteolysis using tobacco etch virus protease. Following digestion, as previously described (211), the sample was reapplied to Ni-NTA beads, and the unbound fraction containing the target protein was collected. Samples were further purified by gel filtration chromatography using either a Superdex 75 (26/60) or Superdex 200 (26/60) column attached to an AKTA format fast protein liquid chromatography (FPLC) instrument (GE Healthcare) with PBS as a running buffer. Elution fractions containing protein were analyzed by SDS-PAGE and Coomassie brilliant blue staining, as described above.

Affinity chromatography for protein-protein interaction. Overnight *E. coli* cultures grown in LB medium plus appropriate antibiotic were subcultured 1:100 into 20 ml LB and grown at 37°C for 3 h, followed by induction with 1 mM IPTG for 4 h or overnight at 16°C. The cultures were centrifuged for 10 min at 1,500 rcf, washed with ice-cold PBS, and pelleted in 1-ml aliquots prior to storage at -20°C for 72 h until use. The pellets were resuspended in 1 ml of cold lysis

buffer (50 mM Tris, pH 8, 100 mM NaCl, 1 mM EDTA) supplemented with 200 μg ml^{-1} lysozyme and complete protease inhibitor and incubated on ice for 30 min. Two millimolar DTT was added to the lysates before sonication on ice. The lysates were then clarified by centrifugation at 12,600 rcf for 15 min at 4°C. The supernatants were collected in fresh, prechilled microcentrifuge tubes. The supernatants were added to either preequilibrated Ni-NTA magnetic beads or magnetic glutathione agarose beads (Pierce) following the manufacturer's protocol for binding His- or GST-tagged fusion proteins, respectively. After the initial batch binding, the beads were washed twice with wash buffer (Ni-NTA [50 mM Na3PO4, 300 mM NaCl, 15 mM imidazole, 0.05% Tween 20, pH 8]; glutathione [125 mM Tris-Cl, 150 mM NaCl, 1 mM DTT, 1 mM EDTA, pH 7.4]) prior to addition of recombinant protein or subsequent cell lysate and batch binding for 1 h at 4°C with rotation. The beads were washed twice with wash buffer before adding the final cell lysate or recombinant protein and incubating for 1 h at 4°C with rotation. Following binding, the beads were washed twice with wash buffer and transferred to fresh, prechilled 1.5-ml microcentrifuge tubes; resuspended in 25 μl of 3x Laemmli sample buffer; and boiled for 10 min. Samples were analyzed by SDS-PAGE and Coomassie brilliant blue staining or Western blotting, as indicated. For experiments to examine eEF1A binding, lysates were derived from either HEK 293T, HEK 293 FcγRII, or HEK293 FcγRII 3xFLAG-MesI cells grown to ~70% confluence on tissue culture (TC)-treated dishes. The cells were washed once with ice-cold PBS and lysed in 1 ml of mammalian lysis buffer (1% NP-40 [vol/vol], 150 mM NaCl, 20 mM Tris-Cl, pH 7.5, 10 mM Na 4P2O7, 50 mM NaF, and complete protease inhibitor). The lysates were collected in prechilled 1.5-ml centrifuge tubes and centrifuged at 11,000 rcf for 20 min at 4°C. The supernatants were collected in prechilled 1.5-ml centrifuge tubes and stored on ice until use.

CyaA effector translocation assay. Translocation of CyaA fusion proteins was performed as described previously (223). Briefly, CHO FcγrII cells were seeded into 24-well plates at $1x10^5$ cells per well 24 h prior to infection. The cells were infected at a multiplicity of infection (MOI) of 30 with *L. pneumophila* Lp01 wild type or Δ*dotA* that had been cultured on CYE supplemented with 10 μg ml^{-1} chloramphenicol and 1 mM IPTG, followed by opsonization by incubation for 30 min with an α-*L. pneumophila* antibody (Invitrogen; PA17227; 1:1,000) at room temperature. The cell culture medium was supplemented with 1 mM IPTG to ensure expression of CyaA-SidI fusion protein. Infected cells were incubated for 1 to 2 h at 37°C-5% CO 2, followed by aspiration of culture medium and washing 3 times with ice-cold PBS. The cells were lysed for 30 min in 200 μl of ice-cold lysis buffer (50 mM HCl, 0.1% Triton X-100) with rocking at 4°C. Samples were either stored at -80°C until use or immediately mixed with 12 μL 0.5 M NaOH in 95% ethanol and centrifuged for 5 min at 11,000 rcf. Supernatants were dried in a Speed Vac and stored at -80°C until use. cAMP was quantified using a cAMP Direct Biotrak enzyme immunoassay (EIA) (nonacetylation) kit (GE Healthcare). Briefly, dried samples were resuspended in 250 μL assay buffer, and ELISA was performed following the manufacturer's protocol. Absorbance at 655 nm was read in a Victor 2 microplate reader (PerkinElmer).

In vitro protein translation assay. Translation assays were performed using the Promega Flexi rabbit reticulocyte lysate (RLL) system (L4540) following the manufacturer's protocol. Briefly, a master mix of RLL was generated and aliquoted into individual tubes. Four nanograms of purified His6-SidI, His6-SidIR453P, or His6-Lgt1 (see above) was added as indicated. Purified recombinant (untagged) MesI or GST was added at the indicated concentrations and molar ratios. The proteins were equilibrated to room temperature before use. All the reaction mixtures were brought to 50 μL with ultrapure water. The reaction mixtures were mixed by pipetting and

briefly centrifuged before incubation at 30°C for 90 min. Translation of firefly luciferase mRNA (Promega) was quantified using a Victor 2 microplate reader (PerkinElmer).

Glycosyltransferase activity assay. Glycosyltransferase activity was evaluated using GDP- or UDP-Glo glycosyltransferase assay kits (Promega) with GDP-mannose (Promega; VA1095), UDP-glucose (Promega; V6991), GDP-fucose (Promega; VA1097), or UDP-GlcNAc (Carbosynth; MU07955) following the manufacturers' recommendations. Briefly, 5 μg of purified His6-SidI, His6-SidIR453P, His6-Lgt1, and/or molar equivalent (or excess, as indicated) MesI was added to 75 μL of 50 mM Tris, pH 7.4, with 10 μM GDP- or UDP-sugar substrate, as specified. One millimolar MnCl2 and 150 mM NaCl were added to His6-Lgt1 reaction mixtures, as previously performed (255). Ten micromolar GDP or UDP was used as a control, as indicated. Reactions were carried out for an hour at 37°C, and quantification of free nucleotide (GDP or UDP) was achieved by addition of GDP- or UDP-Glo nucleotide detection reagent following the manufacturers' instructions and analyzed via luminescence using a Victor 2 microplate reader (PerkinElmer). SDS-PAGE and Western blotting. Boiled protein samples were loaded onto either 4% to 20% gradient SDS-PAGE gels (Bio-Rad) or 12% or 15% SDS-PAGE gels. Following electrophoresis, the proteins were visualized with Coomassie brilliant blue or transferred to polyvinylidene difluoride (PVDF) mem- branes using a Bio-Rad wet transfer cell. The membranes were incubated with blocking buffer (5% nonfat milk powder dissolved in Tris-buffered saline-0.1% Tween 20 [TBST]). Primary antibodies (α-eEF1A [no. 2551S; Cell Signaling Technology], α-Flag-M2 [Sigma], or α-CyaA [3D1; no. EG800; Kerafast]) were used at 1:1,000 in blocking buffer and detected with horseradish peroxidase (HRP)-conjugated secondary antibodies (1:5,000; ThermoFisher). The membranes were washed, incubated with

enhanced chemilu- minescence (ECL) substrate (GE Amersham), and imaged by chemiluminescence using an Azure Biosys- tems c300 darkroom replacer.

Surface plasmon resonance. Direct binding of His6-SidI to MesI was assessed by SPR using a Biacore T-200 instrument (GE Healthcare) at 25°C, according to the general methods previously described (256). Briefly, all experiments were carried out in a running buffer of HBS-T (20 mM HEPES [pH 7.4], 140 mM NaCl, and 0.005% [vol/vol] Tween 20) at a flow rate of 30 μL/min (62). MesI (50 μg ml^{-1} in 10 mM acetate, pH 4.5) was immobilized to a final density of 1,063 resonance units (RU) on one flow cell of a CMD-200M surface (XanTec Bioanalytics GmbH, Dusseldorf, Germany) using standard NHS/EDC coupling. A reference surface was prepared in a similar manner by ethanolamine quenching of the N-hydroxysuccinimide/ ethyl(dimethylaminopropyl) carbodiimide (NHS/EDC)-activated flow cell. Experimental sensorgrams of His 6 -SidI binding to immobilized MesI were obtained in reference-corrected single-cycle mode using sequential concentrations of 0.8, 4, 20, 100, and 500 nM His6-SidI. Each association phase consisted of 2 min of sample injection, followed by a 1.5-min dissociation phase, except for the final injection, which incorporated a 60-min dissociation phase for more accurate determination of the dissociation rate. Kinetic analysis was performed using Biacore T-200 evaluation software v3.1 (GE Healthcare). The sensorgrams were analyzed using both Langmuir and two-state reaction binding models and a local value of Rmax .

Analytical gel filtration chromatography. Samples of recombinant proteins were characterized by analytical-scale gel filtration chromatography as a means of assessing their apparent molecular weights. All samples and standards (500- μL total volume) were separated on a Superdex 200 10/300 column (GE Healthcare) attached to an AKTA format FPLC system using

a flow rate of 0.5 ml/min and PBS as a running buffer. Fractions of 1 ml were collected for subsequent analysis by SDS-PAGE and Coomassie brilliant blue staining, as described above.

Molecular modeling. Homology models were created using four different servers, with the full sequence of SidI as input and default parameters for each server. Using HHPred (224), a number of templates were identified for residues 376 to 868, and the top 25 templates were forwarded for modeling. Using Phyre2 (225), a smaller region, residues 585 to 763, was chosen for modeling. Raptor-X (221) and I-TASSER (226–228) both produce full-length models. Raptor-X predicted residues 350 to 870 to be a domain. I-TASSER presented five models of low confidence, one of which contained a glycosyltransferase domain with a GT-B fold, which was selected as the working model.

Statistical analysis. Statistical analysis was performed with GraphPad Prism software using Student's t test, as indicated, with a 95% confidence interval.

Supplementary Materials

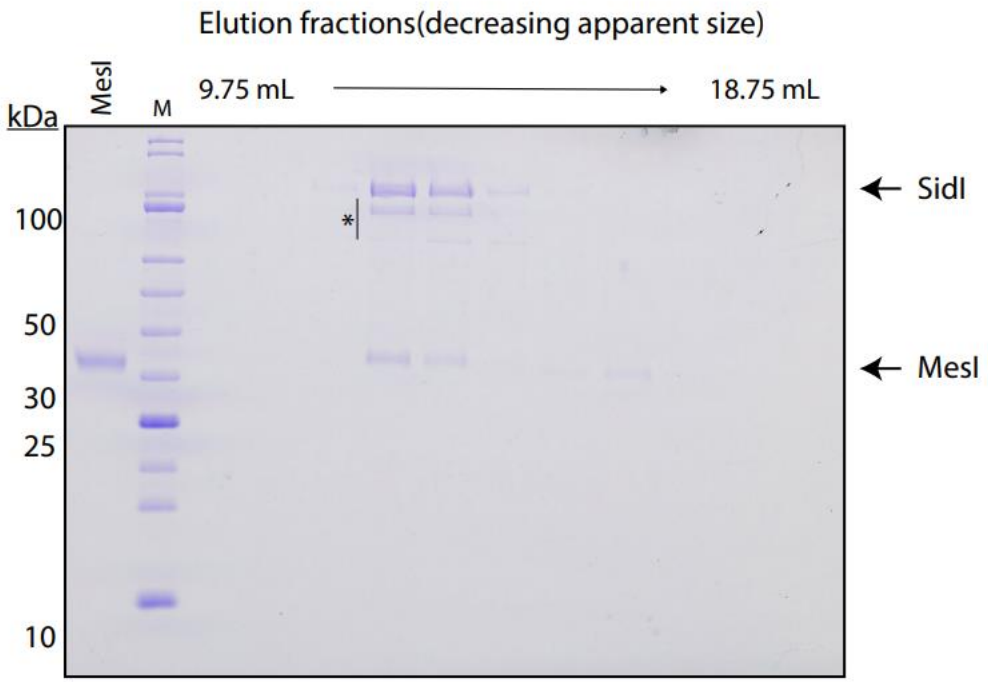

Supplemental Figure 2.1. Co-elution of MesI and SidI by gel filtration chromatography.

A sample of recombinant SidI bound to MesI was separated by analytical scale gel filtration chromatography as presented in Figure 1C. Ten µl of each column fraction were analyzed by SDS-PAGE followed by Coomassie staining to assess the protein content within each fraction. Fractions corresponding to the peak of approximately 150 kDa apparent molecular weight in the sample of SidI bound to MesI (Fig. 1C, red trace) contained both proteins, consistent with formation of a 1:1 complex between these two molecules. Additional bands visible at ~90 kDa represent SidI degradation products and are indicated with an asterisk (*).

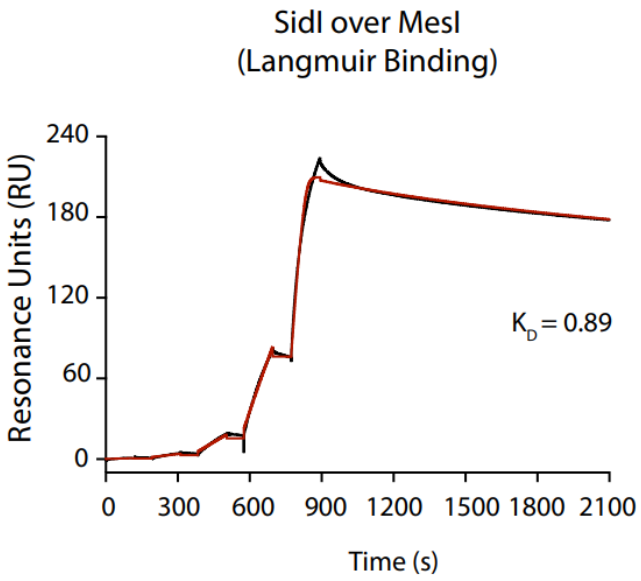

Supplemental Figure 2.2. Binding of His6-SidI to immobilized MesI was assessed by SPR.

The reference corrected sensorgram from a single-cycle experiment is shown in black, while the outcome of fitting to a Langmuir binding model is shown in red. Using this model, the interaction is described by an apparent KD of 0.89 nM where k_{on} = 2.2x10^{5} M^{-1} s^{-1} and k_{off} = 1.9x10^{-4} s^{-1} , respectively.

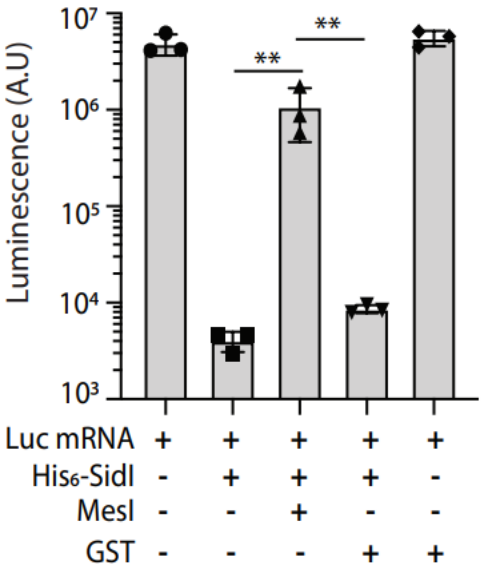

Supplemental Figure 2.3. Inhibition of SidI-mediated protein translation inhibition by MesI is specific.

Translation of luciferase (Luc) mRNA was quantified using a rabbit reticulocyte lysate kit. Translation of luciferase in the presence of 37 fmol His6-SidI alone or in with equimolar amount of purified recombinant MesI or GST. Asterisks denote statistical significance by t-test compared to SidI alone (**P<0.01). Data are representative of two experiments.

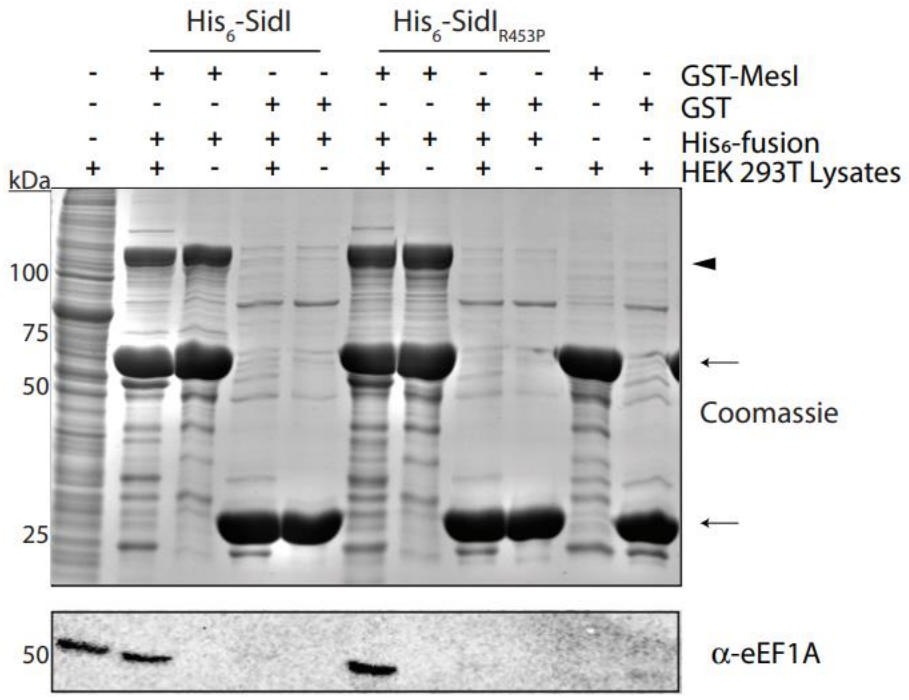

Supplemental Figure 2.4. SidI$_{R453P}$ interacts with MesI and eEF1A.

GST-MesI or GST alone were immobilized on magnetic glutathione agarose beads followed by incubation with 100 µg purified His$_6$-SidI alone or that had been preincubated with lysates from HEK293T cells as indicated (Lysates). Proteins were separated by SDS-PAGE and visualized by Coomassie staining or Western blot as indicated. Arrowhead indicates His$_6$ fusion proteins and arrows indicate GST-MesI (lanes 2-3, 6- 7, and 10) or GST (lanes 4-5, 8-9, 11).

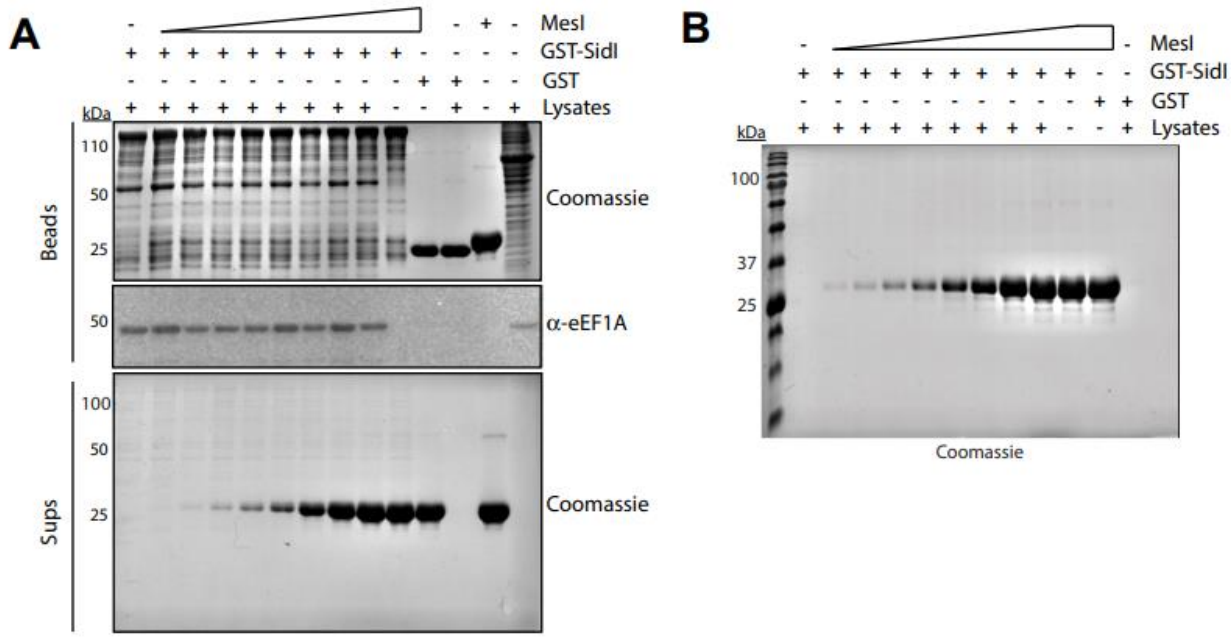

Supplemental Figure 2.5. eEF1A interacts with the SidI-MesI complex.

(A) Lysates from E. coli expressing GSTSidI or GST alone were incubated with magnetic glutathione agarose beads and washed followed by addition of 10, 25, 50, 100, 200, 400, 800 or 1000 µg of purified recombinant MesI (shown as increasing amounts in supernatants from beads). Beads were subsequently incubated with lysates from HEK293T cells. Proteins remaining on the beads were separated by SDS-PAGE and visualized by Coomassie stain or Western blot. (B) Uncropped Coomassie image of supernatant from Figure 3B.

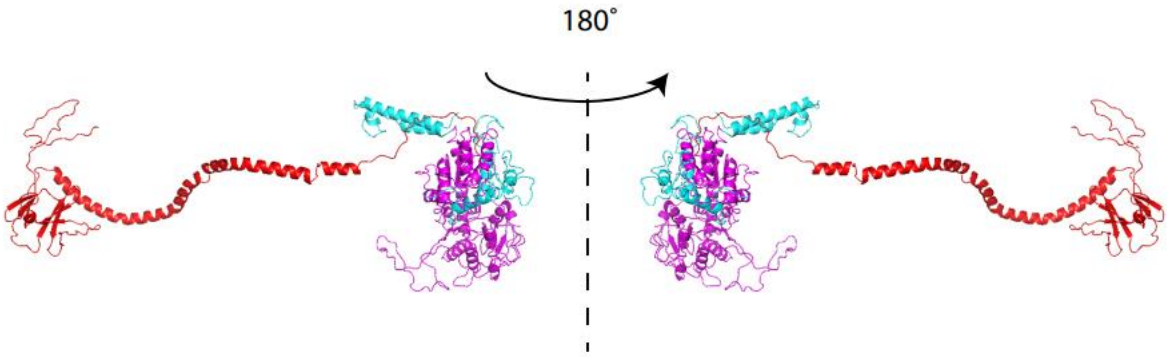

Supplemental Figure 2.6. Molecular model of SidI.

Ribbon cartoons of SidI modeled using the RaptorX webserver. Putative SidI domains are shown in red (residues 1-268), magenta (residues 269-874) and cyan (residues 874-942).

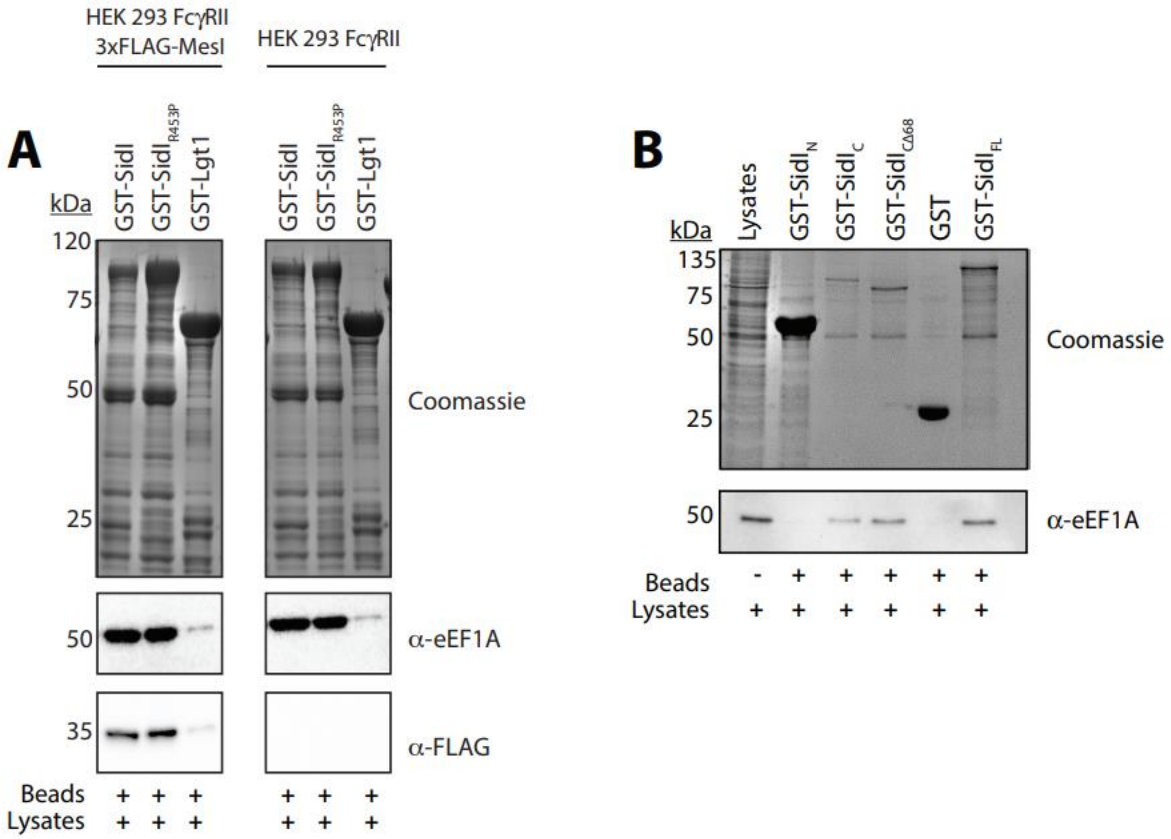

Supplemental Figure 2.7. Specificity of GST-fusion protein binding to MesI and eEF1A.

(A) GST-SidI, GSTSidIR453P or GST-Lgt1 from E. coli lysates were immobilized on glutathione agarose beads followed by incubation with lysates from HEK 293 FcγRII 3xFLAG-MesI or HEK 293 FcγRII cells as indicated. Proteins were separated by SDS-PAGE and visualized by Coomassie staining (GST fusions) or Western blot (eEF1A and 3xFLAG-MesI). Data are representative of two experiments. (B) Interaction between eEF1A and SidI truncations in the absence of MesI. Lysates from *E. coli* expressing GST-SidI constructs were incubated with glutathione agarose beads followed by incubation with lysates from HEK 293 FcγRII cells. Proteins were separated by SDS-PAGE and visualized by Coomassie staining (GST-SidI) or Western blotting (eEF1A). Data are representative of two independent experiments

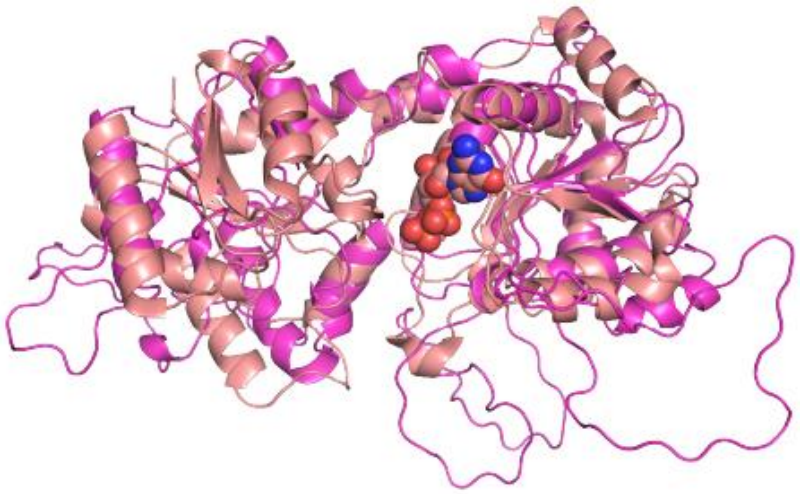

Supplemental Figure 2.8. SidI is modeled as a glycosyltransferase with a GT-B fold.

The model of the putative glycosyltransferase domain is presented in magenta ribbons superimposed to that of PimB (PDB: 3OKA) represented as salmon ribbons, which was identified by DALI as the most similar structure in the PDB. The structure of PimB was solved in the presence of GDP (salmon spheres).

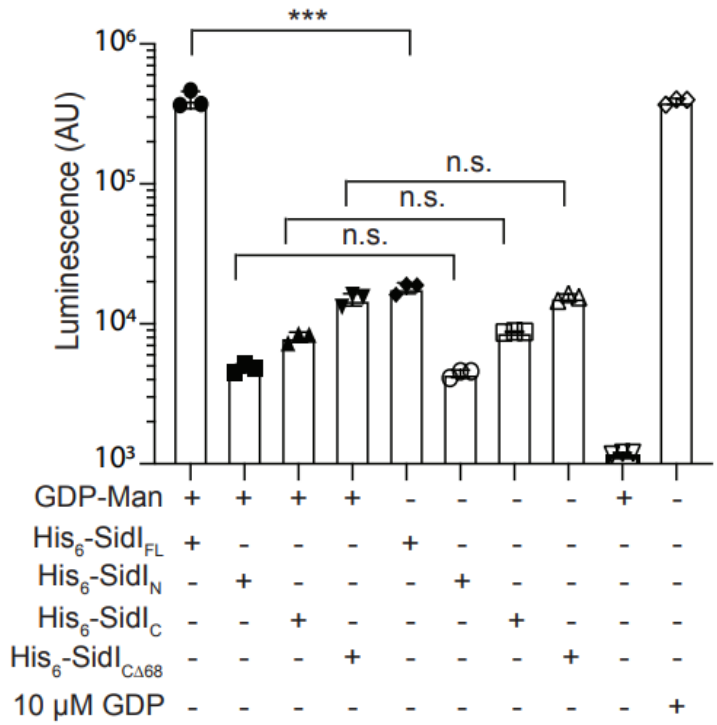

Supplemental Figure 2.9. Full-length SidI is required for glycosyl hydrolase activity.

Luminescence resulting from incubation of 5 μg His6-SidI truncations in the presence or absence of GDP-mannose as indicated. Asterisks denote statistical significance by t-test between samples as indicated (***P<0.001; n.s., not significant). Data are representative of two experiments.

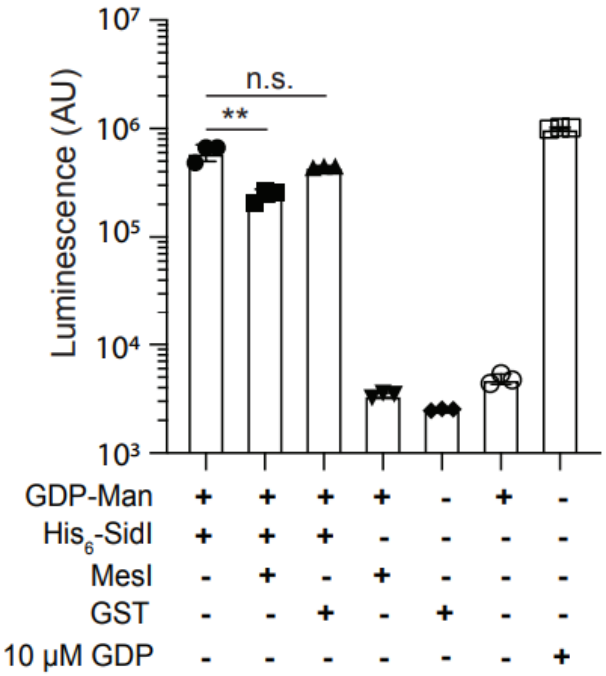

Supplemental Figure 2.10. MesI-mediated attenuation of SidI glycosyl hydrolase is specific.

Liberation of GDP from GDP-mannose by 5 µg His6-SidI and/or molar equivalent of MesI or GST (non-specific control) as indicated. Asterisks denote statistical significance by t-test between samples as indicated (**P<0.01; n.s.,not significant).

Supplemental Table 2.1. Proteins with homology to SidI (HHPred).

No.	PDB		Prob	E-value	P-value	Score	SS	Cols	Query HMM	Template HMM
1	3OKP_A	GDP-mannose-dependent a	99.8	8.2E-20	1.7E-24	181.2	33.6	338	376-868	22-376 (394)
2	4N9W_A	GDP-mannose-dependent a	99.8	3.7E-19	7.5E-24	175.7	36.7	342	370-868	17-364 (390)
3	5D01_B	N-acetyl-alpha-D-glucos	99.8	2.3E-19	4.7E-24	175.8	34.1	347	370-868	15-372 (379)
4	6D9T_A	Glycosyl transferase (E	99.8	1.3E-18	2.6E-23	173.7	33.4	348	370-868	30-387 (400)
5	2JJM_J	GLYCOSYL TRANSFERASE, G	99.8	1.1E-18	2.3E-23	174.8	32.9	346	372-868	27-382 (394)
6	3C48_A	Predicted glycosyltrans	99.8	3.6E-18	7.2E-23	172.6	35.2	352	370-868	40-422 (438)
7	3FRO_B	GlgA glycogen synthase	99.8	5.5E-18	1.1E-22	169.0	34.6	347	370-868	16-427 (439)
8	2R60_A	Glycosyl transferase, g	99.8	1.1E-17	2.3E-22	172.5	37.8	351	370-868	31-456 (499)
9	3OY2_B	Glycosyltransferase B73	99.7	1.3E-18	2.6E-23	176.1	28.3	339	376-868	17-387 (413)
10	6EJI_B	WlaC protein; Glycosylt	99.7	2E-17	4.1E-22	162.9	33.8	333	373-868	15-354 (373)
11	6GNE_A	Probable starch synthas	99.7	8.5E-18	1.7E-22	176.0	31.4	352	369-868	23-494 (508)
12	2QZS_A	PROTEIN; glycosyl-trans	99.7	1.6E-17	3.2E-22	171.3	28.9	347	371-869	16-474 (485)
13	2X6Q_A	TREHALOSE-SYNTHASE TRET	99.7	7.6E-17	1.5E-21	161.9	31.8	386	328-868	8-411 (416)
14	4XYW_A	O-antigen biosynthesis	99.7	1.4E-16	2.8E-21	155.5	31.5	315	376-868	17-336 (338)
15	4XSO_A	Glycosyltransferase (E.	99.7	4.4E-17	8.9E-22	162.6	28.5	291	429-868	81-381 (388)
16	1RZV_A	Glycogen synthase 1 (E.	99.7	2.3E-16	4.6E-21	162.3	33.7	344	371-868	16-472 (485)
17	1V4V_B	UDP-N-Acetylglucosamine	99.7	5.1E-17	1E-21	160.9	25.2	341	370-869	13-366 (376)
18	2IW1_A	LIPOPOLYSACCHARIDE CORE	99.7	4.5E-16	9.2E-21	150.8	31.0	344	372-868	14-368 (374)
19	5ENZ_A	UDP-GlcNAc 2-epimerase	99.6	1.3E-16	2.6E-21	159.1	26.6	344	367-869	6-366 (385)
20	1XV5_A	DNA alpha-glucosyltrans	99.6	8.9E-17	1.8E-21	163.7	25.6	348	370-868	13-399 (401)
21	2X0D_B	WSAF; GT4 FAMILY, TRANS	99.6	9E-16	1.8E-20	155.5	31.7	335	369-868	60-413 (413)
22	5N7Z_A	Lipopolysaccharide 1,6-	99.6	1.5E-15	3.1E-20	147.4	31.5	339	372-868	14-357 (359)
23	5E9T_C	Glycosyltransferase Gtf	99.6	1E-15	2E-20	163.6	32.1	312	388-868	169-497 (503)
24	1VGV_D	UDP-N-acetylglucosamine	99.6	1.9E-16	3.8E-21	156.8	24.3	340	367-868	5-369 (384)
25	3T7D_A	Putative glycosyltransf	99.6	5.8E-16	1.2E-20	169.6	30.2	297	430-868	136-471 (497)
26	4FKZ_B	UDP-N-acetylglucosamine	99.6	2.8E-16	5.7E-21	157.8	24.4	334	377-869	18-368 (388)
27	5DLD_A	UDP-N-Acetylglucosamine	99.6	4.3E-16	8.6E-21	158.4	25.6	338	369-868	16-378 (413)
28	3VUE_A	Granule-bound starch sy	99.6	3.1E-15	6.2E-20	162.0	32.3	350	372-868	26-508 (536)
29	5UOF_B	Alpha,alpha-trehalose-p	99.6	3.9E-16	7.9E-21	167.1	24.3	281	443-868	131-461 (481)
30	3DZC_B	UDP-N-acetylglucosamine	99.6	5.8E-16	1.2E-20	156.0	23.7	331	378-866	41-396 (396)
31	6GNF_A	Glycogen synthase (E.C.	99.6	5.4E-15	1.1E-19	160.0	31.7	345	369-868	35-536 (544)
32	3S28_H	Sucrose synthase 1 (E.C	99.6	3.6E-15	7.3E-20	176.5	32.3	341	382-868	320-766 (816)
33	6GNG_A	Granule-bound starch sy	99.6	5.7E-15	1.2E-19	165.6	32.2	347	368-868	52-556 (612)
34	3OT5_B	UDP-N-acetylglucosamine	99.6	1.1E-15	2.2E-20	154.9	23.3	333	378-869	43-393 (403)
35	4HWG_A	UDP-N-acetylglucosamine	99.6	7.2E-16	1.5E-20	155.2	21.7	342	369-869	16-375 (385)
36	4X7R_B	TarM; Glycosyltransfera	99.6	7.7E-15	1.6E-19	162.3	31.8	283	429-869	204-492 (493)
37	5LQD_D	Alpha,alpha-trehalose-p	99.6	4.7E-15	9.6E-20	159.7	29.0	287	443-868	146-462 (465)
38	4HLN_A	Starch synthase I (E.C.	99.6	1.1E-14	2.2E-19	163.4	33.0	343	369-868	138-622 (633)
39	4PQG_A	Glycosyltransferase Gtf	99.6	4.5E-15	9.1E-20	160.2	28.8	285	427-868	203-505 (511)
40	5JIO_A	Alpha,alpha-trehalose-p	99.5	5.3E-15	1.1E-19	156.1	25.3	307	443-868	136-474 (487)
41	4L22_A	Phosphorylase (E.C.2.4.	99.5	2.8E-15	5.8E-20	176.9	25.4	298	442-868	269-754 (758)
42	5HVO_C	trehalose-6-phosphate p	99.5	4.5E-15	9E-20	160.5	24.7	285	443-868	141-474 (479)
43	3S2U_A	UDP-N-acetylglucosamine	99.5	3.4E-14	7E-19	138.8	27.3	316	372-868	13-355 (365)
44	4W6Q_A	Glcosyltransferase C; G	99.5	4.2E-14	8.4E-19	139.3	27.5	276	417-868	38-330 (333)
45	4NES_A	UDP-N-acetylglucosamine	99.5	3.5E-15	7.2E-20	147.7	20.0	332	367-868	5-361 (374)
46	4RBN_B	Sucrose synthase:Glycos	99.5	7.8E-14	1.6E-18	165.4	31.1	299	430-868	378-754 (794)
47	4AMG_A	SNOGD; TRANSFERASE, POL	99.5	3.9E-14	7.9E-19	140.7	23.7	322	372-869	33-400 (400)
48	3RHZ_B	Nucleotide sugar synthe	99.5	9.8E-14	2E-18	136.6	26.1	279	414-868	44-334 (339)
49	3IA7_A	CalG4; Glycosysltransfe	99.5	3.1E-14	6.3E-19	139.0	22.3	343	372-869	15-398 (402)
50	5W8X_A	Lipid-A-disaccharide sy	99.5	8.6E-14	1.7E-18	137.4	25.3	324	370-868	15-377 (382)
51	2P6P_B	Glycosyl transferase; C	99.4	2.5E-13	5E-18	134.3	27.3	319	372-868	11-378 (384)
52	2IUY_A	GLYCOSYLTRANSFERASE; GL	99.4	1.5E-13	3.1E-18	136.3	25.7	296	370-868	28-332 (342)
53	5VAF_B	Accessory Sec system pr	99.4	6.3E-14	1.3E-18	152.9	24.9	282	429-869	214-520 (533)
54	5V0T_B	Alpha,alpha-trehalose-p	99.4	7.6E-14	1.5E-18	152.3	25.2	303	429-868	116-465 (494)
55	1UQT_B	ALPHA, ALPHA-TREHALOSE-	99.4	1.1E-13	2.3E-18	150.2	26.2	300	430-868	111-451 (482)
56	4RIF_B	Glycosyl transferase ho	99.4	3.8E-14	7.8E-19	140.7	20.1	321	370-868	9-373 (379)
57	5DXF_A	trehalose-6-phosphate p	99.4	2.9E-13	5.8E-18	150.5	29.1	313	430-868	185-523 (534)
58	1F0K_A	E. COLI MURG (E.C. 2.4.	99.4	1.8E-12	3.6E-17	127.8	30.3	311	370-868	15-354 (364)
59	3TSA_A	NDP-rhamnosyltransferas	99.4	2.1E-13	4.3E-18	134.2	23.5	320	372-868	12-387 (391)
60	5HVL_B	trehalose-6-phosphate p	99.4	2.4E-13	4.8E-18	146.1	25.8	286	443-868	134-467 (478)
61	6INF_A	UDP-glycosyltransferase	99.4	5.4E-13	1.1E-17	133.6	26.2	332	373-867	24-454 (466)

62	3RSC_B	CalG2; TDP, enediyne, S	99.4	6.8E-13	1.4E-17	131.3	26.5	320	372-868	31-412 (415)
63	3NB0_C	Glycogen [starch] synth	99.4	1.8E-13	3.6E-18	158.6	25.4	287	429-868	164-630 (725)
64	5I45_A	Glycosyl transferases g	99.4	2.2E-13	4.4E-18	126.1	20.9	181	585-868	27-209 (218)
65	5ZFK_A	UDP-glucose:tetrahydrob	99.4	9.6E-13	1.9E-17	127.7	26.2	325	372-868	21-348 (354)
66	2HY7_A	Crystal Structure of Gu	99.4	3.9E-13	8E-18	137.4	24.7	258	429-867	103-373 (406)
67	2XCI_C	3-DEOXY-D-MANNO-2-OCTUL	99.4	5.3E-13	1.1E-17	138.5	25.6	312	376-868	53-374 (374)
68	5ZLR_A	NeuC protein; NeuC, UDP	99.4	5.2E-13	1.1E-17	132.2	24.0	315	376-868	18-364 (380)
69	3OTI_B	CalG3; Calicheamicin, T	99.3	6.1E-13	1.2E-17	131.7	21.7	323	370-868	29-396 (398)
70	5DU2_A	CalS8; glycosyltransfer	99.3	1.1E-12	2.3E-17	129.9	23.1	322	372-868	37-415 (419)
71	1L5W_A	MALTODEXTRIN PHOSPHORYL	99.3	2.1E-13	4.2E-18	162.7	21.2	346	429-868	277-791 (796)
72	4FZR_A	SsfS6; Structural Genom	99.3	4.4E-13	8.9E-18	132.7	19.6	319	372-866	26-397 (398)
73	3OTG_A	CalG1; Calicheamicin, T	99.3	3.3E-12	6.6E-17	129.3	24.4	324	370-868	29-407 (412)
74	4QLB_D	Probable glycogen [star	99.3	2.6E-12	5.4E-17	150.1	26.4	297	429-868	178-632 (674)
75	3HBJ_A	Flavonoid 3-O-glucosylt	99.3	1.8E-11	3.6E-16	124.1	28.6	328	378-868	30-452 (454)
76	2IYA_B	OLEANDOMYCIN GLYCOSYLTR	99.2	7.4E-12	1.5E-16	122.5	23.6	322	371-868	22-420 (424)
77	4X1T_A	Monogalactosyldiacylgly	99.2	3.8E-11	7.7E-16	120.7	27.5	324	372-868	17-384 (408)
78	2ACV_B	triterpene UDP-glucosyl	99.2	3.7E-11	7.5E-16	122.1	27.2	337	372-868	20-461 (463)
79	2YJN_A	GLYCOSYLTRANSFERASE, DT	99.2	2.5E-12	5.1E-17	129.2	18.4	323	372-869	31-435 (441)
80	2VSY_B	XCC0866; TRANSFERASE, G	99.2	1.9E-11	3.9E-16	135.3	26.9	326	371-868	217-556 (568)
81	3QHP_A	Type 1 capsular polysac	99.2	6.1E-12	1.2E-16	110.8	17.6	163	586-863	1-166 (166)
82	3WAD_B	Glycosyltransferase; GL	99.2	1.6E-11	3.2E-16	121.0	20.8	316	371-868	10-413 (419)
83	4ZHT_B	Bifunctional UDP-N-acet	99.2	2.4E-11	4.9E-16	124.2	22.7	268	429-868	92-374 (411)
84	2C4M_A	GLYCOGEN PHOSPHORYLASE	99.1	2.4E-11	4.9E-16	145.7	25.8	301	442-868	287-785 (796)
85	5DJS_B	Tetratricopeptide TPR_2	99.1	1.1E-10	2.2E-15	128.0	26.9	330	370-868	173-512 (529)
86	2GJ4_A	Glycogen phosphorylase,	99.1	2.6E-10	5.3E-15	137.7	30.3	295	442-868	318-813 (824)
87	5GL5_B	Sterol 3-beta-glucosylt	99.1	2.6E-10	5.3E-15	117.1	25.5	358	373-868	51-459 (498)
88	5E9T_D	Glycosyltransferase Gtf	99.0	6.5E-11	1.3E-15	129.3	21.3	230	475-869	215-446 (447)
89	2BFW_A	GLGA GLYCOGEN SYNTHASE	99.0	1.1E-10	2.2E-15	106.4	18.7	161	585-856	34-200 (200)
90	4LDP_B	NDP-forosamyltransferas	99.0	9.3E-11	1.9E-15	118.1	19.7	323	372-868	27-440 (455)
91	3Q3E_A	HMW1C-like glycosyltran	99.0	2.3E-10	4.7E-15	132.2	24.2	279	425-868	330-624 (631)
92	4BQE_B	ALPHA-GLUCAN PHOSPHORYL	99.0	5.5E-10	1.1E-14	136.0	28.0	315	442-868	364-865 (874)
93	1YGP_A	YEAST GLYCOGEN PHOSPHOR	99.0	5.2E-10	1.1E-14	136.0	27.6	304	439-868	354-872 (879)
94	3H4T_A	Glycosyltransferase Gtf	98.9	2.7E-10	5.5E-15	112.9	17.6	320	373-868	12-381 (404)
95	4REL_A	UDP-glucose:anthocyanid	98.9	3.2E-09	6.4E-14	108.3	24.5	332	378-868	21-443 (446)
96	4BFC_A	3-DEOXY-D-MANNO-OCTULOS	98.8	9E-10	1.8E-14	105.4	18.2	180	586-869	40-232 (235)
97	2F9F_A	first mannosyl transfer	98.8	9.1E-10	1.8E-14	100.5	17.2	157	582-849	18-175 (177)
98	5V2J_A	UDP-glycosyltransferase	98.8	4.5E-09	9.1E-14	106.2	23.7	330	376-868	20-446 (449)
99	5LR8_A	Hv_Pho1 (E.C.2.4.1.1);	98.8	2.8E-09	5.6E-14	130.9	25.4	241	494-868	527-917 (938)
100	6FJ3_A	Parathyroid hormone/par	98.8	1.5E-09	3.1E-14	121.6	20.9	174	585-868	353-532 (602)
101	4M83_A	Oleandomycin glycosyltr	98.8	2.1E-08	4.3E-13	103.3	25.6	318	378-868	24-398 (415)
102	1IIR_A	glycosyltransferase Gtf	98.7	2.8E-09	5.7E-14	105.8	16.5	313	373-868	12-398 (415)
103	1RRV_A	GLYCOSYLTRANSFERASE GTF	98.7	1.5E-08	3.1E-13	101.6	20.7	316	373-869	12-400 (416)
104	6IJ7_A	Rhamnosyltransferase pr	98.6	1.4E-07	2.8E-12	95.8	26.8	281	429-868	102-433 (435)
105	6BK0_A	UDP-glycosyltransferase	98.6	1.4E-07	2.8E-12	96.1	25.7	323	378-868	32-465 (467)
106	2VCH_A	HYDROQUINONE GLUCOSYLTR	98.3	7.9E-06	1.6E-10	84.3	28.7	340	373-868	18-467 (480)
107	3HBM_A	UDP-sugar hydrolase; ud	98.2	4.3E-07	8.7E-12	89.2	17.0	254	377-777	23-281 (282)
108	2PQ6_A	UDP-glucuronosyl/UDP-gl	98.0	1.6E-05	3.2E-10	81.4	22.3	333	378-868	25-477 (482)
109	2C1X_A	UDP-GLUCOSE FLAVONOID 3	97.6	0.00018	3.7E-09	74.3	21.4	284	429-868	95-450 (456)
110	5WQC_A	Orexin receptor type 2,	97.1	0.00055	1.1E-08	76.6	18.4	169	585-863	291-464 (560)
111	2O6L_B	UDP-glucuronosyltransfe	96.5	0.0036	7.2E-08	56.3	12.4	144	584-850	19-168 (170)
112	3L7I_A	Teichoic acid biosynthe	96.4	0.0077	1.6E-07	70.8	16.8	350	355-833	317-725 (729)
113	5U09_A	Cannabinoid receptor 1,	96.0	0.044	8.8E-07	61.4	18.2	177	585-870	243-424 (508)
114	5ZIC_A	Alpha-1,6-mannosylglyco	95.9	0.014	2.8E-07	69.0	13.7	157	585-873	226-407 (523)
115	1PSW_A	ADP-HEPTOSE LPS HEPTOSY	95.3	0.13	2.6E-06	52.7	14.8	166	585-831	179-348 (348)
116	5GVV_A	Glycosyl transferase fa	95.3	0.023	4.6E-07	62.2	9.9	111	606-778	289-401 (406)
117	2GT1_A	Lipopolysaccharide hept	94.9	0.16	3.3E-06	51.5	13.4	145	585-831	177-325 (326)
118	3TOV_B	Glycosyl transferase fa	94.4	0.24	4.8E-06	50.6	12.3	113	585-760	184-299 (349)
119	6JTD_A	C-glycosyltransferase;	92.6	1.7	3.5E-05	46.2	14.0	166	585-868	273-476 (483)
120	5NLM_B	indoxyl UDP-glucosyltra	90.1	8.9	0.00018	40.9	15.2	167	585-868	273-474 (478)
121	6MGB_A	Capsular polysaccharide	87.7	4.1	8.4E-05	43.9	10.4	102	584-746	153-262 (326)
122	5IJO_T	Nuclear pore complex pr	85.2	31	0.00064	41.9	16.5	192	129-377	322-515 (522)
123	6HLP_A	Substance-P receptor,Su	84.5	21	0.00043	40.1	13.9	177	585-870	256-437 (520)
124	6MGC_A	Capsule polysaccharide	83.7	5.7	0.00012	43.7	8.9	101	585-746	147-255 (361)
125	1JIX_A	DNA BETA-GLUCOSYLTRANSF	76.1	8.9	0.00018	43.9	6.9	108	696-855	229-345 (351)
126	6MGD_A	Capsular polysaccharide	66.3	30	0.00061	37.7	7.9	99	585-746	151-259 (332)
127	4RAP_I	Glycosyltransferase Tib	57.6	2.3E+02	0.0047	31.7	12.8	169	585-828	215-389 (406)
128	5IJO_G	Nuclear pore complex pr	57.6	1.2E+02	0.0024	37.8	11.3	178	121-308	241-431 (599)
129	5FA1_A	Cell division protein Z	56.1	57	0.0012	37.3	8.0	91	585-746	219-316 (410)
130	2JZC_A	UDP-N-acetylglucosamine	53.1	2.4E+02	0.0049	30.3	11.5	120	568-748	10-160 (224)

131	4UXV_A	SEPTATION RING FORMATIO	50.5	5.5E+02	0.011	29.9	14.6	150	138-328	361-515 (545)
132	2KS6_A	UDP-N-acetylglucosamine	49.7	1.8E+02	0.0036	30.6	9.6	108	582-750	1-139 (201)
133	5XEI_A	Chromosome partition pr	43.5	7.5E+02	0.015	28.8	21.8	316	136-481	161-482 (540)
134	5ZIB_A	Alpha-1,6-mannosylglyco	42.1	54	0.0011	40.7	5.1	49	697-748	374-423 (626)
135	4P5E_B	2'-deoxynucleoside 5'-p	36.7	3.1E+02	0.0063	25.7	8.2	80	625-746	1-99 (152)
136	5NPS_A	UDP-N-acetylglucosamine	35.2	1.7E+02	0.0034	37.3	7.7	105	590-749	519-625 (718)
137	6QAI_B	deoxyribosyltransferase	34.6	5.5E+02	0.011	24.5	10.1	83	624-746	3-99 (156)
138	3EHD_A	uncharacterized conserv	33.2	4.8E+02	0.0097	24.8	9.0	82	624-746	2-102 (162)
139	4UX3_A	STRUCTURAL MAINTENANCE	32.9	1.2E+03	0.025	28.0	22.5	328	128-482	140-492 (543)
140	6EK8_A	YaxB; pathogens, pore f	25.7	8.4E+02	0.017	27.8	10.6	107	138-244	147-255 (344)
141	6CFZ_H	Ask1, Dad3, Dad2, Duo1,	25.4	1.3E+02	0.0027	26.3	3.4	35	273-308	8-42 (56)
142	5AX7_A	Pyruvyl transferase 1;	23.8	1.3E+03	0.026	25.1	18.0	227	414-746	68-300 (348)
143	3U4Q_B	ATP-dependent helicase/	22.8	1.9E+03	0.039	27.8	13.8	205	215-429	383-615 (1166)
144	3ILW_A	DNA gyrase subunit A (E	21.2	1E+03	0.02	28.1	10.4	155	232-392	298-463 (470)
145	5J0J_A	designed protein 2L6HC3	21.0	7.8E+02	0.016	22.7	7.2	68	139-217	9-76 (79)
146	2KE4_A	Cdc42-interacting prote	20.2	9.1E+02	0.018	22.6	8.0	79	147-225	13-91 (98)

Chapter 3 - Intrabacterial regulation of a cytotoxic effector by its cognate metaeffector promotes *Legionella pneumophila* virulence

Deepika Chauhan[1,2], Ashley M. Joseph[1], Peter McDonald[4], Anuradha Roy[4], Stephanie R. Shames[1,3]

[1] Division of Biology, Kansas State University, Manhattan, KS, USA
[2] College of Veterinary Medicine, Kansas State University, Manhattan, KS, USA
[3] Microbiology and Molecular Genetics, Michigan State University, East Lansing, MI, USA
[4] High-Throughput Screening Laboratory, University of Kansas, Lawrence, KS, USA

Author Contributions

Ashley M. Joseph
- SidI translocation (Figure 1)
- *In vitro* growth curve (Figure 4C)
- MesIΔ10 phenotype (Figure 3C & Figure 6)*
- Degraded & LAMP1 positive bacteria scoring (Figure 7)
- Chemical Inhibitor screening (Figures 8, 9, 10)
- Writing (Figures 1, 4C, 7-10, Editing*, Chemical Inhibitors Content)

Deepika Chauhan
- SidI overexpression (Figure 2)*
- Development of chromosomal inducible strains (Figure 3 A + B, Figure 4 A + B)*
- Live/Dead Staining (Figure 5)*
- Host cell viability (Supplemental Figure 1)*
- Writing & Editing*

Anuradha Roy and Peter McDonald
- High Throughput Small Molecule Screen (Data not shown)

Stephanie R. Shames
- Conceptualization, Writing & Editing*, Figure Formatting*, Funding

* Parts of this chapter have been published to BioRxiv as a pre-print (257). The copyright holder for the pre-print (which was not certified by peer review) is the author/funder, who granted bioRxiv a license to display the preprint in perpetuity.

ABSTRACT

Legionella pneumophila is a natural pathogen of unicellular protozoa that can opportunistically infect macrophages and cause Legionnaires' Disease. Intracellular replication is driven by hundreds of bacterial effector proteins that are translocated into infected host cells by a Dot/Icm type IV secretion system. *L. pneumophila* effectors are temporally regulated in part by a family of translocated regulatory effectors, termed metaeffectors, which bind and modulate the function of a cognate effector in host cells. We discovered that regulation of the cytotoxic effector SidI by its metaeffector, MesI, is critical for *L. pneumophila* virulence in natural and opportunistic hosts. MesI binds and negatively regulates SidI activity *in vitro* but how dysregulation of SidI impairs *L. pneumophila* intracellular replication is unclear. Using a chromosomally-encoded inducible expression system, we discovered that dysregulation of SidI, via loss of MesI, was toxic to *L. pneumophila*. SidI enzymatic activity was required for toxicity since *L. pneumophila* growth was unaffected by induced expression of a catalytically inactive *sidI* allele. We found MesI translocation into host cells was dispensable for intracellular replication and that MesI-deficient bacteria were rapidly degraded within host cells despite low colocalization with LAMP1. Finally, the possibility of exploiting SidI cytotoxicity through small molecule interruption of MesI was explored and a compound capable of attenuating intracellular replication of wild type *L. pneumophila*, but not a strain lacking *sidI-mesI* in *A. castellanii* was identified. Together, our data suggest a unique role for intrabacterial effector regulation by a translocated metaeffector in *L. pneumophila* virulence and demonstrate the potential to target metaeffectors for the development of novel therapeutics.

INTRODUCTION

The development of anti-virulence drug treatments is an emerging trend to combat the emergence of multi-drug resistant pathogens (258). Their development relies on the identification of essential pathogen virulence mechanisms that can be targeted with small molecule inhibitors. Many pathogens use secretion systems and effector proteins to successfully infect their host, making these virulence factors a prime target for anti-virulence drugs. The Gram-negative, extracellular pathogen, *Pseudomonas aeruginosa*, encodes six Type III secretion system (T3SS) effectors and chaperones that are central for pathogen success (259). The effector, Exoenzyme S (ExoS) is a bi-functional enzyme with GTPase-activating and ADP ribosyltransferase activity. The small molecule inhibitor, exosin and two analogs, have been found to modulate ExoS ADP-ribosyltransferase activity *in vitro* and provided significant protection against *P. aeruginosa* infection *in vivo* (260). *Chlamydia trachomatis*, is a Gram-negative, obligate intracellular pathogen that uses a T3SS to translocate effectors into the host cytosol. The inhibitor INP0400, which inhibits translocation of T3SS effectors in the facultative intracellular pathogen, *Yersinia pseudotuberculosis*, was found to be similarly effective against *C. trachomatis* effector translocation (261–263).

Legionella pneumophila is a Gram-negative, facultative intracellular pathogen that infects phagocytic cells. It is a natural environmental pathogen, replicating within free-living amoeba, but gained recognition after it emerged as a human pathogen. When inhaled, *L. pneumophila* replicates within immune macrophages, causing a severe form of pneumonia known as Legionnaires' Disease (LD) and the less severe Pontiac Fever, collectively referred to as legionellosis (264). Critical to its survival intracellularly is the translocation of over 300 effector proteins directly into the host cell (48, 219). Effector proteins modify host cell components to

promote a permissive host and allow for the establishment of a replication niche known as the *Legionella* containing vacuole (LCV) (4, 133, 147, 235). Successful construction of the LCV and propagation intracellularly relies on the tight regulation of effector function. A subset of effectors known as metaeffectors, regulate the activity of other effectors within the host cell (126, 138, 145, 157).

The metaeffector, MesI is critical for *L. pneumophila* replication in bone-marrow derived macrophages (BMDM), *Acanthamoeba castellanii*, and the mouse model of LD, but only in the presence of its target, SidI (162). SidI is a cytotoxic glycosyl hydrolase that inhibits mRNA translation (101, 157) (Chapter 2). MesI binds SidI with high affinity and blocks SidI-mediated translation inhibition *in vitro* (157). The requirement for MesI is relieved when *sidI* is deleted (Δ*sidI*); however, a single amino acid substitution that renders SidI non-toxic and catalytically inactive (R453P) is also sufficient to restore replication of *mesI*-deficient *L. pneumophila* (162). These data have provided key biochemical insights into the regulatory mechanism of MesI but how MesI regulation of SidI promotes intracellular replication is still unclear.

In this study, our lab made the surprising discovery that MesI promotes *L. pneumophila* virulence by regulating SidI intrabacterially. Overexpression of *sidI* was toxic to *L. pneumophila* when uncoupled from MesI *in vitro*. Additionally, MesI translocation was dispensable for *L. pneumophila* intracellular replication and *mesI*-deficient bacteria were rapidly degraded in host cells despite low colocalization with the lysosome associated membrane protein (LAMP1). These data suggest a unique and important role for interkingdom effector regulation in *L. pneumophila* virulence (257).

Following up on this discovery, small molecules were evaluated for their ability to inhibit MesI and imitate the lethal SidI phenotype during *in vitro* and intracellular growth. An initial

screen of 30,000 compounds was performed by the High-Throughput Screening Laboratory at the University of Kansas. In collaboration, compound 5641-1803 was found to inhibit the growth of wild-type *L. pneumophila*, but not strains lacking *sidI* and *mesI, in vitro* and during intracellular replication in *A. castellanii.* These findings not only serve as a basis for the development of novel anti-virulence treatments options for legionellosis but provides valuable insight into the mechanism of effector regulation.

RESULTS

MesI affects SidI translocation into host cells at later timepoints. Previous findings from our lab demonstrated that deletion of *mesI* does not affect SidI translocation into the host cell during early infection (157).These results contrast with those of McCloskey and colleagues who found that deletion of *mesI* resulted in decreased levels of SidI in the host cell three hours post infection (265). These contradictory findings could be an artifact of differing methodologies used to evaluate translocation. Our lab utilized *Bordatella pertussis* adenylate cyclase (CyaA) fusion proteins to quantify increases in cAMP production corresponding to effector translocation in infected cells (157, 223). Adenylate cyclase is an enzyme that catalyzes the conversion of ATP into cAMP. Its activity is dependent on the molecule, calmodulin, which is only present in eukaryotic cells and is therefore only active in eukaryotic cells (266, 267). Thus cAMP production can be used as a proxy for CyaA-fusion protein translocation. McCloskey and colleagues utilized a saponin solubilization assay, analyzed by western blot and densitometry to assess SidI secretion into host cells (265). Another metaeffector, LubX, regulates the translocation of its target effector, SidH during late stages of infection (8 hours), but this is not evident at 1 hour post infection (139). Thus, we investigated the effects of *mesI* on SidI

translocation during late stages of infection. Chinese hamster ovary (CHO) cells ectopically expressing the FcγRII opsonic receptor were infected with opsonized *L. pneumophila* wild-type, Δ*sidI-mesI* (Δ*operon*) or *ΔdotA* strains expressing CyaA-SidI$_{R453P}$ or CyaA-LegC4 for 1- and 8-hours. Since deletion of *dotA* prevents effector translocation, these samples represent levels of cAMP in the host cell unrelated to effector translocation (208, 209). In agreement with our previous findings, there was no difference in SidI translocation with and without *mesI* at 1-hour post infection. Interestingly, translocation of SidI decreased at 8-hours post infection in strains expressing MesI but remained constant throughout infection in strains lacking *mesI* (Fig. 3.1). Therefore, MesI temporally regulates SidI translocation into the host cell, supporting a role for MesI within the bacteria.

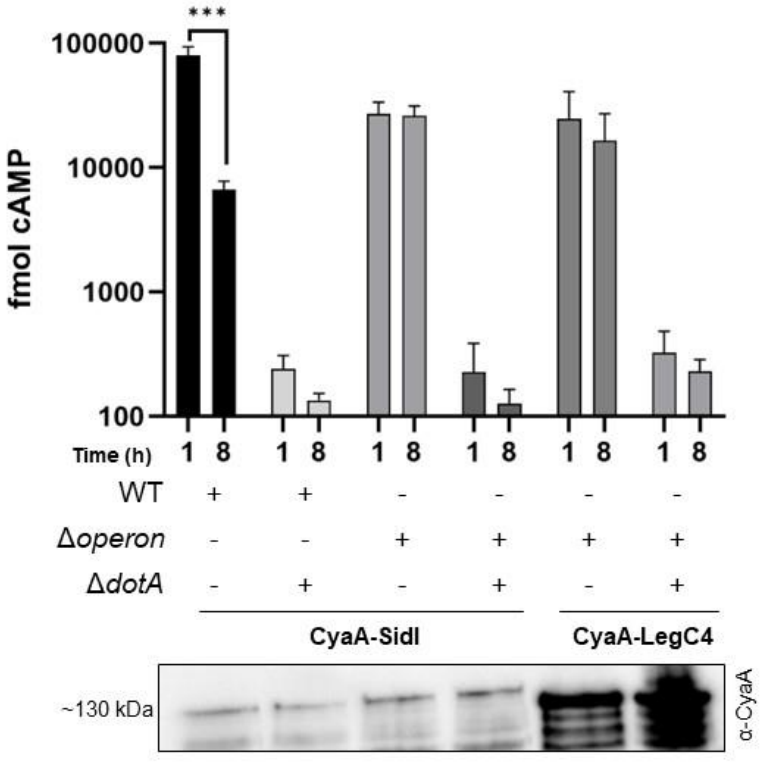

Figure 3.1 *mesI* affects SidI translocation into host cells during late infection

Quantification of cAMP extracted from CHO FcγRII cells infected with the indicated *L. pneumophila* strains. The asterisks denote statistical significance by t test (***, $P < 0.001$). Protein expression was confirmed via CyaA western blot (lower panel). The data are representative of the results of two independent experiments and expressed as means and SD of samples in triplicate.

Overexpression of *sidI* impairs *L. pneumophila* growth *in vitro.* We discovered that the *L. pneumophila* metaeffector MesI promotes bacterial intracellular replication by regulating its cognate effector SidI (162). Our translocation data supports a role for MesI in the bacterial cell but how SidI dysregulation attenuates *L. pneumophila* virulence is unclear. A *L. pneumophila* Δ*mesI* mutant is impaired for intracellular replication but virulence is restored by *sidI* chromosomal deletion (Δ*sidI*Δ*mesI*) or catalytic inactivation (*sidI*$_{R453P}$Δ*mesI*). We validated that dysregulation of SidI impairs *L. pneumophila* intracellular replication by plasmid-based genetic complementation of the Δ*sidI* mutation. We infected primary bone marrow-derived macrophages (BMDMs) from *Nlrc4*$^{-/-}$ mice, which are permissive to flagellated *L. pneumophila* (191, 268). Indeed, induced expression of *sidI* from a complementing plasmid severely attenuated *L. pneumophila* replication within BMDMs (Fig 3.2A). Interestingly, we had to induce *sidI* expression at the time of infection since we were unable to culture *L. pneumophila* Δ*sidI*Δ*mesI* (p*sidI*) on inducing media. Inducible plasmid-based genetic complementation is an established technique to fulfill molecular Koch's postulates and we routinely culture *L. pneumophila* on inducing media (157, 162, 269–271). We hypothesized that overexpression of SidI adversely affects bacterial physiology. Indeed, *L. pneumophila* harboring p*sidI* was unable to replicate in broth under inducing conditions but not in the absence of induction (Fig 3.2B). Impaired growth resulted from SidI enzymatic activity since induced the catalytically inactive sidI$_{R453P}$ allele did not affect *L. pneumophila* growth (Fig 3.2B).

Our initial interpretation was that dysregulation of SidI does not adversely affect *L. pneumophila* physiology since *L. pneumophila* Δ*mesI* is not attenuated for growth in vitro (162). However, *sidI* expression in broth grown bacteria is ~ 3-fold lower than expression during intracellular replication (49), which may be insufficient to impair *L. pneumophila* growth. Induced expression of an effector gene has not previously been associated with impaired bacterial growth and these data suggest that SidI enzymatic activity is deleterious to *L. pneumophila* when stoichiometrically uncoupled from MesI.

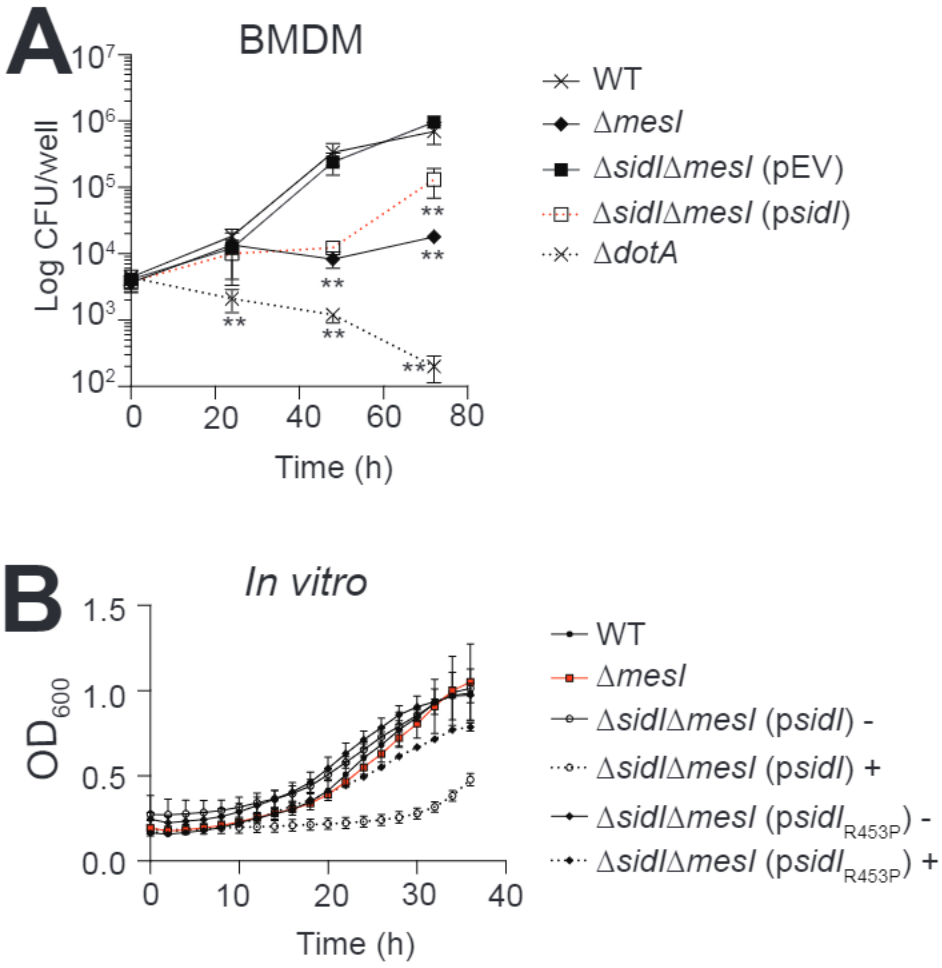

Figure 3.2 Overexpression of *sidI* attenuates *L. pneumophila* replication.

(A) Fold replication of L. pneumophila strains within *Nlrc4*$^{-/-}$ BMDMs over 72 h. Where indicated, infections were performed in the presence of 1 mM IPTG. Data shown are mean ± s.d. on samples in triplicates and asterisks denote statistical significance by Students' t-test

(**P<0.01). (B) Optical density at 600 nm (OD_{600}) of *L. pneumophila* strains grown in AYE broth. Where indicated, bacteria were grown in the presence (+) or absence (-) of 1 mM IPTG. Data shown are mean ± s.d. on samples in triplicates and asterisks denote statistical significance by Students' t-test (**P<0.01). Data shown are representative of at least three independent experiments. Reproduced from (257).

MesI rescues the SidI-mediated growth defect *in vitro*. MesI suppresses SidI toxicity in yeast (162) and our translocation data supports a role for MesI in the bacteria; thus, we hypothesized that MesI also suppresses SidI toxicity in *L. pneumophila*. To test this hypothesis, we generated *L. pneumophila* strains that enable tightly controlled inducible expression of the *sidI-mesI* locus from its endogenous position in the chromosome. We inserted the araC araBAD (araBAD) promoter and an in-frame 3xflag epitope tag directly upstream of *sidI* in the chromosome of WT, Δ*mesI*, and $sidI_{R453P}$Δ*mesI L. pneumophila* strains (Fig 3.3A). Kinetics and abundance of 3xFLAG-SidI fusion protein production was consistent between strains and only observed under arabinose-inducing conditions (Fig 3.3B). We observed a tightly controlled increase in araBAD-mediated *sidI* expression relative to endogenous levels (Fig 3.3C). The ~4-fold increase in *sidI* expression from the araBAD promoter is more physiologically relevant than the >10-fold increase in expression from the Ptac promoter (Fig 3.3C) (49). Thus, we have established *L. pneumophila* strains in which we can control expression of *sidI* and *mesI* in their native stoichiometry and endogenous locus in the chromosome. We leveraged our *L. pneumophila* araBAD strains (Fig 3.3A) to test the hypothesis that stoichiometric production of MesI abrogates SidI-mediated growth attenuation. We quantified replication our *L. pneumophila* araBAD strains under inducing and non-inducing conditions and found that induced expression of *sidI*, but not the inactive $sidI_{R453P}$ allele, significantly attenuated bacterial growth only when uncoupled from *mesI* in broth culture (Fig 3.4A) and within BMDMs (Fig 3.4B).

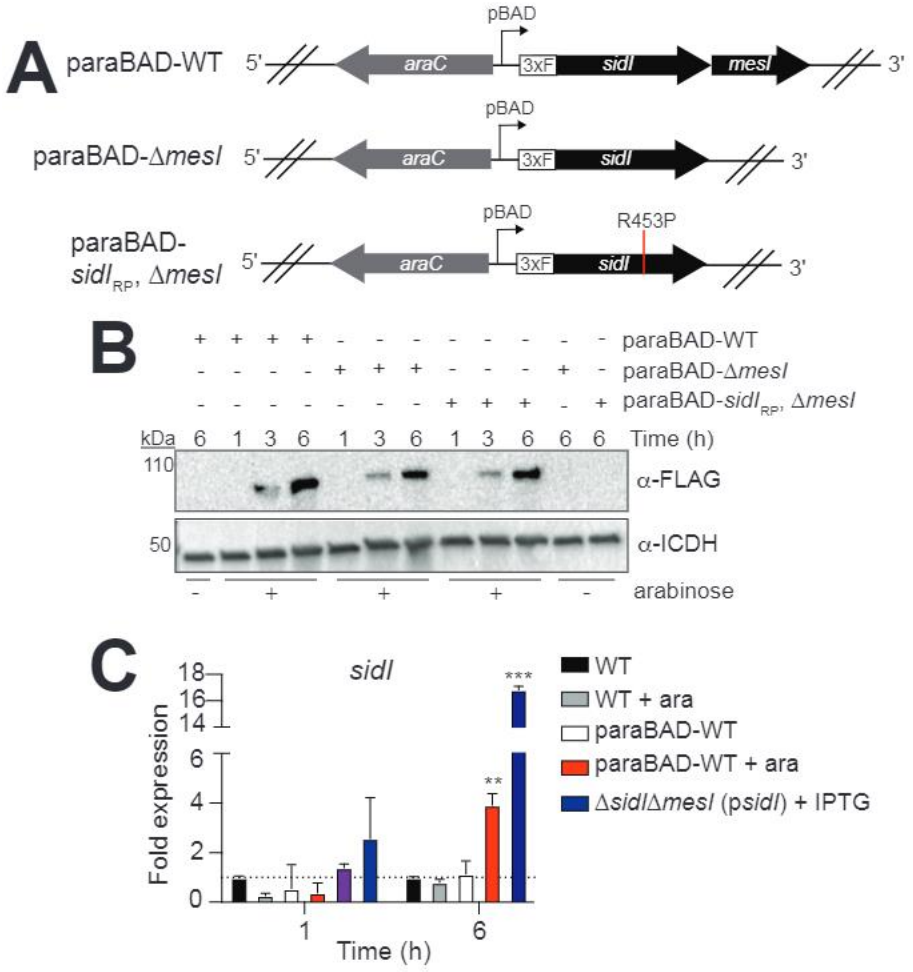

Figure 3.3. Establishment of a chromosomal arabinose-inducible expression system in *L. pneumophila.*

(A) Schematic showing paraBAD insertion upstream of the sidI locus in the L. pneumophila chromosome. 3XF: In-frame 3xflag epitope tag. (B) Western blot showing 3xFLAG-SidI production in the indicated paraBAD strains in the presence (+) or absence (-) of arabinose [ara; 0.6% (w/v)] after growth in AYE broth for 1, 3, or 6 h. (C) Quantitative RT-PCR for expression of sidI grown for 1 or 6 h in AYE broth. Fold expression in OD-normalized cultures (n = 3) was calculated relative to wild-type L. pneumophila at each time point. Asterisks denote statistical significance by Students' t-test (**P<0.01) on samples in triplicates. Data are representative of at least two independent experiments. Reproduced from (257).

MesI suppresses SidI intrabacterial toxicity. SidI impairs *L. pneumophila* growth, but it is unclear whether SidI is bacteriostatic or bactericidal. SidI is toxic to yeast (101); thus, we tested the hypothesis that SidI is bactericidal when uncoupled from MesI. *L. pneumophila* araBAD

strains (Fig 3.3A) were grown for 24 h under arabinose inducing or non-inducing conditions in broth and viability was evaluated using LIVE/DEAD viability staining and confocal microscopy (Fig 3.5). Very few dead bacteria were observed under non-inducing conditions or when induced *sidI* expression was coupled with *mesI* (araBAD-WT) (Fig 3.5). However, significantly more dead bacteria were observed when enzymatically active *sidI* was uncoupled from *mesI* under inducing conditions (Fig 3.5).

To further test that our findings were due to bacterial cell death, we repeated the *in vitro* growth curve with plating to quantify viable bacteria. Cultures of araBAD *ΔmesI* were allowed to grow for 24-hours before half were induced. All cultures grew normally for the first 24-hours under non-inducing conditions. After 24-hours, bacteria grown under inducing conditions began to decline, while those left in non-inducing conditions continued to replicate (Fig 3.5C). Thus, the decreased growth observed in the absence of *mesI* is due to bacterial cell death.

Intrabacterial regulation of SidI by MesI is sufficient for *L. pneumophila* virulence. Based on our observation that SidI is toxic to *L. pneumophila* when uncoupled from MesI, we hypothesized that MesI intrabacterial regulation of SidI is sufficient for *L. pneumophila* virulence. We tested this by evaluating whether an intrabacterially-retained MesI mutant could complement the Δ*mesI* mutation. We generated an allele of *mesI* lacking 10 amino acids from its extreme carboxy terminus; these amino acids are dispensable for SidI binding and contains the putative E-block Dot/Icm translocation signal (46, 222). We cloned this allele into a complementing plasmid downstream of a 3xflag epitope tag (p*mesI*Δ10). We were unable to express a CyaA-tagged *mesI*Δ10 in *L. pneumophila*. We instead opted to evaluate 3xFLAG-MesIΔ10 secretion using Western blot to visualize its abundance in saponin-soluble or -insoluble lysate fractions from *L. pneumophila* infected cells, a technique routinely used to evaluate

effector secretion, since saponin solubilizes eukaryotic membranes but minimally lyses *L. pneumophila* (146, 272). HEK293 FcgRII cells were infected with antibody-opsonized *L.*

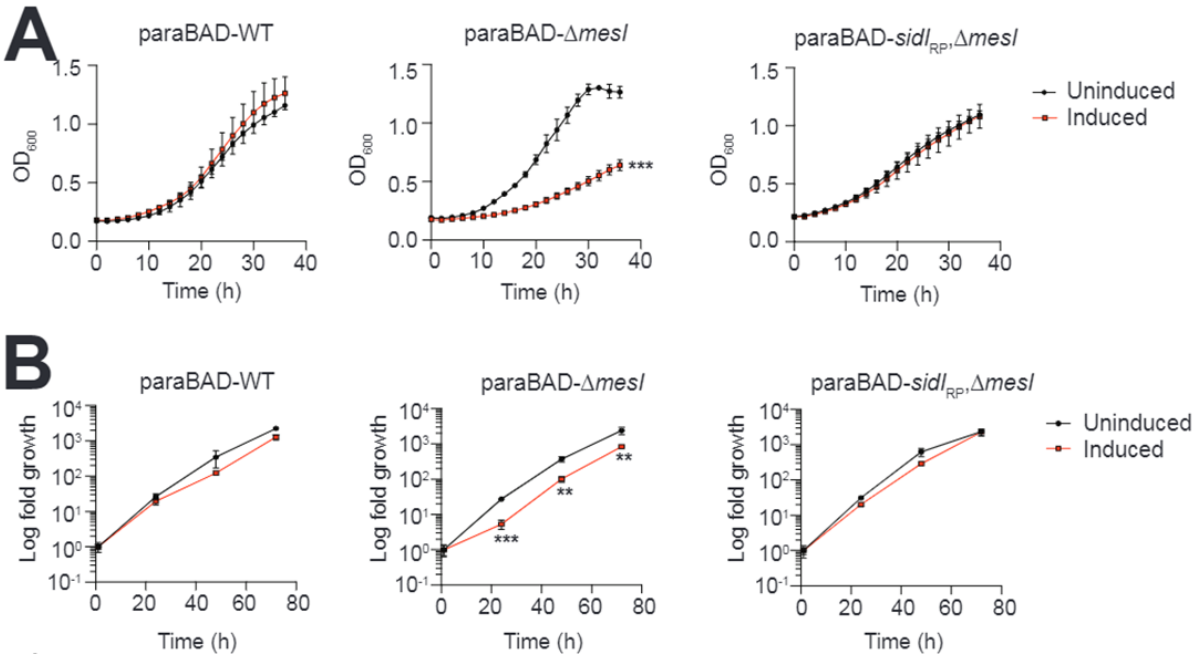

Figure 3.4. SidI impairs *L. pneumophila* growth when uncoupled from MesI.

(A) Replication of the *L. pneumophila* paraBAD strains grown in AYE broth *in vitro* under inducing [1% arabinose (w/v)] or noninducing conditions. Data shown are mean ± s.d. OD_{600} values from samples in triplicates and asterisks denote statistical significance by Students' t-test (**P<0.01). (B) Fold replication of *L. pneumophila* strains within *Nlrc4*$^{-/-}$ BMDMs under inducing [2% arabinose (w/v)] or noninducing conditions. Data shown are mean ± s.d. on samples in triplicates and asterisks denote statistical significance by Students' t-test (**P<0.01). Data shown are representative of at least three independent experiments. Reproduced (257).

---

pneumophila harboring either p*mesI* or p*mesI*Δ10. 3xFLAG-MesIΔ10 was not translocated since it was retained in the insoluble fraction (pellet) and not present in saponin-soluble lysate fractions (Fig 3.6A). As expected, wild-type MesI was secreted into host cells since it was present within saponin-soluble lysate fractions (Fig 3.6A). Isocitrate dehydrogenase (ICDH) and β-actin were used as bacterial lysis and loading controls, respectively. We also confirmed that MesIΔ10 interacts with SidI since it was retained by SidI on beads similarly to full-length MesI (Fig 3.6C). To evaluate a role for intrabacterial SidI regulation by MesI in *L. pneumophila*

virulence, we tested whether the *mesI*Δ10 allele genetically complements that Δ*mesI* mutation. We infected BMDMs and quantified replication of wild-type *L. pneumophila* and Δ*mesI* strains harboring p*mesI*, p*mesI*Δ10, or empty plasmid vector (pEV). We were able to genetically complement the Δ*mesI* with the *mesI*Δ10 allele, demonstrating that MesI translocation into host cells is not necessary for *L. pneumophila* intracellular replication (Fig 3.6B). These data suggest that intrabacterial regulation of SidI by MesI is sufficient for *L. pneumophila* virulence.

***mesI*-deficient bacteria are degraded within host cells.** We found that MesI suppresses intrabacterial SidI toxicity and that MesI translocation into host cells is dispensable for *L. pneumophila* intracellular replication. Since SidI is also toxic to eukaryotic cells, we initially postulated that the virulence defect associated with loss of MesI results from SidI toxicity in host cells. However, we were unable to detect SidI-mediated cytotoxicity in *L. pneumophila*-infected BMDMs (Figure S1) and our new data suggest a potential role for MesI suppression of

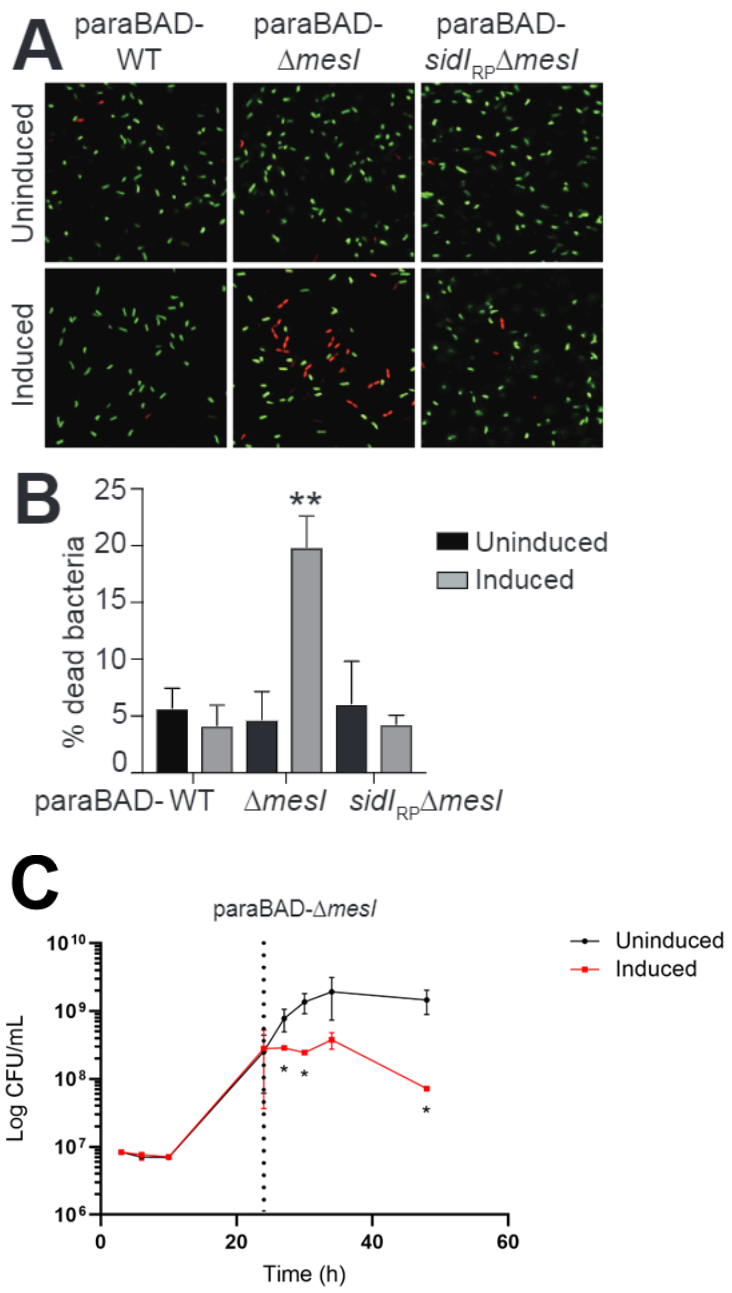

Figure 3.5. SidI is bactericidal in the absence of MesI.

Representative confocal micrographs of Live/Dead-stained *L. pneumophila* paraBAD strains grown in AYE broth under inducing [0.6% arabinose (w/v)] or noninducing conditions [SYTO9 (live; green) and propidium iodide (PI; dead; red)]. (B) Quantification of dead *L. pneumophila* by fluorescence microscopy following Live/Dead staining. Percent dead bacteria was calculated by dividing PI-stained cells by total cells. Data are mean ± s.d. of 650 cells scored blind and asterisks denote statistical significance by Students' t- test (**P<0.01). Data are representative of two independent experiments. (C) Log replication of *L. pneumophila* paraBAD-Δ*mesI* under inducing [1% arabinose (w/v)] or non-inducing conditions. Data shown are mean ± s.d. on

samples in triplicates and asterisks denote statistical significance by Students' t-test (*P<0.05). Data shown are representative of two independent experiments. A + B reproduced from (257).

---

intrabacterial SidI toxicity in *L. pneumophila*'s virulence strategy. Dead and dying bacteria are rapidly degraded within host lysosomes; thus, we rational1ized that *mesI*-deficient bacteria would be robustly degraded within host cells. Degraded *L. pneumophila* are easily identified using immunofluorescence microscopy since they have lost their rod shape and appear instead as diffuse puncta when cells are stained with a *Legionella*-specific antibody (36, 143). Thus, we used immunofluorescence microscopy and blinded scoring to quantify degradation of *L. pneumophila* Δ*mesI* within BMDMs. We infected BMDMs and compared kinetics of *L. pneumophila* Δ*mesI* degradation to virulent *L. pneumophila*, a *mesI*-complemented strain (Δ*mesI*/ 3F-*mesI*) and Δ*dotA*, which is unable to evade lysosomal degradation (208). After 1-hour of infection, most bacteria retained their rod shape and there were no differences between *L. pneumophila* strains; however, at 8-hours post infection, significantly more *L. pneumophila* Δ*mesI* were degraded compared to wild-type, complement and Δ*dotA* control strains (Fig 3.7B). It is unlikely that bacterial degradation was accompanied by host cell death since macrophages harboring degraded bacteria had normal nuclear morphology (Fig 3.7A). The robust degradation of *L. pneumophila* Δ*mesI* compared to the avirulent Δ*dotA* strain suggests a mechanism of bacterial attenuation distinct from the inability to subvert endocytic maturation.

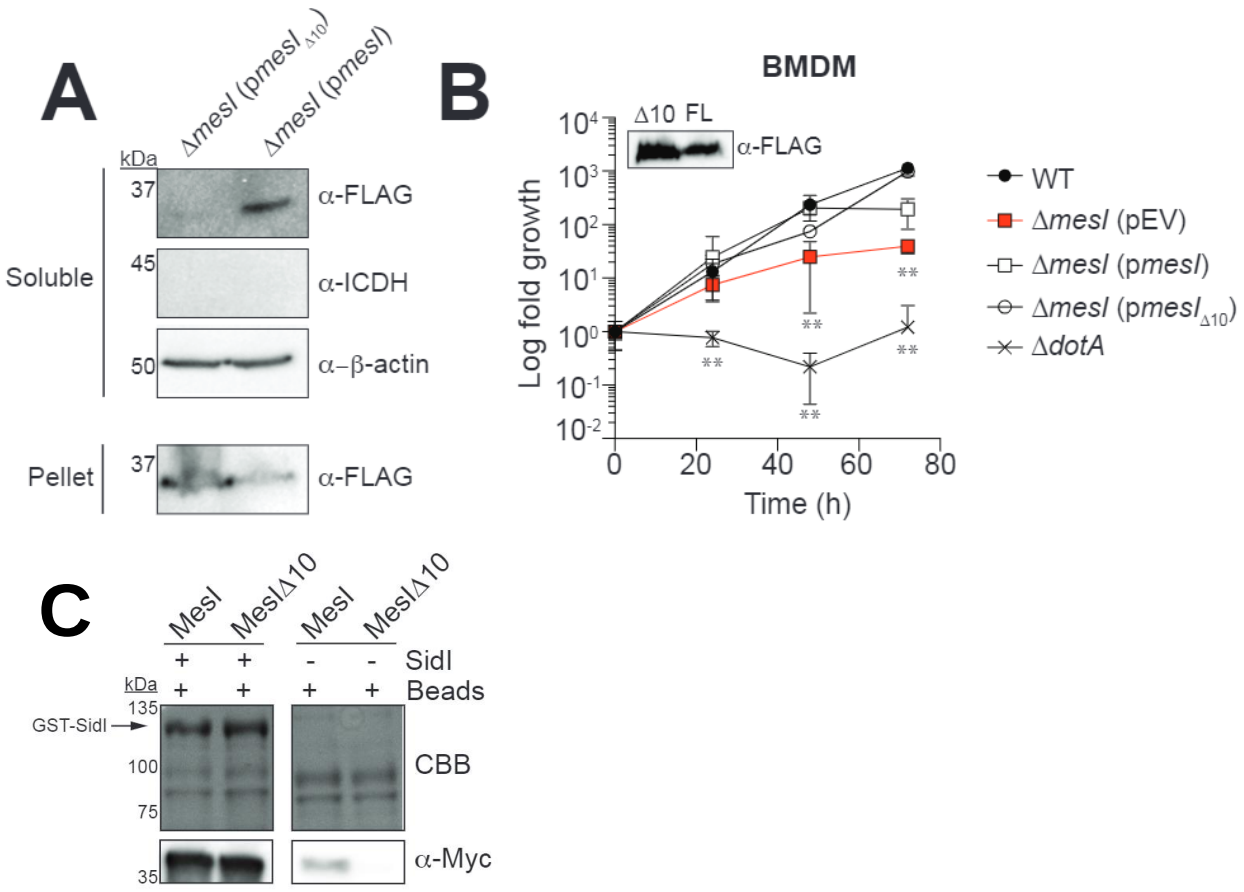

Figure 3.6. MesI translocation is dispensable for *L. pneumophila* intracellular replication.

(A) Western blot for 3xFLAG-MesI fusion proteins in saponin-solubilized lysates of HEK293 FcγRII cells infected with antibody-opsonized L. pneumophila Δ*mesI* harboring p*mesI* (3xFLAG-MesI) or p*mesI*Δ10 (3xFLAG-MesIΔ10). Expression of 3xFLAG-MesI fusions was confirmed by Western blot on saponin-insoluble pellets. ICDH and β-actin were used as controls for bacterial lysis and equal loading, respectively. Data are representative of three independent experiments. (B) Replication of *L. pneumophila* strains within *Nlrc4*$^{-/-}$ BMDMs infected at an MOI of 1. Fold growth was calculated by normalizing CFU counts to internalized bacteria at 1 h post-infection. Plasmid expression of *mesI* alleles was induced with 1 mM IPTG and confirmed by Western blot (inset). Asterisks denote statistical significance (**P<0.05) by Students' t-test on samples in triplicates. Data are representative of three independent experiments. (C) Glutathione agarose beads were incubated with lysates from *E. coli* producing GST-SidI or GST (beads) and subsequently incubated with lysates from *E. coli* producing His_6-Myc-MesI or -MesIΔ10. Proteins on beads were separated by SDS-PAGE and visualized by Coomassie brilliant blue (CBB) staining or a-Myc Western blot, as indicated. Data are representative of three independent experiments. Figure reproduced from (257).

The lysosome associated membrane protein 1 (LAMP1) is a lysosomal degradation marker (273). Intracellular pathogens unable to escape canonical lysosomal degradation, such as

the avirulent *L. pneumophila* Δ*dotA* mutant, will colocalize with LAMP1 indicating phagolysosomal fusion (208). To test our hypothesis that the presence of degraded bacteria was independent from endocytic maturation, we additionally quantified LAMP1 labeling of intact intracellular *L. pneumophila* wild-type, Δ*dotA*, Δ*mesI*, and Δ*mesI*/ 3xFLAG-*mesI*. As expected, Δ*dotA* strains displayed the highest percent of colocalization with LAMP1 at both timepoints (Fig 3.7A + B), which corresponded to observations of degraded intracellular bacteria (Fig 3.7B). Of note, despite Δ*mesI* strains presenting significantly more degraded intracellular bacteria at 8 hours, it displayed low levels of LAMP1 colocalization (Fig 3.7B). These findings suggest that Δ*mesI* bacteria are dying prior to lysosomal degradation and strengthen our conclusion that overexpression of SidI is toxic to *L. pneumophila*.

Screen to identify potential small molecule inhibitors of MesI. Given the finding that SidI is toxic to *L. pneumophila* when uncoupled from *mesI*, the possibility of targeting the metaeffector

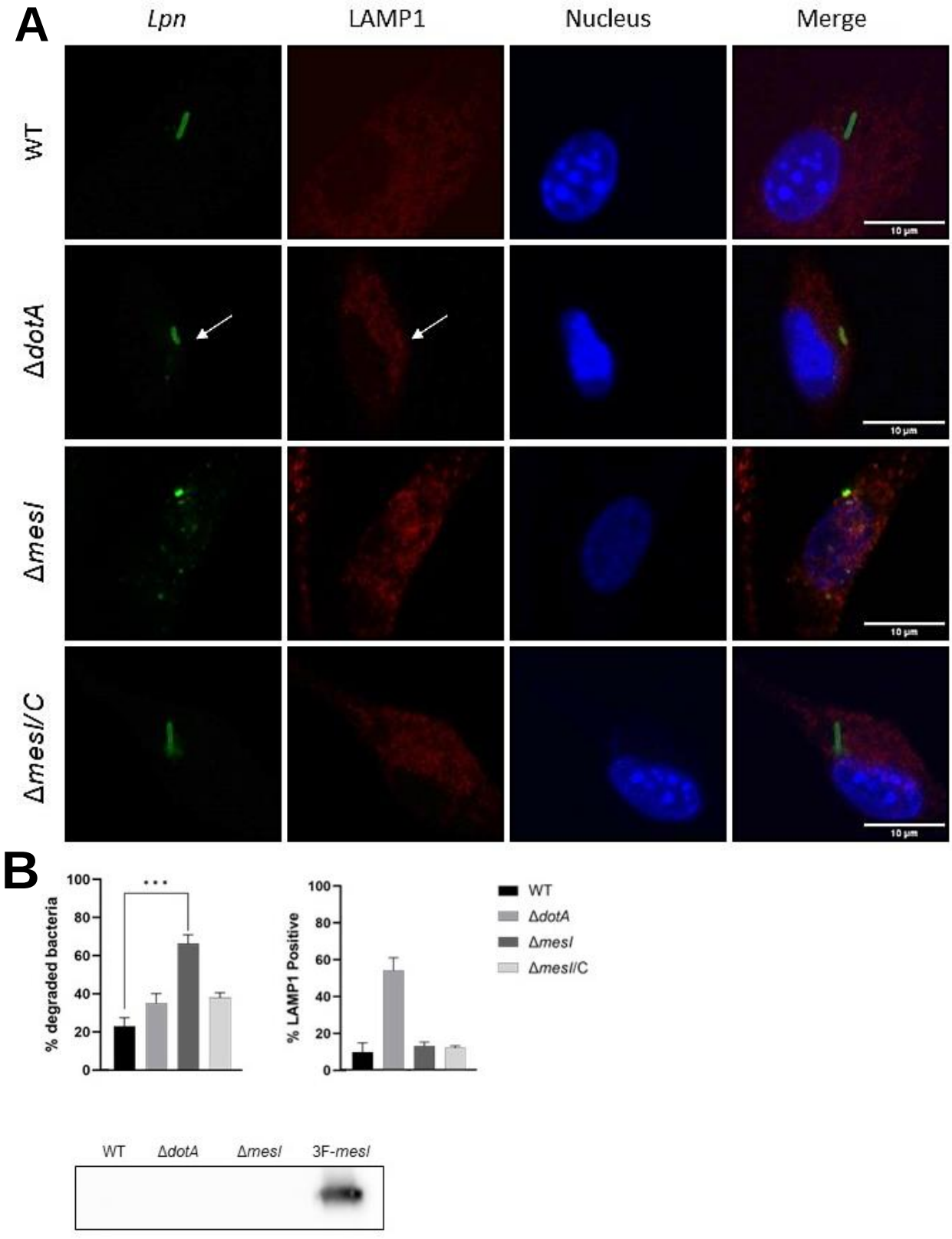

Figure 3.7. MesI-deficient bacteria are efficiently degraded in host cells.

(A) Representative confocal images of *Nlrc4*$^{-/-}$ BMDMs infected for 8 hours with the indicated strains at an MOI of 30. *L. pneumophila* (green), LAMP1 (red), Nuclei (blue), Arrows indicate LAMP1 positive Δ*dotA* bacterial cell. Scale bar is 10 μm. (B) Quantification of degraded (left panel) and LAMP1 positive (right panel) *L. pneumophila* within *Nlrc4*$^{-/-}$ BMDMs infected for 1 8 hours at an MOI of 30. Percent bacteria were enumerated by blinded immunofluorescence scoring of samples in triplicate (n=300). Asterisks denote statistical significance (***P<0.001) by Students' *t*-test. Data shown are representative of two independent experiments. Expression of 3F-*mesI* was confirmed via 3xFLAG western blot (lower panel).

---

with small molecule inhibitors for the development of novel anti-virulence drug treatments was explored. A high-throughput screening of chemical inhibitors was performed by the High-Throughput Screening Laboratory at the University of Kansas (data not shown). The arabinose inducible promoter (pBAD_araC) strains expressing either the wild-type *operon*, Δ*mesI* or the non-toxic *sidI*$_{R453P}$Δ*mesI* were utilized. Compounds of interest would attenuate replication of wild-type *L. pneumophila* but display no effect on *sidI*$_{R453P}$Δ*mesI* or Δ*mesI* strains. Four compounds that met the criteria from the initial screening and were commercially available were further evaluated by our lab (Fig 3.8). Three of the four compounds were broadly inhibitory since substantial growth attenuation was observed in induced and uninduced cultures and their affects cannot be connected to the expression of *sidI* and *mesI*. Compounds G907-0026 0136-0238, 2786-4438 were therefore removed from our analysis (Fig 3.8). Compound 5641-1803 was found to significantly inhibit *L. pneumophila* growth at 1.25 μM when *sidI* and *mesI* were induced but had no effect on the uninduced control (Fig 3.8).

Activity of compounds during *L. pneumophila* intracellular growth. Since *L. pneumophila* is an intracellular pathogen (11), the activity of compound 5641-1803 was tested during intracellular replication in various host model systems. *Nlrc4*$^{-/-}$ BMDMs, human monocyte THP-1 cells and *A. castellanii*, were infected with wild type *L. pneumophila* or a strain lacking both *sidI* and *mesI* (Δ*operon*) for 48- hours. In BMDMs and THP-1 cells, compound 5641-1803

displayed broad

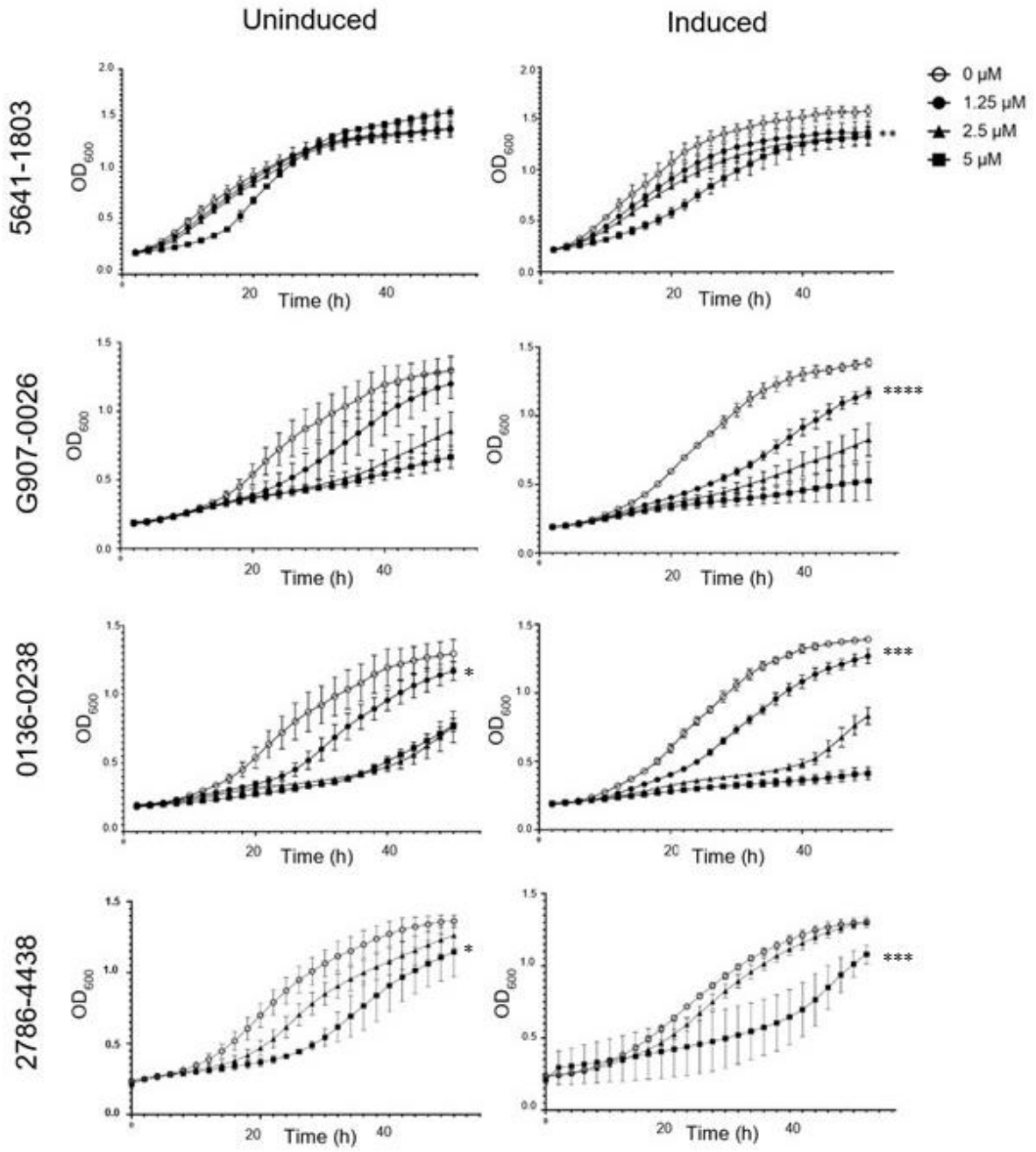

Figure 3.8. Efficacy titration of small molecule compounds against *L. pneumophila*.

Uninduced (left panels) and induced (right panels; 0.6% arabinose) pBAD_araC 3F-SidI strains were grown in the presence of small molecules at 0 (DMSO), 1.25, 2.5 and 5 µM. Data are representative of two independent experiments. Asterisks denote statistical significance as determined by student *t* test (*p<0.05, **p<0.01, ***p<0.001, ****p<0.0001).

inhibition against wild type and Δ*operon* strains in a dose dependent fashion (Figure 3.9). The compound specifically inhibited growth of wild type but not Δ*operon L. pneumophila* in *A. castellanii* by approximately one log at 10 μM compared to the DMSO control (Figure 3.9).

Investigation of Mechanism of Action. To further understand the relationship between SidI and MesI, and investigate the compound's mechanism of action, we tested the ability of 5641-1803 to disrupt known characteristics of the SidI and MesI relationship. SidI is a potent translation inhibitor, but this activity is almost completely abolished by MesI (157). We therefore evaluated the ability of the compound to inhibit MesI suppression of SidI translation inhibition in an *in vitro* rabbit reticulocyte lysate (RLL) system. Equimolar amounts of purified His_6-SidI and MesI were added to the RLL with the indicated concentrations of 5641-1803 or DMSO. While the compound appeared to have a slight effect on translation, no specificity was identified for the SidI-MesI interaction (Fig 3.10A).

We also investigated the ability of the compound to inhibit direct interaction between SidI and MesI. Since it is known that MesI binds at two distinct locations, on the N- and C-termini of SidI (157), we utilized truncations of SidI containing those binding regions ($SidI_N$ and $SidI_C$), in addition to the full-length protein. Affinity chromatography was performed with GST-SidI, GST-$SidI_N$ and GST-$SidI_C$, bound to magnetic glutathione agarose beads. 1 mM of compound in wash buffer (see materials and methods) was added followed by 75 μg of purified His_6-MesI. The compound did not interfere with MesI binding to SidI or its truncations, and we observed more MesI was retained by the GST controls in the presence of 5641-1803 compared to the DMSO controls (Fig 3.10B). It is still possible that compound 5641-1803 affects the binding affinity between SidI and MesI, however, further investigation is needed to elucidate the mechanism of action.

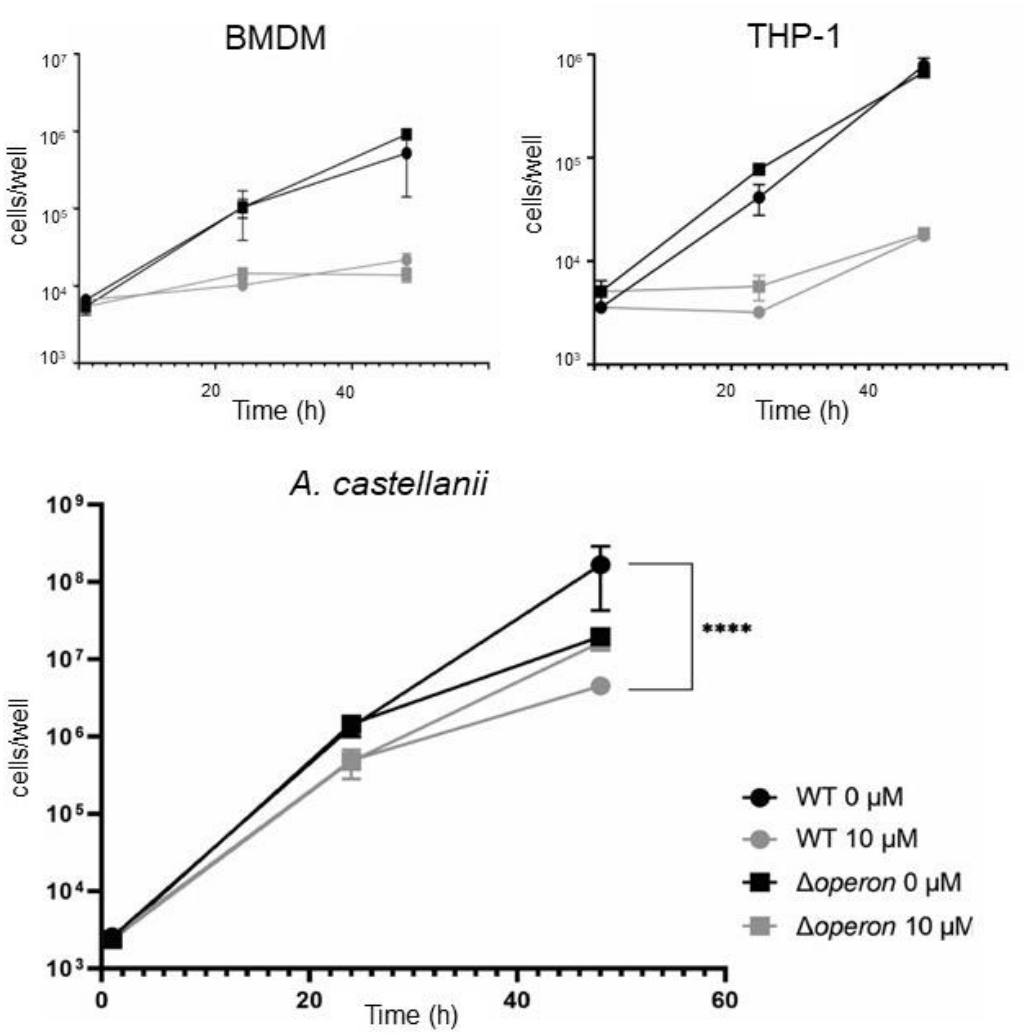

Figure 3.9. Efficacy of compound 5641-1803 during *L. pneumophila* intracellular replication.

Intracellular replication of *L. pneumophila* SRS43 wild type (WT) or *sidI-mesI* knock outs (Δ*operon*) in *Nlrc4*$^{-/-}$ BMDMs, THP-1 and *A. castellanii* in the presence of 0 µM (DMSO) or 10 µM 5641-1803. Data are representative of three independent experiments. Asterisks denote statistical significance as determined by a student *t* test (****P<0.0001).

DISCUSSION

This study supports a unique model whereby the *L. pneumophila* metaeffector MesI drives virulence by intrabacterial regulation its cognate effector SidI. Several *L. pneumophila* effectors

are toxic to eukaryotic cells; however, effector bactericidal activity in *L. pneumophila* has not been previously observed. Furthermore, our data challenge the dogma that metaeffectors promote *L. pneumophila* virulence by functioning exclusively within host cells. SidI and MesI bear resemblance to canonical toxin-antitoxin (TA) and effector-immunity (E-I) pairs (274–276). However, they are distinct from TA pairs as these perform counteracting functions against a common target (277). While immunity proteins in E-I pairs provide protection against antibacterial effectors, they are not secreted (278). This also distinguishes MesI from canonical chaperones, which remain intrabacterial (279). MesI negatively regulates SidI subversion of eukaryotic homeostasis (157) and a role for

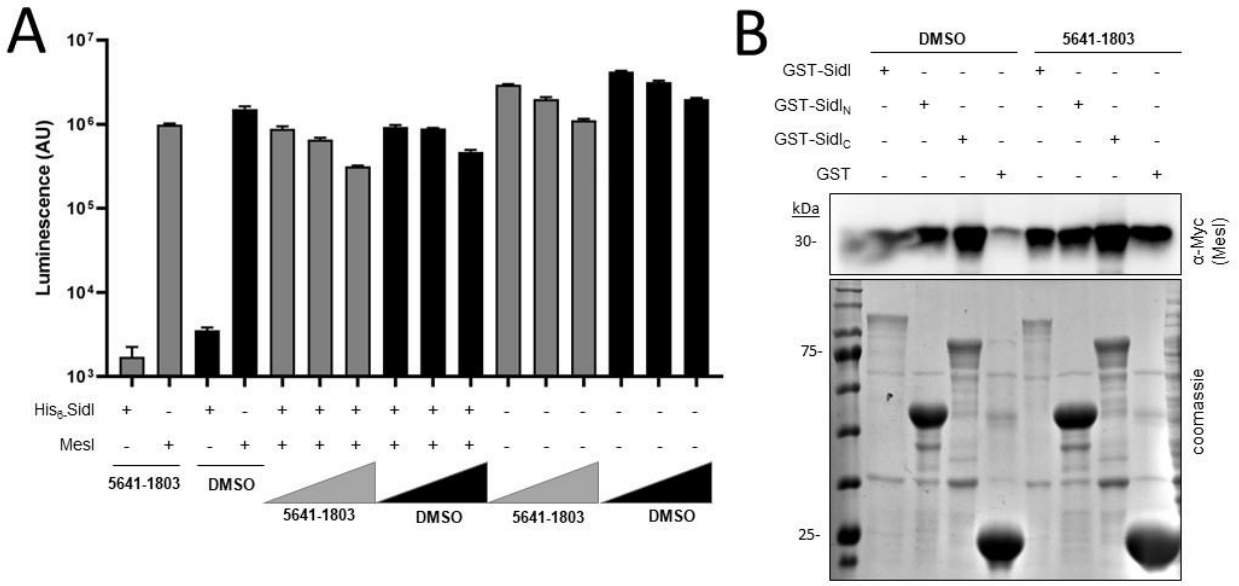

Figure 3.10. Investigation of 5641-1803 mechanism of action.

(A) Translation of luciferase mRNA in the presence of compound 5641-1803 (gray) or equal volumes of DMSO (black) using an *in vitro* Rabbit Reticulocyte Lysate kit. 10, 50 or 100 μM 5641-1803 or equal volume of DMSO (0.1, 0.5, 1 μL) was added to the reaction before addition of 5 ng of His_6-SidI (46.17 fmol) and/or 1.56 ng MesI (46.17 fmol). Reactions with just one protein received 100 μM compound or 1 μL DMSO. (AU, arbitrary units). (B) GST-tagged SidI, $SidI_N$, $SidI_C$ or GST alone were bound to magnetic glutathione beads and then incubated with 75 μg of purified His_6-MesI that had been pre-incubated with 1 mM 5641-1803 or equal volume of DMSO. Proteins were separated by SDS-Page and visualized by Myc western blot (MesI) and coomassie.

host cell pathways in the MesI regulatory mechanism cannot be fully excluded. However, our data suggest a novel mechanism by which *L. pneumophila* virulence hinges on effector regulation by a metaeffector within the bacterium and explores the possibility of exploiting metaeffector regulation for the development of novel therapeutics.

Interkingdom SidI toxicity suggests that its target is highly conserved between *L. pneumophila* and host cells. SidI is one of at least seven *L. pneumophila* effectors that subvert host protein synthesis (101, 124), one of the most conserved cellular processes across the kingdoms of life (280). Effector mediated suppression of host mRNA translation is important for *L. pneumophila's* acquisition of host-derived amino acids, which are essential for intracellular replication and the main driver of bacterial phase switching within host cells (36, 107). The mechanism by which SidI inhibits protein synthesis is unclear; however, SidI binds eEF1A and likely functions as a mannosyltransferase, so it could be speculated that SidI blocks translation by modifying eEF1A (101, 157). However, the significance of eEF1A binding remains unclear since binding alone is insufficient for translation inhibition and the inability of MesI to disrupt binding (101, 157). Although a stable interaction is not always required for target modification. For example, the effector Lgt1 blocks eukaryotic translation by glycosylating eEF1A at Ser-53 but does not form a stable interaction with eEF1A that can be visualized with standard affinity chromatography techniques. Additionally, *L. pneumophila* potentially evades intrabacterial suppression of translation by Lgt1 by targeting Ser-53 which is conserved in eukaryotes but not the bacterial eEF1A homolog, EF-Tu (102, 232). The mechanistic underpinnings of intrabacterial MesI activity is unclear; however, it is tempting to speculate that MesI may function in part to preserve protein synthesis within the bacterium.

Recent work has challenged the dogma that bacterial effectors function exclusively within host cells. Hardwidge and colleagues revealed that the pathogenic *E. coli* effector NleB and *Salmonella enterica* Typhimurium effector SseK1 function intrabacterially (281). NleB confers resistance to oxidative stress and SseK1 confers resistance to methylglyoxal and regulates UDP-GlcNAc biosynthesis (281–283). The pathogenic *E. coli* effector NleC can also function intrabacterially, but the endogenous, biologically relevant substrates are unknown (284). Our data suggest that intrabacterial MesI activity confers a fitness advantage on *L. pneumophila* by suppressing intrabacterial SidI activity. However, MesI is produced at later time points than SidI when *L. pneumophila* is grown in broth (265), which could contribute to our observation that MesI regulates SidI translocation into the host cell during late infection. Although SidI secretion alone cannot explain the intrabacterially toxicity of the effector. Another possibility is that that low levels of SidI activity within the bacterium may be beneficial at early stages of the *L. pneumophila* lifecycle. There is emerging evidence that bacterial TA pairs can shape pathogen physiology by modulating transcriptional gene expression (285). For instance, the toxin MqsR from *E. coli* stimulates the expression of the stress-induced DNA replication inhibitor, *cspD*, while the antitoxin MqsA suppresses it (286). However, this activity must be highly regulated by the antitoxin to prevent toxicity. Our data challenges our initial assumption that MesI promotes *L. pneumophila* intracellular replication by preventing SidI-mediated host cell toxicity. We found no SidI-mediated differences in host cell death and observed that macrophages infected with MesI-deficient bacteria had normal morphology. Recent phylogenetic analysis suggests ancient and extensive co-evolution between the order Legionellales, which includes *Legionella* spp., and unicellular eukaryotes (287). Thus, metaeffectors may represent an ancient mechanism evolved by pathogenic bacteria for adaptation to eukaryotic hosts.

The potential to target MesI with small molecules to inhibit *L. pneumophila* replication was also demonstrated. The identified compound inhibited both wild-type and Δ*sidI-mesI L. pneumophila* intracellular growth in macrophages, and therefore specific activity against SidI and MesI has not been demonstrated in these cells. The compound did significantly inhibit the growth of wild-type *L. pneumophila* but not Δ*sidI-mesI* cells in *A. castellanii*. We previously found that the interaction between SidI and MesI was extremely strong, suggesting that if both proteins are present, they will interact (157). This led us to hypothesize that direct interaction was critical for suppression of SidI toxicity. However, we were unable to detect disruption of protein interaction or observe interference of SidI and MesI in a functional assay. Addition of 5641-1803 to a rabbit reticulocyte lysate *in vitro* translation system led to a dose dependent decrease in translation regardless of the presence of SidI and MesI. It could be speculated that the compound mimics SidI toxicity in vitro, rather than inhibits SidI interactions with MesI, however this falls outside of the scope of our study.

Together, this study revealed a unique role for intrabacterial regulation of a translocated effector by its cognate metaeffector in *L. pneumophila* virulence. Our data, in the context of previously published studies (101, 157), suggest that the target of SidI is conserved between host and pathogen. While we were unable to elucidate the mechanism of action of compound 5641-1803, our findings demonstrate the potential to exploit *L. pneumophila* effectors for anti-virulence therapeutics and future studies will aim to uncover and refine its mechanism of action. This study marks a promising milestone in the treatment of Legionnaires' Disease that may be applied to other effectors and intracellular pathogens.

METHODS

Bacterial Strains. Bacterial strains, plasmids, primers, and culture conditions. Escherichia coli Top10 (cloning), DH5alpir (allelic exchange) and BL21 (DE3) (protein production) were maintained at 37˚C in Luria-Bertani (LB) medium supplemented with appropriate antibiotics for plasmid maintenance [50 µg mL-1 kanamycin, 25 µg mL-1 chloramphenicol, or 100 µg mL-1 ampicillin]. Protein production in *E. coli* BL21 (DE3) was induced with 1 mM isopropyl-b-D-1-thiogalactopyranoside (IPTG). All Legionella pneumophila strains in this study were derived from *L. pneumophila* Philadelphia-1 SRS43 (162) and cultured at 37˚C on charcoal–N (2-acetamido)-2-aminoethanesulfonic acid (ACES)-buffered yeast extract (CYE) supplemented with L-cysteine and ferric pyrophosphate as described previously (251). Single colonies were isolated after 4 days of growth on CYE agar and used to generate 48 h heavy patches of bacteria. Where indicated, liquid cultures were grown from heavy-patched bacteria at 37°C in L-cysteine- and ferric pyrophosphate-supplemented ACES buffered yeast extract broth (AYE)(252). Media were supplemented with 10 µg mL-1 chloramphenicol (plasmid maintenance), 10 µg mL-1 kanamycin (allelic exchange), 1 mM IPTG (Ptac gene expression), or 0.6-2% L-arabinose (w/v; paraBAD gene expression). Plasmids and oligonucleotide primers used in this study are listed in Table 1 and Table 2, respectively.

Molecular cloning and strain construction. *L. pneumophila* gDNA was isolated using the Illustra genomicPREP DNA spin kit (GE Healthcare) and used as a template for cloning *sidI* and *mesI* into the indicated plasmid vectors. *sidI* was amplified from *L. pneumophila* gDNA using SidIBamHI-F/SidISphI-R, which includes 60 base-pairs (bp) downstream of the *sidI* open reading frame, and cloned as a BamHI/SphI fragment into pJB1806 (288) or downstream of an in-frame 3xflag epitope tag in pSN85 (289) to generate pJB1806::sidI (p*sidI*) and pSN85::*sidI*.

To generate p*sidI*$_{R453P}$, p*sidI* was mutagenized using site-directed mutagenesis with primer pairs SidIR453P-sense/SidIR453P-asense (162). To generate p*mesI* complementation plasmids, *mesI* and *mesI*Δ10 open reading frames were amplified from *L. pneumophila* gDNA using MesIBglII-F/MesISphI-R or MesIBglII-F/MesIΔ10SphI-R primer pairs, respectively, and cloned into pSN85 in-frame with the 3xflag epitope tag. Ligations were transformed into chemically competent *E. coli* Top10 and sequences confirmed by Sanger sequencing (Eton Biosciences). *L. pneumophila* complementation strains were generated by electroporation of plasmids into competent *L. pneumophila* strains using a BioRad Gene Pulser at 2.4 kV, 200 Ω, and 0.25 μF and plated on CYE supplemented with 10 μg mL-1 chloramphenicol.

For production of recombinant His$_6$-Myc-MesIΔ10, *mesI*Δ10 was amplified from *L. pneumophila* gDNA using MesIT7SalI-F/MesIΔ10NotI-R and cloned as a SalI/NotI fragment into pT7HMT (211) downstream of an in-frame His$_6$-Myc epitope tag. pT7HMT::*mesI* and pGEX::*sidI* were generated previously (Table 2) (157). Ligation reactions were transformed into chemically competent *E. coli* Top10 and sequences were confirmed by Sanger sequencing (Eton Biosciences). The *dotA* open reading was deleted from the *L. pneumophila* chromosome using allelic exchange, as described (290). To generate a clean in-frame deletion of *dotA*, 5' and 3' regions flanking the *dotA* open reading frame (726 bp upstream and 1,012 bp downstream) were amplified using DotAKOSacI-F/DotAKONotI-R and DotAKONotI-F/DotAKOSalI-R to generate SacI/NotI and NotI/SalI fragments which were ligated into SacI/SalI digested pSR47s to generate pSR47s::Δ*dotA*, which was conjugated into *L. pneumophila* SRS43 for selection of double crossover events, as described. Sequences were confirmed by Sanger sequencing (Eton Biosciences) and the Δ*dotA* phenotype was confirmed by comparison the established SRS43 dotA::Tn strain (162). For allelic exchange to insert the paraBAD promoter and a 3xflag epitope

tag upstream of *sidI* in the *L. pneumophila* chromosome, overlapping primers were used to generate a fusion construct consisting of 1,000 bp upstream of *sidI* (SidIUTR-F/SidIUTR-R; from *L. pneumophila* gDNA), araBAD promoter [araC-pBAD-F/araC-pBAD-R; from pMRBAD::z-CspGFP (a gift from Dr. Brian McNaughton; Addgene #40730) (291)], and 3xflag fused to the first 1,200 nucleotides of *sidI* (3FLAG-SidI-F/3FLAG-SidI-R; from pSN85::*sidI*), which was ligated as a SacI/SalI fragment into pSR47s to generate pSR47S::araBAD. Plasmids were transformed into chemically competent *E. coli* DH5alpir and sequences were confirmed by Sanger sequencing (Eton Biosciences). To generate paraBAD strains, pSR47s::paraBAD was conjugated into *L. pneumophila* SRS43 wild type, Δ*mesI*, and *sidI*$_{R453P}$ΔmesI (162) and selection of double crossover events was performed as described (290). Sucrose resistant, kanamycin sensitive colonies were screened by PCR to verify gene insertion.

Table 3.1. Plasmids used in this study.

Name	Description	Resistance	Ref/sources
PROTEIN PRODUCTION			
pT7HMT	Production of His$_6$-Myc Fusion	Kan^R	(211)
pT7HMT::*mesI*	Production of His$_6$-Myc-MesI	Kan^R	(157)
pT7HMT::*mesIΔ10*	Production of His$_6$-Myc-MesIΔ10	Kan^R	This study
pGEX6P1	Production of GST	Amp^R	GE healthcare
pGEX6P1::*sidI*	Production of GST-SidI	Amp^R	(157)
ALLELIC EXCHANGE			
pSR47s	Allelic exchange vector	Kan^R	(290)
pSR47s::*paraBAD*	For chromosomal integration of *araBAD-3xflag* upstream of *sidI*	Kan^R	This study
pSR47s::Δ*dotA*	For in-frame deletion of *dotA*	Kan^R	This study
GENETIC COMPLEMENTATION AND CLONING			
pJB1806	*Legionella* expression vector		(288)
pJB1806::*sidI (psidI)*	*sidI* expression from P*tac*	Cm^R	This study
pJB1806::*sidI*$_{R453P}$ *(psidI*$_{RP}$*)*	*sidI*$_{R453P}$ expression from P*tac*	Cm^R	This study
pSN85	*Legionella* vector with in-frame N-terminal *3xflag* epitope tag		(289)
pSN85::*sidI*	To generate *3xflag-sidI*	Cm^R	This study
pSN85::*mesI (pmesI)*	*3xflag-mesI* expression from P*tac*	Cm^R	This study
pSN85::*mesIΔ10*	*3xflag-mesIΔ10* expression from P*tac*	Cm^R	This study

(pmesIΔ10)

Table 3.2. Oligonucleotide primers used in this study.

Name	Sequence
PROTEIN PRODUCTION	
MesIT7SalI-F	attgtcgacaatgataaaaggaaaacttatgcc
MesIΔ10NotI-F	attgcggccgcttactcatcgtctttacc
ALLELIC EXCHANGE	
DotAKOSacI-F	attgtcgacgccctagctgtttcattgc
DotAKONotI-R	attgcggccgcacattctttctcacccaataac
DotAKONotI-F	attgcggccgcataacattcaaaaacaatata
DotAKOSalI-R	attgagctcccaaaacaaaataaccagctg
SidIUTR-F	cccccgagctcgagcatcaataatatcctgc
SidIUTR-R	gtagccgtcaagttgtcaaaattactttagtaaaatttttgtcatggtg
AraC-pBad-F	caccatgacaaaaattttactaaagtaattttgacaacttgacggctacatc
AraC-pBad-R	catggtctttgtagtccatatatctccttcttaaagttaaacaaaattatttc
3flagSidI-F	gtttaactttaagaaggagatatatggactacaaagaccatgacg
3flagSidI-R	cccccgtcgactgactacacccctctttattggc
GENETIC COMPLEMENTATION	
SidIBamH1-F	ttaggatccttatgactaaaatatacttattaac
SidISphI-R	attgcatgctcaatcacaaattaatttttgcacatc
MesIBgllI-F	tggagatctttatgataaaaggaaaacttatgc
MesISphI-R	attgcatgcttataaaataattggtcgag
MesIΔ10SphI-R	attgcatgcttactcatcgtctttaccagc
QRT-PCR	
SIDIRT-F	atcaggcaaaccgacgtgac
SIDIRT-R	ccgcaatctggtggacgaat
16SRT-F	tcagtggggaggagggttga
16SRT-R	cgctcgcaccctccgtatta
SITE-DIRECTED MUTAGENESIS	
SidIR453P-sense	ccgcaatctggtggaggaatatgaatatcaagatgagta
SidIR453P-asense	tactcatcttgatattcatattcctccaccagattgcgg

Mice. C57Bl/6 *Nlrc4* -/- mice (a gift from Dr. Craig Roy) have been described (292). In-house colonies were maintained under specific pathogen-free conditions at Kansas State University. Bone marrow was harvested from 8- to 15-week-old mice as previously described (293). All experiments involving animals were approved by the Kansas State University Institutional

Animal Care and Use Committee (IACUC-4501 and -4022) and performed in compliance with the Animal Welfare Act and National Institutes of Health guidelines

Cell culture. All mammalian cells were grown at 37˚C/5% CO2. HEK293 FcγRII cells (a gift from Dr. Craig Roy) were cultured in Dulbecco's Modified Eagle Medium (DMEM; Gibco) supplemented with 10% heat-inactivated fetal bovine serum (HIFBS; Biowest) for up to 25 passages. Primary mouse bone marrow-derived macrophages (BMDMs) were differentiated in RPMI supplemented with 20% HIFBS (Biowest) and 15% L-929 conditioned medium (Differentiation media) for 6 days prior to infection, as described (293). Differentiated BMDMs were seeded for infections in RMPI supplemented with 10%HIFBS and 7.5% L-929 conditioned medium (Seeding medium).

THP-1 were propagated in suspension in tissue culture flasks containing DMEM + 10% HIFBS at 37°C 5% CO2. Cells were kept below $1x10^6$ cells/mL by either passaging or addition of fresh media. THP-1 cells were quantified and differentiated in DMEM + 5% HIFBS + PMA for 3 days in 24-well plates.

Growth curves. Eukaryotic cells were seeded into 24-well tissue culture dishes at 2.5×10^5 per well one day prior to infection. *L. pneumophila* were cultured on CYE agar and heavy patch grown bacteria were used to infect BMDM and THP-1 at a MOI of 1 or *A. castellanii* at an MOI of 0.1 in triplicates and CFU were enumerated as previously described (162, 269). Fold growth was calculated by normalizing CFU at 24 h, 48 h, 337 and 72 h to internalized bacteria at 1 h post-infection. For genetic complementation, either 1 mM IPTG or 2% L-arabinose (w/v) were added to the media as indicated at the time of infection and maintained throughout.

In vitro growth curves. *L. pneumophila* heavy patches were resuspended in fresh AYE broth and sub-cultured for consistent 600 nm optical density (OD_{600}). Cultures were split into triplicates in

wells of a 96-well round-bottom plate and incubated at 37˚C with continuous orbital shaking using an Agilent BioTek Epoch2 plate reader. OD_{600} from triplicate wells was read every two hours for 36 h. Plasmids were maintained with 10 µg mL-1 chloramphenicol and IPTG (1 mM) or 1% L-arabinose (w/v) were added to the media to induce gene expression, as indicated. When bacterial were plated, cultures at an OD_{600} or 0.2 were split into 6- 14-mL culture tubes and incubated at 37°C with continuous shaking for 48 h. At each timepoint, cultures were diluted and plated on CYE agar. After 24 h, half the tubes were induced with 1% L-arabinose (w/v) or plain water (uninduced) as a control.

Quantitative RT-PCR. *L. pneumophila* strains were grown for 1 or 6 h in AYE broth of incubation with and without arabinose (2%), and total RNA was purified with the Direct-zol RNA miniprep kit with TRI-reagent (Zymo Research) following manufacturer's instructions. RNA samples were treated with DNase (Sigma) before reverse transcription with Superscript III (Invitrogen). Quantitative RT-PCR was performed using the Invitrogen SuperScript III Platinum SYBR Green One Step qRT-PCR kit. Transcript abundance was quantified using sidIRT-F/sidIRT-R (*sidI*) and 16SRT-F/16SRT-R (16S rRNA) primer pairs on a BioRad CFX96 Real-Time PCR machine. Fold expression (2^ΔΔCt) was calculated by normalizing *sidI* transcript abundance to 16S rRNA and standardizing values to wild-type *L. pneumophila.*

Bacterial viability and LIVE/DEAD staining. *L. pneumophila* paraBAD strains were resuspended in AYE media from a heavy patch (48 h). Strains were grown for 24 h at 37˚C in the presence or absence of 0.6% L-arabinose (w/v). Cell viability was quantified using a LIVE/DEAD™ Bac361 Light™ Bacterial Viability kit according to manufacturer's instructions. Bacteria were stained with 5 µM SYTO9 (live; green) and 10 µM propidium iodide (dead; red) (ThermoFisher) and incubated for 15 min at room temperature in the dark. To determine the

baseline threshold for dead cells a negative control was used, where cells were treated with 90% ethanol for 1 h. After staining, cells were washed with sterile water and 5 µL of resuspended cells were loaded on a glass slide with a coverslip. Images were acquired at the KSU Division of Biology Microscopy Facility using a Zeiss LSM5 Laser Scanning Confocal Microscope using a 100x oil-immersion objective. Percent dead bacteria was calculated by normalizing dead bacteria (red) to total bacteria using ImageJ software. At least 500 cells were evaluated for each strain and culture condition and the researcher performing the analysis was blinded to sample identity.

Western blot. Protein was boiled in Laemmli Buffer and separated by SDS-PAGE and were transferred to polyvinylidene difluoride (PVDF; Fisher Scientific) membranes using a BioRad wet transfer apparatus. The membranes were incubated with blocking buffer [5% nonfat milk powder dissolved in Tris-buffered saline-0.1% Tween 20 (TBST)] for 30 min. Membranes were incubated with primary antibodies [mouse α-FLAG M2 (1:1000; Sigma); rabbit α-ICDH (1:1,000; Sigma); rabbit α-β-actin (Cell Signaling); rabbit α-Myc TAG mAb (71D10) (1:1,000; Cell Signaling)] at 1:1,000 in blocking buffer overnight at 4˚C with rocking and subsequently with HRP-conjugated goat α-rabbit or α-mouse secondary antibodies at 1:5,000 (ThermoFisher) in blocking buffer for 2 h at room temperature with rocking. Membranes were washed, incubated with ECL reagent (GE Amersham), and imaged by chemiluminescence using an Azure Biosystems c300 Darkroom Replacer.

Saponin solubilization assay. HEK293 FcγRII cells (253) were seeded in 10 cm poly-L-lysine coated tissue culture dishes (4×10^6) one day prior to infection. *L. pneumophila* strains were patched from fresh single colonies onto CYE agar supplemented with 10 µg mL-1 chloramphenicol and 1 mM IPTG to induce gene expression. Bacteria were opsonized with α-*L. pneumophila* antibody [1:1,000 (Invitrogen; PA17227)] in DMEM 10%HIFBS supplemented

with 1 mM IPTG for 20 min at room temperature (RT) with rotation. Cells were infected with opsonized bacteria at a MOI of 50 in for 2 h in 2 mL DMEM 10% HIFBS supplemented with 1 mM IPTG. Cells were washed 3X with ice-cold PBS to remove extracellular bacteria and lysed for 10 min in 500 µL ice cold Hank's Balanced Salt Solution (HBSS) supplemented with 0.2% saponin and ProBlock™ Gold Mammalian Protease Inhibitor Cocktail (GoldBio). Lysates were treated with RNAse A (10 µg mL-1) and DNase I (10 µg mL-1), incubated at RT for 15 min, and centrifuged for 15 min at 17,000 r.c.f at 4˚C. Saponin-soluble supernatants were filtered using a 0.22 µM syringe filter and transferred to a fresh 1.5 mL microcentrifuge tube. Saponin-insoluble pellets were resuspended in 50 µL TE buffer (10 mM Tris-HCl, 1 mM EDTA). Fifty microliters of supernatant and pellet fractions were diluted in 3X Laemmeli sample buffer, boiled for 10 min, and the whole sample was loaded into wells of a 1.5 mm 15% SDS-PAGE gel for Western blot. Proteins were separated by SDS-PAGE and visualized using Coomassie brilliant blue or Western Blot, as indicated.

Affinity chromatography. Affinity chromatography from *E. coli* lysates was performed as described (157). Briefly, *E. coli* BL21 (DE3) harboring pT7HMT::*mesI,* pT7HMT::*mesI*Δ10, pGEX6P1::*sidI*, or pGEX6P1 were grown overnight with shaking at 37˚C overnight and sub-cultured at 1:100 in LB media. Sub-cultures were grown for 3 h followed by induction with 1 mM IPTG and growth overnight at 16˚C. Clarified lysates from bacteria producing GST-fusion proteins were incubated with pre-equilibrated glutathione magnetic agarose beads (Pierce) for 1h at 4˚C with rotation. Beads were washed twice in washing buffer (125 mM Tris-Cl, 150 mM NaCl, 1mM DTT, 1 mM EDTA, pH 7.4) and incubated with clarified lysates from bacteria producing His_6-Myc fusion proteins at 4˚C for 1 h with rotation. Beads were washed twice in

washing buffer transferred to a fresh 1.5 mL microcentrifuge tube and boiled in 25 µM 3X Laemmli Sample buffer.

Cytotoxicity Assay. Cytotoxicity was evaluated by quantifying lactate dehydrogenase (LDH) activity in supernatants of *L. pneumophila*-infected BMDMs. BMDMs were seeded in 24-well tissue culture dishes at $2.5x10^5$ in Seeding medium one day prior to infection. Cells were infected with *L. pneumophila* strains at an MOI of 50 for 1 h, washed 3 times with sterile phosphate-buffered saline ($PBS^{-/-}$), and incubated in seeding media for additional 5 h or 9 h. At the indicated times, plates were centrifuged at 250 r.c.f. and supernatants were transferred to a sterile non-tissue culture treated 96 well plate. For the 1 h timepoint, supernatants were collected from cells without washing. LDH was quantified using the CytoTox™ 96 Non-radioactive Cytotoxicity Assay (Promega) and according to manufacturer's instructions. Absorbance at 490 nm was read on a BioTek Epoch2 microplate reader and percent cytotoxicity was calculated by normalizing absorbance values to cells treated with lysis buffer.

Quantification of bacterial degradation and LAMP1 colocalization within macrophages. BMDMs (1×10^5) were seeded on poly-L-lysine-coated glass coverslips in 24-well tissue culture dishes one day prior to infection. BMDMs were infected in triplicate wells with the indicated *L. pneumophila* strains at an MOI of 30 for 1 h or 8 h. For the 8 h timepoint, extracellular bacteria were removed after 1 h by washing coverslips three times in $PBS^{-/-}$ and incubated with fresh media for 7 h. Coverslips were fixed in 3.7% paraformaldehyde for 15 min and permeabilized with ice-cold methanol. Coverslips were stained with 1:1,000 rabbit α-*L. pneumophila* and rat α-LAMP1 primary antibodies (Invitrogen; PA17227) followed by 1:500 Alexa488-conjugated goat α-rabbit and Alexa594-conjugated α-rat secondary antibodies (ThermoFisher). Nuclei were stained with 1:2,000 Hoeshst (ThermoFisher) and coverslips were mounted on slides with

ProLong™ Gold Antifade Mountant (Invitrogen). Degraded and intact bacteria were scored blind on a Leica DMiL LED inverted epifluorescence microscope (n=300 per strain and time point). Intact bacteria were further categorized as LAMP1 positive or negative (n=300 per strain and time point). Representative images were acquired at the KSU College of Veterinary Medicine Confocal Core using a Zeiss LSM 880 inverted confocal microscope and processed using Fiji ImageJ and Adobe Photoshop software.

Chemical Inhibitor Screen. 2-day heavy patches of pBAD_araC *L. pneumophila* were resuspended in AYE broth containing appropriate supplements. The OD_{600} was determined, and bacteria were seeded into 384-well plates at an OD_{600} of 0.1 in supplemented AYE broth in the presence or absence of (0.6% or 2%) arabinose. Chemical inhibitors were added at 5 or 10 μM and cells were grown over 24-hours at 37°C. The minimum amount of compound needed to inhibition 50% of growth (IC_{50}) was determined by OD_{600}.

In vitro Small Molecule Growth Curves. *L. pneumophila* were were cultured as described above. The OD_{600} was determined, and bacteria were seeded into 96-well plates at a final OD_{600} of 0.2 in supplemented AYE broth. Protein production was induced using 1% arabinose at the start of the growth curve. Chemical inhibitors in DMSO were titrated at the indicated concentrations based on the IC_{50} identified in the initial chemical inhibitor screening. The growth curve was carried out as described above.

Small molecule efficacy during intracellular replication. Growth curves were performed as described above. After 1 hour, the infection media was aspirated and cells were washed 3x with PBS before replacing with appropriate media containing the chemical inhibitor and continued as described. *Acanthamoeba castellanii* were cultured in PYE media within tissue culture flasks incubated at 22°C. One day prior to infection, cells were split 1:10 and incubated overnight at

22°C. The day of infection, cells were washed with warm Ac infection media, resuspended in PYE media and quantified. Cells were seeded into 24-well plates and incubated for 1-2 hours at 37°C until cells became adherent. Amoeba were infected at a multiplicity of infection of 0.1 for 45 minutes at 37°C and washed 3x with Ac infection media. Infected cells were incubated at 37°C in 1mL of Ac infection media containing the chemical inhibitor. At each timepoint, cells were detached by pipetting and appropriate dilutions were made in diH2O before plating on CYE agar. CYE plates were incubated for 4-days at 37°C and quantified.

In vitro Translation Assay. Translation assays were conducted following manufacturer's protocol (Promega). A master mix of rabbit reticulocyte lysate, amino acid solutions (-Met and -Leu as indicated by the manufacturer), potassium chloride and luciferase mRNA was combined in a 1.5 mL microcentrifuge tube. Appropriate volumes of ultra-pure water were added to PCR tubes followed by the indicated concentration of inhibitor or equal volume of DMSO. His_6-tagged SidI and/or untagged MesI were added to the appropriate reactions before addition of the master mix. Tubes were briefly spun down and incubated at 30°C for 90 minutes. Following incubation, 2.5 µL of reaction was mixed with 50 µL of luciferase detection reagent and immediately quantified using the Victor plate reader.

Small Molecule Affinity Chromatography. Glutathione S-transferase (GST) tagged SidI truncations from E. coli lysates (157) were bound to magnetic glutathione agarose beads for 1 hour with rotation at 4°C. Beads were washed 2x with glutathione wash buffer (recipe here) before adding 1mM of inhibitor in 250 µL PBS, followed by 75 µg (250 µL) of purified His_6-MesI. Beads were washed 2x with glutathione wash buffer and transferred to a fresh microcentrifuge tube. Supernatants were removed and beads were resuspended in 25 µL of 3x Laemelli buffer, boiled and ran in duplicate on 10% SDS-Page gels. Gels were either transferred

to PVDF membrane and western blotted for α-Myc (rabbit, Cell Signaling) or stained with Coomassie

Statistical analysis. Statistical analysis was performed with GraphPad Prism 9 software using unpaired two-tailed t-test with a 95% confidence interval. Unless otherwise indicated, data are presented as mean ± standard deviation (s.d.) and statistical analysis was performed on triplicate biological replicates.

Supplementary Materials

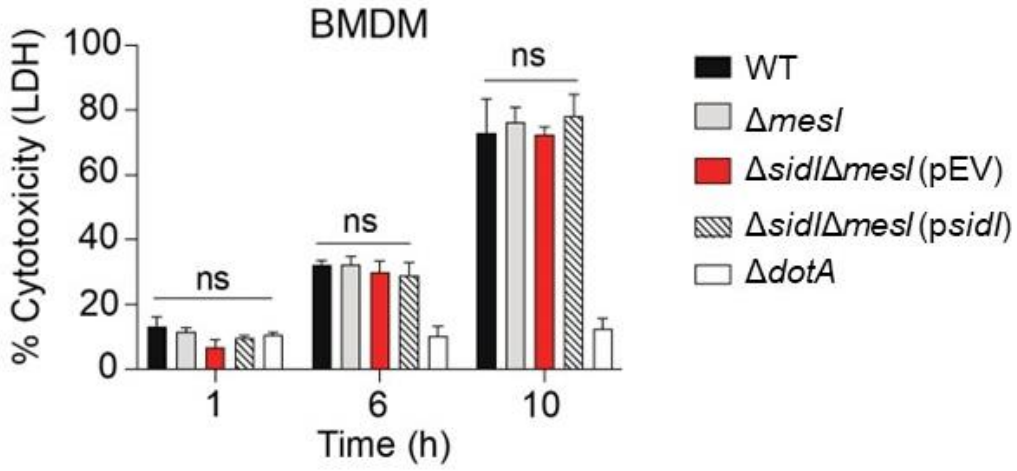

Supplemental Figure 3.1. Host cell death is not increased by SidI-producing L. pneumophila.

Lactate dehydrogenase activity in supernatants of *Nlrc4*$^{-/-}$ BMDMs infected with the indicated *L. pneumophila* strains (MOI of 30) for 1, 6, or 10 h. Plasmid expression of *sidI* was induced with 1 mM IPTG. Data are representative of three independent experiments and statistical analysis was performed using Students' *t*-test (ns, not significant).

Chapter 4 - The *Legionella pneumophila* metaeffector, LegA11, regulates the inhibitory activities of its target effector

Ashley M. Joseph[1] and Stephanie R. Shames[1,2]

[1] Division of Biology, Kansas State University, Manhattan, KS, USA
[2] Microbiology and Molecular Genetics, Michigan State University, East Lansing, MI, USA

Author Contributions

Ashley Joseph
- Experiments
- Figure Formatting
- Writing
- Hypothetical Models

Stephanie Shames
- Conceptualization, Funding, Editing

ABSTRACT

Legionella pneumophila is an intracellular pathogen that can infect a plethora of phagocytic hosts cells using an arsenal of over 300 different effector proteins. Effector proteins are virulence factors that are translocated directly into the host cell following pathogen uptake. Effectors hijack host pathways to promote *L. pneumophila* survival. Successful establishment and maintenance of infection relies on intricate regulation of effector protein activity throughout the infection process. *L. pneumophila* employs a subset of effector regulatory proteins called metaeffectors. LegA11 is a predicted metaeffector that alleviates yeast toxicity of another effector, SidL. SidL inhibits actin polymerization, likely as a result of direct actin binding and also inhibits host mRNA translation. How LegA11 suppresses SidL toxicity and its effect on SidL activity are unknown. We have confirmed that LegA11 and SidL directly interact, solidifying LegA11 as a bona fide metaeffector. It was additionally discovered that LegA11 suppresses SidL inhibitory activities *in vitro,* while increasing actin retention. Loss of a functional *legA11* from the *L. pneumophila* genome incurred a replication advantage during intracellular replication in *Nlrc4*-deficient macrophages, but not in THP-1 or *Acanthamoeba castellanii* that was not attributed to enhanced establishment of the *Legionella* containing vacuole or an increased growth rate. These findings demonstrate novel regulation of a translation inhibiting effector and provide insight into the contributions of metaeffectors to *L. pnuemophila* growth.

INTRODUCTION

Legionella pneumophila is a facultative, intracellular pathogen that naturally infects free living amoebae and is an accidental human pathogen (4). To successfully infect its host cell, *L. pneumophila* translocates over 330 unique effector proteins directly into the host cell using a Dot/Icm Type IVB secretion system (T4SS). Proper coordination of effector proteins is required for successful infection and establishment of a replication niche known as the *Legionella* containing vacuole (LCV). Development of the LCV requires modulation of vesicle trafficking within the host cell and several *L. pneumophila* effectors alter actin dynamics to avoid the endocytic pathway (69–71, 90, 294). VipA is an actin nucleator that enhances polymerization of actin microfilaments and alters endosome trafficking (69). In contrast, the effector kinase, LegK2, inhibits nucleation of branched actin filaments by phosphorylating the ARP2/3 complex on phagosomes to evade the late endocytic pathway (70). WipA destabilizes the N-WASP-ARP2/3 complex through dephosphorylation, and a double mutant lacking *wipA* and *legK2,* displays impaired replication at late stages of infection (71).

Actin is an abundant and essential protein in eukaryotic cells, responsible for maintaining cell shape, phagocytosis, and mRNA translational fidelity (82, 86, 295–298). Proper protein synthesis requires assembly of translation machinery such as elongation factors 1 A (eEF1A) and β (eEF1β), aminoacyl-tRNA synthetases, initiation factors and ribosomes on actin filaments (84, 86, 299–301). Filamentous actin comprises several actin monomers (G-actin) bound to ATP (ATP-actin) at the growing (barbed) end and ADP-actin near the minus (pointed) end. As the actin filament elongates with ATP-actin from the barbed end, ADP-actin is removed from the pointed end by the protein, cofilin. The free ADP-actin subunits are then captured by profilin, which catalyzes the conversion of ADP to ATP. The Profilin-ATP-actin complex is recruited to

the barbed end by nucleating formins, enabling elongation. However, if the barbed end is bound by a capping protein, profilin will rapidly depolymerize the filament (79–81, 302–306). In addition to its role with actin dynamics, profilin is important for many other processes in the cell. Profilin interacts with mRNA process and translation initiation proteins and has been connected to cell cycle progression between G1- and S- phases in the parasite *Leishmania* (125).

L. pneumophila is auxotrophic for seven amino acids and must acquire them from their environment or host cell to survive (7, 94). Translation inhibiting effectors have been linked to pathogen nutrient acquisition, cytokine induction and host cell cycle arrest (100, 124, 133). The effector, SidL, is one of seven known translation inhibiting effectors that also inhibits actin polymerization (90, 124). SidL is toxic when expressed in yeast, but this toxicity can be alleviated by a threonine to asparagine substitution at amino acid 623 ($SidL_{T623N}$) or with overexpression of yeast profilin. Profilin can bind to actin in the presence of SidL and actin binding is essential for suppression of SidL toxicity (90). Given that the actin profiles of polymerization reactions containing SidL alone and SidL with profilin are indistinguishable, it is unclear if inhibition of actin polymerization is solely responsible for SidL toxicity (90). SidL toxicity may instead be related to inhibition of mRNA translation or cell cycle arrest, as profilin plays a role in both of those processes (125)

SidL yeast toxicity can additionally be suppressed by co-expression with another *L. pneumophila* effector, LegA11 (126). LegA11 belongs to a class of effectors known as metaeffectors. Metaeffectors directly interact with other effectors and regulate their activity in the host cell (138). Previous studies found that deletion of *legA11* decreased *L. pneumophila* replication in some protozoan hosts and human monocyte derived macrophages (215, 307). How LegA11 alleviates SidL toxicity and the mechanism responsible for the decreased replication

observed in some host cells is unknown. In this study, our lab set out to investigate how LegA11 regulates SidL and if this regulation contributes to *L. pneumophila* survival. It was found that LegA11 suppresses SidL inhibitory effects on both translation and actin polymerization but did not interrupt SidL binding to actin. Unexpectedly, we discovered that deletion of *legA11* increased intracellular replication in *Nlrc4*-deficient bone marrow derived macrophages (BMDM) but presented no observable phenotype in *Acanthamoeba castellanii* or human THP-1 cells. These findings provide insight into the contributions of metaeffectors to *L. pneumophila* intracellular replication. Uncovering host specific phenotypes aid in elucidating effector function and benefit our understanding of host-pathogen interactions, that can be applied to other intracellular pathogens.

RESULTS

LegA11 suppresses SidL translation inhibition in vitro. SidL is one of 7 known translation inhibiting effectors (103). The activity of another translation inhibiting effector, SidI, is regulated by its metaeffector *in vitro* (157, 265).We therefore examined the ability of LegA11 to suppress SidL translation inhibition *in vitro.* Since SidL translation inhibiting activities have been demonstrated through incorporation of ^{35}S-Methionine during *L. pneumophila* infection (100), we first confirmed the activity of purified SidL in an *in vitro* system. Purified His_6-tagged SidL and $SidL_{T623N}$ were added at 5, 25 and 50 ng to rabbit reticulocyte lysates containing luciferase mRNA and compared to 5 ng of His_6-SidI. While 5 ng of His_6-SidL caused a significant decrease in luciferase mRNA translation compared to the positive control, its effects were minimal compared to the same amount of His_6-SidI (Fig 4.1A). Even up to 50 ng of His_6-SidL did not display the same translation inhibition as 5 ng His_6-SidI, indicating that SidL is not as potent *in*

vitro as SidI. His_6-$SidL_{T623N}$ showed a minimal, yet statistically significant decrease in translation compared to the controls and addition of His_6-LegA11 had no effect on this (Fig 4.1B). When an equimolar amount of His_6-LegA11 was added to reactions containing His_6-SidL, there was a significant increase in translation, that did not change with increasing molar ratios (Fig 4.1C). Pre-incubation of His_6-SidL and His_6-LegA11 increased LegA11 efficacy (Fig 4.1D).

LegA11 binds SidL directly and does not interfere with actin binding

Previous reports found that SidL and LegA11 interacted in a LUMIER prey-and-bait assay during mammalian cell expression (126). Direct interaction is a hallmark of *L. pneumophila* metaeffectors, so we sought to confirm that SidL and LegA11 bind directly. Recombinantly expressed GST-tagged SidL or GST alone were immobilized on magnetic glutathione agarose beads and incubated with His_6-LegA11 from *E. coli* lysates. In support of previous reports, His_6-LegA11 was retained on GST-SidL coated beads, but not GST alone (Fig 4.2A), demonstrating a direct interaction and supporting classification of LegA11 as a bona fide metaeffector.

Some metaeffectors regulate their cognate effectors by inhibiting interactions with host cell targets, but some effectors can bind their metaeffector and host target simultaneously (126, 157). To investigate how LegA11 affects SidL interactions with its known host target, we subsequently added HEK293T lysates as a source of actin. In agreement with previous reports (90), GST-SidL independently bound actin (Fig 4.2A). While we hypothesized that LegA11 would disrupt SidL-actin binding, actin was retained by GST-SidL in the presence of His_6-LegA11 (Fig 4.2A). Based on the western blot, we predicted that LegA11 increased SidL binding to actin, however analysis by densitometry indicated that this was not statistically

significant (Fig 4.2B).

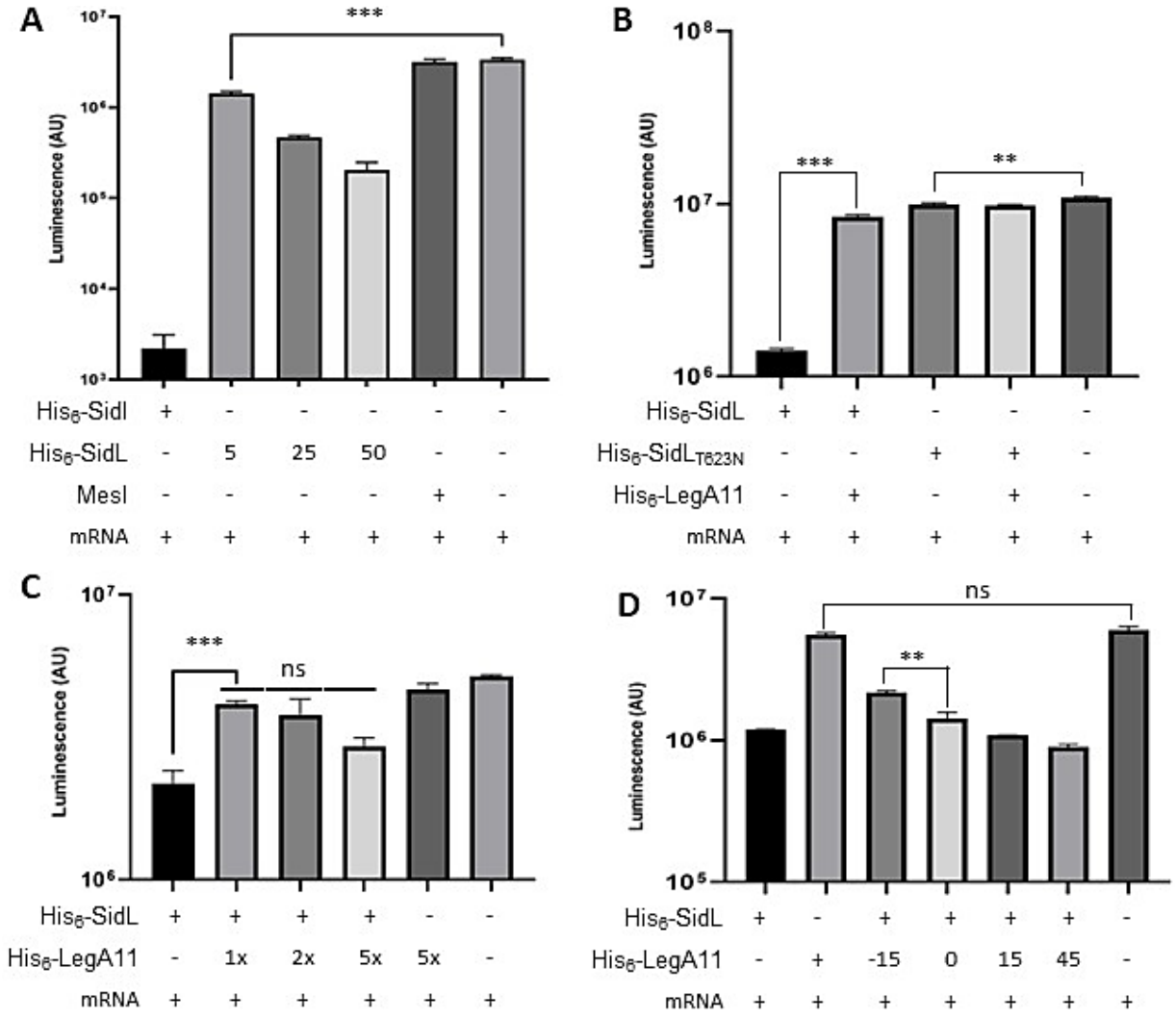

Figure 4.1. LegA11 suppresses SidL translation inhibition in vitro.

Translation of luciferase mRNA was quantified within rabbit reticulocyte lysates in the presence of (A) 5 ng of His_6-SidI (67 fmol), 5, **25** and **50** ng of His_6-SidL (70, 352, and 704 fmol) or 22 ng of untagged MesI (704 fmol). (B) 50 ng His_6-SidL or His_6-$SidL_{T623N}$ with and without equimolar amounts of His_6-LegA11. (C) 50 ng His_6-SidL in the presence of 1x, 2x, 5x molar amounts of His_6-LegA11. (D) 50 ng His_6-SidL with equimolar amounts of His_6-LegA11 added at different timepoints- 15-minute incubation prior to the start of the experiment (**-15**), at the start of the experiment (**0**) and 15 and 45 minutes after His_6-SidL. Results are representative of at least 3 independent experiments and expressed as means ± standard deviation of samples in triplicate. Statistical significance determined by *t* test with a 95% confidence interval (*, $p<0.05$, **$p<0.01$, ***$p<0.001$, ****$p<0.0001$, ns, not significant)

The LegA11 sequence contains three putative ankyrin repeats, a common sequence motif used for protein interactions (160, 215). The observation that LegA11 did not interrupt SidL binding to actin and could potentially be increasing this interaction, led us to evaluate if LegA11 interacted with actin independent from SidL. We incubated HEK293T lysates with magnetic glutathione agarose beads coated with GST-LegA11 or GST alone in the presence and absence of His_6-SidL. Actin was retained in the presence of His_6-SidL, but not by GST-LegA11 or GST alone, indicating that LegA11 does not directly bind actin (Fig 4.2C).

LegA11 promotes SidL binding to actin from DMSO treated cells, but not cytochalasin D treated cells

Actin is present as either monomeric (G) actin or as filaments (F-actin), consisting of several actin monomers bound together (80). Recombinant SidL has been shown to co-sediment with F-actin (90), but the effect of LegA11 on this interaction is unknown and we therefore evaluated the effect of LegA11 on F-actin binding. We repeated the affinity chromatography as before with GST-SidL and His_6-LegA11 from lysates incubated with magnetic glutathione agarose beads in succession. HEK293T cells were treated with 5 μM cytochalasin D or equivalent volume of DMSO as a control for 2 hours. Cytochalasin D (CytoD) is a potent actin polymerization inhibitor. Treatment of mammalian cells with CytoD causes an increase in G-actin monomers and decreased podia formation resulting in a spherical appearance to the cell (308). HEK293T cells treated with DMSO retained their shape with visible podia and were expected to have a higher abundance of F-actin compared to cells treated with CytoD.

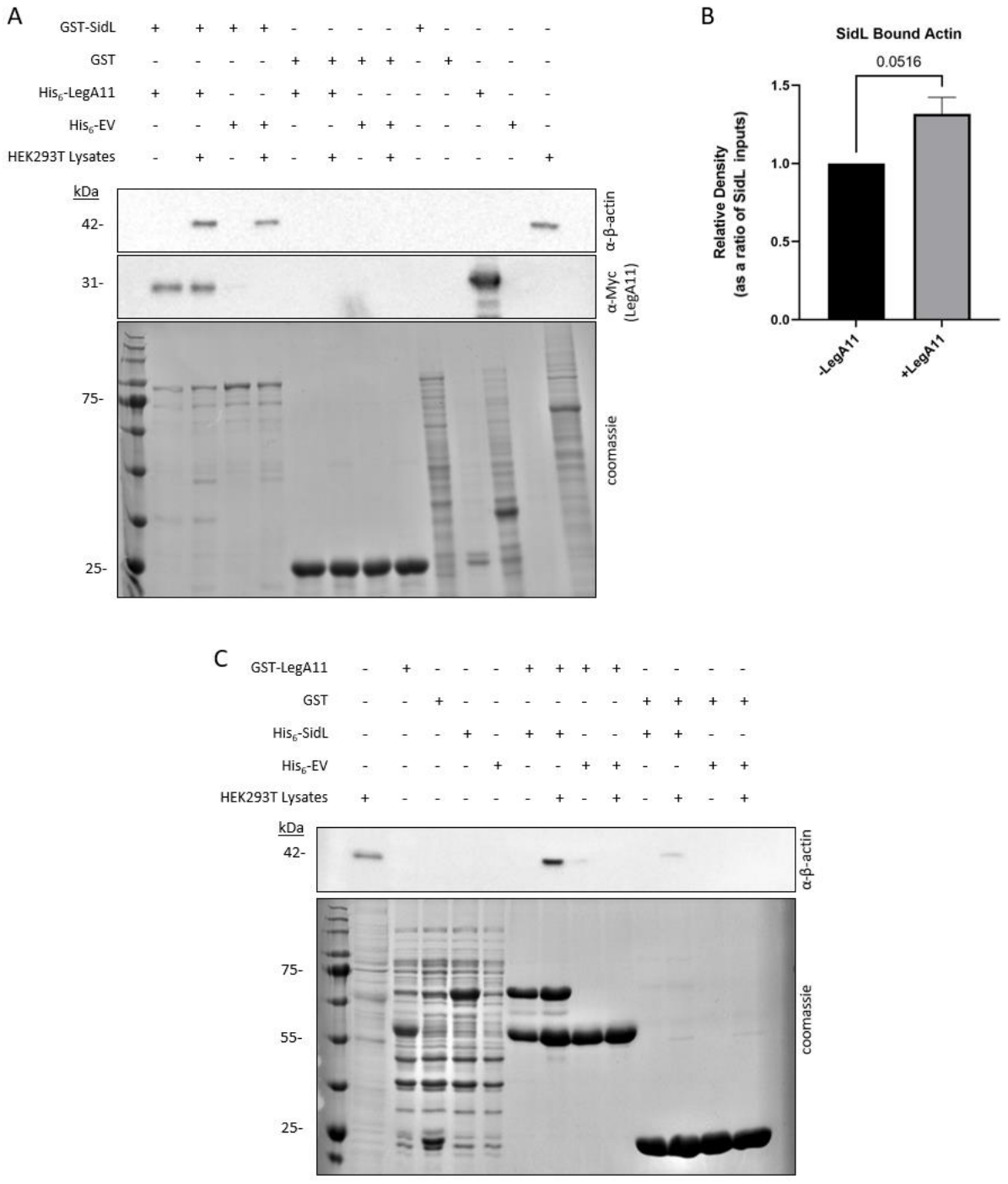

Figure 4.2. LegA11 does not interrupt SidL binding to actin.

(A) Recombinantly expressed GST-SidL or GST alone was immobilized on glutathione magnetic agarose beads, followed by incubation with recombinantly expressed His_6-LegA11 or empty vector control (His_6-EV) and then HEK293T lysates as a source of actin. Proteins were separated by SDS-Page and visualized by Coomassie or western blotting for β-actin and Myc (LegA11). (B) The amount of retained actin was quantified using densitometry as a ratio of SidL

inputs and shown as the mean ± standard deviation across five independent experiments. Statistical significance was determined using a *t* test with 95% confidence interval. (C) Recombinantly expressed GST-LegA11 or GST alone were immobilized on glutathione magnetic agarose beads, followed by incubation with recombinant His_6-SidL or empty vector control and then HEK293T lysates as a source of actin. Proteins were separated by SDS-Page and visualized by Coomassie or western blotting for β-actin.

Before lysis, HEK293T cells were inspected for morphological changes consistent with CytoD treatment. CytoD was additionally added to treated HEK293T cell lysates to discourage spontaneous polymerization during the incubation process. Regardless of His_6-LegA11 presence, more actin was retained by GST-SidL from HEK293T lysates treated with the DMSO control compared to CytoD treated cells, however this could be an artifact of F-actin filaments giving the appearance of increased binding (Fig 4.3A & B). There was no significant difference in the amount of actin retained by GST-SidL between CytoD treated lysates with and without His_6-LegA11 when quantified across five independent experiments (Fig 4.3B). There was a significant increase in the amount of actin retained by GST-SidL from control lysates (DMSO treated) in the presence of His_6-LegA11, suggesting that LegA11 promotes interactions between SidL and F-actin. Interestingly, the $SidL_{T623N}$ mutant that has decreased activity against actin polymerization (90), and does not bind actin retained actin in the presence of His_6-LegA11 (Fig 4.3A & B). Although there was no significant difference in the amount of actin retained by $SidL_{T623N}$ - LegA11 between CytoD and DMSO treatments (Fig 4.3A & B) . These data suggest that LegA11 enhances wild type SidL binding to actin filaments. To confirm these findings, we repeated the experiment using purified actin incubated in either G-actin buffer or F-actin buffer (see materials and methods) and ultracentrifuged to isolate the two species. However, the experiment was underpowered and thus excluded from the report. Further experimentation using purified actin is needed to fully support if LegA11 promotes SidL binding to F-actin.

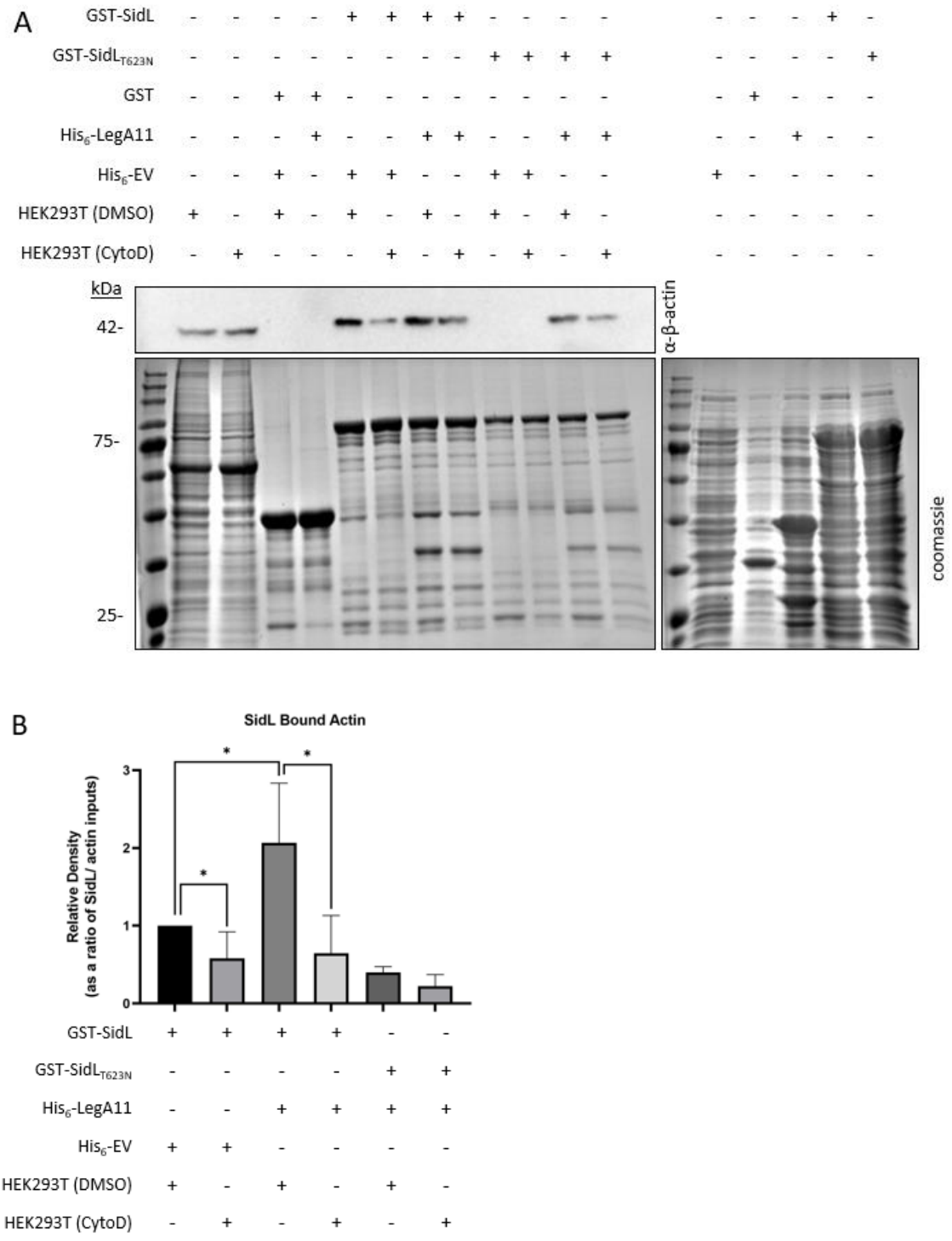

Figure 4.3. LegA11 promotes SidL binding to actin from HEK293T cells treated with DMSO but not Cytochalasin D

Recombinantly expressed GST-SidL, GST-SidL$_{T623N}$ or GST alone were immobilized on beads, followed by incubation with His$_6$-LegA11 or empty vector control. (A) HEK293T lysates treated

with 5 μM cytochalasin D or an equal volume of DMSO for 2 hours were added as a source of actin. (B) The amount of actin retained was quantified using densitometry as a ratio of SidL and actin inputs and shown as the mean ± standard deviation across five independent experiments. Statistical significance was determined using a *t* test with a 95% confidence interval. *p<0.05

LegA11 regulates SidL actin polymerization inhibition *in vitro*. The findings that LegA11 promotes SidL binding to actin yet suppresses SidL translation inhibition, led us hypothesize that it may have the opposite effect on SidL inhibition of actin polymerization. We investigated the ability of LegA1l to promote SidL inhibition of actin polymerization *in vitro* using a pyrene-labeled actin polymerization assay. In agreement with previous reports (90), His_6-SidL significantly inhibited actin polymerization while His_6-$SidL_{T623N}$ showed no inhibitory effects. In contrast to our hypothesis, addition of an equimolar amount of His_6-LegA11 to His_6-SidL reactions fully restored actin polymerization (Fig. 4.4). The ability of LegA11 to suppress both SidL translation and actin polymerization inhibitory activities *in vitro* could indicate that these functions are related, but further investigation is needed to confirm a connection.

SidL and LegA11 colocalize during ectopic expression in COS7 cells.

It was previously demonstrated that SidL and LegA11 interact within mammalian cells (126). Our results confirm that this is a direct interaction and additionally discovered that LegA11 promotes SidL binding to actin. We therefore hypothesized that LegA11 may direct SidL to actin filaments within the host cell and examined their localization during ectopic expression. We co-transfected

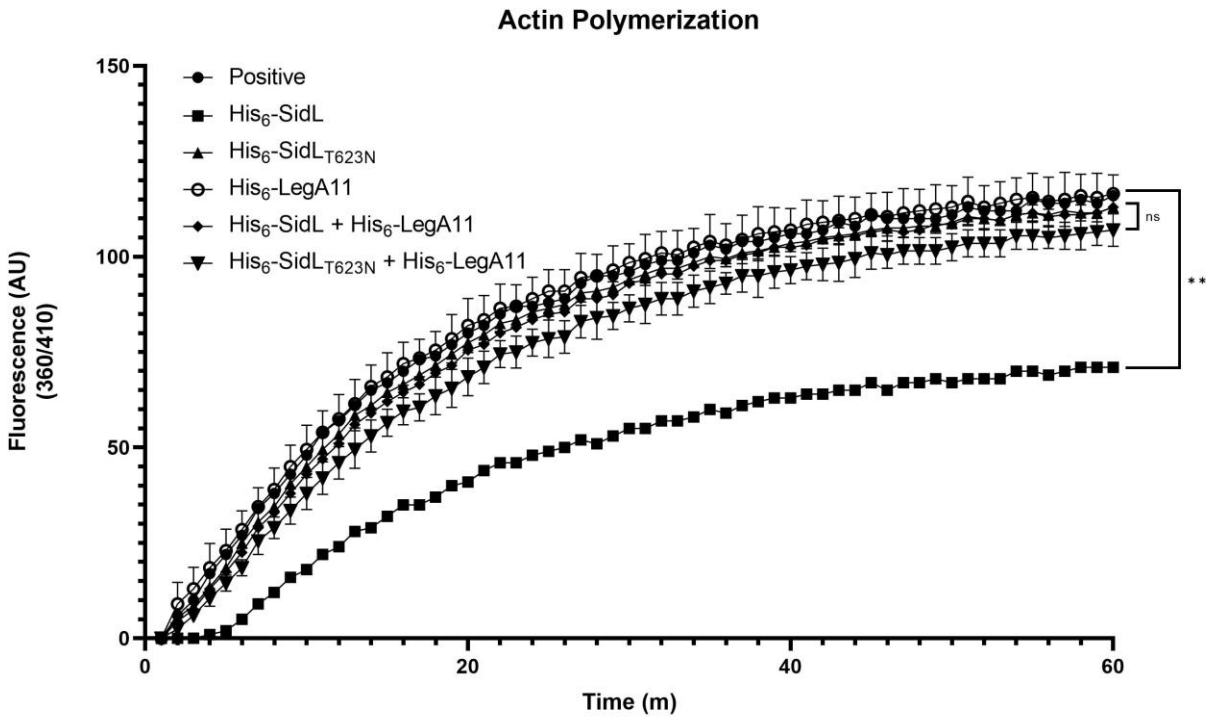

Figure 4.4. LegA11 suppresses SidL inhibition of actin polymerization in vitro

Kinetics of actin polymerization using a pyrene-labeled actin polymerization kit. 1 μM of purified His_6-SidL or, His_6-$SidL_{T623N}$ with and without an equimolar amount of His_6-LegA11 was added to pyrene labeled G-actin following the manufacturer's protocol. Fluorescence intensity (ex. 360/ em. 410) was recorded every minute for 60 minutes. Data shown are representative of 3 independent experiments consisting of 2 replicates per sample, with the exception of His_6-SidL which only consists of 1 replicate. Statistical significance was determined using multiple *t* tests with 95% confidence interval. **p<0.01; ns, not significant.

African green monkey fibroblasts (COS7) with GFP-SidL and 3xFLAG-LegA11 along with GFP and 3xFLAG controls and observed localization using immunofluorescence. As expected, GFP-SidL was not expressed in cells co-transfected with the 3xFLAG control, likely due to inhibition of its own translation, while 3xFLAG-LegA11 was well expressed regardless of the co-transfected plasmid (Fig 4.5). GFP, 3xFLAG and 3xFLAG-LegA11 all localized to the cytoplasm when co-transfected with each other. In support of previous findings (126) co-transfected 3xFLAG-LegA11 and GFP-SidL staining colocalized within the cell (Fig 4.5). We

were unable to confirm localization of GFP-SidL and 3xFLAG-LegA11 with actin filaments, and further investigation is required to support this hypothesis.

L. pneumophila lacking functional *legA11* have a growth advantage in *Nlrc4*-deficient macrophages

We discovered that LegA11 suppresses the activity of SidL, similar to another metaeffector-effector pair, MesI and SidI (157). The metaeffector, MesI is required for *L. pneumophila* survival as unregulated SidI is toxic to the bacteria (162, 257). Previous reports found that loss of LegA11 causes a growth defect in some protozoan hosts and human monocyte-derived macrophages (215, 307). Since this phenotype has not been observed in all hosts cells (159), we examined how loss of *legA11* impacted *L. pneumophila* intracellular replication in *Nlrc4*-deficient bone marrow-derived macrophages (BMDMs), which has not been previously investigated. We additionally evaluated the impact of loss of *sidL* on *L. pneumophila* intracellular replication to evaluate if our findings agree with previous reports that *sidL* is dispensable (90). We utilized loss of function transposon mutants (162) and evaluated their growth intracellularly over 48 hours. Murine *Nlrc4*$^{-/-}$ BMDM were used to avoid activation of the NLRC4/NAIP5 inflammasome by bacterial flagella that restricts *L. pneumophila* intracellular growth (178, 191, 309). In agreement with previous reports (90) *sidL*::Tn grew similar to wild-type *L. pneumophila.* In contrast to previous findings, *legA11::*Tn had a growth advantage compared to wild type after 48 hours (Fig 4.6A). To confirm that the growth phenotype in *Nlrc4*$^{-/-}$ BMDMs was associated with the loss of effector function, rather than a polar effect of transposon insertion (310), we created clean deletions of *legA11 (ΔlegA11)* and *sidL* (*ΔsidL)* and complemented the deletion with expression of the genes from a plasmid. Consistent with transposon mutant phenotypes, Δ*legA11* grew better after 48 hours (Fig 4.6B), while no

difference in growth was observed between wild type, Δ*sidL* and Δ*sidL*/ 3F-*sidL* strains (Fig 4.6C). Expression of 3xFLAG-LegA11 from a plasmid restored growth to wild type levels (Fig

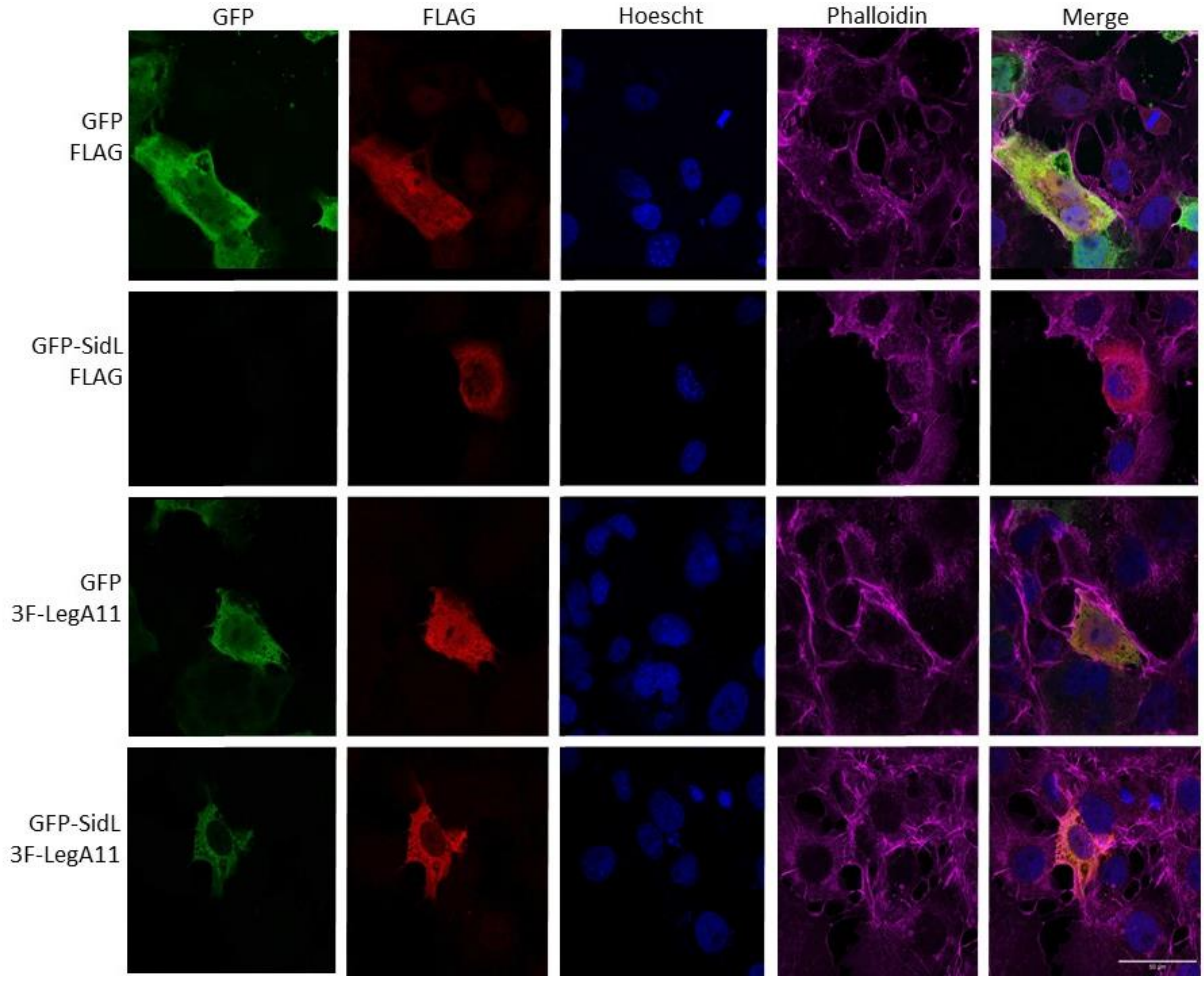

Figure 4.5. SidL and LegA11 colocalize during ectopic expression in COS7 cells.

COS7 cells seeded on coverslips were transfected with GFP-SidL, GFP, 3xFLAG-LegA11 or 3xFLAG for 24 hours after which the cells were fixed and imaged with a Zeiss 880 confocal microscope at 63x magnification and processed using ImageJ Fiji software. Scale bar is 50 μm. Images are representative of 3 independent experiments.

4.6B). All strains grew similarly in *A. castellanii* and human THP-1 cells, suggesting that this phenotype may be host cell specific (Fig 4.6B & C).

One explanation for the increased growth observed with loss of *legA11* could be improved establishment of the LCV. SidL inhibits actin polymerization and modulation of actin

dynamics is important for construction of the LCV (21, 90, 311, 312). Furthermore, translation inhibiting effectors can induce host cell cycle arrest that is beneficial for bacterial replication (133, 313). We therefore performed a replicative vacuole assay to evaluate if *ΔlegA11* strains displayed enhanced establishment of the LCV compared to wild type bacteria and observe if the phenotype was detectable at earlier time points. Vacuoles containing 1-2 bacteria were considered immature, 3-5 bacteria represent newly established LCVs and more than 6 bacteria indicate a mature LCV (143). *Nlrc4*$^{-/-}$ BMDMs seeded on poly-L-lysine coated coverslips were infected with wild type, Δ*dotA*, and *ΔlegA11/* 3xFLAG bacteria for 1 and 10 hours. As expected, all strains predominantly displayed LCVs containing 1-2 bacteria at 1 hour (Fig 4.7A). After 10 hours, wild type, *ΔlegA11/* 3xFLAG and Δ*legA11/*3xFLAG::*legA11* presented mostly mature LCVs, containing 6 or more bacteria, indicating that improved LCV establishment was not responsible for the increased growth associated with loss of *legA11* (Fig 4.7A). The complemented strain was eliminated as the results were inconsistent across experiments and no significance difference between wildtype and *ΔlegA11/* 3xFLAG strains was observed.

Another possibility for the Δ*legA11* phenotype could be an increased growth rate. To test this, we grew wild type, Δ*legA11,* Δ*sidL* and their complemented strains *in vitro* and measured their absorbance (OD_{600}) over 48 hours. Δ*legA11/*3xFLAG (EV) and Δ*legA11/*3xFLAG::*legA11* strains grew similar to wild type, indicating that enhanced bacterial replication was not responsible for the increased growth intracellularly (Fig 4.7B). Interestingly, strains overexpressing *sidL* exhibited impaired growth (Fig 4.7B & C), despite growing similar to wild type strains during intracellular growth.

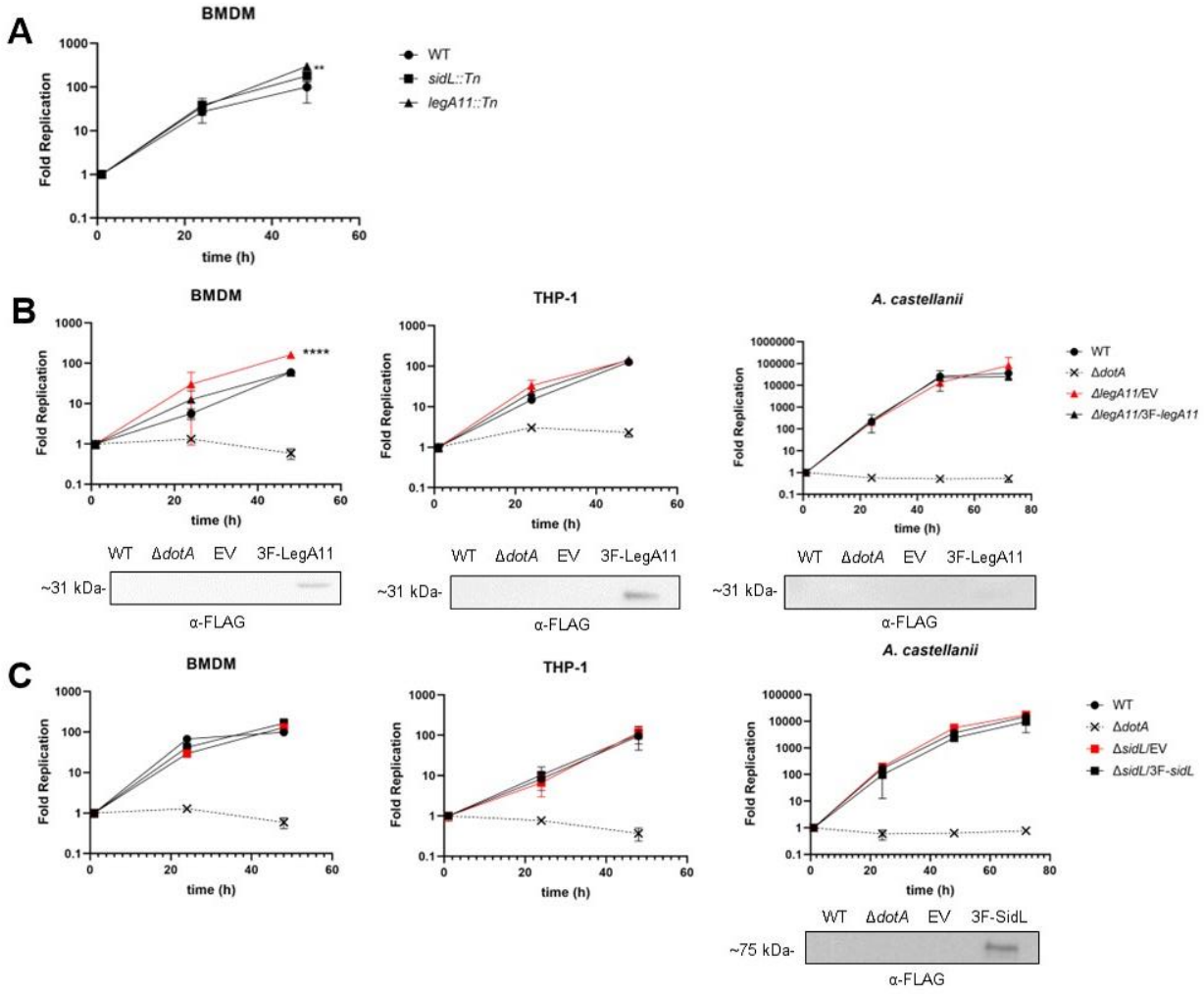

Figure 4.6. *L. pneumophila* lacking functional *legA11* have a growth advantage in *Nlrc4*$^{-/-}$ macrophages

Nlrc4$^{-/-}$ BMDMs and THP-1 cells were infected with an MOI=1 for 48-hours and *A. castellanii* were infected with an MOI=0.1 for72-hours. Fold replication of *L. pneumophila* wild type and *dotA* deletion strain (Δ*dotA*) in the indicated host cell compared to (A) *sidL* and *legA11* transposon mutants (B) *legA11* deletion strain harboring pSN85 empty vector (Δ*legA11*/EV) or pSN85::*legA11* compliment strain (Δ*legA11*/ 3F-*legA11*) or (C) *sidL* deletion strain harboring pSN85 empty vector (Δ*sidL*/EV) or pSN85::*sidL* compliment strain (Δ*sidL*/ 3F-*sidL*). 3xFLAG-LegA11 expression was induced by heavy patching on IPTG containing media for 2-days and confirmed by western blotting. 3xFLAG-SidL expression was induced at the time of infection (BMDMs & THP-1) or heavy patching on IPTG containing media for 2-days (*A. castellanii)*. Data are representative of at least 2 independent experiments and shown as means ± standard

deviation of samples in triplicate. Statistical significance was determined using a *t* test with 95% confidence interval. **p<0.01, ****p<0.0001

---

legA11 and *sidL* deletion mutants cannot outcompete wild type bacteria in a mouse model of Legionnaires' Disease

The observation that loss of *legA11* incurs a growth advantage during intracellular replication in *Nlrc4*$^{-/-}$ macrophages led us to hypothesize that this would also result in an advantage in a mouse model of Legionnaires' Disease. Despite *sidL*-deletion strains growing similar to wild type bacteria during intracellular replication, the impaired growth observed during overexpression *in vitro*, led us to additionally evaluate loss of *sidL*. We performed a competitive index evaluation in the mouse lung. Age- and sex- matched C57JB/6 *Nlrc4*$^{-/-}$ mice

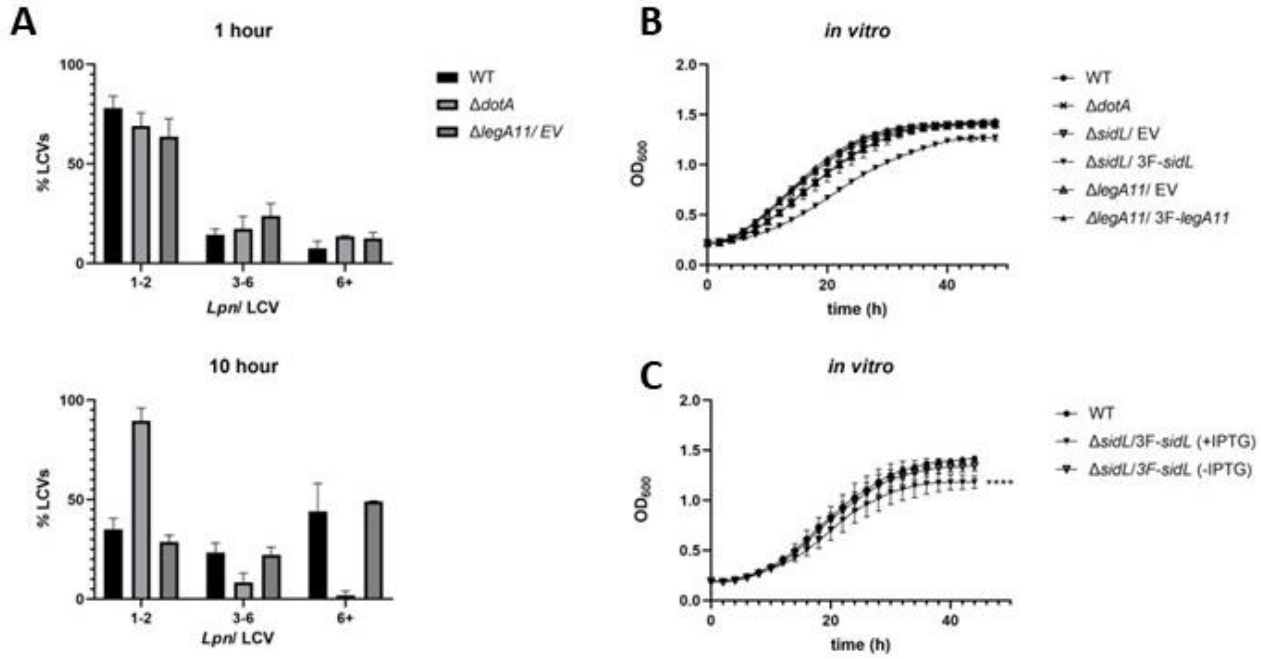

Figure 4.7. Improved maturation of the LCV, nor, increased bacterial growth rate are responsible for the Δ*legA11* phenotype.

(A) *Nlrc4*$^{-/-}$ BMDMs seeded on coverslips were infected at an MOI=30 for the indicated time. Cells were fixed, blinded, and visualized using a fluorescent microscope. 150 LCVs per sample, across three replicates were scored. Data are representative of two independent experiments. (B + C) *L. pneumophila* strains were grown *in vitro* in a 96-well plate over 48-hours. Growth was recorded every 2 hours as OD_{600}. Protein expression was induced using IPTG at the start of the

experiment. Data are shown as mean ± standard deviation of 5 sample replicates and are representative of at least two independent experiments. Statistical significance was determined using a *t* test with 95% confidence interval. *p<0.05, **p<0.01, ****p<0.0001

---

were infected intranasally with a 1-to-1 ratio of wild type *L. pneumophila* and the Δ*legA11* mutant or Δ*sidL* mutant harboring a plasmid that encodes a chloramphenicol resistant gene for 48-hours. Lung tissue was subsequently harvested, homogenized, and plated on CYE and CYE agar supplemented with 5 μM chloramphenicol. Bacteria were enumerated and the competitive index (CI) was calculated (See materials and methods). No significant competitive advantage or disadvantage was observed for either mutant (Fig 4.8A & B)

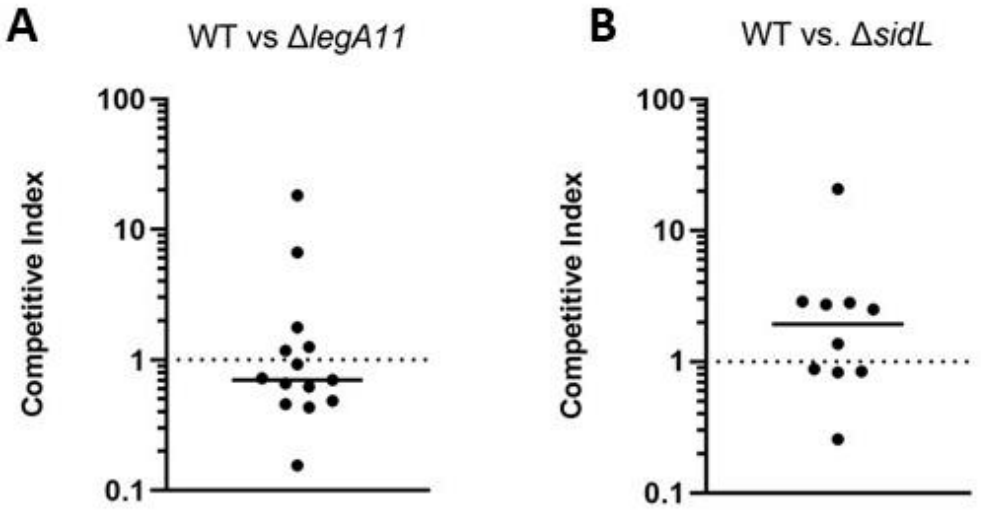

Figure 4.8. *sidL* and *legA11* mutants cannot outcompete wild type bacteria during *in vivo* replication.

Competitive index (CI) of *L. pneumophila* wild type SRS43 versus (A) Δ*legA11/* pJB1806 or (B) Δ*sidL*/ pJB1806 from the lungs of *Nlrc4*$^{-/-}$ mice. Mice were infected intranasally, and lungs were harvested after 48 hours. Data are compiled from 3 independent (Δ*legA11*) or 2 independent (Δ*sidL*) experiments with an n=5, or an n=4 for a single Δ*legA11* CI. Each symbol represents an individual animal, and the line indicates the mean CI value.

DISCUSSION

In the present study we sought to understand the relationship between the *L. pneumophila* effector, SidL, and its metaeffector, LegA11. SidL is one of seven known translation inhibiting effectors (SidL, SidI, LegK4, Lgt1-3, and RavX), at least two of which are regulated by metaeffectors (124, 126, 138, 157). Our lab previously demonstrated that the metaeffector of SidI, MesI, is required for *L. pneumophila* intracellular survival and suppresses SidI activity *in vitro* (157, 162, 257). We therefore hypothesized that the metaeffector, LegA11, would have a similar relationship with SidL. We found that LegA11 suppressed both SidL translation inhibition and actin polymerization inhibition *in vitro* but this was not due to disruption of actin binding. Instead, LegA11 increased SidL binding to actin from DMSO treated HEK293T cells, but not from cells treated with the actin polymerization inhibitor, cytochalasin D, suggesting that F-actin binding is improved. In agreement with previous studies, *sidL* was dispensible for intracellular replication. Loss of *legA11* resulted in increased replication in *Nlrc4*$^{-/-}$ BMDMs that was not attributed to enhanced development of the LCV or an increased growth rate and did not translate to a competitive advantage in a mouse model of Legionnaires' disease. From these findings we propose that LegA11 facilitates SidL binding to the actin filament but must release SidL to enable full activity.

Actin is critical for many cellular processes including preservation of cell shape, transcription regulation and organization of translation machinery (80, 84, 86, 300). Polymerization and depolymerization of the actin filament is controlled by several actin binding proteins that could compete with SidL. Polymerization can be halted by the actin capping protein (CP) which competes with formins on the barbed end of the filament. The actin filmalent is a two-stranded helix with staggered ends that must both be capped to prevent polymerization (314)

CP behaves as a single protein in terms of its stability and denaturation, but it contains two subunits, alpha (α) and beta (β) that interact with actin independently (79). Deletion of the α-subunit significantly reduced actin affinity while removal of the β-subunit results in an increased off-rate from actin and decreased filamentous actin in lamellipodia (314, 315). It is possible that the SidL-LegA11 complex behaves similarly to CP, with LegA11 acting like the β-subunit, which could explain the increase retention of actin by SidL in the presence of LegA11. The SidL-LegA11 complex is distinct from CP as we were unable to detect direct interactions between LegA11 and actin. The possibility of SidL alone acting analogously to CP has previously been dismissed as SidL is still toxic when expressed in yeast lacking CP and the low affinity between SidL and actin (90). However, affinity between SidL and actin was not directly measured, and CPs are not universally interchangeable between organisms (90, 316, 317). Evaluating the affinity of SidL and the SidL-LegA11 complex for actin using an analytical method such as surface plasmon resonance (318) would provide insight into how LegA11 contributes to SidL-actin interactions.

Many metaeffectors temporally regulate their target effector by suppressing their activity. The metaeffector, LubX, ubiquitinates the effector, SidH, marking it for proteasomal degradation (139). LupA deubiquitinates its target, LegC3, and SidJ polyglutamylates the SidE family of effectors, all resulting in effector deactivation (126, 149–152). Secretion of LegA11 is upregulated during exponential and post-exponential growth of *L. pneumophila* (28). Previous reports indicate that *sidL* is constitutively expressed throughout the *L. pneumophila* life cycle (90). From this, it can be speculated that LegA11 regulates SidL activity during multiple phases of growth and there is evidence to support bi-functional metaeffector activity. The metaeffector, MesI has been shown to exhibit chaperone-like activity, controlling the levels of translocated

SidI during late infection in addition to suppressing SidI activity ((265), Chapter 3). The metaeffector SdjA is a bifunctional enzyme, capable of glutamylating the effectors, SdeB and SdeC, while deglutamylating SdeA (319). Results from our affinity chromatography experiments indicate that LegA11 increases actin retention by SidL despite suppressing both mRNA translation inhibition and inhibition of actin polymerization. It is therefore possible that LegA11 regulates SidL activity throughout infection by modulating the affinity of SidL for actin.

Loss of *legA11* provided a growth advantage during intracellular replication in *Nlrc4*-deficient BMDMs but not in *A. castellanii* nor THP-1 cells, suggesting that the effect is related to immune function. While THP-1 cells and *Nlrc4*-deficient BMDMs are both permissive to *L. pneumophila* infection, THP-1 cells have reduced levels of the full-length NAIP adaptor protein and deletion of *Nlrc4* increases their susceptibility (196, 320). It has been proposed that NAIP5 functions independent from inflammasome activation as A/J mice carrying a defective *Naip5* allele, still activate caspase-1 in response to *L. pneumophila* infection (167). Our findings also contradict previous literature that demonstrate that deletion of *legA11* decreases survival in human monocyte derived macrophages (hMDMs) (307). However, hMDMs express a functional, full length NAIP that is known to respond to multiple bacterial ligands (321).These differences in host cell immune deficiencies may account for the contrasting responses to loss of *legA11*. Our data indicate that LegA11 suppresses SidL inhibitory activities, and it can therefore be speculated that the growth advantage associated with loss of *legA11* is the result of unregulated SidL activity. BMDMs produce TNF in response to *L. pneumophila* infection that is crucial for innate immunity in the absence of NLRC4-mediated responses (56). Disruption of β-actin impairs TNF production by adherent monocytes (322). Therefore, it could be speculated that disruption of actin polymerization by SidLin the absence of LegA11 leads to decreased

antimicrobial TNF production and decreased restriction of replication. Further investigation is required to elucidate the mechanism behind the Δ*legA11* replicative advantage.

Actin dynamics and protein synthesis are tightly intertwined processes and SidL toxicity could be the result of a combination of factors. The ability of profilin to suppress SidL toxicity could be related to translation inhibition and/or cell cycle arrest, rather than modulation of actin. Expression of a single translation inhibiting effector, Lgt1, is sufficient to reduce cyclin D1 levels and induce cell cycle arrest between G1- and S-phases in HEK293 cells (133). *Leishmania* parasites deficient in profilin similarly display reduced levels of cyclin-like proteins (125). In this context, overexpression of profilin may override cell cycle arrest induced by the translation inhibiting effector. SidL has not been shown to independently induce cell cycle arrest, and this would have to be addressed to support this hypothesis. Profilin has also been shown to interact with the eukaryotic initiation factor 4A1 (EIF4A1) translation initiator and profilin-deficient cells differentially express genes in DNA transcription and mRNA translation, including EIF4A1 (125). SidL enhances the translation inhibitory effects exhibited by Lgt1-3 and SidI (100). Since this was demonstrated by incorporation of ^{35}S-methionine, it could be speculated that the observed enhancement is due to disruption of translation initiation, rather than elongation as seen with the Lgt effector family (100, 101, 106, 232). Indeed, defects in actin organization affect translation initiation, rather than elongation (86). It could therefore be hypothesized that overexpression of profilin may offset SidL translation inhibition and toxicity through regulation of mRNA translation initiation. Further investigation will likely tease out the specific mechanism of SidL function and toxicity.

Overexpression of *sidL in vitro* produced a slight, but significant decrease in *L. pneumophila* replication that was not observed during intracellular growth. Many effector

proteins are upregulated during intracellular growth that are not well expressed during *in vitro* replication (323). The lack of an intracellular phenotype with *sidL* overexpression could be due the upregulation of other effector proteins, that does not occur during *in vitro* growth. If the decreased growth *in vitro* is the result of SidL activity, it could be hypothesized that SidL can interact with the bacterial actin homolog, MreB. MreB localizes to the midcell prior to cell division and interacts with the protein, FtsZ (324). FtsZ is a tubulin homolog essential for cell division in rod-shaped bacteria and *E. coli* MreB mutants deficient in FtsZ binding display decreased replication (324, 325). *L. pneumophila* MreB and human β-actin share ~15% identity (NCBI BLAST), which could translate to weak interactions between SidL and MreB and explain the minimal phenotype. Further investigation is needed to deduce if this phenotype is due to slight SidL intrabacterial toxicity or simply an artifact of *in vitro* replication.

There is growing evidence supporting the presence of metaeffectors in other pathogens (216, 326, 327). This study expands our understanding of effector-metaeffector relationships and provides insight into how those relationships contribute to effector triggered immune responses. Further research will tease out the mechanism behind LegA11 regulation of SidL and how metaeffectors regulation affects the host effector triggered response.

METHODS

Bacterial Strains. *Legionella pneumophila* strains were grown on supplemented charcoal-*N*-(2-acetamido)-2-aminoethanesulfonic acid (ACES)-buffered yeast extract (CYE). When appropriate, bacteria were grown in the presence of 10 μg mL^{-1} chloramphenicol for plasmid maintenance, or 5 μg mL^{-1} chloramphenicol for transposon maintenance. *Escherichia coli* strains used for cloning (Top10; Invitrogen) and protein expression [BL21(DE3); a gift from Craig Roy, Yale University] were cultured in Luria-Bertani (LB) broth in the presence of 50 μg mL^{-1}

kanamycin (Gold Bio), 100 μg mL^{-1} ampicillin (Gold Bio) or 25 μg mL^{-1} chloramphenicol (Gold Bio) as needed for plasmid maintenance. Bacterial strains were grown at 37°C. Protein expression in *E. coli* and *L. pneumophila* was induced with 1 mM isopropyl-β-D-1-thiogalactopyranoside (IPTG) (Gold Bio). For intracellular growth curves, expression of 3xFLAG::*legA11* was induced by heavy patching on IPTG containing media. Induction of 3xFLAG::*sidL* by heavy patching on IPTG containing media hinders the growth of *L. pneumophila*, so expression was induced at the time of infection.

Clean chromosomal deletions of *sidL*, *legA11*, and *dotA* genes in SRS43 *L. pneumophila* were constructed using homologous recombination. Upstream and downstream regions of target genes were amplified as either Sac1/Not1 or Not1/Sal1 fragments using iProof high fidelity PCR kit (BioRad) (LegA11_KO-F/LegA11_KO1-R, LegA11_KO2-F/KO2-R; SidL_KO1-F/SidL_KO1-R, SidL_KO2-F/SidL_KO2-R; DotA_KO1-F/DotA_KO1-R, DotA_KO2-F/ DotA_KO2-R) (see Table 4.1) and cloned into the pSR47s vector and transformed into Top10 *E. coli. E.coli* harboring the donor knock-out plasmid were patched onto CYE agar with CR19 *E. coli* (helper) and SRS43 *L. pneumophila* (recipient) and incubated for 4-6 hours. The entire patch was then collected and plated on CYE + 10 μg mL^{-1} kanamycin and 100 μg mL^{-1} streptomycin (CYE + Kan10 + Sm100) and incubated for 4-days. Single colonies were streaked onto CYE + Kan10 + Sm100 and incubated for 4-days until single colonies arose. Individual colonies were then streaked onto CYE agar and incubated for 3-days. Colonies were finally streaked onto CYE + Sm100 + sucrose and incubated for 4-days. Individual colonies were duplicate patched on CYE + Kan10 + Sm100 and CYE agar and gene deletion was confirmed by colony PCR using the QUICK-LOAD Taq 2x Master Mix (New England Biolabs). Positive knockout colonies were

sensitive to kanamycin, confirming plasmid rejection, and have an amplicon of ~2 kbp when observed on a 1% agarose gel.

Legionella pneumophila transposon mutants were generated as part of Shames et al. 2017 using *Mariner* Tn insertion into the chromosome (162). iProof polymerase chain reaction (PCR) amplification of gene targets was used to confirm the transposon presence. Briefly, transposon mutants were streaked on CYE + CM5 and incubated as described above. Two isolated colonies were heavy patched on CYE + CM5 in duplicate. One heavy patch was collected and stocked, while the other was used for gDNA extraction (Illustra genomicPREP DNA isolation spin kit, GE healthcare). *sidL* and *legA11* genes were amplified from the transposon gDNA and wild-type *L. pneumophila* SRS43 gDNA using SidL_BamH1-F/SidL_Not1-R and LegA11_BamH1-F/LegA11_Not1-R respectively and ran on a 1% agarose gel. Bacteria positive for the transposon insertion amplified genes ~1 kb larger than the control amplicon from wild-type *L. pneumophila.* The *sidL*::Tn mutant carried a transposon positioned 25% into the gene, while the *legA11*::Tn insertion occurred 12% into the gene.

Vectors containing *sidL* and *legA11* were generated by amplifying the genes from SRS43 wildtype gDNA using an iProof PCR kit (see Table 4.1). GFP-tagged SidL and and $SidL_{T623N}$ was generated using BgIII_SidL-F/SalI_SidL-R and ligated into peGFP-C1 vector as a BglII/SalI fragment. Flag-tagged LegA11 for transfections was generated using BamH1_LegA11-F/LegA11_Not1-R and ligated into pcDNA-3FLAG as a BamH1/Not1 fragment. Flag-tagged LegA11 for intracellular growth curves was generated using BamH1_LegA11-F/ SalI_LegA11-R and ligated into PSN85 as a BamH1/Sal1 fragment. Flag-tagged SidL for intracellular growth curves was generated using SidLJBBamH1-F/Sal1_SidL-R and ligated into PSN85 as a BamH1/Sal1 fragment. GST-tagged SidL was generated using SidL_BamH1-F/Sal1_SidL-R and

ligated into pGEX-6P-1 as a BamH1/Sal1 fragment. GST-tagged LegA11 was generated using BamH1_LegA11-F/LegA11_Not1-R and ligated into pGEX-6P-1 as a BamH1/Not1 fragment. His-/Myc- tagged SidL was generated using BamH1_SidL-F/NotI_SidL-R and ligated into pT7HMT as BamH1/Not1 fragments. His-/Myc- tagged LegA11 was generated using BamH1_LegA11-F/Sal1_LegA11-R and ligated into pT7HMT as a BamH1/Sal1 fragment. $SidL_{T623N}$ was generated using SidL_T623N-F/SidL_T623N-R primers to mutate pT7HMT::SidL using iProof.

Table 4.1. Oligonucleotide primers used in this study.

Name	Sequence (5'-3')
LegA11_KO1-F	ATT**GTCGAC**GGGATCACCAATCGATGGACG
LegA11_KO1-R	ATT**GCGGCCGC**ACACCTATTTTCTATCGCCATAG
LegA11_KO2-F	ATT**GCGGCCGC**ATAAATTTTTTATCCTATCTATTAA
LegA11_KO2-R	ATT**GAGCTC**GATCAATCTATCTAAATCGGC
SidL_KO1-F	ATT**GTCGAC**CCGGTCATAAAGAAAAGAC
SidL_KO1-R	ATT**GCGGCCGC**ACATATAACCCTCTACCTCTTAG
SidL_KO2-F	ATT**GCGGCCGC**ATAAAGGATAATTTGGGTTCC
SidL_KO2-R	ATT**GAGCTC**CCCTAAAAGTGACTATTCAC
DotA_KO1-F	ATT**GTCGAC**GCCCTAGCTGTTTCATTGC
DotA_KO1-R	ATT**GCGGCCGC**ACATTCTTTCTCACCCAATAAC
DotA_KO2-F	ATT**GCGGCCGC**ATAACATTCAAAAACAATATA
Dota_KO2-R	ATT**GAGCTC**CCAAAACAAAATAACCAGCTG
BamH1_LegA11-F	ATT**GGATCC**TTGTGATTAAAATGGGTAGAAG
Sal1_LegA11-R	ATT**GTCGAC**TTAAAGTGCGTTTTTAGGGG
LegA11_Not1-R	ATT**GCGGCCGC**TAAAGTGCGTTTTTAGGGG
XBal_SidL-R	ATT**TCTAGA**TTAGCACCCATAAACAGTTCC
SidL_T623N-F	AACAAGAGCCTGATTATAAGTGGTTGCATCATTCATCGC
SidL_T623N-R	GCGATGAATGATGCAACCACTTATAATCAGGCTCTTGTT
BgIII_SidL-F	ATT**AGATCT**ATGCAAAACTTAGATGAGATTC
Sal1_SidL-R	ATT**GTCGAC**TTAGCACCCATAAACAGTTC
SidLJBBamHI-F	ATT**GGATCC**TTATGCAAAACTTAGATGAGATTC
Sidl_BamH1-f	ATT**GGATCC**ATGCAAAACTTAGATGAGATTC

Mice. C57Bl/6 *Nlrc4* -/- mice (a gift from Dr. Craig Roy) have been described (292). In-house colonies were maintained under specific pathogen-free conditions at Kansas State University. Bone marrow was harvested from 8- to 12-week-old mice as previously described (293). All

experiments involving animals were approved by the Kansas State University Institutional Animal Care and Use Committee (IACUC-4501 and -4022) and performed in compliance with the Animal Welfare Act and National Institutes of Health guidelines.

Intracellular Growth Curves. Mammalian cells were grown at 37˚C-5% CO_2. Bone marrow-derived macrophages were differentiated in RPMI 1640 media supplemented with 10% HI-FBS (Gibco) and 7.5% L929 cell supernatant. HEK293T (ATCC). BMDMs were seeded at $2.5x10^5$ cells per well one day prior to infection. BMDMs were infected with an MOI of 1 for 1 hour before washing 3x with PBS and replacing with fresh media.

Human leukemia monocytic cells (THP-1) were cultured in Dulbecco's modified Eagle medium (DMEM) (Gibco) supplemented with 10% HI-FBS (Gibco). THP-1 cells were seeded into 24-well plates at $5x10^5$ cells per well and differentiated with 100 nM phorbal 12-myristate 13-acetate (PMA) for 3 days before replacing with fresh PMA-free media and incubating for 24-hours. THP-1 cells were infected with an MOI of 1 for 1 hour before washing with PBS and replacing with fresh media.

Acanthamoeba castellanii was cultured at room temperature (~22˚C) in PYG broth [proteose peptone 0.75% (w/v), yeast extract 0.75% (w/v) and glucose 1.5% (w/v)] supplemented with $MgSO_4$, Sodium citrate, $Fe(NH_4)_2(SO_4)_2$, KH_2PO_4, Na_2PO_4 and $CaCl_2$ (328) within tissue culture flasks and infected at 37˚C in Ac infection media. One day prior to infection, cells were split 1:10 and incubated overnight. Prior to infection, cells were washed with warm Ac infection media, resuspended in PYG and quantified. Amoeba were seeded into 24-well plates and incubated for 1 hour at 37°C. Amoeba were inspected for adherence and then infected at a MOI of 0.1 for 45 minutes before washing 3x with Ac infection media and replaced with 1 mL fresh Ac infection media.

For all intracellular growth curves at each time point, cells were hypotonically lysed in sterile diH2O and detached by pipetting. Appropriate dilutions were made in sterile diH2O before plating on CYE agar. CYE plates were incubated for 4-days at 37°C and quantified.

Competitive Index. 8- to 12-week-old age- and sex- matched C57Bl/6 *Nlrc4* $^{-/-}$ mice were infected for competitive index (CI) experiments as previously described (162). Briefly, Bacterial inoculums containing a 1:1 mixture of indicated strains were delivered by intranasal inhalation. Inoculums were diluted and plated on plain and selective (10 μg ml^{-1} chloramphenicol) CYE. 48 hours post infection, mice were euthanized and whole lung tissue was harvested. The tissue was homogenized in 300 μL sterile water using a Bullet Blender (Next Advance). Dilutions were plated on plain and selective media as described above. CFU were counted and the CI values were calculated [$(CFUcm^{R}_{48h}/CFUwt_{48h})/(CFUcm^{R}_{IN}/CFUwt_{IN})$].

Recombinant protein expression and purification. Proteins of interest were recombinantly expressed in *E. coli* BL21 (DE3). Overnight cultures were grown in LB supplemented with appropriate antibiotic before subculturing 1:100. Subcultures were incubated at 37°C, 250 rpm for 3 hours and then protein expression was induced with 1 mM IPTG. Induction proceeded overnight (~18 hours) at 16°C. Cultures were centrifuged for 10 minutes at 3,000 rpm at 4°C to pellet the bacteria. Pellets were washed with ice-cold PBS and then lysed in bacterial lysis buffer (50 mM Tris, pH 8, 100 mM NaCl, 200 g ml^{-1} lysozyme, 2 mM dithiothreitol [DTT], 10 μg ml^{-1} DNase, and complete protease inhibitor) for >30 minutes on ice. Lysates were sonicated and centrifuged at 10,000 rpm for 30 minutes at 4°C to pellet cell debris. Supernatants were transferred to fresh, pre-chilled centrifuge bottles and centrifuged at 18,000 rpm for 25 minutes at 4°C to remove insoluble materials. The final supernatants were added Ni-NTA agarose beads (ThermoSci) plus 75 mM imidazole and incubated at 4°C with rotation for 1 hour. The bead-

protein solution was then added to BioRad Poly Prep chromatography columns and gravity filtered at 4°C. Beads were washed once with wash buffer (50 mM Tris, pH 8, 100 mM NaCl, 40 mM imidazole) and then eluted in 50 mM Tris, pH 8, 100 mM NaCl, 200 mM imidazole. Elutions were collected in 1.5 mL centrifuge tubes in 1 mL aliquots and protein production was analyzed via SDS-Page Coomassie staining. Protein containing aliquots were combined and dialyzed into 10 mM HEPES + 140 mM NaCl buffer for 48-hours. Protein concentration was quantified using Bradford Coomassie Brilliant Blue (ThermoFisher) and used immediately.

Translation Assay. Translation assays were performed using the Promega Flexi rabbit reticulocyte lysate (RLL) system (L4540) following the manufacturer's protocol. Briefly, a master mix of RLL was generated and aliquoted into individual tubes. Indicated amounts of purified His_6-SidL, His_6-$SidL_{T623N}$, or His_6-SidI (see above) were added to appropriate tubes. Purified recombinant (untagged) MesI or His_6-LegA11 was added at the indicated concentrations, molar ratios and timepoints. Proteins were kept on ice before use. Reaction mixtures were brought to 25 µL with ultrapure water and mixed by pipetting and briefly centrifuged before incubation at 30°C for 90 min. Translation of firefly luciferase mRNA (Promega) was quantified using a Victor 2 microplate reader (PerkinElmer).

Actin Polymerization. Actin polymerization was quantified using the Abcam actin polymerization kit (Product Number) following the manufacturer's protocol. Briefly, pyrene-labeled actin was reconstituted in the provided G-actin buffer supplemented with ATP for 1 hour on ice. 1 µM of His_6-SidL, His_6-$SidL_{T623N}$ or molar equivalent of His_6-LegA11 were added to supplemented G-actin buffer in a 96-well, clear bottom, black walled plate. Supplemented polymerization buffer (P-buffer) was added to appropriate wells and mixed briefly by pipetting up and down. Reactions were carried out for 1 hour at room temperature (~23°C) in the Synergy

Fluorescence plate reader. Fluorescence readings (excitation 365/ emission 410) were taken every 60 seconds.

Affinity chromatography. Overnight cultures of *E. coli* BL21 (DE3) grown in LB medium plus appropriate antibiotic were subcultured 1:100 into 20 ml LB and incubated at 37°C for 3 hours. Protein expression was induced with 1 mM IPTG overnight at 16°C. Cultures were centrifuged for 10 min at 3,000 rpm and washed with ice-cold PBS. Pellets were resuspended in 2 ml of cold lysis buffer (50 mM Tris, pH 8, 100 mM NaCl, 200 g ml^{-1} lysozyme, complete protease inhibitor) and incubated on ice for >30 min. 2 mM DTT was added to the lysates before sonicating on ice. Lysates were then clarified by centrifugation at 15,000 rpm for 15 min at 4°C. The supernatants were added to preequilibrated magnetic glutathione agarose beads (Pierce) following the manufacturer's protocol and incubated for 1 hour at 4°C with rotation. Beads were washed 2x with wash buffer (125 mM Tris-Cl, 150 mM NaCl, 1 mM DTT, pH 7.4) before adding subsequent cell lysates and incubating for 1 h at 4°C with rotation. This was repeated for additional proteins. Following binding, beads were washed 2x with wash buffer and transferred to fresh, prechilled 1.5-ml microcentrifuge tubes. Beads resuspended in 25 µl of 3x Laemmli sample buffer and boiled for 10 min. Samples were analyzed by SDS-PAGE and Coomassie brilliant blue staining or Western blotting, as indicated. For experiments to examine actin binding, HEK 293T cells grown to >70% confluence on tissue culture (TC)-treated dishes. Cells were washed once with ice-cold PBS and lysed in 1 ml of mammalian lysis buffer (1% NP-40 [vol/vol], 150 mM NaCl, 20 mM Tris-Cl, pH 7.5, 10 mM Na 4P2O7, 50 mM NaF, and complete protease inhibitor). Lysates were collected in prechilled 1.5-ml centrifuge tubes and centrifuged at 14,000 rpm for 20 min at 4°C. Supernatants were collected in prechilled 1.5-ml centrifuge tubes and stored on ice until use.

Cytochalasin D treatment. HEK293T were grown to >80% confluence in poly-L-lysine coated 10 cm TC-treated dishes. Media was removed from the cells and replaced with 5 mL DMEM + 10% HIFBS containing either 5 mM cytochalasin D (CytoD) (Tocris; 1233) in DMSO or equivalent volume of DMSO alone. Treated cells were incubated for 2 hours at 37°C 5% CO_2 and inspected for morphology changes indicative of CytoD treatment before lysing as described above. 5 mM CytoD or equivalent volume of DMSO alone were added to the supernatants following centrifuging to prevent spontaneous actin polymerization in treated samples.

Purified Actin. Unlabeled, lyophilized pure actin from rabbit skeletal muscle was purchased from Cytoskeleton, Inc (AKL99) and stored at 4°C. The proteins were suspended in 100 μL of sterile ultra pure water for 10 minutes, on ice with intermittent pipetting per manufacturer's protocol. The concentrated protein was then diluted to 200 μg/ mL in ice-cold general actin buffer (5 mM Tris-HCl pH 8.0, 0.2 mM $CaCl_2$) supplemented with 0.2 mM ATP and 0.5 mM DTT). Depolymerization was carried out on ice for 1 hour. The actin was then divided into 2 batches and 50 mM KCl and 2 mM $MgCl_2$ was added to one tube to induce polymerization (F-actin buffer.) Actin polymerization was carried out at 4°C for 1 hour. An equal volume of G-actin buffer was added to the other tube and left on ice. Equal amounts of G-actin and F-actin solutions were transferred to pre-chilled 5 mL ultracentrifuge tubes and centrifuged for 1 hour at 100,000 g at 4°C to pellet F-actin. The supernatant containing unpolymerized G-actin was removed from the F-actin tube and replaced with fresh F-actin buffer. The supernatant from the G-actin tube was transferred to a fresh tube, being careful not to disturb pelleted F-actin. 100 g (500 μL) of F-actin or G-actin was added to appropriate affinity chromatography samples following the protocol outlined above.

Densitometry. Western Blot and Coomassie images were inverted using Adobe Photoshop and the intensity of each sample band was measured using Fuji Image J software. Actin binding was normalized to the amount of GST-SidL present in each sample and actin inputs when appropriate. Background intensity was subtracted from all sample measures to account for image variability.

Confocal Microscopy. African green monkey fibroblasts (COS7) were cultured in Dulbecco's modified Eagle medium (DMEM) (Gibco) supplemented with 10% HI-FBS (Gibco). Cells were seeded 5 x 10^4 on poly-L-lysine-coated glass coverslips in 24-well tissue culture dishes one day prior to transfection. Cells were transfected using the Lipofectamine 3000 transfection kit (Invitrogen; L3000001) for 24 hours following manufacturers protocol. Coverslips were washed 3x with $PBS^{+/+}$ then fixed with 4% paraformaldehyde for 15 minutes and washed 3x with $PBS^{-/-}$ before staining with 1:1,000 rabbit a-GFP (Cell Signaling) and mouse α-FLAG primary antibodies (Sigma). Secondary 1:500 Alexa488-conjugated goat a-rabbit and Alexa546-conjugated α-mouse antibodies (ThermoFisher) and Phalloidin CruzFluor-633 (Santa Cruz Bio) were then added. Nuclei were stained with 1:2,000 Hoeshst (ThermoFisher) and coverslips were mounted on slides with ProLong™ Gold Antifade Mountant (Invitrogen). Representative images were acquired at the KSU College of Veterinary Medicine Confocal Core using a Zeiss LSM 880 inverted confocal microscope and processed using Fiji ImageJ and Adobe Photoshop software.

Replicative Vacuole Assay. Differentiated BMDMs were seeded 1x10^5 one day prior to infection on poly-L-Lysine coated coverslips. Cells were infected in triplicate wells with the indicated *L. pneumophila* strains at an MOI of 30 for 1 h or 10 h. For the 10 h timepoint, extracellular bacteria were removed after 1 h by washing coverslips three times in PBS-/- and incubated with fresh media for 9 h. Coverslips were fixed in 4% paraformaldehyde for 15 min

and permeabilized with ice-cold methanol. Coverslips were stained with 1:1,000 rabbit a-L. pneumophila (Invitrogen; PA17227) and mouse α-FLAG (Sigma) primary antibodies followed by 1:500 Alexa488-conjugated goat a-rabbit and Alexa546-conjugated α-mouse secondary antibodies (ThermoFisher). Nuclei were stained with 1:2,000 Hoeshst (ThermoFisher) and coverslips were mounted on slides with ProLong™ Gold Antifade Mountant (Invitrogen). Bacteria were scored blind on a Leica DMiL LED inverted epifluorescence microscope (n=300 per strain and time point).

Statistical analysis. Statistical analysis was performed with GraphPad 9 Prism software using analyses denoted in the figure legends.

Chapter 5- Conclusions

L. pneumophila intracellular replication is dependent on the secretion and function of effector proteins within its host cell. Effectors enter the host cell via a polar Dot/Icm T4SS tethered to the phagosome membrane (43). *L. pneumophila* encodes over 330 different effector proteins that function at various stages of infection to support survival. A large group of effectors modulate vesicle and organelle trafficking and recruit host components to the phagosome (4, 124). With this the phagosome expands and becomes embedded with ribosomes (4, 329). The modified phagosome presents an ideal environment for bacterial replication and is referred to as the *Legionella* containing vacuole (LCV) (11).

Following LCV biogenesis, *L. pneumophila* continues to regulate its host to support bacterial survival. *L. pneumophila* lacks the ability to synthesize several amino acids and the bacteria encodes at least 7 effectors that target host protein synthesis (124, 133, 235). Translation inhibiting effectors also facilitate cell cycle arrest in G phases that further promote bacterial survival (133). SidI and SidL are two translation inhibiting effectors in *L. pneumophila* (90, 100, 101, 124, 138). SidI is a mannosyl hydrolase that interacts with and likely modifies host translation machinery (Chapter 2). SidL has no predicted enzymatic activity but is hypothesized to inhibit translation through disruption of actin dynamics (Chapter 4). The activities of SidI and SidL are regulated by effector specific metaeffectors, MesI and LegA11. MesI and LegA11 contain protein-protein interaction domains characteristic of metaeffectors (126, 138, 158). The crystal structure of MesI consists of 14 α-helices and one single-turn helix that separates the protein into two distinct domains. The domains create grooves on either side of the protein that are predicted to interact with SidI within its tetratricopeptide repeats (TPR) (158). This aligns with data indicating that MesI binds SidI at both its N- and C- terminus (157, 158). The crystal

structure of LegA11 has not been solved but the sequence contains three predicted tandem ankyrin repeats that are commonly involved in protein-protein interactions in eukaryotic cells (160, 215, 330). LegA11 increased actin retention by SidL and we were unable to detect a direct interaction between LegA11 and actin. It is possible that LegA11 modulates SidL actin affinity, or weakly interacts with actin. The dynamics of these interactions could be evaluated using an analytical method such as surface plasmon resonance that is more sensitive to changes in binding affinity compared to affinity chromatography (318).

The metaeffector, LegL1 possesses no enzymatic activity but regulates its target effector, RavJ, through competitive inhibition (126). We initially hypothesized that MesI and LegA11 similarly regulated SidI and SidL respectively, given the lack of evidence to support enzymatic activity. Unexpectedly, while both metaeffectors suppressed the activities of their target effectors, neither were able to outcompete known host binding targets and SidL retained more actin in the presence of LegA11. It could be speculated that metaeffector binding induces a conformational change to SidI and SidL that renders them inactive, however, the possibility of LegA11 possessing enzymatic activity has not been eliminated. Conformational changes during protein-protein interactions can be evaluated using crystallography (331), however, not all proteins readily crystallize. Other methods such as fluorescence resonance energy transfer (FRET) or selective labeling with pyrene can provide insight into conformational changes without the need for crystallography (332, 333). Further research is needed to elucidate the mechanisms by which MesI and LegA11 regulate their effectors.

It is hypothesized that the SidL-LegA11 complex may behave similarly to host cell capping protein (CP), with LegA11 acting as the β-subunit which increases actin retention of the α-subunit . Immunoprecipitation experiments with actin immobilized on α-actin protein G beads

incubated with purified SidL, LegA11 and CP could investigate if the proteins compete for actin binding. This could similarly be attempted using host cell infection with a high multiplicity of infection with *L. pneumophila* overexpressing *sidL*. To examine metaeffector contributions to this interaction, a *3xflag*-LegA11 could be ectopically expressed in HEK293 FcγRII cells prior to infection. This could be examined through immunoprecipitation of actin or CP to determine their interactions with each other in the presence of SidL and LegA11. If LegA11 is required to effectively outcompete CP, the *legA11*-deficient phenotype could be attributed to decreased SidL activity and consequently decreased effector triggered immunity to *L. pneumophila* infection.

We discovered a novel intrabacterial role for the translocated metaeffector, MesI. MesI modulates SidI translocation into host cells at late stages of infection and a non-translocated MesIΔ10 construct can support intracellular survival (Chapter 3, (265)). It is widely accepted that secreted bacterial effectors target host cell components and therefore do not function within the bacteria (334, 335). Our findings challenge this dogma and demonstrate the need for effector regulation within the bacterial cell. Previous studies have examined the expression and production of effectors throughout the *L. pneumophila* life cycle (28, 101, 265). Although these studies provide valuable insight, they are largely conducted *in vitro* and do not always reflect effector expression during infection (49, 336). Ideally, effector mRNA expression would be evaluated during intracellular growth using reverse transcriptase quantitative polymerase chain reaction (RT-qPCR) (337). RT-qPCR combined with observation of protein levels and effector translocation following expression from the endogenous promoter would provide a better picture of temporal effector regulation by metaeffectors. As we observed, translocated substrates can be difficult to detect using western blot, even when overexpressed. This could potentially be circumvented by fusion of the *Bordetella pertussis* adenylate cyclase (CyaA) active domain to

genes of interest within the *L. pneumophila* genome (338). Given the temporal regulation of SidI translocation into the host cell, it is hypothesized that SidI expression precedes that of MesI and *in vitro* studies support this hypothesis (265).

This does not necessarily explain the cause or regulation of SidI toxicity. If MesI suppresses intrabacterial toxicity by binding SidI in an inactive state, it could be argued that expression occurs simultaneously. Therefore it would be prudent to examine SidI activity within the bacterial cell. Mass spectrometry could potentially identify modifications to bacterial proteins during *in vitro* growth with and without *mesI.* SidI is known to interact with host eEF1A, eEF1Bγ,and Valyl-tRNA synthetase as well to activate the heat shock response (101). These are conserved processes, and it is hypothesized that SidI toxicity is a result of modifications to bacterial homologs of translational machinery. Bacterial global translation can be examined using incorporation of ^{35}S-methionine or the non-radioactive L-methionine analog, L-azidohomoalanine (AHA). Incorporated AHA in newly synthesized proteins can be coupled to biotin via Copper (II)-TBTA complex click chemistry and isolated using streptavidin (339). If SidI targets bacterial translation machinery, we would anticipate less AHA or ^{35}S-methionine incorporation in the absence of *mesI*, representing decreased global translation. It may also be possible to measure translation by detection of adenylate cyclase from a plasmid in *L. pneumophila* pBAD_araC arabinose inducible strains. Western blotting is a common tool used by researchers to detect protein production overtime (129, 130, 145, 146). Target reporter protein levels would be measured by western blot and densitometry and normalized to bacterial titer using a loading control such as isocitrate dehydrogenase (ICDH). *L. pneumophila* pBAD_araC strains harboring a reporter plasmid would be grown without induction to subvert SidI growth attenuation. Once an adequate bacterial titer is achieved (>10^6 cells/mL), expression of *sidI* and

the reporter protein would be induced, and western blotting of samples would detect protein production overtime.

Unlike SidI, SidL has no predicted enzymatic activity and hasn't been shown to interact with translation machinery. It is unclear if *sidL* overexpression is deleterious to *L. pneumophila* replication or if the decreased growth is an artifact of *in vitro* growth. If the observation is related to SidL function, it could be speculated that the effector is able interact with the bacterial actin analog, MreB. MreB must interact with FtsZ to enable effective cell division (324, 340). If SidL competitive inhibition of MreB-FtsZ binding is responsible for the *in vitro* phenotype, we would anticipate that cells sampled from exponentially growing cultures would display shorter, rounder morphologies characteristic of MreB inhibition (324). Affinity chromatography using a GST-SidL immobilized on glutathione beads and incubated with *L. pneumophila* cell lysates could reveal if interactions between SidL and Mreb are possible. Overexpressing *sidL* in the absence of *legA11* would provide further insight into an intrabacterial role for LegA11, similar to observations between SidI and MesI.

Loss of *legA11* during intracellular growth in *Nlrc4*-deficient macrophages proved beneficial for *L. pneumophila*. Although the cause of this advantage is unknown, it can be deduced that it is cell line specific given the lack of phenotype in *Acanthamoeba castellanii* and THP-1 cells and the contrasting phenotype in human macrophages (hMDM) and *Hartmannella vermiformis* (215). LegA11 suppressed the inhibitory activities of SidL and it could be argued that the phenotype associated with the loss of *legA11* is a result of SidL activity, however the possibility of LegA11 inducing an immune response has not been eliminated. Evaluating the ability of LegA11 to interact with host cell components using mass spectrometry could provide evidence to support activation of the immune response by LegA11. It is known the BMDMs

produce TNF in response to *L. pneumophila* infection and that disruption of β-actin dampens TNF production (322, 341). If the phenotype is the result of SidL activity, it could be hypothesized that disruption of actin by SidL dampens TNF production in response to *L. pneumophila ΔlegA11*. The cytokine response to *L. pneumophila* strains lacking *legA11* could be quantified by RT-PCR and ELISA and compared to those infected with wild type bacteria to observe if circumvention of this immune response is responsible for the phenotype (103, 269, 337).

Here we described the regulation of two translation inhibition effectors by metaeffectors in the intracellular pathogen, *L. pneumophila.* Although SidI and SidL demonstrate different modes of action, both are similarly regulated by their metaeffectors. The metaeffectors, MesI and LegA11, suppress the translation inhibitory activities of their cognate effectors, in addition to the mannosyl hydrolase activity of SidI (MesI), and actin polymerization activities of SidL (LegA11). While other metaeffectors enzymatically alter their target effectors (126, 138, 149–152, 156, 319, 342), our data currently suggest that MesI and LegA11 regulate their cognate effectors through direct interactions alone. Future studies will aim to fully elucidate the mechanism(s) by which these metaeffectors control their target effectors and understand the consequences of unregulated effector activity. The research presented in this dissertation and ongoing efforts will expand our knowledge of *L. pneumophila* virulence and complex host-pathogen interactions.

References

1. Whiley H, Bentham R. 2011. Legionella longbeachae and Legionellosis - Volume 17, Number 4—April 2011 - Emerging Infectious Diseases journal - CDC. Emerg Infect Dis 17:579–583.

2. Heijnsbergen E van, Schalk JAC, Euser SM, Brandsema PS, Boer JW den, Husman AM de R. 2015. Confirmed and Potential Sources of Legionella Reviewed. Environ Sci Technol 49:4797–4815.

3. Gomez-Valero L, Rusniok C, Carson D, Mondino S, Pérez-Cobas AE, Rolando M, Pasricha S, Reuter S, Demirtas J, Crumbach J, Descorps-Declere S, Hartland EL, Jarraud S, Dougan G, Schroeder GN, Frankel G, Buchrieser C. 2019. More than 18,000 effectors in the Legionella genus genome provide multiple, independent combinations for replication in human cells. Proc National Acad Sci 116:201808016.

4. Chauhan D, Shames SR. 2021. Pathogenicity and Virulence of Legionella: Intracellular replication and host response. Virulence 12:1122–1144.

5. Appelt S, Heuner K. 2017. The Flagellar Regulon of Legionella—A Review. Front Cell Infect Mi 7:454.

6. Dietrich C, Heuner K, Brand BC, Hacker J, Steinert M. 2001. Flagellum of Legionella pneumophila Positively Affects the Early Phase of Infection of Eukaryotic Host Cells. Infect Immun 69:2116–2122.

7. George JR, Pine L, Reeves MW, Harrell WK. 1980. Amino acid requirements of Legionella pneumophila. J Clin Microbiol 11:286–291.

8. Murga R, Forster TS, Brown E, Pruckler JM, Fields BS, Donlan RM. 2001. Role of biofilms in the survival of Legionella pneumophila in a model potable-water system. Microbiology+ 147:3121–3126.

9. Temmerman R, Vervaeren H, Noseda B, Boon N, Verstraete W. 2006. Necrotrophic Growth of Legionella pneumophila. Appl Environ Microb 72:4323–4328.

10. Taylor M, Ross K, Bentham R. 2009. Legionella, Protozoa, and Biofilms: Interactions Within Complex Microbial Systems. Microbial Ecol 58:538–547.

11. Isberg RR, O'Connor TJ, Heidtman M. 2009. The Legionella pneumophila replication vacuole: making a cosy niche inside host cells. Nat Rev Microbiol 7:13–24.

12. Graells T, Ishak H, Larsson M, Guy L. 2018. The all-intracellular order Legionellales is unexpectedly diverse, globally distributed and lowly abundant. Fems Microbiol Ecol 94:fiy185.

13. Vandersmissen L, Buck ED, Saels V, Coil DA, Anné J. 2010. A Legionella pneumophila collagen-like protein encoded by a gene with a variable number of tandem repeats is involved in the adherence and invasion of host cells. Fems Microbiol Lett 306:168–176.

14. Chang B, Kura F, Amemura-Maekawa J, Koizumi N, Watanabe H. 2005. Identification of a Novel Adhesion Molecule Involved in the Virulence of Legionella pneumophila. Infect Immun 73:4272–4280.

15. Palusinska-Szysz M, Luchowski R, Gruszecki WI, Choma A, Szuster-Ciesielska A, Lück C, Petzold M, Sroka-Bartnicka A, Kowalczyk B. 2019. The Role of Legionella pneumophila Serogroup 1 Lipopolysaccharide in Host-Pathogen Interaction. Front Microbiol 10:2890.

16. Abdel-Nour M, Duncan C, Prashar A, Rao C, Ginevra C, Jarraud S, Low DE, Ensminger AW, Terebiznik MR, Guyard C. 2014. The Legionella pneumophila Collagen-Like Protein Mediates Sedimentation, Autoaggregation, and Pathogen-Phagocyte Interactions. Appl Environ Microb 80:1441–1454.

17. HORWITZ M. 1984. Phagocytosis of the legionnaires' disease bacterium (legionella pneumophila) occurs by a novel mechanism: Engulfment within a Pseudopod coil. Cell 36:27–33.

18. Bozue JA, Johnson W. 1996. Interaction of Legionella pneumophila with Acanthamoeba castellanii: uptake by coiling phagocytosis and inhibition of phagosome-lysosome fusion. Infect Immun 64:668–673.

19. Williams SK, Weiner ZP, Gilmore RD. 2018. Human neuroglial cells internalize Borrelia burgdorferi by coiling phagocytosis mediated by Daam1. Plos One 13:e0197413.

20. Naj X, Hoffmann A-K, Himmel M, Linder S. 2013. The Formins FMNL1 and mDia1 Regulate Coiling Phagocytosis of Borrelia burgdorferi by Primary Human Macrophages. Infect Immun 81:1683–1695.

21. Linder S, Heimerl C, Fingerle V, Aepfelbacher M, Wilske B. 2001. Coiling Phagocytosis of Borrelia burgdorferi by Primary Human Macrophages Is Controlled by CDC42Hs and Rac1 and Involves Recruitment of Wiskott-Aldrich Syndrome Protein and Arp2/3 Complex. Infect Immun 69:1739–1746.

22. Horwitz MA. 1983. Formation of a novel phagosome by the Legionnaires' disease bacterium (Legionella pneumophila) in human monocytes. J Exp Medicine 158:1319–1331.

23. Escoll P, Song O-R, Viana F, Steiner B, Lagache T, Olivo-Marin J-C, Impens F, Brodin P, Hilbi H, Buchrieser C. 2017. Legionella pneumophila Modulates Mitochondrial Dynamics to Trigger Metabolic Repurposing of Infected Macrophages. Cell Host Microbe 22:302-316.e7.

24. Swanson MS, Isberg RR. 1995. Association of Legionella pneumophila with the macrophage endoplasmic reticulum. Infect Immun 63:3609–20.

25. Robinson CG, Roy CR. 2006. Attachment and fusion of endoplasmic reticulum with vacuoles containing Legionella pneumophila. Cell Microbiol 8:793–805.

26. Heidtman M, Chen EJ, Moy M, Isberg RR. 2009. Large-scale identification of Legionella pneumophila Dot/Icm substrates that modulate host cell vesicle trafficking pathways. Cell Microbiol 11:230–248.

27. Sauer J-D, Bachman MA, Swanson MS. 2005. The phagosomal transporter A couples threonine acquisition to differentiation and replication of Legionella pneumophila in macrophages. Proc National Acad Sci 102:9924–9929.

28. Aurass P, Gerlach T, Becher D, Voigt B, Karste S, Bernhardt J, Riedel K, Hecker M, Flieger A. 2016. Life Stage-specific Proteomes of Legionella pneumophila Reveal a Highly Differential Abundance of Virulence-associated Dot/Icm effectors. Mol Cell Proteomics 15:177–200.

29. Personnic N, Striednig B, Lezan E, Manske C, Welin A, Schmidt A, Hilbi H. 2019. Quorum sensing modulates the formation of virulent Legionella persisters within infected cells. Nat Commun 10:5216.

30. Schell U, Simon S, Sahr T, Hagar D, Albers MF, Kessler A, Fahrnbauer F, Trauner D, Hedberg C, Buchrieser C, Hilbi H. 2015. The α-hydroxyketone LAI-1 regulates motility, Lqs-dependent phosphorylation signalling and gene expression of Legionella pneumophila 99:778–793.

31. Tiaden A, Spirig T, Carranza P, Brüggemann H, Riedel K, Eberl L, Buchrieser C, Hilbi H. 2008. Synergistic Contribution of the Legionella pneumophila lqs Genes to Pathogen-Host Interactions. J Bacteriol 190:7532–7547.

32. Spirig T, Tiaden A, Kiefer P, Buchrieser C, Vorholt JA, Hilbi H. 2008. The Legionella Autoinducer Synthase LqsA Produces an α-Hydroxyketone Signaling Molecule*. J Biol Chem 283:18113–18123.

33. Tiaden A, Spirig T, Sahr T, Wälti MA, Boucke K, Buchrieser C, Hilbi H. 2010. The autoinducer synthase LqsA and putative sensor kinase LqsS regulate phagocyte interactions, extracellular filaments and a genomic island of Legionella pneumophila. Environ Microbiol 12:1243–1259.

34. Hochstrasser R, Hutter CAJ, Arnold FM, Barlocher K, Seeger MA, Hilbi H. 2020. The structure of the Legionella response regulator LqsR reveals amino acids critical for phosphorylation and dimerization. Molecular Microbiology 113:1070–1084.

35. Abu-Zant A, Asare R, Graham JE, Kwaik YA. 2006. Role for RpoS but Not RelA of Legionella pneumophila in Modulation of Phagosome Biogenesis and Adaptation to the Phagosomal Microenvironment. Infect Immun 74:3021–3026.

36. Dalebroux ZD, Edwards RL, Swanson MS. 2009. SpoT governs Legionella pneumophila differentiation in host macrophages. Mol Microbiol 71:640–658.

37. Verdon J, Labanowski J, Sahr T, Ferreira T, Lacombe C, Buchrieser C, Berjeaud J-M, Héchard Y. 2011. Fatty acid composition modulates sensitivity of Legionella pneumophila to warnericin RK, an antimicrobial peptide. Biochimica Et Biophysica Acta Bba - Biomembr 1808:1146–1153.

38. Ferhat M, Atlan D, Vianney A, Lazzaroni J-C, Doublet P, Gilbert C. 2009. The TolC Protein of Legionella pneumophila Plays a Major Role in Multi-Drug Resistance and the Early Steps of Host Invasion. Plos One 4:e7732.

39. Vandewalle-Capo M, Massip C, Descours G, Charavit J, Chastang J, Billy PA, Boisset S, Lina G, Gilbert C, Maurin M, Jarraud S, Ginevra C. 2017. Minimum inhibitory concentration (MIC) distribution among wild-type strains of Legionella pneumophila identifies a subpopulation with reduced susceptibility to macrolides owing to efflux pump genes. Int J Antimicrob Ag 50:684–689.

40. Personnic N, Striednig B, Hilbi H. 2021. Quorum sensing controls persistence, resuscitation, and virulence of Legionella subpopulations in biofilms. Isme J 15:196–210.

41. Lüneberg E, Zähringer U, Knirel YA, Steinmann D, Hartmann M, Steinmetz I, Rohde M, Köhl J, Frosch M. 1998. Phase-variable Expression of Lipopolysaccharide Contributes to the Virulence of Legionella pneumophila. J Exp Medicine 188:49–60.

42. Qiu J, Luo Z-Q. 2017. Legionella and Coxiella effectors: strength in diversity and activity. Nat Rev Microbiol 15:591–605.

43. Böck D, Hüsler D, Steiner B, Medeiros JM, Welin A, Radomska KA, Hardt W-D, Pilhofer M, Hilbi H. 2021. The Polar Legionella Icm/Dot T4SS Establishes Distinct Contact Sites with the Pathogen Vacuole Membrane. Mbio 12:e02180-21.

44. Jeong KC, Ghosal D, Chang Y-W, Jensen GJ, Vogel JP. 2017. Polar delivery of Legionella type IV secretion system substrates is essential for virulence. Proc National Acad Sci 114:8077–8082.

45. Durie CL, Sheedlo MJ, Chung JM, Byrne BG, Su M, Knight T, Swanson M, Lacy DB, Ohi MD. 2020. Structural analysis of the Legionella pneumophila Dot/Icm Type IV Secretion System Core Complex. Elife 9:e59530.

46. Burstein D, Zusman T, Degtyar E, Viner R, Segal G, Pupko T. 2009. Genome-Scale Identification of Legionella pneumophila Effectors Using a Machine Learning Approach. Plos Pathog 5:e1000508.

47. Segal G, Shuman HA. 1999. Legionella pneumophila Utilizes the Same Genes To Multiply within Acanthamoeba castellanii and Human Macrophages. Infect Immun 67:2117–2124.

48. Best A, Kwaik YA. 2018. Evolution of the Arsenal of Legionella pneumophila Effectors To Modulate Protist Hosts. Mbio 9:e01313-18.

49. Faucher SP, Mueller CA, Shuman HA. 2011. Legionella Pneumophila Transcriptome during Intracellular Multiplication in Human Macrophages. Front Microbiol 2:60.

50. Park JM, Ghosh S, O'Connor TJ. 2020. Combinatorial selection in amoebal hosts drives the evolution of the human pathogen Legionella pneumophila. Nat Microbiol 5:599–609.

51. O'Connor TJ, Boyd D, Dorer MS, Isberg RR. 2012. Aggravating Genetic Interactions Allow a Solution to Redundancy in a Bacterial Pathogen. Science 338:1440–1444.

52. Li X, Rydzewski N, Hider A, Zhang X, Yang J, Wang W, Gao Q, Cheng X, Xu H. 2016. A molecular mechanism to regulate lysosome motility for lysosome positioning and tubulation. Nat Cell Biol 18:404–417.

53. Keller S, Berghoff K, Kress H. 2017. Phagosomal transport depends strongly on phagosome size. Sci Rep-uk 7:17068.

54. Liebl D, Griffiths G. 2009. Transient assembly of F-actin by phagosomes delays phagosome fusion with lysosomes in cargo-overloaded macrophages. J Cell Sci 122:2935–2945.

55. Nguyen JA, Yates RM. 2021. Better Together: Current Insights Into Phagosome-Lysosome Fusion. Frontiers in Immunology 12.

56. Ziltener P, Reinheckel T, Oxenius A. 2016. Neutrophil and Alveolar Macrophage-Mediated Innate Immune Control of Legionella pneumophila Lung Infection via TNF and ROS. Plos Pathog 12:e1005591.

57. Zhang C-S, Jiang B, Li M, Zhu M, Peng Y, Zhang Y-L, Wu Y-Q, Li TY, Liang Y, Lu Z, Lian G, Liu Q, Guo H, Yin Z, Ye Z, Han J, Wu J-W, Yin H, Lin S-Y, Lin S-C. 2014. The Lysosomal v-ATPase-Ragulator Complex Is a Common Activator for AMPK and mTORC1, Acting as a Switch between Catabolism and Anabolism. Cell Metab 20:526–540.

58. Ratto E, Chowdhury SR, Siefert NS, Schneider M, Wittmann M, Helm D, Palm W. 2022. Direct control of lysosomal catabolic activity by mTORC1 through regulation of V-ATPase assembly. Nat Commun 13:4848.

59. Rybicka JM, Balce DR, Khan MF, Krohn RM, Yates RM. 2010. NADPH oxidase activity controls phagosomal proteolysis in macrophages through modulation of the lumenal redox environment of phagosomes. Proc National Acad Sci 107:10496–10501.

60. Xia Y, Liu N, Xie X, Bi G, Ba H, Li L, Zhang J, Deng X, Yao Y, Tang Z, Yin B, Wang J, Jiang K, Li Z, Choi Y, Gong F, Cheng X, O'Shea JJ, Chae JJ, Laurence A, Yang X-P. 2019. The macrophage-specific V-ATPase subunit ATP6V0D2 restricts inflammasome activation and bacterial infection by facilitating autophagosome-lysosome fusion. Autophagy 15:960–975.

61. Fernandez-Moreira E, Helbig JH, Swanson MS. 2006. Membrane Vesicles Shed by Legionella pneumophila Inhibit Fusion of Phagosomes with Lysosomes. Infect Immun 74:3285–3295.

62. Xu L, Shen X, Bryan A, Banga S, Swanson MS, Luo Z-Q. 2010. Inhibition of Host Vacuolar H+-ATPase Activity by a Legionella pneumophila Effector. Plos Pathog 6:e1000822.

63. Prevost MS, Pinotsis N, Dumoux M, Hayward RD, Waksman G. 2017. The Legionella effector WipB is a translocated Ser/Thr phosphatase that targets the host lysosomal nutrient sensing machinery. Sci Rep-uk 7:9450.

64. Shohdy N, Efe JA, Emr SD, Shuman HA. 2005. Pathogen effector protein screening in yeast identifies Legionella factors that interfere with membrane trafficking. Proc National Acad Sci 102:4866–4871.

65. Felipe KS de, Glover RT, Charpentier X, Anderson OR, Reyes M, Pericone CD, Shuman HA. 2008. Legionella Eukaryotic-Like Type IV Substrates Interfere with Organelle Trafficking. Plos Pathog 4:e1000117.

66. West ZE, Aitcheson SM, Semmler ABT, Murray RZ. 2021. The trans-SNARE complex VAMP4/Stx6/Stx7/Vti1b is a key regulator of Golgi to late endosome MT1-MMP transport in macrophages. Traffic 22:368–376.

67. Bennett TL, Kraft SM, Reaves BJ, Mima J, O'Brien KM, Starai VJ. 2013. LegC3, an Effector Protein from Legionella pneumophila, Inhibits Homotypic Yeast Vacuole Fusion In Vivo and In Vitro. Plos One 8:e56798.

68. Shi X, Halder P, Yavuz H, Jahn R, Shuman HA. 2016. Direct targeting of membrane fusion by SNARE mimicry: Convergent evolution of Legionella effectors. Proc National Acad Sci 113:8807–8812.

69. Franco IS, Shohdy N, Shuman HA. 2012. The Legionella pneumophila Effector VipA Is an Actin Nucleator That Alters Host Cell Organelle Trafficking. Plos Pathog 8:e1002546.

70. Michard C, Sperandio D, Baïlo N, Pizarro-Cerdá J, LeClaire L, Chadeau-Argaud E, Pombo-Grégoire I, Hervet E, Vianney A, Gilbert C, Faure M, Cossart P, Doublet P. 2015. The Legionella Kinase LegK2 Targets the ARP2/3 Complex To Inhibit Actin Nucleation on Phagosomes and Allow Bacterial Evasion of the Late Endocytic Pathway. Mbio 6:e00354-15.

71. He L, Lin Y, Ge Z, He S, Zhao B, Shen D, He J, Lu Y. 2019. The Legionella pneumophila effector WipA disrupts host F-actin polymerisation by hijacking phosphotyrosine signalling. Cell Microbiol 21:e13014.

72. Gaspar AH, Machner MP. 2014. VipD is a Rab5-activated phospholipase A1 that protects Legionella pneumophila from endosomal fusion. Proc National Acad Sci 111:4560–4565.

73. Machner MP, Isberg RR. 2006. Targeting of Host Rab GTPase Function by the Intravacuolar Pathogen Legionella pneumophila. Dev Cell 11:47–56.

74. Tan Y, Luo Z-Q. 2011. Legionella pneumophila SidD is a deAMPylase that modifies Rab1. Nature 475:506–509.

75. Ingmundson A, Delprato A, Lambright DG, Roy CR. 2007. Legionella pneumophila proteins that regulate Rab1 membrane cycling. Nature 450:365–369.

76. Müller MP, Peters H, Blümer J, Blankenfeldt W, Goody RS, Itzen A. 2010. The Legionella Effector Protein DrrA AMPylates the Membrane Traffic Regulator Rab1b. Science 329:946–949.

77. Horwitz MA. 1983. The Legionnaires' disease bacterium (Legionella pneumophila) inhibits phagosome-lysosome fusion in human monocytes. J Exp Medicine 158:2108–2126.

78. Chong A, Lima CA, Allan DS, Nasrallah GK, Garduño RA. 2009. The Purified and Recombinant Legionella pneumophila Chaperonin Alters Mitochondrial Trafficking and Microfilament Organization. Infect Immun 77:4724–4739.

79. Edwards M, Zwolak A, Schafer DA, Sept D, Dominguez R, Cooper JA. 2014. Capping protein regulators fine-tune actin assembly dynamics. Nat Rev Mol Cell Bio 15:677–689.

80. Dominguez R, Holmes KC. 2011. Actin Structure and Function. Annu Rev Biophys 40:169–186.

81. Kovar DR, Harris ES, Mahaffy R, Higgs HN, Pollard TD. 2006. Control of the Assembly of ATP- and ADP-Actin by Formins and Profilin. Cell 124:423–435.

82. Kandl K, Munshi R, Ortiz P, Andersen G, Kinzy T, Adams A. 2002. Identification of a role for actin in translational fidelity in yeast. Mol Genet Genomics 268:10–18.

83. Amberg DC, Basart E, Botstein D. 1995. Defining protein interactions with yeast actin in vivo. Nature Structural Biology 2:28–35.

84. Furukawa R, Jinks TM, Tishgarten T, Mazzawi M, Morris DR, Fechheimer M. 2001. Elongation factor 1β is an actin-binding protein. Biochimica Et Biophysica Acta Bba - Gen Subj 1527:130–140.

85. Klyachko N, Aksenova L, Dunaeva M, Kulikova A. 2000. INTERACTION OF PLANT POLYSOMES WITH THE ACTIN CYTOSKELETON. Cell Biol Int 24:351–358.

86. Gross SR, Kinzy TG. 2007. Improper Organization of the Actin Cytoskeleton Affects Protein Synthesis at Initiation ▿ . Mol Cell Biol 27:1974–1989.

87. Németh ZH, Deitch EA, Davidson MT, Szabó C, Vizi ES, Haskó G. 2004. Disruption of the actin cytoskeleton results in nuclear factor-κB activation and inflammatory mediator production in cultured human intestinal epithelial cells. J Cell Physiol 200:71–81.

88. Elliott JA, Winn WC. 1986. Treatment of alveolar macrophages with cytochalasin D inhibits uptake and subsequent growth of Legionella pneumophila. Infect Immun 51:31–36.

89. King CH, Fields BS, Shotts EB, White EH. 1991. Effects of cytochalasin D and methylamine on intracellular growth of Legionella pneumophila in amoebae and human monocyte-like cells. Infect Immun 59:758–763.

90. Guo Z, Stephenson R, Qiu J, Zheng S, Luo Z-Q. 2014. A Legionella effector modulates host cytoskeletal structure by inhibiting actin polymerization. Microbes Infect 16:225–236.

91. Eylert E, Herrmann V, Jules M, Gillmaier N, Lautner M, Buchrieser C, Eisenreich W, Heuner K. 2010. Isotopologue Profiling of Legionella pneumophila ROLE OF SERINE AND GLUCOSE AS CARBON SUBSTRATES*. J Biol Chem 285:22232–22243.

92. Gillmaier N, Schunder E, Kutzner E, Tlapák H, Rydzewski K, Herrmann V, Stämmler M, Lasch P, Eisenreich W, Heuner K. 2016. Growth-related Metabolism of the Carbon Storage Poly-3-hydroxybutyrate in Legionella pneumophila *. J Biol Chem 291:6471–6482.

93. Häuslein I, Sahr T, Escoll P, Klausner N, Eisenreich W, Buchrieser C. 2017. Legionella pneumophila CsrA regulates a metabolic switch from amino acid to glycerolipid metabolism. Open Biol 7:170149.

94. Price CTD, Al-Quadan T, Santic M, Rosenshine I, Kwaik YA. 2011. Host proteasomal degradation generates amino acids essential for intracellular bacterial growth. Sci New York N Y 334:1553–7.

95. Zhang N, Yin S, Zhang W, Gong X, Zhang N, Fang K, Ge H. 2017. Crystal Structure and Biochemical Characterization of an Aminopeptidase LapB from Legionella pneumophila. J Agr Food Chem 65:7569–7578.

96. Rossier O, Starkenburg SR, Cianciotto NP. 2003. Legionella pneumophila Type II Protein Secretion Promotes Virulence in the A/J Mouse Model of Legionnaires' Disease Pneumonia. Infect Immun 72:310–321.

97. Rossier O, Dao J, Cianciotto NP. 2008. The Type II Secretion System of Legionella pneumophila Elaborates Two Aminopeptidases, as Well as a Metalloprotease That Contributes to Differential Infection among Protozoan Hosts. Appl Environ Microb 74:753–761.

98. White RC, Gunderson FF, Tyson JY, Richardson KH, Portlock TJ, Garnett JA, Cianciotto NP. 2018. Type II Secretion-Dependent Aminopeptidase LapA and Acyltransferase PlaC Are Redundant for Nutrient Acquisition during Legionella pneumophila Intracellular Infection of Amoebas. Mbio 9:e00528-18.

99. Wieland H, Ullrich S, Lang F, Neumeister B. 2005. Intracellular multiplication of Legionella pneumophila depends on host cell amino acid transporter SLC1A5. Mol Microbiol 55:1528–1537.

100. Fontana MF, Banga S, Barry KC, Shen X, Tan Y, Luo Z-Q, Vance RE. 2011. Secreted Bacterial Effectors That Inhibit Host Protein Synthesis Are Critical for Induction of the Innate Immune Response to Virulent Legionella pneumophila. Plos Pathog 7:e1001289.

101. Shen X, Banga S, Liu Y, Xu L, Gao P, Shamovsky I, Nudler E, Luo Z. 2009. Targeting eEF1A by a Legionella pneumophila effector leads to inhibition of protein synthesis and induction of host stress response. Cell Microbiol 11:911–926.

102. Belyi Y, Tabakova I, Stahl M, Aktories K. 2008. Lgt: a Family of Cytotoxic Glucosyltransferases Produced by Legionella pneumophila ▿ †. J Bacteriol 190:3026–3035.

103. Barry KC, Fontana MF, Portman JL, Dugan AS, Vance RE. 2013. IL-1α Signaling Initiates the Inflammatory Response to Virulent Legionella pneumophila In Vivo. J Immunol 190:6329–6339.

104. Moss SM, Taylor IR, Ruggero D, Gestwicki JE, Shokat KM, Mukherjee S. 2019. A Legionella pneumophila Kinase Phosphorylates the Hsp70 Chaperone Family to Inhibit Eukaryotic Protein Synthesis. Cell Host Microbe 25:454-462.e6.

105. Belyi Y, Niggeweg R, Opitz B, Vogelsgesang M, Hippenstiel S, Wilm M, Aktories K. 2006. Legionella pneumophila glucosyltransferase inhibits host elongation factor 1A. Proc National Acad Sci 103:16953–16958.

106. Tzivelekidis T, Jank T, Pohl C, Schlosser A, Rospert S, Knudsen CR, Rodnina MV, Belyi Y, Aktories K. 2011. Aminoacyl-tRNA-charged eukaryotic elongation factor 1A is the bona fide substrate for Legionella pneumophila effector glucosyltransferases. Plos One 6:e29525.

107. Leon JAD, Qiu J, Nicolai CJ, Counihan JL, Barry KC, Xu L, Lawrence RE, Castellano BM, Zoncu R, Nomura DK, Luo Z-Q, Vance RE. 2017. Positive and Negative Regulation of the Master Metabolic Regulator mTORC1 by Two Families of Legionella pneumophila Effectors. Cell Reports 21:2031–2038.

108. Zoncu R, Bar-Peled L, Efeyan A, Wang S, Sancak Y, Sabatini DM. 2011. mTORC1 Senses Lysosomal Amino Acids Through an Inside-Out Mechanism That Requires the Vacuolar H+-ATPase. Science 334:678–683.

109. Sancak Y, Bar-Peled L, Zoncu R, Markhard AL, Nada S, Sabatini DM. 2010. Ragulator-Rag Complex Targets mTORC1 to the Lysosomal Surface and Is Necessary for Its Activation by Amino Acids. Cell 141:290–303.

110. Sancak Y, Peterson TR, Shaul YD, Lindquist RA, Thoreen CC, Bar-Peled L, Sabatini DM. 2008. The Rag GTPases Bind Raptor and Mediate Amino Acid Signaling to mTORC1. Science 320:1496–1501.

111. Thoreen CC, Chantranupong L, Keys HR, Wang T, Gray NS, Sabatini DM. 2012. A unifying model for mTORC1-mediated regulation of mRNA translation. Nature 485:109–113.

112. Ben-Sahra I, Manning BD. 2017. mTORC1 signaling and the metabolic control of cell growth. Curr Opin Cell Biol 45:72–82.

113. Gross JD, Pears CJ. 2021. Possible Involvement of the Nutrient and Energy Sensors mTORC1 and AMPK in Cell Fate Diversification in a Non-Metazoan Organism. Frontiers Cell Dev Biology 9:758317.

114. Willows R, Sanders MJ, Xiao B, Patel BR, Martin SR, Read J, Wilson JR, Hubbard J, Gamblin SJ, Carling D. 2017. Phosphorylation of AMPK by upstream kinases is required for activity in mammalian cells. Biochem J 474:3059–3073.

115. Jaiswal P, Kimmel AR. 2019. mTORC1/AMPK responses define a core gene set for developmental cell fate switching. Bmc Biol 17:58.

116. Kim J, Kundu M, Viollet B, Guan K-L. 2011. AMPK and mTOR regulate autophagy through direct phosphorylation of Ulk1. Nat Cell Biol 13:132–141.

117. Rolando M, Escoll P, Nora T, Botti J, Boitez V, Bedia C, Daniels C, Abraham G, Stogios PJ, Skarina T, Christophe C, Dervins-Ravault D, Cazalet C, Hilbi H, Rupasinghe TWT, Tull D, McConville MJ, Ong SY, Hartland EL, Codogno P, Levade T, Naderer T, Savchenko A, Buchrieser C. 2016. Legionella pneumophila S1P-lyase targets host sphingolipid metabolism and restrains autophagy. Proc National Acad Sci 113:1901–1906.

118. Kajiwara C, Kusaka Y, Kimura S, Yamaguchi T, Nanjo Y, Ishii Y, Udono H, Standiford TJ, Tateda K. 2018. Metformin Mediates Protection against Legionella Pneumonia through Activation of AMPK and Mitochondrial Reactive Oxygen Species. J Immunol 200:623–631.

119. Choy A, Dancourt J, Mugo B, O'Connor TJ, Isberg RR, Melia TJ, Roy CR. 2012. The *Legionella* Effector RavZ Inhibits Host Autophagy Through Irreversible Atg8 Deconjugation. Science 338:1072–1076.

120. Horenkamp FA, Kauffman KJ, Kohler LJ, Sherwood RK, Krueger KP, Shteyn V, Roy CR, Melia TJ, Reinisch KM. 2015. The Legionella Anti-autophagy Effector RavZ Targets the Autophagosome via PI3P- and Curvature-Sensing Motifs. Dev Cell 34:569–576.

121. Craig EA, Gambill BD, Nelson RJ. 1993. Heat shock proteins: molecular chaperones of protein biogenesis. Microbiol Rev 57:402–414.

122. Shalgi R, Hurt JA, Krykbaeva I, Taipale M, Lindquist S, Burge CB. 2013. Widespread Regulation of Translation by Elongation Pausing in Heat Shock. Mol Cell 49:439–452.

123. Shamovsky I, Ivannikov M, Kandel ES, Gershon D, Nudler E. 2006. RNA-mediated response to heat shock in mammalian cells. Nature 440:nature04518.

124. Belyi Y. 2020. Targeting Eukaryotic mRNA Translation by Legionella pneumophila. Frontiers Mol Biosci 7:80.

125. Ambaru B, Gangadharan GM, Subramanya HS, Gupta CM. 2022. Profilin is involved in G1 to S phase progression and mitotic spindle orientation during Leishmania donovani cell division cycle. Plos One 17:e0265692.

126. Urbanus ML, Quaile AT, Stogios PJ, Morar M, Rao C, Leo RD, Evdokimova E, Lam M, Oatway C, Cuff ME, Osipiuk J, Michalska K, Nocek BP, Taipale M, Savchenko A, Ensminger AW. 2016. Diverse mechanisms of metaeffector activity in an intracellular bacterial pathogen, Legionella pneumophila. Mol Syst Biol 12:893.

127. Barry KC, Ingolia NT, Vance RE. 2017. Global analysis of gene expression reveals mRNA superinduction is required for the inducible immune response to a bacterial pathogen. Elife 6:e22707.

128. Ivanov SS, Roy CR. 2013. Pathogen signatures activate a ubiquitination pathway that modulates the function of the metabolic checkpoint kinase mTOR. Nat Immunol 14:1219–1228.

129. Shin S, Case CL, Archer KA, Nogueira CV, Kobayashi KS, Flavell RA, Roy CR, Zamboni DS. 2008. Type IV Secretion-Dependent Activation of Host MAP Kinases Induces an Increased Proinflammatory Cytokine Response to Legionella pneumophila. Plos Pathog 4:e1000220.

130. Fontana MF, Shin S, Vance RE. 2012. Activation of Host Mitogen-Activated Protein Kinases by Secreted Legionella pneumophila Effectors That Inhibit Host Protein Translation. Infect Immun 80:3570–3575.

131. ZHANG W, LIU HT. 2002. MAPK signal pathways in the regulation of cell proliferation in mammalian cells. Cell Res 12:9–18.

132. Asrat S, Dugan AS, Isberg RR. 2014. The Frustrated Host Response to Legionella pneumophila Is Bypassed by MyD88-Dependent Translation of Pro-inflammatory Cytokines. Plos Pathog 10:e1004229.

133. Sol A, Lipo E, Jesús-Díaz DA de, Murphy C, Devereux M, Isberg RR. 2019. Legionella pneumophila translocated translation inhibitors are required for bacterial-induced host cell cycle arrest. Proc National Acad Sci 116:201820093.

134. Welsh CT, Summersgill JT, Miller RD. 2004. Increases in c-Jun N-Terminal Kinase/Stress-Activated Protein Kinase and p38 Activity in Monocyte-Derived Macrophages following the Uptake of Legionella pneumophila. Infect Immun 72:1512–1518.

135. Quaile AT, Stogios PJ, Egorova O, Evdokimova E, Valleau D, Nocek B, Kompella PS, Peisajovich S, Yakunin AF, Ensminger AW, Savchenko A. 2018. The Legionella pneumophila effector Ceg4 is a phosphotyrosine phosphatase that attenuates activation of eukaryotic MAPK pathways. J Biol Chem 293:3307–3320.

136. Schwebs DJ, Hadwiger JA. 2015. The Dictyostelium MAPK ERK1 is phosphorylated in a secondary response to early developmental signaling. Cell Signal 27:147–155.

137. Schwebs DJ, Pan M, Adhikari N, Kuburich NA, Jin T, Hadwiger JA. 2018. Dictyostelium Erk2 is an atypical MAPK required for chemotaxis. Cell Signal 46:154–165.

138. Joseph AM, Shames SR. 2021. Affecting the Effectors: Regulation of Legionella pneumophila Effector Function by Metaeffectors. Pathogens 10:108.

139. Kubori T, Shinzawa N, Kanuka H, Nagai H. 2010. Legionella Metaeffector Exploits Host Proteasome to Temporally Regulate Cognate Effector. Plos Pathog 6:e1001216.

140. Kubori T, Hyakutake A, Nagai H. 2008. Legionella translocates an E3 ubiquitin ligase that has multiple U-boxes with distinct functions. Mol Microbiol 67:1307–1319.

141. Ghosh S, O'Connor TJ. 2017. Beyond Paralogs: The Multiple Layers of Redundancy in Bacterial Pathogenesis. Front Cell Infect Mi 7:467.

142. Laguna RK, Creasey EA, Li Z, Valtz N, Isberg RR. 2006. A Legionella pneumophila-translocated substrate that is required for growth within macrophages and protection from host cell death. Proc National Acad Sci 103:18745–18750.

143. Creasey EA, Isberg RR. 2012. The protein SdhA maintains the integrity of the Legionella-containing vacuole. Proc National Acad Sci 109:3481–3486.

144. Havey JC, Roy CR. 2015. Toxicity and SidJ-Mediated Suppression of Toxicity Require Distinct Regions in the SidE Family of Legionella pneumophila Effectors. Infect Immun 83:3506–3514.

145. Jeong KC, Sexton JA, Vogel JP. 2015. Spatiotemporal Regulation of a Legionella pneumophila T4SS Substrate by the Metaeffector SidJ. Plos Pathog 11:e1004695.

146. Liu Y, Luo Z-Q. 2007. The Legionella pneumophila Effector SidJ Is Required for Efficient Recruitment of Endoplasmic Reticulum Proteins to the Bacterial Phagosome ▿ . Infect Immun 75:592–603.

147. Qiu J, Luo Z-Q. 2017. Hijacking of the Host Ubiquitin Network by Legionella pneumophila. Front Cell Infect Mi 7:487.

148. Qiu J, Yu K, Fei X, Liu Y, Nakayasu ES, Piehowski PD, Shaw JB, Puvar K, Das C, Liu X, Luo Z-Q. 2017. A unique deubiquitinase that deconjugates phosphoribosyl-linked protein ubiquitination. Cell Res 27:865–881.

149. Gan N, Zhen X, Liu Y, Xu X, He C, Qiu J, Liu Y, Fujimoto GM, Nakayasu ES, Zhou B, Zhao L, Puvar K, Das C, Ouyang S, Luo Z-Q. 2019. Regulation of phosphoribosyl ubiquitination by a calmodulin-dependent glutamylase. Nature 572:387–391.

150. Bhogaraju S, Bonn F, Mukherjee R, Adams M, Pfleiderer MM, Galej WP, Matkovic V, Lopez-Mosqueda J, Kalayil S, Shin D, Dikic I. 2019. Inhibition of bacterial ubiquitin ligases by SidJ–calmodulin catalysed glutamylation. Nature 572:382–386.

151. Black MH, Osinski A, Gradowski M, Servage KA, Pawłowski K, Tomchick DR, Tagliabracci VS. 2019. Bacterial pseudokinase catalyzes protein polyglutamylation to inhibit the SidE-family ubiquitin ligases. Science 364:787–792.

152. Sulpizio A, Minelli ME, Wan M, Burrowes PD, Wu X, Sanford EJ, Shin J-H, Williams BC, Goldberg ML, Smolka MB, Mao Y. 2019. Protein polyglutamylation catalyzed by the bacterial calmodulin-dependent pseudokinase SidJ. Elife 8:e51162.

153. Toulabi L, Wu X, Cheng Y, Mao Y. 2013. Identification and Structural Characterization of a Legionella Phosphoinositide Phosphatase. J Biol Chem 288:24518–24527.

154. Valleau D, Quaile AT, Cui H, Xu X, Evdokimova E, Chang C, Cuff ME, Urbanus ML, Houliston S, Arrowsmith CH, Ensminger AW, Savchenko A. 2018. Discovery of Ubiquitin Deamidases in the Pathogenic Arsenal of Legionella pneumophila. Cell Reports 23:568–583.

155. Gan N, Guan H, Huang Y, Yu T, Fu J, Nakayasu ES, Puvar K, Das C, Wang D, Ouyang S, Luo Z. 2020. Legionella pneumophila regulates the activity of UBE2N by deamidase-mediated deubiquitination. Embo J 39:e102806.

156. Sulpizio AG, Minelli ME, Mao Y. 2019. Glutamylation of Bacterial Ubiquitin Ligases by a Legionella Pseudokinase. Trends Microbiol 27:967–969.

157. Joseph AM, Pohl AE, Ball TJ, Abram TG, Johnson DK, Geisbrecht BV, Shames SR. 2020. The Legionella pneumophila Metaeffector Lpg2505 (MesI) Regulates SidI-Mediated Translation Inhibition and Novel Glycosyl Hydrolase Activity. Infect Immun 88.

158. Machtens DA, Willerding JM, Eschenburg S, Reubold TF. 2020. Crystal structure of the metaeffector MesI (Lpg2505) from Legionella pneumophila. Biochem Bioph Res Co https://doi.org/10.1016/j.bbrc.2020.05.027.

159. Felipe KS de, Pampou S, Jovanovic OS, Pericone CD, Ye SF, Kalachikov S, Shuman HA. 2005. Evidence for Acquisition of Legionella Type IV Secretion Substrates via Interdomain Horizontal Gene Transfer. J Bacteriol 187:7716–7726.

160. Mosavi LK, Cammett TJ, Desrosiers DC, Peng Z. 2004. The ankyrin repeat as molecular architecture for protein recognition. Protein Sci 13:1435–1448.

161. Burstein D, Amaro F, Zusman T, Lifshitz Z, Cohen O, Gilbert JA, Pupko T, Shuman HA, Segal G. 2016. Genomic analysis of 38 Legionella species identifies large and diverse effector repertoires. Nat Genet 48:167–175.

162. Shames SR, Liu L, Havey JC, Schofield WB, Goodman AL, Roy CR. 2017. Multiple Legionella pneumophila effector virulence phenotypes revealed through high-throughput analysis of targeted mutant libraries. Proc National Acad Sci 114:E10446–E10454.

163. Fraser DW, Tsai TR, Orenstein W, Parkin WE, Beecham HJ, Sharrar RG, Harris J, Mallison GF, Martin SM, McDade JE, Shepard CC, Brachman PS. 1977. Legionnaires' Disease — Description of an Epidemic of Pneumonia. New Engl J Medicine 297:1189–1197.

164. CDC. 2021. Legionnaires' Disease and Pontiac Fever. https://www.cdc.gov/legionella/index.html. Retrieved 22 September 2022.

165. McDade JE, Shepard CC, Fraser DW, Tsai TR, Redus MA, Dowdle WR. 1977. Legionnaires' Disease — Isolation of a Bacterium and Demonstration of Its Role in Other Respiratory Disease. New Engl J Medicine 297:1197–1203.

166. Diez E, Yaraghi Z, MacKenzie A, Gros P. 2000. The Neuronal Apoptosis Inhibitory Protein (Naip) Is Expressed in Macrophages and Is Modulated After Phagocytosis and During Intracellular Infection with Legionella pneumophila. J Immunol 164:1470–1477.

167. Lightfield KL, Persson J, Brubaker SW, Witte CE, Moltke J von, Dunipace EA, Henry T, Sun Y-H, Cado D, Dietrich WF, Monack DM, Tsolis RM, Vance RE. 2008. Critical function for Naip5 in inflammasome activation by a conserved carboxy-terminal domain of flagellin. Nat Immunol 9:1171–1178.

168. Halff EF, Diebolder CA, Versteeg M, Schouten A, Brondijk THC, Huizinga EG. 2012. Formation and Structure of a NAIP5-NLRC4 Inflammasome Induced by Direct Interactions with Conserved N- and C-terminal Regions of Flagellin*. THE JOURNAL OF BIOLOGICAL CHEMISTRY 287:38460 –38472.

169. Pereira MSF, Morgantetti GF, Massis LM, Horta CV, Hori JI, Zamboni DS. 2011. Activation of NLRC4 by Flagellated Bacteria Triggers Caspase-1–Dependent and –Independent Responses To Restrict Legionella pneumophila Replication in Macrophages and In Vivo. J Immunol 187:6447–6455.

170. Silveira TN, Zamboni DS. 2010. Pore Formation Triggered by Legionella spp. Is an Nlrc4 Inflammasome-Dependent Host Cell Response That Precedes Pyroptosis ▿ . Infect Immun 78:1403–1413.

171. Cai S, Batra S, Wakamatsu N, Pacher P, Jeyaseelan S. 2012. NLRC4 Inflammasome-Mediated Production of IL-1β Modulates Mucosal Immunity in the Lung against Gram-Negative Bacterial Infection. J Immunol 188:5623–5635.

172. He W, Wan H, Hu L, Chen P, Wang X, Huang Z, Yang Z, Zhong C-Q, Han J. 2015. Gasdermin D is an executor of pyroptosis and required for interleukin-1β secretion. Cell Research 2015:1285–1298.

173. Broz P, Pelegrín P, Shao F. 2020. The gasdermins, a protein family executing cell death and inflammation. Nat Rev Immunol 20:143–157.

174. Jiang M, Qi L, Li L, Li Y. 2020. The caspase-3/GSDME signal pathway as a switch between apoptosis and pyroptosis in cancer. Cell Death Discov 6:112.

175. Sarhan J, Liu BC, Muendlein HI, Li P, Nilson R, Tang AY, Rongvaux A, Bunnell SC, Shao F, Green DR, Poltorak A. 2018. Caspase-8 induces cleavage of gasdermin D to elicit pyroptosis during Yersinia infection. Proc National Acad Sci 115:E10888–E10897.

176. Rogers C, Fernandes-Alnemri T, Mayes L, Alnemri D, Cingolani G, Alnemri ES. 2017. Cleavage of DFNA5 by caspase-3 during apoptosis mediates progression to secondary necrotic/pyroptotic cell death. Nat Commun 8:14128.

177. Rogers C, Erkes DA, Nardone A, Aplin AE, Fernandes-Alnemri T, Alnemri ES. 2019. Gasdermin pores permeabilize mitochondria to augment caspase-3 activation during apoptosis and inflammasome activation. Nat Commun 10:1689.

178. Wu Y, Zhang J, Yu S, Li Y, Zhu J, Zhang K, Zhang R. 2022. Cell pyroptosis in health and inflammatory diseases. Cell Death Discov 8:191.

179. Sikora A, Kozioł-Montewka M, Książek A, Wójtowicz M, Paluch-Oleś J, Magryś A, Grzebalska A, Bednarek-Skublewska A, Steć A, Rudzki S, Furmaga J, Matuszewska R, Krogulska B. 2013. Assessment of Cytokine Release After in Vitro Stimulation of Whole Blood with Legionella Pneumophila in Immunocompromised Patients. Immunol Invest 42:1–17.

180. Fernandez-Serrano S, Dorca J, Coromines M, Carratala J, Gudiol F, Manresa F. 2003. Molecular Inflammatory Responses Measured in Blood of Patients with Severe Community-Acquired Pneumonia. Clinical and Diagnostic Laboratory Immunology 10:813–820.

181. Archer KA, Roy CR. 2006. MyD88-Dependent Responses Involving Toll-Like Receptor 2 Are Important for Protection and Clearance of Legionella pneumophila in a Mouse Model of Legionnaires' Disease. Infect Immun 74:3325–3333.

182. Archer KA, Alexopoulou L, Flavell RA, Roy CR. 2009. Multiple MyD88-dependent responses contribute to pulmonary clearance of Legionella pneumophila. Cell Microbiol 11:21–36.

183. Sporri R, Joller N, Albers U, Hilbi H, Oxenius A. 2006. MyD88-dependent IFN-y Production by NK cells is key for control of Legionella pneumophila infection. The Journal of Immunology 176:6162–6171.

184. Horwitz MA, Silverstein SC. 1980. Legionnaires' Disease Bacterium (Legionella pneumophila) Multiplies Intracellularly in Human Monocytes. J Clin Invest 66:441–450.

185. Yamamoto Y, Klein TW, Brown K, Friedman H. 1992. Differential morphologic and metabolic alterations in permissive versus nonpermissive murine macrophages infected with Legionella pneumophila. Infect Immun 60:3231–3237.

186. Dietrich WF, Damron DM, Isberg RR, Lander ES, Swanson MS. 1995. Lgn1, a gene that determines susceptibility to Legionella pneumophila, maps to mouse chromosome 13. Genomics 26:443–450.

187. Brieland J, Freeman P, Kunkel R, Chrisp C, Hurley M, Fantone J, Engleberg C. 1994. Replicative Legionella pneumophila lung infection in intratracheally inoculated A/J mice. A murine model of human Legionnaires' disease. Am J Pathology 145:1537–46.

188. Ricci ML, Torosantucci A, Scaturro M, Chiani P, Baldassarri L, Pastoris MC. 2005. Induction of protective immunity by Legionella pneumophila flagellum in an A/J mouse model. Vaccine 23:4811–4820.

189. Susa M, Ticac B, Rukavina T, Doric M, Marre R. 1998. Legionella pneumophila Infection in Intratracheally Inoculated T CellDepleted or -Nondepleted A/J Mice. The Journal of Immunology 160:316–321.

190. Derré I, Isberg RR. 2004. Macrophages from Mice with the Restrictive Lgn1 Allele Exhibit Multifactorial Resistance to Legionella pneumophila. Infect Immun 72:6221–6229.

191. Ren T, Zamboni DS, Roy CR, Dietrich WF, Vance RE. 2006. Flagellin-Deficient Legionella Mutants Evade Caspase-1- and Naip5-Mediated Macrophage Immunity. Plos Pathog 2:e18.

192. Edelstein PH, Beer KB, DeBoynton ED. 1987. Influence of growth temperature on virulence of Legionella pneumophila. Infect Immun 55:2701–2705.

193. Celada A, Gray PW, Rinderknecht E, Schreiber RD. 1984. Evidence for a gamma-interferon receptor that regulates macrophage tumoricidal activity. J Exp Medicine 160:55–74.

194. Thomas ED, Ramberg RE, Sale GE, Sparkes RS, Golde DW. 1976. Direct Evidence for a Bone Marrow Origin of the Alveolar Macrophage in Man. Science 192:1016–1018.

195. Takemura H, Yamamoto H, Kunishima H, Ikejima H, Hara T, Kanemitsu K, Terakubo S, Shoji Y, Kaku M, Shimada J. 2000. Evaluation of a human monocytic cell line THP-1 model for assay of the intracellular activities of antimicrobial agents against Legionella pneumophila. J Antimicrob Chemoth 46:589–594.

196. Kortmann J, Brubaker SW, Monack DM. 2015. Cutting Edge: Inflammasome Activation in Primary Human Macrophages Is Dependent on Flagellin. J Immunol 195:815–819.

197. Tsuchiya S, Yamabe M, Yamaguchi Y, Kobayashi Y, Konno T, Tada K. 1980. Establishment and characterization of a human acute monocytic leukemia cell line (THP-1). Int J Cancer 26:171–176.

198. Shin D, Bhattacharya A, Cheng Y-L, Alonso MC, Mehdipour AR, Noort GJ van der H van, Ovaa H, Hummer G, Dikic I. 2020. Bacterial OTU deubiquitinases regulate substrate ubiquitination upon Legionella infection. Elife 9:e58277.

199. Kitao T, Taguchi K, Seto S, Arasaki K, Ando H, Nagai H, Kubori T. 2020. Legionella Manipulates Non-canonical SNARE Pairing Using a Bacterial Deubiquitinase. Cell Reports 32:108107.

200. Uribe-Querol E, Rosales C. 2017. Control of Phagocytosis by Microbial Pathogens. Front Immunol 8:1368.

201. KUMAR A, MURPHY R, ROBINSON P, WEI L, BORIE AM. 2004. Cyclic mechanical strain inhibits skeletal myogenesis through activation of focal adhesion kinase, Rac-1 GTPase, and NF-kB transcription factor. Faseb J 18:1524–1535.

202. Payne NR, Horwitz MA. 1987. Phagocytosis of Legionella pneumophila is mediated by human monocyte complement receptors. J Exp Medicine 166:1377–1389.

203. Mancuso P, Peters-Golden M. 2000. Modulation of Alveolar Macrophage Phagocytosis by Leukotrienes Is Fc Receptor–Mediated and Protein Kinase C-Dependent. Am J Resp Cell Mol 23:727–733.

204. Donini R, Haslam SM, Kontoravdi C. 2021. Glycoengineering Chinese hamster ovary cells: a short history. Biochem Soc T 49:915–931.

205. Goswami J, Sinskey AJ, Steller H, Stephanopoulos GN, Wang DIC. 1999. Apoptosis in batch cultures of Chinese Hamster Ovary cells. Biotechnol Bioeng 62:632–640.

206. Thomas P, Smart TG. 2005. HEK293 cell line: A vehicle for the expression of recombinant proteins. J Pharmacol Toxicol 51:187–200.

207. Nagai H, Roy CR. 2001. The DotA protein from Legionella pneumophila is secreted by a novel process that requires the Dot/Icm transporter. Embo J 20:5962–5970.

208. Roy CR, Berger KH, Isberg RR. 1998. Legionella pneumophila DotA protein is required for early phagosome trafficking decisions that occur within minutes of bacterial uptake. Mol Microbiol 28:663–674.

209. Berger KH, Merriam JJ, Isberg RR. 1994. Altered intracellular targeting properties associated with mutations in the Legionella pneumophila dotA gene. Mol Microbiol 14:809–822.

210. Roy CR, Isberg RR. 1997. Topology of Legionella pneumophila DotA: an inner membrane protein required for replication in macrophages. Infect Immun 65:571–578.

211. Geisbrecht BV, Bouyain S, Pop M. 2006. An optimized system for expression and purification of secreted bacterial proteins. Protein Expres Purif 46:23–32.

212. Jeong H, Barbe V, Lee CH, Vallenet D, Yu DS, Choi S-H, Couloux A, Lee S-W, Yoon SH, Cattolico L, Hur C-G, Park H-S, Ségurens B, Kim SC, Oh TK, Lenski RE, Studier FW, Daegelen P, Kim JF. 2009. Genome Sequences of Escherichia coli B strains REL606 and BL21(DE3). J Mol Biol 394:644–652.

213. Edwards CP, Aruffo A. 1993. Current applications of COS cell based transient expression systems. Curr Opin Biotech 4:558–563.

214. Fehr M, Lalonde S, Ehrhardt DW, Frommer WB. 2004. Live Imaging of Glucose Homeostasis in Nuclei of COS-7 Cells. J Fluoresc 14:603–609.

215. Habyarimana F, Al-khodor S, Kalia A, Graham JE, Price CT, Garcia MT, Kwaik YA. 2008. Role for the Ankyrin eukaryotic-like genes of Legionella pneumophila in parasitism of protozoan hosts and human macrophages. Environ Microbiol 10:1460–1474.

216. Olawole OI, Gleason ML, Beattie GA. 2022. Expression and Functional Analysis of the Type III Secretion System Effector Repertoire of the Xylem Pathogen Erwinia tracheiphila on Cucurbits. Mol Plant-microbe Interactions MPMI01220002R.

217. Smith EP, Cotto-Rosario A, Borghesan E, Held K, Miller CN, Celli J. 2020. Epistatic Interplay between Type IV Secretion Effectors Engages the Small GTPase Rab2 in the Brucella Intracellular Cycle. mBio 11:e03350-19.

218. Okujava R, Guye P, Lu Y-Y, Mistl C, Polus F, Vayssier-Taussat M, Halin C, Rolink AG, Dehio C. A Translocated Effector Required for Bartonella Dissemination from Derma to Blood Safeguards Migratory Host Cells from Damage by Co-translocated Effectors. Plos Pathogens 10:e1004187.

219. Ensminger AW. 2016. Legionella pneumophila, armed to the hilt: justifying the largest arsenal of effectors in the bacterial world. Curr Opin Microbiol 29:74–80.

220. Belyi Y, Jank T, Aktories K. 2013. Cytotoxic glucosyltransferases of Legionella pneumophila. Curr Top Microbiol 376:211 226.

221. Källberg M, Wang H, Wang S, Peng J, Wang Z, Lu H, Xu J. 2012. Template-based protein structure modeling using the RaptorX web server. Nat Protoc 7:1511–1522.

222. Huang L, Boyd D, Amyot WM, Hempstead AD, Luo Z, O'Connor TJ, Chen C, Machner M, Montminy T, Isberg RR. 2011. The E Block motif is associated with Legionella pneumophila translocated substrates. Cell Microbiol 13:227–245.

223. Nagai H, Cambronne ED, Kagan JC, Amor JC, Kahn RA, Roy CR. 2005. A C-terminal translocation signal required for Dot/Icm-dependent delivery of the Legionella RalF protein to host cells. Proc National Acad Sci 102:826–831.

224. Söding J, Biegert A, Lupas AN. 2005. The HHpred interactive server for protein homology detection and structure prediction. Nucleic Acids Res 33:W244 8.

225. Kelley LA, Mezulis S, Yates CM, Wass MN, Sternberg MJE. 2015. The Phyre2 web portal for protein modeling, prediction and analysis. Nat Protoc 10:845–858.

226. Yang J, Zhang Y. 2015. I-TASSER server: new development for protein structure and function predictions. Nucleic Acids Res 43:W174–W181.

227. Roy A, Kucukural A, Zhang Y. 2010. I-TASSER: a unified platform for automated protein structure and function prediction. Nat Protoc 5:725–738.

228. Yang J, Yan R, Roy A, Xu D, Poisson J, Zhang Y. 2015. The I-TASSER Suite: protein structure and function prediction. Nat Methods 12:7–8.

229. Holm L. 2019. Benchmarking fold detection by DaliLite v.5. Bioinformatics 35:5326–5327.

230. Kim DE, Chivian D, Malmström L, Baker D. 2005. Automated prediction of domain boundaries in CASP6 targets using Ginzu and RosettaDOM. Proteins Struct Funct Bioinform 61:193–200.

231. Belyi I, Popoff MR, Cianciotto NP. 2003. Purification and Characterization of a UDP-Glucosyltransferase Produced by Legionella pneumophila. Infect Immun 71:181–186.

232. Belyi Y, Tartakovskaya D, Tais A, Fitzke E, Tzivelekidis T, Jank T, Rospert S, Aktories K. 2012. Elongation Factor 1A Is the Target of Growth Inhibition in Yeast Caused by Legionella pneumophila Glucosyltransferase Lgt1. J Biol Chem 287:26029–26037.

233. Dever TE, Green R. 2012. The Elongation, Termination, and Recycling Phases of Translation in Eukaryotes. Csh Perspect Biol 4:a013706.

234. Belyi Y, Stahl M, Sovkova I, Kaden P, Luy B, Aktories K. 2009. Region of Elongation Factor 1A1 Involved in Substrate Recognition by Legionella pneumophila Glucosyltransferase Lgt1 IDENTIFICATION OF Lgt1 AS A RETAINING GLUCOSYLTRANSFERASE. J Biol Chem 284:20167–20174.

235. Rolando M, Buchrieser C. 2014. Legionella pneumophila type IV effectors hijack the transcription and translation machinery of the host cell. Trends Cell Biol 24:771–778.

236. Naegeli A, Michaud G, Schubert M, Lin C-W, Lizak C, Darbre T, Reymond J-L, Aebi M. 2014. Substrate Specificity of Cytoplasmic N-Glycosyltransferase. J Biol Chem 289:24521–24532.

237. Vera M, Pani B, Griffiths LA, Muchardt C, Abbott CM, Singer RH, Nudler E. 2014. The translation elongation factor eEF1A1 couples transcription to translation during heat shock response. Elife 3:e03164.

238. Yan L, Cerny RL, Cirillo JD. 2004. Evidence that hsp90 Is Involved in the Altered Interactions of Acanthamoeba castellanii Variants with Bacteria. Eukaryot Cell 3:567–578.

239. Dong Y, Mu Y, Xie Y, Zhang Y, Han Y, Zhou Y, Wang W, Liu Z, Wu M, Wang H, Pan M, Xu N, Xu C-Q, Yang M, Fan S, Deng H, Tan T, Liu X, Liu L, Li J, Wang J, Fang X, Feng Y. 2018. Structural basis of ubiquitin modification by the Legionella effector SdeA. Nature 557:674–678.

240. Wang Y, Shi M, Feng H, Zhu Y, Liu S, Gao A, Gao P. 2018. Structural Insights into Non-canonical Ubiquitination Catalyzed by SidE. Cell 173:1231-1243.e16.

241. Qiu J, Sheedlo MJ, Yu K, Tan Y, Nakayasu ES, Das C, Liu X, Luo Z-Q. 2016. Ubiquitination independent of E1 and E2 enzymes by bacterial effectors. Nature 533:120–124.

242. Liang G, Hai T. 1997. Characterization of Human Activating Transcription Factor 4, a Transcriptional Activator That Interacts with Multiple Domains of cAMP-responsive Element-binding Protein (CREB)-binding Protein (CBP)*. J Biol Chem 272:24088–24095.

243. Sethi MK, Buettner FFR, Ashikov A, Bakker H. 2013. Glycosyltransferases, Methods and Protocols. Methods Mol Biology 1022:307–320.

244. Mishra AK, Krumbach K, Rittmann D, Batt SM, Lee OY-C, De S, Frunzke J, Besra GS, Eggeling L. 2012. Deletion of manC in Corynebacterium glutamicum results in a phospho-myo-inositol mannoside- and lipoglycan-deficient mutant. Microbiology+ 158:1908–1917.

245. Rodrigo-Unzueta A, Martínez MA, Comino N, Alzari PM, Chenal A, Guerin ME. 2016. Molecular Basis of Membrane Association by the Phosphatidylinositol Mannosyltransferase PimA Enzyme from Mycobacteria*. J Biol Chem 291:13955–13963.

246. Panda SK, Saxena S, Guruprasad L. 2019. Homology modeling, docking and structure-based virtual screening for new inhibitor identification of Klebsiella pneumoniae heptosyltransferase-III. J Biomol Struct Dyn 38:1–16.

247. Batt SM, Jabeen T, Mishra AK, Veerapen N, Krumbach K, Eggeling L, Besra GS, Fütterer K. 2010. Acceptor Substrate Discrimination in Phosphatidyl-myo-inositol Mannoside Synthesis

STRUCTURAL AND MUTATIONAL ANALYSIS OF MANNOSYLTRANSFERASE CORYNEBACTERIUM GLUTAMICUM PimB′. J Biol Chem 285:37741–37752.

248. Coates SW, Gurney T, Sommers LW, Yeh M, Hirschberg CB. 1980. Subcellular localization of sugar nucleotide synthetases. J Biol Chem 255:9225–9229.

249. Kawakita M, Ishida N, Miura N, Sun-Wada G-H, Yoshioka S. 1998. Nucleotide Sugar Transporters: Elucidation of Their Molecular Identity and Its Implication for Future Studies. J Biochem 123:777–785.

250. Berger KH, Isberg RR. 1993. Two distinct defects in intracellular growth complemented by a single genetic locus in Legionella pneumophila. Mol Microbiol 7:7–19.

251. Feeley JC, Gibson RJ, Gorman GW, Langford NC, Rasheed JK, Mackel DC, Baine WB. 1979. Charcoal-yeast extract agar: primary isolation medium for Legionella pneumophila. J Clin Microbiol 10:437–441.

252. Saito A, Rolfe RD, Edelstein PH, Finegold SM. 1981. Comparison of liquid growth media for Legionella pneumophila. J Clin Microbiol 14:623–627.

253. Arasaki K, Roy CR. 2010. Legionella pneumophila Promotes Functional Interactions between Plasma Membrane Syntaxins and Sec22b. Traffic 11:587–600.

254. Joiner KA, Fuhrman SA, Miettinen HM, Kasper LH, Mellman I. 1990. Toxoplasma gondii: Fusion Competence of Parasitophorous Vacuoles in Fc Receptor-Transfected Fibroblasts. Science 249:641–646.

255. Lü W, Du J, Stahl M, Tzivelekidis T, Belyi Y, Gerhardt S, Aktories K, Einsle O. 2010. Structural Basis of the Action of Glucosyltransferase Lgt1 from Legionella pneumophila. J Mol Biol 396:321–331.

256. Stapels DAC, Woehl JL, Milder FJ, Tromp AT, Batenburg AA van, Graaf WC de, Broll SC, White NM, Rooijakkers SHM, Geisbrecht BV. 2018. Evidence for multiple modes of neutrophil serine protease recognition by the EAP family of Staphylococcal innate immune evasion proteins. Protein Sci 27:509–522.

257. Chauhan D, Joseph AM, Shames SR. 2022. Intrabacterial regulation of a cytotoxic effector by its cognate metaeffector promotes Legionella pneumophila virulence. Biorxiv 2022.06.12.495833.

258. Ghazaei C. 2021. Anti-virulence Therapy Against Bacterial Infections: Mechanisms of Action and Challenges. J Kermanshah Univ Medical Sci 25.

259. Hauser AR. 2009. The type III secretion system of Pseudomonas aeruginosa: infection by injection. Nat Rev Microbiol 7:654–665.

260. Arnoldo A, Curak J, Kittanakom S, Chevelev I, Lee VT, Sahebol-Amri M, Koscik B, Ljuma L, Roy PJ, Bedalov A, Giaever G, Nislow C, Merrill AR, Merrill RA, Lory S, Stagljar I. 2008. Identification of Small Molecule Inhibitors of Pseudomonas aeruginosa Exoenzyme S Using a Yeast Phenotypic Screen. Plos Genet 4:e1000005.

261. Muschiol S, Bailey L, Gylfe A, Sundin C, Hultenby K, Bergstrom S, Elofsson M, Wolf-Watz H, Normark S, Henriques-Normark B. 2006. A small-molecule inhibitor of type III secretion inhibits different stages of the infectious cycle of Chlamydia trachomatis. PNAS 103:14566–14571.

262. Kauppi AM, Nordfelth R, Uvell H, Wolf-Watz H, Elofsson M. 2003. Targeting Bacterial Virulence: Inhibitors of Type III Secretion in Yersinia. Chemistry & Biology 10:241–249.

263. Nordfelth R, Kauppi AM, Norberg HA, Wolf-Watz H, Elofsson M. 2005. Small-Molecule Inhibitors Specifically Targeting Type III Secretion. Infect Immun 73:3104–3114.

264. Mondino S, Schmidt S, Rolando M, Escoll P, Gomez-Valero L, Buchrieser C. 2019. Legionnaires' Disease: State of the Art Knowledge of Pathogenesis Mechanisms of Legionella. Annu Rev Pathology Mech Dis 15:1–28.

265. McCloskey A, Perri K, Chen T, Han A, Luo Z-Q. 2021. The metaeffector MesI regulates the activity of the Legionella effector SidI through direct protein-protein interactions. Microbes Infect 104794.

266. Ladant D. 1988. Interaction of Bordetella pertussis adenylate cyclase with calmodulin. Identification of two separated calmodulin-binding domains. J Biol Chem 263:2612–2618.

267. Hewlett EL, Underhill LH, Cook GH, Manclark CR, Wolf J. 1079. A protein activator for the adenylate cyclase of Bordetella pertussis. | Elsevier Enhanced Reader. THE JOURNAL OF BIOLOGICAL CHEMISTRY 254:5602–5605.

268. Molofsky AB, Byrne BG, Whitfield NN, Madigan CA, Fuse ET, Tateda K, Swanson MS. 2006. Cytosolic recognition of flagellin by mouse macrophages restricts Legionella pneumophila infection. J Exp Medicine 203:1093–1104.

269. Ngwaga T, Hydock AJ, Ganesan S, Shames SR. 2019. Potentiation of Cytokine-Mediated Restriction of Legionella Intracellular Replication by a Dot/Icm-Translocated Effector. J Bacteriol 201.

270. Falkow S. 2004. Molecular Koch's postulates applied to bacterial pathogenicity — a personal recollection 15 years later. Nat Rev Microbiol 2:67–72.

271. Falkow S. 1988. Molecular Koch's Postulates Applied to Microbial Pathogenicity. Clin Infect Dis 10:S274–S276.

272. Puvar K, Iyer S, Fu J, Kenny S, Terón KIN, Luo Z-Q, Brzovic PS, Klevit RE, Das C. 2020. Legionella effector MavC targets the Ube2N~Ub conjugate for noncanonical ubiquitination. Nat Commun 11:2365.

273. Akasaki K, Michihara A, Mibuka K, Fujiwara Y, Tsuji H. 1995. Biosynthetic Transport of a Major Lysosomal Membrane Glycoprotein, Lamp-1: Convergence of Biosynthetic and Endocytic Pathways Occurs at Three Distinctive Points. Exp Cell Res 220:464–473.

274. Benz J, Meinhart A. 2014. Antibacterial effector/immunity systems: it's just the tip of the iceberg. Curr Opin Microbiol 17:1–10.

275. Altindis E, Dong T, Catalano C, Mekalanos J. 2015. Secretome Analysis of Vibrio cholerae Type VI Secretion System Reveals a New Effector-Immunity Pair. Mbio 6:e00075-15.

276. Kirchberger PC, Unterweger D, Provenzano D, Pukatzki S, Boucher Y. 2017. Sequential displacement of Type VI Secretion System effector genes leads to evolution of diverse immunity gene arrays in Vibrio cholerae. Sci Rep-uk 7:45133.

277. Goeders N, Melderen LV. 2014. Toxin-Antitoxin Systems as Multilevel Interaction Systems. Toxins 2014:304–324.

278. Yang X, Long M, Shen X. 2018. Effector–Immunity Pairs Provide the T6SS Nanomachine its Offensive and Defensive Capabilities. Molecules 23:1009.

279. Feldman MF, Cornelis GR. 2003. The multitalented type III chaperones: all you can do with 15 kDa. Fems Microbiol Lett 219:151–158.

280. Ganoza MC, Kiel MC, Aoki H. 2002. Evolutionary Conservation of Reactions in Translation. Microbiol Mol Biol R 66:460–485.

281. Qaidi SE, Scott NE, Hays MP, Geisbrecht BV, Watkins S, Hardwidge PR. 2020. An intra-bacterial activity for a T3SS effector. Sci Rep-uk 10:1073.

282. Qaidi SE, Scott NE, Hardwidge PR. 2021. Arginine glycosylation enhances methylglyoxal detoxification. Sci Rep-uk 11:3834.

283. Qaidi SE, Scott NE, Hays MP, Hardwidge PR. 2022. Arginine glycosylation regulates UDP-GlcNAc biosynthesis in Salmonella enterica. Sci Rep-uk 12:5293.

284. Hasan MK, Qaidi SE, Hardwidge PR. 2021. The T3SS Effector Protease NleC Is Active within Citrobacter rodentium. Pathogens 10:589.

285. Bertram R, Schuster CF. 2014. Post-transcriptional regulation of gene expression in bacterial pathogens by toxin-antitoxin systems. Front Cell Infect Mi 4:6.

286. Kim Y, Wang X, Zhang X, Grigoriu S, Page R, Peti W, Wood TK. 2010. Escherichia coli toxin/antitoxin pair MqsR/MqsA regulate toxin CspD. Environ Microbiol 12:1105–1121.

287. Hugoson E, Guliaev A, Ammunét T, Guy L. 2022. Host Adaptation in Legionellales Is 1.9 Ga, Coincident with Eukaryogenesis. Mol Biol Evol 39:msac037.

288. Merriam JJ, Mathur R, Maxfield-Boumil R, Isberg RR. 1997. Analysis of the Legionella pneumophila fliI gene: intracellular growth of a defined mutant defective for flagellum biosynthesis. Infect Immun 65:2497–2501.

289. Folly-Klan M, Alix E, Stalder D, Ray P, Duarte LV, Delprato A, Zeghouf M, Antonny B, Campanacci V, Roy CR, Cherfils J. 2013. A Novel Membrane Sensor Controls the Localization and ArfGEF Activity of Bacterial RalF. Plos Pathog 9:e1003747.

290. Bardill JP, Miller JL, Vogel JP. 2005. IcmS-dependent translocation of SdeA into macrophages by the Legionella pneumophila type IV secretion system. Mol Microbiol 56:90–103.

291. Blakeley BD, Chapman AM, McNaughton BR. 2012. Split-superpositive GFP reassembly is a fast, efficient, and robust method for detecting protein – protein interactions in vivo. Mol Biosyst 8:2036–2040.

292. Lara-Tejero M, Sutterwala FS, Ogura Y, Grant EP, Bertin J, Coyle AJ, Flavell RA, Galán JE. 2006. Role of the caspase-1 inflammasome in Salmonella typhimurium pathogenesis. J Exp Medicine 203:1407–1412.

293. Case CL, Roy CR. 2012. Legionella, Methods and Protocols. Methods Mol Biology 954:479–491.

294. Liu Y, Zhu W, Tan Y, Nakayasu ES, Staiger CJ, Luo Z-Q. 2017. A Legionella Effector Disrupts Host Cytoskeletal Structure by Cleaving Actin. Plos Pathog 13:e1006186.

295. Li J, Li Q, Xie C, Zhou H, Wang Y, Zhang N, Shao H, Chan SC, Peng X, Lin S-C, Han J. 2004. β-actin is required for mitochondria clustering and ROS generation in TNF-induced, caspase-independent cell death. J Cell Sci 117:4673–4680.

296. Gross SR, Kinzy TG. 2005. Translation elongation factor 1A is essential for regulation of the actin cytoskeleton and cell morphology. Nat Struct Mol Biol 12:772–778.

297. Davidson AJ, Wood W. 2020. Macrophages Use Distinct Actin Regulators to Switch Engulfment Strategies and Ensure Phagocytic Plasticity In Vivo. Cell Reports 31:107692.

298. Rasmussen I, Pedersen LH, Byg L, Suzuki K, Sumimoto H, Vilhardt F. 2010. Effects of F/G-actin ratio and actin turn-over rate on NADPH oxidase activity in microglia. Bmc Immunol 11:44–44.

299. Mirande M, Corre DL, Louvard D, Reggio H, Pailliez J-P, Waller J-P. 1985. Association of an aminoacyl-tRNA synthetase complex and of phenylalanyl-tRNA synthetase with the cytoskeletal framework fraction from mammalian cells. Exp Cell Res 156:91–102.

300. Dang CV, Yang DC, Pollard TD. 1983. Association of methionyl-tRNA synthetase with detergent-insoluble components of the rough endoplasmic reticulum. J Cell Biology 96:1138–1147.

301. Howe JG, Hershey JWB. 1984. Translational initiation factor and ribosome association with the cytoskeletal framework fraction from HeLa cells. Cell 37:85–93.

302. Bubb MR, Yarmola EG, Gibson BG, Southwick FS. 2003. Depolymerization of Actin Filaments by Profilin EFFECTS OF PROFILIN ON CAPPING PROTEIN FUNCTION*. J Biol Chem 278:24629–24635.

303. Goode BL, Eck MJ. 2007. Mechanism and Function of Formins in the Control of Actin Assembly. Biochemistry-us 76:593–627.

304. Kabsch W, Vandekerckhove J. 1992. Structure and Function of Actin. Annu Rev Bioph Biom 21:49–76.

305. Krishnan K, Moens PDJ. 2009. Structure and functions of profilins. Biophysical Rev 1:71–81.

306. Kardos R, Pozsonyi K, Nevalainen E, Lappalainen P, Nyitrai M, Hild G. 2009. The Effects of ADF/Cofilin and Profilin on the Conformation of the ATP-Binding Cleft of Monomeric Actin. Biophys J 96:2335–2343.

307. Habyarimana F, Price CT, Santic M, Al-Khodor S, Kwaik YA. 2010. Molecular Characterization of the Dot/Icm-Translocated AnkH and AnkJ Eukaryotic-Like Effectors of Legionella pneumophila. Infect Immun 78:1123–1134.

308. Carlier MF, Criquet P, Pantaloni D, Korn ED. 1986. Interaction of cytochalasin D with actin filaments in the presence of ADP and ATP. J Biol Chem 261:2041–2050.

309. Vance RE. 2015. The NAIP/NLRC4 inflammasomes. Curr Opin Immunol 32:84–89.

310. Hutchison CA, Merryman C, Sun L, Assad-Garcia N, Richter RA, Smith HO, Glass JI. 2019. Polar Effects of Transposon Insertion into a Minimal Bacterial Genome. J Bacteriol 201:e00185-19.

311. Castellano F, Chavrier P, Caron E. 2001. Actin dynamics during phagocytosis. Semin Immunol 13:347–355.

312. Jaumouillé V, Cartagena-Rivera AX, Waterman CM. 2019. Coupling of β2 integrins to actin by a mechanosensitive molecular clutch drives complement receptor-mediated phagocytosis. Nat Cell Biol 21:1357–1369.

313. Jesús-Díaz DA de, Murphy C, Sol A, Dorer M, Isberg RR. 2017. Host Cell S Phase Restricts Legionella pneumophila Intracellular Replication by Destabilizing the Membrane-Bound Replication Compartment. Mbio 8:e02345-16.

314. Wear MA, Yamashita A, Kim K, Maeda Y, Cooper JA. 2003. How Capping Protein Binds the Barbed End of the Actin Filament. Current Biology 13:1531–1537.

315. Funk J, Merino F, Schaks M, Rottner K, Raunser S, Bieling P. 2021. A barbed end interference mechanism reveals how capping protein promotes nucleation in branched actin networks. Nature Communications 12:1–17.

316. Kim K, Yamashita A, Wear MA, Maeda Y, Cooper JA. 2004. Capping protein binding to actin in yeast: biochemical mechanism and physiological relevance. The Journal of Cell Biology 164:567–580.

317. Schafer DA, Korshunova YO, Schroer TA, Cooper JA. 1994. Differential Localization and Sequence Analysis of Capping Protein B-Subunit Isoforms of Vertebrates . The Journal of Cell Biology 127:453–465.

318. Schuck P. 1997. Reliable determination of binding affinity and kinetics using surface plasmon resonance biosensors. Curr Opin Biotech 8:498–502.

319. Song L, Xie Y, Li C, Wang L, He C, Zhang Y, Yuan J, Luo J, Liu X, Xiu Y, Li H, Gritsenko M, Nakayasu ES, Feng Y, Luo Z-Q. 2021. The Legionella Effector SdjA Is a Bifunctional Enzyme That Distinctly Regulates Phosphoribosyl Ubiquitination. Mbio 12:e02316-21.

320. Vinzing M, Eitel J, Lippmann J, Hocke AC, Zahlten J, Slevogt H, N'Guessan PD, Gunther S, Schmeck B, Hippenstiel S, Flieger A, Suttorp N, Opitz B. 2008. NAIP and Ipaf Control Legionella pneumophila Replication in Human Cells. The Journal of Immunology 180:6808–6815.

321. Ruiz VMR, Ramirez J, Naseer N, Palacio NM, Siddarthan IJ, Yan BM, Boyer MA, Pensinger DA, Sauer J-D, Shin S. 2017. Broad detection of bacterial type III secretion system and flagellin proteins by the human NAIP/NLRC4 inflammasome. PNAS 114:13242–13247.

322. Rosengart MR, Arbabi S, Bauer GJ, Garcia I, Jelacic S, Maier RV. 2002. The Actin Cytoskeleton: An Essential Component for Enhanced TNFa Production by Adherent Monocytes. Shock 17:109–113.

323. Brüggemann H, Hagman A, Jules M, Sismeiro O, Dillies M, Gouyette C, Kunst F, Steinert M, Heuner K, Coppée J, Buchrieser C. 2006. Virulence strategies for infecting phagocytes

deduced from the in vivo transcriptional program of Legionella pneumophila. Cell Microbiol 8:1228–1240.

324. Fenton AK, Gerdes K. 2013. Direct interaction of FtsZ and MreB is required for septum synthesis and cell division in Escherichia coli. Embo J 32:1953–1965.

325. Zupan JR, Cameron TA, Anderson-Furgeson J, Zambryski PC. 2013. Dynamic FtsA and FtsZ localization and outer membrane alterations during polar growth and cell division in Agrobacterium tumefaciens. Proc National Acad Sci 110:9060–9065.

326. Martel A, Ruiz-Bedoya T, Breit-McNally C, Laflamme B, Desveaux D, Guttman DS. 2021. The ETS-ETI cycle: evolutionary processes and metapopulation dynamics driving the diversification of pathogen effectors and host immune factors. Curr Opin Plant Biol 62:102011.

327. Martel A, Laflamme B, Breit-McNally C, Lonjon F, Desveaux D, Guttman DS. 2021. Metaeffector interactions modulate the type III effector-triggered immunity load of Pseudomonas syringae. Biorxiv 2021.11.18.469137.

328. Greub G, Raoult D. 2002. Crescent Bodies of Parachlamydia acanthamoeba and Its Life Cycle within Acanthamoeba polyphaga : an Electron Micrograph Study. Appl Environ Microb 68:3076–3084.

329. Weber MM, Faris R. 2018. Subversion of the Endocytic and Secretory Pathways by Bacterial Effector Proteins. Frontiers Cell Dev Biology 6:1.

330. Brüggemann H, Cazalet C, Buchrieser C. 2006. Adaptation of Legionella pneumophila to the host environment: role of protein secretion, effectors and eukaryotic-like proteins. Curr Opin Microbiol 9:86–94.

331. Håkansson K, Doherty AJ, Shuman S, Wigley DB. 1997. X-Ray Crystallography Reveals a Large Conformational Change during Guanyl Transfer by mRNA Capping Enzymes. Cell 89:545–553.

332. Bains G, Patel AB, Narayanaswami V. 2011. Pyrene: A Probe to Study Protein Conformation and Conformational Changes. Molecules 16:7909–7935.

333. Truong K, Ikura M. 2001. The use of FRET imaging microscopy to detect protein–protein interactions and protein conformational changes in vivo. Curr Opin Struc Biol 11:573–578.

334. Anderson DM, Feix JB, Frank DW. 2015. Cross Kingdom Activators of Five Classes of Bacterial Effectors. Plos Pathog 11:e1004944.

335. Popa CM, Tabuchi M, Valls M. 2016. Modification of Bacterial Effector Proteins Inside Eukaryotic Host Cells. Frontiers in Cellular and Infection Microbiology 6.

336. Mangan JA, Monahan IM, Butcher PD. 2002. Gene expression during host—pathogen interactions: Approaches to bacterial mRNA extraction and labelling for microarray analysis. Method Microbiol 33:137–151.

337. Isla A, Haussmann D, Vera T, Kausel G, Figueroa J. 2014. Identification of the clpB and bipA genes and an evaluation of their expression as related to intracellular survival for the bacterial pathogen Piscirickettsia salmonis. Vet Microbiol 173:390–394.

338. Altman E, Segal G. 2008. The Response Regulator CpxR Directly Regulates Expression of Several Legionella pneumophila icm/dot Components as Well as New Translocated Substrates ▿ †. J Bacteriol 190:1985–1996.

339. Ma Y, III JRY. 2018. Proteomics and pulse azidohomoalanine labeling of newly synthesized proteins: what are the potential applications? Expert Rev Proteomic 15:545–554.

340. Soufo HJD, Reimold C, Linne U, Knust T, Gescher J, Graumann PL. 2010. Bacterial translation elongation factor EF-Tu interacts and colocalizes with actin-like MreB protein. Proc National Acad Sci 107:3163–3168.

341. Copenhaver AM, Casson CN, Nguyen HT, Fung TC, Duda MM, Roy CR, Shin S. 2014. Alveolar Macrophages and Neutrophils Are the Primary Reservoirs for Legionella pneumophila and Mediate Cytosolic Surveillance of Type IV Secretion. Infect Immun 82:4325–4336.

342. Quaile AT, Urbanus ML, Stogios PJ, Nocek B, Skarina T, Ensminger AW, Savchenko A. 2015. Molecular Characterization of LubX: Functional Divergence of the U-Box Fold by Legionella pneumophila. Struct Lond Engl 1993 23:1459–69.

1.